Abstract
Biomechanics and remodeling of free-floating tissue equivalents

David Dale Simon
2014

Since its introduction in 1979, the free-floating fibroblast-populated collagen lattice (FF-FPCL) has been employed in hundreds of studies examining cell-matrix interactions and cell contractility mechanisms. While it has been shown in constrained tissue equivalents that fibroblasts seek to develop and maintain a preferred mechanical environment, little work has been done to mechanically characterize the free-floating construct as it was assumed, since the lattices are unconstrained, cells cannot develop tension in the matrix. Similarly, the FF-FPCL is often used to examine remodeling during the wound healing process, yet very few studies have been carried out to determine how cells "lock-in" or entrench the matrix after actively remodeling it. The overall goal of this dissertation is to shed light on the mechanical environment of the FF-FPCL and to determine the mechanisms by which cells remodel and entrench the extant matrix to increase its utility as a model system for mechanobiological studies.

First, initiation of collagen lattice compaction was examined mechanically using an incompressibility assumption and traction-free radial and axial boundary conditions. It was found that radially varying material properties and active cell stresses were required to allow for nontrivial solutions and that a residual-type stress field would develop with equibiaxial compression in the central region transitioning to circumferential tensile stress in the periphery of the lattice. Next, the mechanical framework was adjusted to allow for compressibility as the FF-FPCL undergoes a significant change in volume during culture. Again, it was shown mathematically that the experimentally observed

deformations are possible when considering radially varying material properties and active cell stresses and this results in the development of a residual-type stress field. The presence of residual stresses was verified experimentally by applying a radial cut from the center of the gel to the outer edge the relieve the circumferential stresses, which resulted in the development of an opening angle, and the application of a circular punch in the central region, which resulted in an equibiaxial contraction of the applied hole, indicative of the release of an equibiaxial compressive stress.

To examine the remodeling and entrenchment of the FF-FPCL, the role of covalent crosslinkers, namely tissue transglutaminase (tTG) and lysyl oxidase (LOX), was examined, as well as the contractile mechanisms (Ca^{2+}-dependent vs. –independent) by which the cells actively deform the matrix. It was found that tTG was necessary for normal FF-FPCL remodeling at early times (through 2 days) and the preferred contractile mechanism up to day 1 appeared to be Ca^{2+}-dependent. While LOX was not necessary in early remodeling, its inhibition reduced further compaction at later times (3 to 4 days in culture). Similarly, there was a shift towards Ca^{2+}-independent contractility dominating at later times.

Finally, a growth & remodeling (G&R) theory-based constrained mixture model was developed to computationally examine the evolution of the first 2 days of culture of the FF-FPCL when little to no new matrix deposition occurs. This approach employs the idea that the cells seek to develop a preferred level of stress and remodel the matrix in an effort to achieve this homeostatic value and that remodeling of the extant matrix results in a composite of original and remodeled matrix that are constrained to deform together. With this approach, the gross geometric evolution of the FF-FPCL can be modeled

including the development of opening angles in the reference configuration. This model also provides the first approximation of how the stresses within the FF-FPCL can evolve over time as the resident cells seek to establish their preferred mechanical environment.

In conclusion, this work provides a mechanical framework for the FF-FPCL and its variants that accounts for prior experimental observations related to cell and matrix orientations and provides experimental verification of the presence of a residual-type stress field. This mechanical framework allows for radially varying cellular responses to be correlated to the mechanical environment and improves the utility of the FF-FPCL in mechanobiological investigations. The results related to tTG and LOX inhibition provide a potential timeline for how cells initially remodel extant matrix in an attempt to quickly develop or restore a preferred mechanical environment. Finally, the computational model provides the first model of FF-FPCL evolution to account for the changing mechanical environment and the entrenchment of the matrix and provides a hypothesis testing framework to guide future cell-matrix interaction studies utilizing the FF-FPCL. Future investigation related to this work includes the refinement of the computational model as new experimental data become available and implementation of this framework in biaxially constrained tissue equivalents to allow for precise control of the mechanical environment.

Biomechanics and remodeling of free-floating tissue equivalents

A Dissertation
Presented to the Faculty of the Graduate School
of
Yale University
in Candidacy for the Degree of
Doctor of Philosophy

by
David Dale Simon

Dissertation Director: Jay D. Humphrey

December 2014

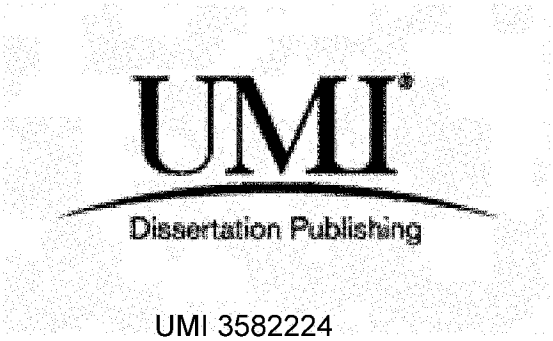

ProQuest LLC
789 East Eisenhower Parkway
P.O. Box 1346
Ann Arbor, MI 48106-1346

Table of Contents

List of Figures

List of Tables

Biographical Sketch

David Dale Simon was born in Kendallville, Indiana to Steven and Debra Simon in 1985. He has two older brothers, Steven Jr. and Russell, and an older sister, Marillyn. David attended high school at West Noble in Ligonier, Indiana and was an active participant in the National Honors Society, Boy Scouts of America, 4-H, and competed on the varsity cross-country and track teams.

As a recipient of the Distinguished Scholars Award and W.E. Koch Engineering Scholarship, he enrolled in Tulane University in 2003 and received a Bachelor of Science degree in Biomedical Engineering and a minor in Mathematics. David also received a Master of Science degree in Biomedical Engineering under the guidance of Dr. Darryl R. Overby at Tulane University in 2009. His Master's thesis research was on the development and verification of a novel experimental system to image Schlemm's canal endothelial cells during basal-to-apical constant pressure perfusion. This system allowed for the visualization of cellular dynamics and the formation of giant vacuoles in response to pressure and can be employed in studies focused on understanding the causes of open-angle glaucoma. At Tulane, David was the recipient of the Outstanding Achievement in Biomedical Engineering Studies award and a member of the National Biomedical Engineering Honor Society.

After completion of his Master's degree, David began working on his Doctoral research under the guidance of Professor Jay D. Humphrey examining the mechanics and remodeling of tissue equivalents. At present, David is pursuing an industry career in research and development.

Acknowledgements

I would first like to express my sincere gratitude to my dissertation advisor, Professor Jay Humphrey for all I have learned from him and for his continuous help and support in all stages of this work. Thank you for your mentorship, inspiring wisdom, and providing me with this exceptional opportunity. This experience has been very rewarding. I would also like to thank the members of my committee, Professor Laura Niklason, Professor Eric Dufresne, and Professor Stuart Campbell for your guidance and input in completing my studies.

Thank you to the members of Professor Humphrey's Continuum Biomechanics Lab for your feedback and more importantly your friendship. I am grateful for your advice, encouragement, and stimulating discussions. I would like to offer thanks to the members of the labs of Professor Martin Schwartz and Professor Eric Dufresne that are a part of the Mechanotransduction Group at Yale for your advice, criticism, and discussions related to this project. I would like to thank Professor Cornelius Horgan at the University of Virginia for his help and collaboration on the development of the compressible mechanical model. I would also like to thank the wonderful staff in the Yale BME department for always being so helpful and friendly.

I would like to thank my wonderful family. I am grateful for your love, constant support, and prayers through my academic endeavors. I would like to especially thank my wife Aubrey for her personal support, love, and great patience. Most importantly, I would like to thank my Lord and Savior Jesus Christ for the perseverance that he has bestowed upon me during my graduate studies.

This research was supported by NIH Grant R01 EB-008366 and a grant from the National Science Foundation (CMMI-1161423) through the Biomechanics and Mechanobiology Program.

Chapter 1: Introduction and Outline

Portions of the chapter were published in *Bio-inspired Materials for Biomedical Engineering* (Eds. AB Brennan, CM Kirschner) Ch. 15, John Wiley & Sons: 2014, 281-308

1.1 Introduction

Advances in tissue engineering and regenerative medicine have been tremendous over the past decade. Clinical successes include a number of implantable tissues, with the majority of available products being in orthopedic and wound healing arenas [1]. Still, a major challenge in research and development is optimization, both in the performance of the tissue engineered construct and in the scale-up of processes required for commercialization.

Tissue engineering approaches also benefit basic research in biomechanics and mechanobiology. Tissue equivalents represent excellent model systems for studying cellular responses to mechanical and chemical stimuli, both of which can be well controlled in vitro. Whereas biomechanics seeks to understand bulk material behavior in terms of microstructure, which can be manipulated in a tissue engineered construct, mechanobiology seeks to correlate cellular responses with mechanical stimuli, which is often difficult to infer in vivo and even in native tissues in vitro. Mechanically stimulated cells can alter their local environment, often by working on and remodeling the local extracellular matrix and hence bulk material behavior. Such changes, in turn, can alter the mechanical stimuli sensed by the cell and thereby lead to additional cell-mediated changes of the construct.

A combined approach using tissue equivalent-based experiments and computational models of cell-matrix mechanics promises to provide increased insight

into these complex couplings. Quantitative measurement of cellular gene expression and protein synthesis can be correlated with mechanical stimuli via mechanical testing and characterization of tissue equivalents. This information can then inform computational simulations to correlate how the mechanical stimuli and subsequent cellular responses lead to matrix remodeling.

1.2 Specific Aims

The free-floating fibroblast-populated collagen lattice (FPCL), first introduced in 1979 by Bell et al. [2], is a simple tissue equivalent that has provided tremendous insight into cell-matrix interactions and cell contractility mechanisms [3,4]. A solution containing a known concentration of cells and collagen is cast in a circular mold, allowed sufficient time to gel, released from its mold, and allowed to free-float during culture for a given period of time and under conditions of interest. Because the construct is allowed to free-float, it is not influenced by any substantial external mechanical stimuli. Though the tissue equivalent is unconstrained geometrically, the traction-free boundary conditions restrict the possible constitutive mechanical formulations that allow experimentally observed deformations.

Although the free-floating FPCL and its variants have been employed in hundreds of studies, very little work has been done to mechanically characterize the tissue equivalent or to examine the mechanisms by which the cells entrench applied deformations during remodeling. Because the free-floating FPCL is unconstrained, it has been previously assumed that the cells and matrix remain randomly or isotropically oriented and any contractile forces are balanced by the response of the matrix resulting in

a net stress-free environment [4,5]. Without a mathematically rigorous examination of the mechanics, however, the precise mechanical environment of the free-floating FPCL cannot be known and cellular responses cannot be properly correlated to the mechanical stimuli. The overall goal of this dissertation is to provide a theoretical and computational framework to assess the mechanical environment the free-floating FPCL and to examine its remodeling process to increase its utility as a tool in mechanobiological studies. To this end, the specific aims of this dissertation are:

Aim 1: To develop an appropriate constitutive framework to examine the mechanical environment of the free-floating fibroblast-populated collagen lattice that accounts for prior experimental observations.

Aim 2: To assess the time course of remodeling of the free-floating fibroblast-populated collagen lattice and determine the mechanisms that allow for the remodeling and entrenchment of the matrix.

Aim 3: To implement a computational model of the remodeling and entrenchment of the free-floating fibroblast-populated collagen lattice to allow for the determination of the evolving mechanical environment of the tissue equivalent.

1.3 Outline of Dissertation

Chapter 2 provides background on the free-floating FPCL as well as uniaxially and biaxially constrained tissue equivalents. Included are observations on cellular genetic responses, cell and matrix orientation, mechanical homeostasis, prior mechanical models,

and motivation for the need of combined computational and experimental approaches to further mechanobiological research.

Chapter 3 focuses on Aim 1 and introduces an incompressible constitutive model of the mechanics of the free-floating FPCL. This model can represent the initiation of cell-driven compaction before remodeling of the matrix begins. This model also preliminarily indicates that the free-floating FPCL is indeed not stress-free, but likely develops a residual-type stress distribution.

Chapter 4 focuses on Aim 1 and improves upon the model proposed in Chapter 3 to account for the compressible nature of the free-floating FPCL. Included in this chapter is the theoretical derivation of the model and experimental verification of the model assumptions and results. This chapter also postulates the idea that the stress developed within the free-floating FPCL is the result of the cells attempt to achieve a preferred mechanical environment.

Chapter 5 focuses on Aim 2 and examines experimentally both the means by which cells actively stress the free-floating FPCL and the mechanisms employed to entrench applied deformations and remodel the matrix. This chapter provides an initial timeline of the modes of contractility and nature of enzymatic crosslinking used to alter the global geometry and organization of the free-floating FPCL during matrix compaction.

Chapter 6 focuses on Aim 3. It builds upon the theoretical model developed in Chapters 3 and 4 and introduces a growth and remodeling (G&R)-based computational model of the matrix compaction and mechanical evolution of the free-floating FPCL. Initial model parameters are chosen to fit closely the prior experimental results and the

simulation results examined to assess the evolving stresses and material properties. Hypothesis tests are performed to examine alternative constitutive relations and preliminary mechanical testing is carried out to examine the evolving material behavior.

Chapter 7 summarizes the findings and conclusions of this dissertation. This chapter also provides guidance for future work including the refinement of the proposed computational model and the development of a planar biaxial bioreactor to provide a tissue equivalent system that allows precise control of external mechanical loads.

Chapter 2: Background and Motivation – Learning from Tissue Equivalents: Biomechanics and Mechanobiology

Portions of the chapter were published in *Bio-inspired Materials for Biomedical Engineering* (Eds. AB Brennan, CM Kirschner) Ch. 15, John Wiley & Sons: 2014, 281-308

In this chapter, we review prior observations of three types of tissue equivalents (free-floating, uniaxially constrained, and biaxially constrained; see Figure 2.1), prior work in the mechanical characterization of the tissue equivalents, and prior theoretical work on mathematically modeling the growth and remodeling of tissue equivalents. Finally, we propose a possible methodology for combining experiments and computational simulations to examine cell-mediated remodeling of tissue equivalents.

2.1 Background

2.1.1 Matrix Composition & Integrins

The composition of the extracellular matrix (ECM) varies depending on tissue type, in vivo location, and tissue health. Most components of the ECM are proteins, with collagen often being the most prevalent. Collagens consist of large domains of the repeating peptide sequence Glycine-X-Y that are folded into a triple-helix structure, with X and Y representing different amino acids, often proline or hydroxyproline. The collagens are divided into subfamilies, mainly fibrillar (e.g. type I, II, and III) and network-like (e.g. type IV), with most of the other collagen types playing accessory roles for the two dominant subfamilies [6]. Of the fibrillar collagens, type I is found throughout the body and is a substantial structural component in tissues such as skin, arteries,

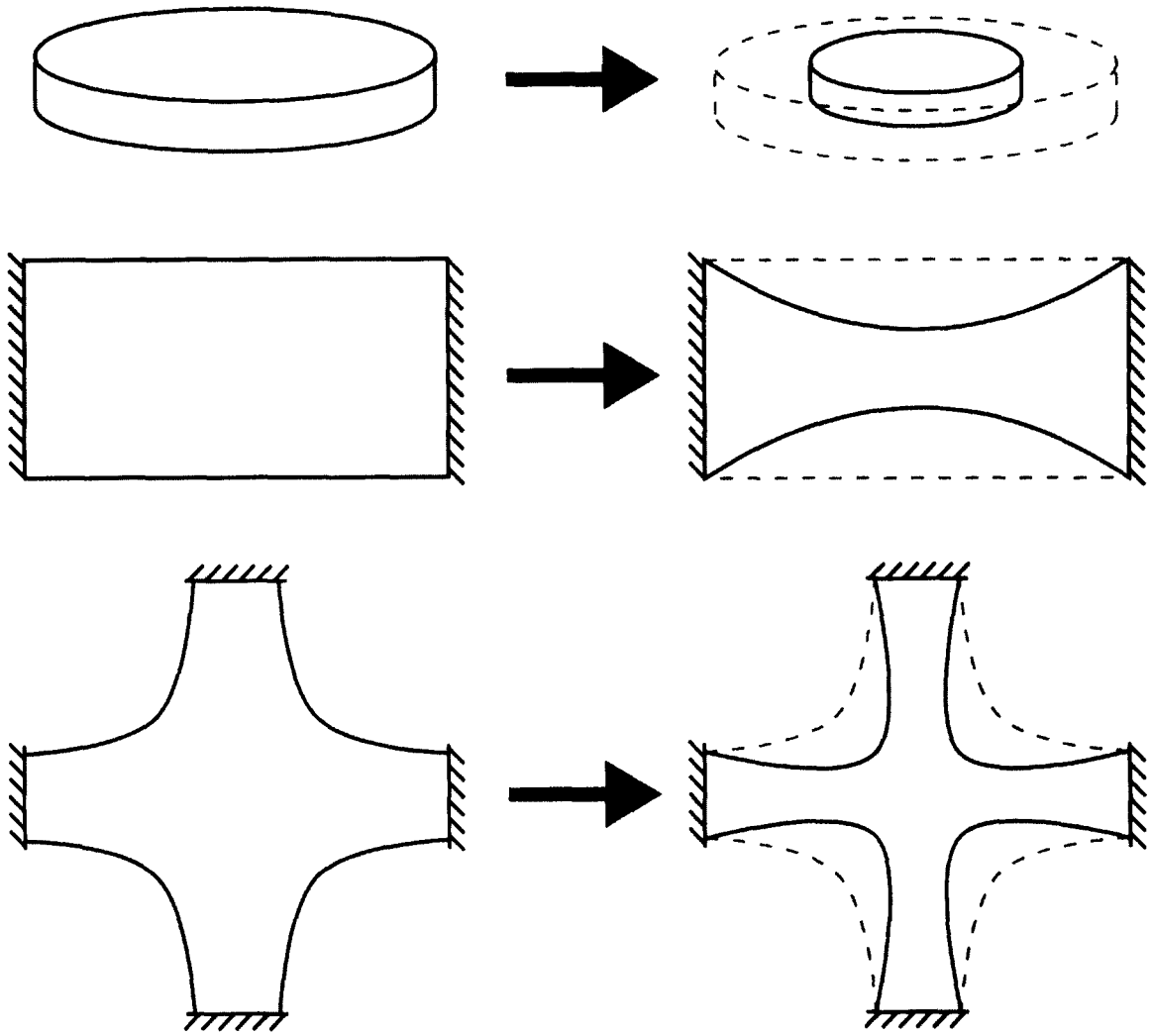

Figure 2.1: Tissue equivalent examples. Schematic drawings of cell-mediated matrix compaction for free-floating (top), uniaxially constrained (middle), and biaxially constrained (bottom) tissue equivalents. From an initial geometry (left), cells begin to spread and retract, resulting in matrix compaction that changes the overall geometry of the tissue equivalents (right).

tendons, and ligaments. Type II collagen is found primarily in cartilage, whereas type III collagen is often associated with type I, except during early wound healing when it precedes type I. During the formation of collagen fibers, lysyl oxidases convert some of the hydroxylysine and lysine residues into aldehydes, which allows the formation of covalent cross-links between fibrils and aids in the aggregation of collagen fibers [7]. Collagen is continually turned over by cells (i.e., degraded, removed, and replaced), which allows tissue to adapt to changes in both the mechanical and chemical environment [8].

Other common extracellular matrix components include elastic fibers, adhesion molecules, and proteoglycans (PGs), which consist of a protein core and associated glycosaminoglycans (GAGs). Elastic fibers consist primarily of elastin, but also associated glycoproteins such as the fibrillins and fibulins; elastic fibers endow tissues with resilience, recoil, and greater degrees of extensibility than does collagen alone. Elastin tends to be produced primarily during the perinatal period; hence, it has a minimal role in tissue adaptation and wound repair [9]. Amongst the many adhesion molecules, fibronectin is a glycoprotein that is important in the migration and localization of many cell types due to its repeated arginine-glycine-aspartic acid (RGD) domains, which serve as ligands for multiple cell-matrix adhesion receptors. Fibronectin can also bind a variety of growth factors that can contribute to cellular differentiation [9]. PGs and GAGs play diverse roles in tissue maintenance and adaptation. They are important in the assembly or organization of other matrix components, including collagen, through the creation of a swelling pressure due to abundant fixed negative charges. By sequestering water, they help resist compressive loads, which is particularly important in tissues such as cartilage.

PGs and GAGs can also sequester growth factors and thereby modulate cell behavior [10].

Cell-matrix interactions are important in mechanical sensing by cells and the regulation of cellular gene expression and protein synthesis, which together enable physical remodeling of the matrix. The primary receptors responsible for cell attachment to the ECM are the integrins. These heterodimeric structures consist of one α and one β subunit, each of which span the plasma membrane of cells. The extracellular domain binds to ECM molecules and the intracellular domain is anchored to the cytoskeleton. This association with the cytoskeleton allows the transduction of mechanical stimuli (outside–in signaling) as well as the transmission of actomyosin-based forces to the matrix (inside-out signaling), and can thus affect multiple signaling pathways [11]. The α and β subunit pairing determines the ligands with which the integrin will associate. For example, α_v based integrins associate with the RGD peptide found in fibronectin and vitronectin, while $\alpha_1\beta_1$ and $\alpha_2\beta_1$ associate with collagen through the GFOGER peptide sequence.

2.1.2 Fibroblasts

The cell type often associated with connective tissue development, maintenance, and remodeling is the fibroblast. They are found in many tissues of the body and can display different cellular behaviors depending on embryonic origin, surrounding matrix, and biochemical cues [12]. Fibroblasts can produce a wide range of extracellular matrix proteins, including collagens, fibronectin, and a wide array of PGs and GAGs [13]. Fibroblasts can also differentiate into the myofibroblast phenotype, which is often

indicated by the cellular expression of alpha smooth muscle actin, denoted αSMA [14]. This phenotypic change to a myofibroblast appears to require a tensile mechanical environment and cell exposure to transforming growth factor–beta (e.g., TGF-β1, one of three primary isoforms); it increases the magnitude of force the cell can apply to the surrounding matrix [5].

2.1.3 Growth Factors & Culture Media

The terms "cytokine" and "growth factor" are often used interchangeably. These biomolecules are soluble proteins or glycoproteins that are secreted by cells and act non-enzymatically to regulate cellular functions via both paracrine and autocrine stimulation [15]. Functions regulated by growth factors can be diverse, and a single growth factor can elicit opposite effects (e.g., proliferation or apoptosis) in the same cell type due to differences in other cellular cues like the matrix environment or the presence of other growth factors. Two growth factors of importance for fibroblasts and collagen maintenance are platelet-derived growth factor (PDGF) and TGF-β1. PDGF can act as a chemotactic agent, which is important for wound healing to induce fibroblasts and other cell types to infiltrate the wound site. Further, PDGF can induce proliferation, and it can stimulate the production of matrix components and matrix metalloproteinases (MMPs) that contribute to the degradation of many ECM proteins. Hence, PDGF can play an important role in tissue maintenance and remodeling [16]. TGF-β1 has diverse effects on cells that depend strongly on other environmental factors. It has been shown, for example, to stimulate both proliferation and apoptosis, to be required for cell phenotypic modulation, and to increase matrix deposition while downregulating MMPs. In terms of

cellular activity, TGF-β1 "seems capable of doing just about everything" [17]. Other cytokines of importance include the interleukins (e.g., IL-2 or IL-6). They are produced by leukocytes and often play important roles in vivo in tissue remodeling, wound healing, and disease progression.

Cell culture media for in vitro cell and tissue experiments is necessary to ensure the viability of resident cells as well as to serve as a source of molecules needed for matrix production and other cell-mediated processes. Some commonly used formulations include Ham's nutrient mixture F12, minimal essential medium, and Dulbecco's modified Eagle's medium (DMEM). Basic constituents of culture media include organic salts that maintain osmolality and act as pH buffers, essential amino acids needed for protein synthesis, vitamins for metabolic activities, and glucose for energy. To provide other factors needed for cell maintenance, serum is often added to culture media. Serum provides a broad spectrum of growth factors and other proteins including albumin. In lieu of serum, individual growth factors and proteins can be added to allow delineation of their individual effects in a given experiment [18].

2.1.4 Mechanics & Mechanobiology

It has been known at least since the time of Borelli (1608-1678) that mechanics plays important roles in biology. Nevertheless, it was not until the mid-1970s that it was shown experimentally that cells respond directly to changes in their mechanical environment, often via changes in gene expression. Indeed, more recently it was even shown that matrix stiffness can contribute to stem cell differentiation. Whereas continuum biomechanics focuses on mechanical responses of cells, tissues, and organs to

applied loads (under conditions of interest), mechanobiology focuses on biological responses of cells to mechanical stimuli. Mechanics and mechanobiology are thus allied fields – biological responses by cells can change tissue geometry, properties, and even loads, which in turn can alter the mechanical properties and hence mechanical responses by that tissue, which in turn can change the mechanical stimulus sensed by the cell. Mechanobiology often involves transduction (i.e., conversion of a mechanical stimulus to a chemical signal), transcription (i.e., an associated change in gene expression), and translation (i.e., the resulting production of a protein). Clearly, therefore, systems biology is also a natural ally of biomechanics and mechanobiology and there is a pressing need for multiscale models that address the multiple levels of response [19]. One of the key questions in mechanobiology is actually how the mechanical stimuli are transduced via corresponding signaling pathways [20]. Toward this end, there is a need for continued quantification of both the mechanical loads that act on cells and the subsequent biological responses, and to correlate how the former affects the latter. Results from studies on tissue equivalents promise to improve tissue engineering and regenerative medicine through proper mechanical and biological characterization [21].

2.2 Prior Experiments

2.2.1 Free-Floating Cell Populated Lattice

Although observing cells plated on different ECM proteins can lead to the collection of considerable information, adherent cells behave differently within three-dimensional (3D) matrices than when attached to two-dimensional (2D) surfaces [22–25]. Over thirty years ago, Bell et al. introduced the circular, free-floating, fibroblast-

populated collagen lattice (FPCL) [2]. Collagen gels containing embedded fibroblasts were suspended in culture media, and over a period of days, the cells compacted the lattices and thus reduced the gel diameter. The resulting tissue was noted as resembling skin and having a rubber-like consistency. The rate and extent of compaction could be varied depending on a number of factors, including cell concentration, collagen density, cell passage number, and the presence of inhibitors of cell contractility such as cytochalasin B. Many investigators point to this work as the beginning of tissue engineering, but it also provided a simple experimental framework for studying cell-matrix interactions in a 3D matrix.

The FPCL has been used predominantly as an in vitro model in wound healing research to examine cell-matrix interactions with an emphasis on understanding factors associated with wound contraction and closure. Detailed methods for the casting and culturing of FPCLs are described by Ehrlich [26]. Briefly, a solution containing known densities of collagen (usually type I) and fibroblasts is cast into a circular mold, often a bacteriological or tissue culture dish, allowed to undergo gelation, and then suspended in culture media. Over time (on the order of days to weeks), the embedded cells compact the collagen, which expels fluid from the matrix and reduces the overall volume of the lattice. The standard protocol described in [26] results in an initial density of collagen ~1.25 mg/mL and an initial concentration of fibroblasts of 50,000 cells/mL. The compaction of this standard configuration is characterized as occurring in two phases: an initial "lag" phase and a subsequent "log" phase (Figure 2.2) [27]. During the lag phase, there is little to no lattice compaction. This observation is likely due to the time required for the cells to begin adhering to and spreading within their surrounding matrix. After

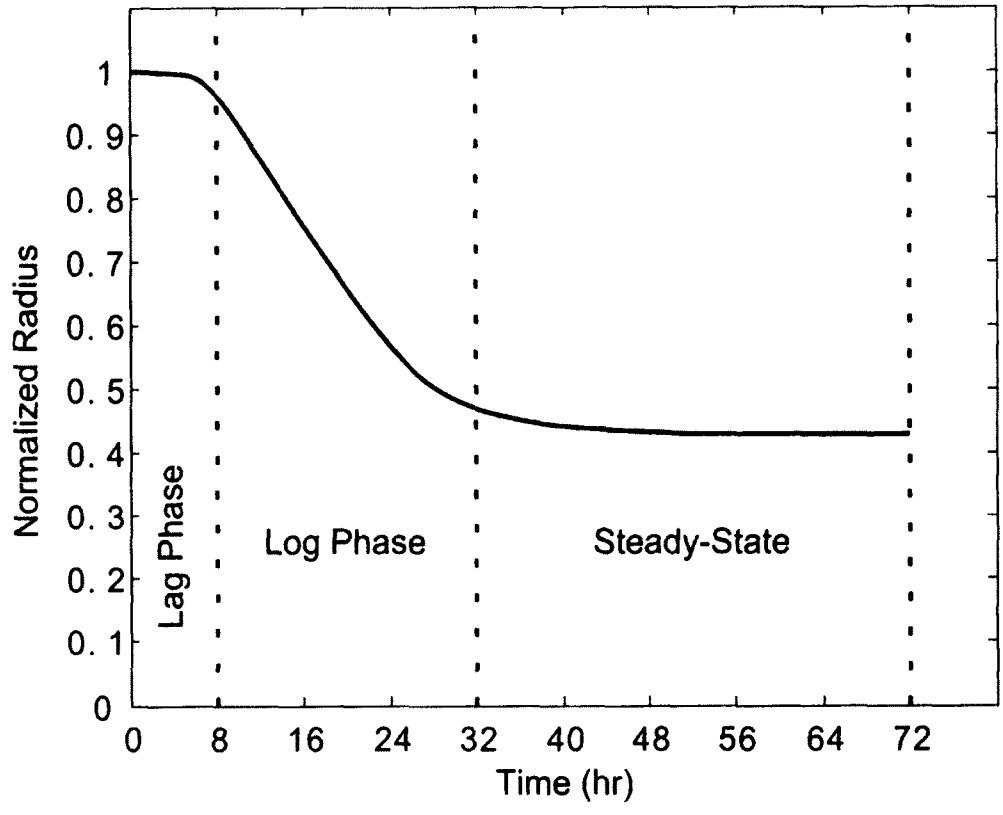

Figure 2.2: Free-floating FPCL compaction over time. General trend of radius reduction during cell-mediated compaction of a free-floating cell-populated lattice. During the "lag" phase, cells adhere to and begin to spread within the matrix. The "log" phase is characterized by a rapid reduction in the radius. Eventually, the lattice reaches a steady state when compaction ceases. The duration of each phase is dependent on many factors and can vary considerably depending on experimental protocol.

approximately 6 to 8 hours, lattices enter the log phase when the rate of compaction can increase greatly, then decrease gradually over multiple days until yielding an apparent steady-state where compaction becomes minimal or ceases altogether. The compaction in this phase is believed to arise from cellular contractions (cycling of protrusion and retraction) associated with locomotion plus associated matrix reorganization. The degree of compaction is usually reported as a percent decrease in the circular surface area or diameter, which in standard experiments is on the order of 50-70%. These studies can be modified to examine changes in the rate of compaction, cell morphology and phenotype, and lattice organization due to a number of factors, including different cell types and concentrations, matrix compositions and densities, and the presence of exogenous growth factors.

In the initial experiments performed in [2], differences in the rate and extent of compaction were noted when modifying either the collagen density or number of fibroblasts. Increasing the collagen density while using the same number of cells resulted in slower compaction with the final extent of compaction reduced. The cessation of compaction is considered by some as a state of "equilibrium" at which the size and organization of collagen fibrils or fibers prevents further compaction [26]. For lattices with higher collagen densities, cells are surrounded locally by more collagen and can achieve such an equilibrium without reducing the overall volume of the lattice to the same extent as a lower density matrix.

Conversely, if the collagen density is held fixed and fibroblast concentration is increased, both the rate and the extent of lattice compaction increase [2]. When the cell concentration is increased in the standard protocol by an order of magnitude (0.5×10^5 to

5.0×10^5), the lag phase is decreased by 4 to 6 hours, and the log phase is completed after 6 hours rather than the 24 hours needed for the lower densities [27]. This change in the compaction profile is thought to be caused by forces generated by recently passaged cells that are spreading and elongating. Though spreading-related forces are weak when compared with cellular forces linked with migration and especially contractility, increased cell densities can increase greatly the total force applied to the lattice during cell spreading [28]. Of course, these forces may only affect the matrix in the immediate vicinity of a spreading cell. Yet, at high cell concentrations, individual cells may reside within close proximity to each other such that many collectively applied forces are exerted on the same volume of matrix during initial spreading.

Different cell types produce different compaction rates and final degrees of overall compaction. Fibroblasts from different species as well as those from different tissue sources compact collagen at varying rates [29]. Increased passage number for a given cell line has also been shown to reduce the rates at which collagen is compacted [2,29]. For example, when comparing normal rat skin fibroblasts to a line of transformed rat sarcoma cells, it was found that normal cells compacted the matrix much more than did the transformed line [30]. By 7 days, however, the total extent of compaction was approximately equal for both cell lines and remained equal for the remaining period of culture (14 days). This pattern of compaction is likely due to differences in cell proliferation as the number of transformed cells at 7 days was almost 100 times greater than the normal cells. When comparing bovine vascular smooth muscle cells to human dermal fibroblasts, the latter compacted gels more quickly and to a greater extent [31]. This difference is possibly due to the fibroblasts having a more elongated morphology

compared with the smooth muscle cells, which would allow cellular locomotion and contractility to influence more surrounding matrix. Aortic adventitial fibroblasts and medial smooth muscle cells from the cynomolgus monkey were found to compact collagen lattices similarly over a 24-hour period [32]. Cells from different aged donors as well as those from pathological conditions can also exhibit differing degrees and rates of compaction [33]. Smooth muscle cells isolated from balloon-induced intimal thickening in rat aortas compacted collagen to a lesser degree than smooth muscle cells from the underlying media or from normal aortas. If cultured in plasma-derived serum instead of fetal bovine serum, compaction was decreased for all cell types; plasma-derived serum similarly resulted in less compaction by newborn (4 day old) rat smooth muscle cells compared to those from young (8-10 weeks) and old (16-18 months) adult rats.

Matrix composition similarly plays an important role in the rate and extent of the cell-driven compaction of lattices. Multiple fibroblast lines have been shown to compact lattices comprised of different collagen types at different rates and to varying degrees [34,35]. Dermal fibroblasts compact type III collagen more quickly and to a greater extent than type I while type II collagen is compacted more slowly and to a lesser degree than either type I or type III [34]. These cells had similar morphologies across all three collagen types, however. Yet, others have found the opposite to be true with MRC5 fibroblasts compacting type I collagen more than type III [35]. These differences could be attributed to a number of factors, including duration of pepsin digestion during collagen isolation, differences in initial collagen and cell densities, and potential differences between dermal and MRC5 fibroblasts [34–36].

Dermal fibroblasts also tend to compact collagen lattices to a greater extent than fibrin lattices whereas gingival fibroblasts compact collagen to the same degree as dermal fibroblasts while compacting fibrin more and completely degrading it after 7 days in culture [37]. The addition of ε-amino-caproic acid (an inhibitor of fibrinolysis) to gingival fibroblast-fibrin cultures resulted in compactions similar to the untreated dermal fibroblast-fibrin lattices. This finding suggests that gingival fibroblasts may have increased fibrinolytic capability compared to dermal fibroblasts.

The addition of GAGs and PGs to collagen lattices can affect the compaction of the lattices. The addition of hyaluronan to collagen lattices has been shown to increase the degree to which smooth muscle cells can compact the matrix compared with collagen alone [32]. When CD44 binding of hyaluronan is blocked, compaction is comparable to collagen alone, which indicates that the cells may be able to use hyaluronan as an indirect linker to collagen to expedite matrix compaction. In contrast, the addition of decorin can reduce lattice compaction by hypertrophic scar fibroblasts, likely through the sequestration of TGF-β1, which is highly expressed by these cells [38].

The ability of cells to cross-link collagen is also important in the compaction of collagen lattices. Collagen is enzymatically cross-linked primarily through the action of lysyl oxidase, but can also be cross-linked by transglutaminases [39]. Pre-treatment of dermal fibroblasts with a lysyl oxidase inhibitor, β-aminopropionitrile (BAPN), delayed the onset of compaction and subsequent exposure during culture reduced the final degree of compaction [40]. If BAPN is only added during lattice compaction, lung fibroblasts maintain normal levels of compaction early in culture (~2 days) but exhibit reduced compaction at later times compared with untreated lattices [41]. Early compaction of the

lattices may proceed normally assuming that BAPN does not inhibit cell spreading or attachment to surrounding collagen. That is, the cells may continue to actively pull in collagen and compact the matrix. With the inhibition of lysyl oxidase, however, prior data suggest the cells are unable to covalently cross-link the collagen following the initial compaction and thereby they cannot entrench any of applied deformations within the matrix. In the normal culture environment, cells could cross-link their surrounding collagen to entrench the local compaction, then detach and adhere to other collagen to continue the process of compaction and cross-linking. Cross-linking may thus allow resident cells to develop a "residual matrix tension" in an attempt to stiffen their local matrix environment to achieve a preferred mechanical environment; this process or mechanism has been referred to as "tensional homeostasis", which appears to be an in vitro example of a general process of mechanical homeostasis that promotes tissue formation, maintenance, remodeling, and adaptation [42–44].

Compaction of collagen lattices by fibroblasts also depends on specific integrin-matrix interactions [3]. Multiple reports have shown that fibroblast compaction of lattices formed from reconstituted type I collagen is achieved primarily through cell-matrix interactions via the $\alpha_2\beta_1$ integrin [45–47]. Altered matrix composition can allow compaction even in the presence of $\alpha_2\beta_1$ directed antibodies through cell attachment to other matrix components that are entangled with the collagen [32]. Moreover, cells that are deficient of the $\alpha_2\beta_1$ integrin are still capable of compacting collagen lattices via the $\alpha_v\beta_3$ integrin [48,49]. This difference in adhesion can also lead to changes in mechanobiological and biochemical responses as, for example, PDGF increases compaction in $\alpha_2\beta_1$-mediated gels but not in those mediated via $\alpha_v\beta_3$ [48].

The culture environment of collagen lattices can greatly affect their compaction. It has been shown that serum is required for compaction of FPCLs, likely due to the presence of myriad growth factors [30,50]. Lattices cultured in the absence of serum can also compact if the culture media is supplemented with growth factors such as TGF-β1 and PDGF [51–54]. Compaction of lattices exposed to PDGF suggests that part of the process may be mediated through cell migratory processes [53,55]. Exposure to TGF-β1 leads to lattice compaction, but the stimulated cellular mechanism may be augmented when cells express the αPDGF receptor [51,54]. This suggests that TGF-β1 may induce PDGF release and subsequently increase compaction [54,56]. TGF-β1 has also been shown to increase the expression of integrins, which would allow cells to adhere to more collagen and to transmit more force to the matrix [57,58]. TGF-β1 is also necessary for fibroblasts to differentiate into the more contractile myofibroblasts, thus increasing the contractile force they can apply to their surrounding matrix in the free-floating collagen lattice, possibly through increased actin expression [5,59].

Gene and protein expression have been examined in free-floating lattices and are usually compared to levels expressed by cells in lattices that are allowed to adhere to the surface of the culture dish. It has been assumed by many that adhered matrices develop a tensile mechanical environment while free-floating gels remain mechanically relaxed though the mechanical environment has not been explicitly measured or derived [5]. Cells in floating lattices have a reduced response to PDGF compared to adhered gels as measured by level of receptor autophosphorylation [60]. Type I collagen expression is also decreased in floating constructs compared to monolayer cell cultures while MMP-1 levels are increased [46]. Blocking $\alpha_1\beta_1$ and $\alpha_2\beta_1$ integrins further down-regulates type I

collagen expression and up-regulates MMP-1 in floating gels [46]. Expression of MMPs by ocular fibroblasts has similarly been shown to change throughout culture time [61]. MMP-1 expression is elevated at 9 hours and increases to day 1 before dropping off by day 7. MMP-2 and MMP-3 showed similar trends; however, total expression of both at 9 hours is markedly lower compared to MMP-1, with MMP-2 levels being significantly higher than MMP-1 and -3 at day 7. Total protein measures for MMP-2 were also much greater than levels of MMP-1 and -3. The varying levels of MMP activity throughout lattice compaction could possibly arise from a continually evolving mechanical environment. In examining cellular contractile components, anchored and floating lattices show similar levels of β-actin expression but anchored gels show higher levels of α-SMA. In both configurations, TGF-β1 increases the ratio of α-SMA to β-actin [52].

Measures of gene and protein expression show that there are global differences between adhered and floating lattice cultures, but such measurements do not account for the potential of local variations within the matrix. Free-floating lattice compaction has been shown to lead to regional variations in cell and matrix alignment as well as cell phenotype [27,62]. After 24 hours in culture, two distinct fibroblast phenotypes and states of matrix organization can arise. The center of the lattice is populated by randomly oriented fibroblasts with densely compacted, randomly oriented collagen whereas the periphery of the gel contains fibroblasts that have differentiated into myofibroblasts with both cells and collagen aligned parallel to the outer edge of the lattice. Similar results were shown by Costa et al. [63] in various constrained geometries – cell compaction of collagen lattices leads to fiber alignment parallel to any free or unconstrained edge (Figure 2.3). Although there are no externally applied loads or constraints on the system,

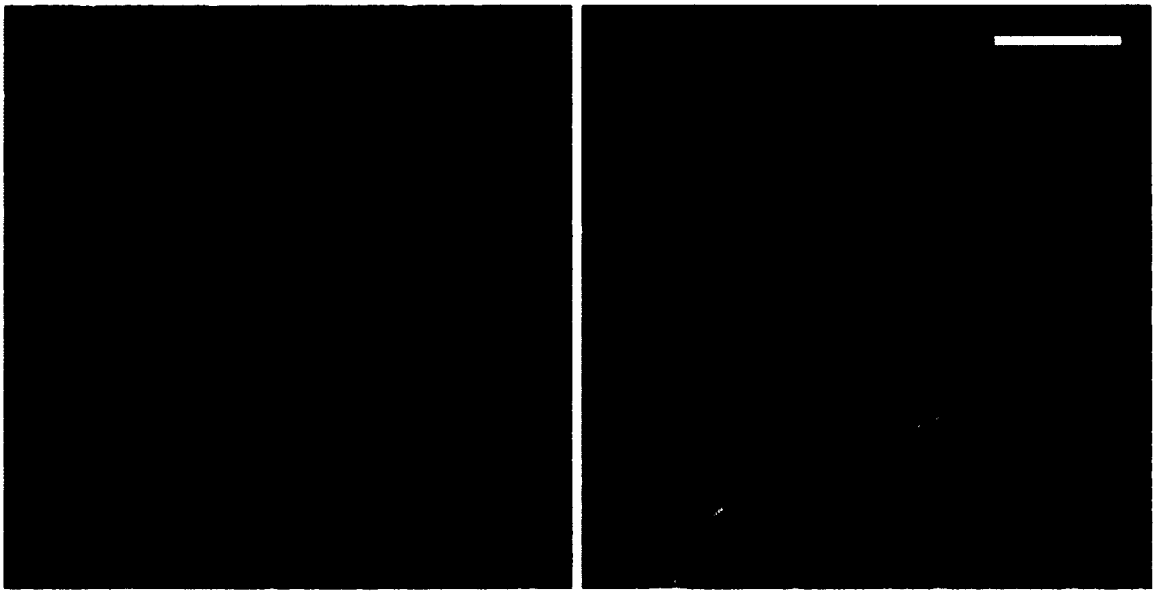

Figure 2.3: Example of free-floating FPCL collagen orientation. Picrosirius red stained free-floating fibroblast populated collagen lattice under circularly polarized light to show birefringent collagen. Central region (left) shows dense, randomly oriented collagen fibers while the outer edge of the lattice (right) shows aligned fibers for a lattice that has reached steady state (See Figure 2.2). Scale bar is 50 μm.

the peripheral alignment is potentially due to the development of different local mechanical environments that could lead to differences in local gene and protein expression.

2.2.2 Uniaxial Collagen Gels

Externally applied mechanical loads can greatly alter cellular activity, and tissue equivalents represent controllable systems suitable for examining the mechanobiological responses of cells to such applied loads. Uniaxially constrained collagen gels are simple systems wherein the axial, or in-line, force can be measured and the axial strain can be controlled accurately and precisely. One of the first experiments carried out on uniaxial tissue equivalents sought to characterize cellular forces associated with locomotion [64]. A collagen solution containing either normal or diseased skin fibroblasts from human or calf explants was cast in a rectangular mold and allowed to polymerize around Velcro constraints; one end was connected to a strain gauge to infer the force generation and the other to a mobile vernier to adjust the length of the gel. It was reported that tension developed within 30 to 60 minutes of polymerization and increased rapidly over 6 to 12 hours with increases in tension slowing or ceasing by 24 to 48 hours. During the period of observation, the geometry of the gel changed due to cellular compaction, including development of a parabolic shape (maximal gel width at the end restraints, minimal width at mid axial location) and reduction in thickness. After tension reached a steady state, the gels were lengthened or shortened to cause a step increase or decrease of 2 grams of load. The cells restored the in-line force to the previous steady level in both cases within 1 hour.

This investigational setup has been modified, characterized, and used by multiple groups [43,65,66]. It can be used to perform experiments similar to those for the free-floating lattice to examine the effect of different initial or continual culture conditions on the mechanobiological responses to uniaxial constraints. Easy to implement variations include different cell types, cell concentrations, matrix type, matrix composition and density, static or cyclic loading conditions, and the effects of different growth factors and pharmacological agents. For example, Delvoye et al. noted that calf skin fibroblasts generated larger forces compared to human skin fibroblasts [64]. They also observed that calf dermatosparatctic skin fibroblasts were less effective at generating tension within the uniaxial lattice when compared with normal fibroblasts, which likely results from reduced cell-matrix interactions observed previously in animals [67].

A similar experimental setup has been employed to measure forces generated by endothelial cells [65]. Instead of casting the cells within the collagen, an acellular collagen solution was cast, and following gelation, endothelial cells were seeded on the apical surface to form a monolayer. Whereas fibroblasts were found to reach a steady state force within 2 days, endothelial cells required 4 to 5 days in culture and only reached force levels an order of magnitude lower than the fibroblasts. This finding could have been due to the different casting methods, though no corresponding experiments were performed with fibroblast monolayers. Uniaxial equivalents also allow direct comparisons between cell types. For example, they have been employed to compare and characterize differences between human dermal and Tenon's capsule (ocular) fibroblasts [68]. The ocular fibroblasts showed a gradual increase in force generation that achieved only one-third of the force generated by dermal fibroblasts after 24 hours.

Tissue origin can also play a role in cellular responses as smooth muscle cells from different layers of piglet pulmonary arteries developed tensile forces in uniaxial tissue equivalents at different rates and to different extents in 24 hours [69]. Cells from the outer medial layers generated force more quickly than those from inner layers and they also generated more force. Cells sourced from hypoxic animals generated smaller forces overall, with cells from the inner media producing more tension than those from the outer layers.

Free-floating lattices have increased rates of compaction when cell concentrations are increased; the same holds for uniaxial tissue equivalents. Along the same line, increased collagen density increases the rate of force generation in tethered gels while reducing the rate and extent of compaction in free-floating constructs [64]. Increasing collagen density would increase initial substrate stiffness and apparently require less cellular compaction to achieve homeostatic or preferred forces [43]. The role of initial cell and matrix densities is likely important when trying to engineer potential regenerative therapies as well [70]. Too high of a cell seeding can lead to overly compacted and damaged constructs.

Uniaxial tissue equivalents also allow measurement of contractility by cells [65]. Similar to [64], force generation began within three hours of casting fibroblast populated uniaxial tissue equivalents, increased rapidly over 24 hours, and reached a steady level in 48 to 72 hours that was maintained in cultures taken out to 7 days. To assess contractility, constructs were exposed to thrombin after reaching steady state, which induced an increase in force within 5 to 10 minutes that was sustained for several days. Once

exposed to cytochalasin D to disrupt actin filaments, all tension in the system was lost within 10 minutes.

Whereas it was expected that disruption of actin would diminish tension development, it appears that microtubules can also influence cellular forces applied to matrices [65,71]. Disrupting microtubules within fibroblasts leads to an initial increase in force in uniaxial constructs that is gradually returned to prior steady state levels. Microtubules help maintain cell shape and buffer the tension of actin filaments by acting as compressive supports. When disrupted, the tension in the actin cytoskeleton can no longer compress the microtubules, hence leading to a net increase in the tensile force on the tissue equivalent. Over time, the cells seem to want to maintain a homeostatic level of tension and potentially relax intracellular tension to restore preferred levels [43,71].

As stated previously, cells appear to establish and then maintain a preferred level of tension, which is referred to as tensional homeostasis [43]. By cycling the length of uniaxial tissue equivalents, it became clear that the cells sought to restore a preferred force level. Upon reaching steady state, constructs were then shortened abruptly, which resulted in a sharp decrease in force. Almost immediately thereafter, however, the force began to increase quickly before plateauing at a steady state value. Lattices were also cycled between lengthening and shortening. The cycling regimen started with an applied 0.6 mN increase above endogenous force, then followed a pattern of a 15 minute rest, a 1.2 mN unloading over 15 minutes, 15 minute rest, and a 1.2 mN loading over 15 minutes. This protocol kept the cycled force measurements centered about the endogenous force. Other variations of this cycling regimen have been used to cycle from the endogenous tension level to either 1.2 mN above or below it. When constructs were

lengthened, force increased throughout loading and then immediately started to decrease during the resting cycle; when they were shortened, forces decreased and then gradually started to increase once at rest. These results again suggest that cells attempt to maintain a certain mechanical environment and they respond quickly to perturbations to actively restore a preferred state.

The idea of tensional homeostasis is supported further by the work of Marenzana et al [42]. After adding cytochalasin D to release fibroblast induced forces at various time points in culture, it was found that not all tension is released from the matrix and the amount of this residual matrix tension seems to increase linearly between 4 and 60 hours in culture. During this time, the total axial force in the uniaxial tissue equivalents reaches a steady level in 24 hours. It appears that the cells actively deform the matrix in an attempt restore tensional homeostasis. To aid in this process, they will also remodel their resident matrix to build in tension (the aforementioned residual matrix tension) and potentially reduce the amount of active force they need to apply to maintain the preferred mechanical environment.

Growth factors and cytokines can also alter cell contractility and matrix compaction in uniaxial constructs. In particular, TGF-β1 has been investigated extensively [42,72,73]. TGF-β1 tends to increase the rate and extent of force generation, although it has been shown that high concentrations of this cytokine could potentially inhibit increases in force [72]. Exposure to TGF-β1 also appears to speed the development of the residual matrix tension and to increase fibroblast contractile forces greatly, possibly by inducing the myofibroblast phenotype [42]. TGF-β1 also alters cell responses to lengthening of the tissue equivalent as treated fibroblasts initially increase

then reduce the tension relative to controls, which begin reducing matrix tension almost immediately following the perturbation [73].

The uniaxial mechanical environment can also lead to the up- or down-regulation of multiple genes and proteins. If constructs are pre-strained to increase matrix stiffness before the onset of force generation, the expression of multiple genes can be altered [74]. Pre-strain significantly increases the expression of MMP-2 and tissue inhibitor of metalloproteinase-2 (TIMP-2) in human dermal fibroblasts while collagen type III expression is increased only at a high pre-strain (10%), though not significantly due to a broad range of expression in control expression. Cyclic loading (1 cycle per hour) of dermal fibroblast-populated constructs also leads to changes in protease expression [75,76]. MMP-2, MMP-9, and tissue plasminogen activator (tPA) levels are increased by cyclic loading while MMP-3 and urokinase-type plasminogen activator (uPA) levels are reduced. These levels can also be altered by construct geometry [76]. The up-regulation of both MMPs and TIMPs due to increased mechanical loads suggests that the resident cells attempt to remodel the constructs to reduce the amount of tension in the system and restore tensional homeostasis.

2.2.3 Biaxial Collagen Gels

While an extensive number of studies have been carried out employing free-floating and uniaxially constrained collagen lattices, biaxial tissue equivalent-based investigations have been relatively few in number. Most of this work has focused on the design and characterization of biaxial systems, measurement of cell and mechanically

induced tissue anisotropy, and mechanical characterization of equivalents following prescribed culture periods [77–79].

Similar to uniaxial tissue equivalents, a collagen solution containing cells is cast in a mold containing restraints, usually a porous plastic, to facilitate mechanical manipulation of the constructs. Two mold shapes are usually employed, either a square with restraints on each side or a cruciform-shape with restraints at the end of each arm [77,78]. Upon gelation, the specimens can be mechanically loaded in culture either through the attachment of weights to the restraining bars to prescribe an isotonic load or by holding the specimen dimensions static and allowing the resident cells to compact the matrix isometrically and thereby develop endogenous loads [77,78]. Biaxial systems also allow multiple loading protocols, including equibiaxial stretching or loading (i.e., same stretch or force along each axis), non-equibiaxial stretching or loading (often proportionally), or strip biaxial stretching (one axis held fixed at original length while other axis is loaded).

Measuring biaxial strains in the central region (or arms of the cruciform specimens) can be achieved by tracking the positions of embedded markers within the gel, often microspheres [77]. The tracking of marker positions during both cell-mediated compaction and mechanical testing allows calculation of the deformation gradient tensor, **F**, in 2D and calculation of associated strain measures. Other groups have also used histological stains or ink on the specimen surface to track strains [79]. It has been shown that strain is often inhomogeneous across biaxial specimens during cell compactions, though they may be nearly homogeneous within the central region of the specimens [77].

Boundary conditions in culture can be used to change the organization of collagen fibers. In comparing the structure and mechanical behavior of biaxially and uniaxially constrained gels, it has been shown uniaxial constraints result in a marked increase in tissue anisotropy following three days of cell-driven remodeling [80]. In biaxial gels, collagen fiber orientations remain randomly oriented in the central region during equibiaxial stretching or mechanical testing, indicative of an isotropic response. In contrast, uniaxial gels develop a preferred collagen alignment parallel to the constrained axis, which thus exhibits a markedly stiffer response in mechanical testing compared to the unconstrained axis.

The degree of tissue anisotropy may also be altered by imposing unequal initial stretches to constructs [78]. Applying two different magnitudes of stretch to each axis will increase collagen alignment toward the direction of larger initial stretch. With a cruciform-shaped sample, it is noted that the mechanical environment of the arms is uniaxial and thus results in distinct alignment parallel to the corresponding axis regardless of the "biaxial" loading protocol. Moreover, if the arms of one axis of a cruciform sample are wider than the other axis, the fibers tend to align in the center of the tissue equivalent toward the axis of the wider arms [79]. As the ratio of widths of the arms is increased, the degree of alignment also increases. This finding is most likely due to a greater force generated by the larger number of cells in the wider arms of the gel compared to the narrower arms.

The application of external loads also leads to some initial alignment of collagen fibers [78,81]. As stated before, uniaxial constraining leads to alignment along the constrained axis during cell-mediated compaction. If that axis is then unloaded and the

gel constrained or loaded perpendicular to the original constraint, the collagen lattice can become isotropically distributed [81]. If cultured out further, the cells will begin to reorganize the matrix and align collagen predominately with the new constrained axis. Polarized light microscopy has also been employed to monitor fiber alignment even during biaxial mechanical testing [82–84]. Displacement along one axis shows a shift in collagen fiber alignment towards the direction of the applied motion [82].

Fibroblast-populated fibrin tissue equivalents have also been used to examine the role of fiber alignment in a biaxial constrained environment [85]. After 10 weeks in culture, fibrin-based tissue equivalents showed marked changes in tissue composition. Collagen accounted for approximately 3-4% of the total dry weight of cruciforms at 10 weeks, with low levels of elastin present (~0.10-0.15 % dry weight). Regional differences were also found with the most pronounced being a higher percentage of collagen content in the narrow arms of cruciforms with geometrically induced fiber alignment.

2.3 Prior Mechanical Analyses

Given that embedded cells are highly responsive to their mechanical environment and changes therein, there is clear motivation to quantify the states of stress and strain imposed upon a tissue equivalent during culture as well as to quantify changes that result due to the action of the cells on the matrix. It is surprising; therefore, that appropriate mechanical quantification remains wanting in many regards. Indeed, not only has there been little attention to the macroscopic stress or strain fields, there has been less attention to the cell-matrix interactions.

2.3.1 Free-Floating Lattices

The first mechanical model of the free-floating collagen lattice sought to quantify the "traction force" associated with the cell [86]. A spherical geometry was employed as spherical symmetry simplifies both the problem formulation and solution. The ECM was modeled as a linear viscoelastic material described by the following stress-strain-strain rate relation:

$$\boldsymbol{\sigma}_{ECM} = \mu_1 \frac{\partial \boldsymbol{\epsilon}}{\partial t} + \mu_2 \frac{\partial \theta}{\partial t}\mathbf{I} + \frac{E}{1+\nu}\left[\boldsymbol{\epsilon} + \frac{\nu}{1-2\nu}\theta\mathbf{I}\right] \tag{2.1}$$

with material parameters μ_1 and μ_2 related to the shear, μ, and bulk, K, viscosities ($\mu_1 = 2\mu, \mu_2 = K - 2/3\mu$), E is the Young's modulus, ν is the Poisson's ratio, $\mathbf{I}$ is the identity tensor, $\boldsymbol{\epsilon}$ is the infinitesimal strain tensor, and θ is the dilatation. The active stress (stress applied by the cells on the ECM) was modeled as a "negative pressure" having the form

$$\boldsymbol{\sigma}_{Cell/ECM} = \tau_0 \frac{\rho n}{1+\lambda n^2}\mathbf{I} \tag{2.2}$$

where τ_0 is a traction parameter (units of force per matrix density, ρ, and cell density, n) and λ is a contact inhibition parameter. A constant value was applied for the cell traction parameter and the boundary value problem was solved for the displacement field by imposing a traction-free (zero stress) boundary condition at the outer surface. The model showed that increasing the value of the traction parameter resulted in an increased rate of compaction or diameter reduction. Similar to experimental data, increasing the initial cell

density also resulted in faster compaction. This model has been modified using a different material model and a time varying traction parameter to incorporate the lag in the onset of compaction in one variation as well as the incorporation of a cell-cell interaction force [87,88].

This viscoelastic model shows that the application of an active cellular stress can lead to overall compaction with corresponding changes in matrix and cell densities [86]. One drawback, however, is the assumption of linear material behavior and infinitesimal strains despite the actual gels experiencing large deformations (10% reduction in diameter). Moreover, the model was not implemented to explicitly solve for the stress within the gel, which could modulate cellular responses and lead to changes in the cell traction parameter. Finally, use of a viscoelastic model may be most appropriate to collagen gels that are subjected to step increases in force or displacement whereas the time scale of cell-induced traction and contractility may be long enough that any viscous effects are negligible.

A second model of the free-floating collagen lattice employed finite element analysis [89]. The collagen matrix was modeled as a 3D isotropic solid disc with a Young's modulus, E, between 25 and 50 kPa and a Poisson's ration, ν, of 0.33 to allow compressibility. Cell traction was then simulated as a change in temperature, noting that most solids contract in response to a decrease in temperature. The simulation for a free floating or unconstrained gel resulted in an inward contraction of the solid with negligible stress development. Although the model simulates a compaction of an unconstrained solid material, as noted by the authors, the use of thermal contraction has no physical

meaning. That is, it models cell traction as an imposed internal strain or displacement, not as an internal or active force that leads to deformation of the solid.

As stated previously, some have observed that the organization of the free-floating lattice varies regionally, namely, the cells and collagen fibers in the center remain randomly oriented while at the periphery of the construct they become highly aligned, parallel to the outer edge [27,62]. It appears, therefore, that the FPCL could be modeled as a cylindrical annulus exhibiting a nonlinear compressible material behavior, with axisymmetric properties that can vary with radial position [90]. Whereas an initial solution focused on the initiation of the compaction, assuming incompressibility, a subsequent development of the model assumed an extended Blatz-Ko constitutive behavior to allow compressibility, resulting in the following general form for the Cauchy stress – stretch response:

$$\mathbf{t} = \varphi_{iso}(r)\left(\frac{\mu}{III_C^{1/2}}\left(III_C^{1/2}\mathbf{I} - \mathbf{B}^{-1}\right) + t_a\mathbf{I}\right)$$
$$+\varphi_{ani}(r)\left(\frac{c}{III_C^{1/2}}\left(IV_C^2 - IV_C\right) + t_c\right)\boldsymbol{e}_\vartheta \otimes \boldsymbol{e}_\vartheta \qquad (2.3)$$

where μ and c are material parameters for the isotropic and anisotropic materials, respectively, and φ_{iso} and φ_{ani} are mass fractions for the respective materials. III_C and IV_C are invariants of the right Cauchy-Green tensor, $\mathbf{C} = \mathbf{F}^T\mathbf{F}$, with $III_C = \det\mathbf{C}$ and $IV_C = \mathbf{M}\cdot\mathbf{C}\boldsymbol{M}$ where $\mathbf{M}$ is a unit vector defining the preferred direction for the anisotropic material. $\mathbf{B}$ is the left Cauchy-Green tensor, $\mathbf{B} = \mathbf{F}\mathbf{F}^T$. At any point along the radius, r, $\varphi_{iso} + \varphi_{ani} = 1$, with $\varphi_{iso} = 1$ at the center and $\varphi_{ani} = 1$ at the outer edge.

The terms t_a and t_c are the actively applied stresses by the cells, which were determined from the solution, not prescribed a priori [91].

In satisfying equilibrium given the traction-free boundary conditions at the outer edge and the apical and basal surfaces, nontrivial deformations were admitted only in the presence of a residual-type stress field. The radial stress was compressive in the center of the gel and transitioned to a zero at the outer edge, satisfying the outer boundary condition. The circumferential stress was also compressive in the center, but tensile near the outer edge. The possible existence of this type of residual stress field was examined qualitatively through the experiments on compacted gels. A radial cut from the center of the gel to the outer edge resulted in a pronounced opening angle that is consistent with the release of residual stresses. Further, creating a circular hole near the center of a compacted gel resulted in a narrowing of the hole, which is consistent with the presence of local compressive stresses and lengthening of compressed collagen fibers [91].

Although this analysis did not explicitly determine the stress state of a particular free-floating lattice, it provided a general characterization of the mechanical environment based on experimental observations of cell and matrix alignment. Although the assumption of global isotropy within the gel also mathematically admits a compaction that results in a zero stress field, such a solution requires the thickness of the matrix to decrease by the same degree as the radius, which is not realized experimentally [91]. Hence, it appears that the residual stress type field is most likely. The initial mechanical model [90] will be discussed in Chapter 3. The compressible mechanical model [91] will be examined in depth in Chapter 4.

The free-floating lattice construct can continue to serve as a great tool for understanding mechanobiological responses of cells, but the evolving mechanical environment still needs to be characterized precisely. That is, current mechanical models need to be extended to capture the evolution of the gel from a dilute isotropic construct to a dense, non-homogeneous tissue-like structure, with improved estimates of applied cell tractions throughout. Prior generalized inferences on gene and protein expression may be confounded by a non-zero, radially varying stress field rather than the prior assumed relaxed or stress-free environment.

2.3.2 Uniaxial and Biaxial Lattices

The mechanical characterization of uniaxially and biaxially constrained collagen lattices follows more traditional methods of analysis as the nature of their construction provides a simple shift from culture to mechanical testing. One major detriment of the uniaxial setup, however, is these tissue equivalents are often only characterized uniaxially, which only provides information on material behavior in one dimension. Finally, careful consideration needs to be given with regard to a number of factors, such as how the sample is gripped, which can alter measured responses from the tissue [92,93].

Mechanical analysis is either carried out on a region of interest within the tissue construct or on the entire sample. Focusing analysis on the central region usually invokes Saint-Venant's principle; namely, the assumption that any inhomogeneity in force or displacement caused by loading at the boundaries of a sample is negligible at a sufficient distance from the sample edge, hence distributions of stresses and strains can be assumed

to be homogeneous away from the edges. Assessment of whole constructs is more complicated as constrained tissue equivalents develop complex geometries and the local distribution of cells and matrix can lead to complex material properties. Clearly, finite element methods become essential in such studies [94].

The primary focus of mechanical modeling of uniaxially and biaxially constrained tissue equivalents has been on the relation of matrix orientation to the mechanical state of the tissue. Some investigators have incorporated imaging systems into mechanical testing rigs to monitor matrix alignment throughout testing. Imaging modalities include confocal and polarized light microscopy [95–97]. Both approaches have advantages and disadvantages. Confocal systems can provide detailed images of individual matrix fibers and cells as well as their volumetric distributions, but the long acquisition times may allow stress relaxation to occur. Polarized light microscopy allows a quicker acquisition of images and a larger field of view, but it does not provide volumetric assessment of alignment; it assesses alignment as perturbations to polarized light as it passes through a sample. Confocal microscopy may be more readily implemented in studies focusing on only the central region of constructs while the nature of polarized light microscopy makes it better suited for studies assessing the mechanics of entire tissue equivalents.

Mechanical models of constrained tissue equivalents typically employ either structural analog models or continuum models. Structural network-based models attempt to capture effects of individual matrix fibers [98]. Noting that collagen exhibits a nonlinear stress-strain behavior due to fiber crimp, an "effective" fiber stress-strain relation of the following form is often used:

$$S_f = A[\exp(BE_f) - 1]. \tag{2.4}$$

Here, S_f is the second Piola-Kirchhoff stress of a fiber, E_f is the Green's strain of a fiber, and A and B are material parameters with A having units of stress. The next step is to prescribe an initial orientation to individual fibers, which is usually accomplished via a distribution function that describes fiber distributions acquired via imaging.

Fiber-based models have also been implemented in analytical continuum formulations, when focusing on the central region of a tissue equivalent or through the use of representative volume elements (RVEs) in finite element models [82,83,94,99]. In a continuum, the total stress is equal to the sum of the stresses in all the modeled collagen fibers for a given deformation. Such models do not account for interactions between individual fibers, however [99]. In some finite element based approaches, RVEs are constructed to prescribe the microscopic fiber network at Gauss points of each element of the model. For more information on the implementation of this model, see [94]. This method allows modeling of entire tissue constructs having complex geometries and seeks to describe the macroscopic mechanical behavior via representative microscale fiber networks. A current drawback of these models is they only account for the fibrous collagen network. During compaction and remodeling of collagen lattices, other matrix components may be deposited and influence mechanical responses of the tissue.

Another method of modeling the mechanics of tissue equivalents is via traditional continuum approaches. This methodology typically involves specifying a strain energy function to describe the constitutive response. One model that could potentially apply to tissue engineered constructs is an n-fiber family model that has been employed to

characterize arterial mechanics; such models are meant to capture overall responses, not to describe fiber-level mechanics per se [100]. The strain energy takes the following form:

$$W = \frac{c_1}{2}(I_C - 3) + \sum_{\alpha}^{n} \frac{c_2^{\alpha}}{4c_3^{\alpha}} \left[\exp\left(c_3^{\alpha}\left(\lambda^{\alpha 2} - 1\right)^2\right) - 1\right] \quad 2.5$$

Where c_1, c_2, and c_3 are material parameters with c_1 and c_2 having units of Pa, α is the index of each fiber family, n is the total number of fiber families, λ^{α} is the stretch experienced by the α fiber family, and I_C is the first invariant of $\mathbf{C}$, $I_C = \mathrm{tr}\mathbf{C}$. For the case of a constrained biaxial tissue equivalent, $n = 2$ fiber families could describe a matrix aligned with each of the principal axes. Again, however, there is a need in tissue equivalents to model the cell-mediated tractions.

2.4 Growth and Remodeling (G&R) Models

A major need in the study of tissue equivalents is models capable of predicting the evolving nature of the constructs in terms of myriad factors, including externally applied loads (boundary conditions), internally applied loads (cell traction forces and contractility), cell mediated matrix production and removal, and the effects of soluble factors on cellular activity. Toward this end, however, there is also a need for better experimental data. For example, the free-floating construct is mechanically simple and thus mathematically tractable, yet there is currently no way to estimate the regionally varying force development within the matrix without applying a physical constraint to the system. Measuring the compaction of the lattice would provide some indirect information

regarding cell-generated forces, yet the evolving residual matrix tension would complicate such inferences beyond the early stages of compaction.

There has been some initial work on modeling the G&R of uniaxially and biaxially constrained tissue equivalents, for which more data are available, including information on net forces generated during compaction. For example, matrix remodeling has been described using the theory of kinematic growth, which assumes that the total deformation gradient **F** can be decomposed in to an elastic part (in response to externally applied loads) and a growth part (due to biological activity), which is assumed to occur in stress-free configurations [101]. Kroon adopted such an approach, with the contribution of the cells representing a rotation to realign matrix based on a mechanical cue (e.g., stress, strain, or stiffness) [102,103]. This approach indirectly accounts for cellular activity and models changes in the matrix as deformation instead of direct changes in the material constitution.

Other attempts to account for the evolution of tissue equivalents have sought to model changes in cell and matrix alignment as time varying entities without directly accounting for the mechanical cues that may drive or augment the remodeling process [81]. Such an approach is simple to implement as it only requires the assessment of cell and matrix orientation at multiple time points to fit a desired function, but it neglects contributions of other cell mediated factors such as cross-linking and the development of residual matrix tension.

Another candidate approach to modeling the evolving properties of tissue equivalents, which could capture cell-driven alterations to the matrix in terms of changes to the strain energy function for the individual constituents, could be borrowed from

modeling soft tissue G&R. A constrained mixture theory of G&R allows one to model separately the mechanical properties, rates and extents of turnover, and natural configurations of individual constituents [104]. Put simply, the stress in a body depends on the sum of the stresses in individual constituents, which need not be the same. Stress develops when a constituent deforms from its natural, or stress-free, configuration, which can evolve. For example, cross-linking of some fibers to build in a residual matrix tension could render their natural configuration different from the original natural configuration of similar fibers. The basic model requires that one construct a rule-of-mixtures strain energy function (i.e., $W = \sum W^{\alpha}$), where:

$$W^{\alpha}(s) = \frac{\rho^{\alpha}(0)}{\rho(s)} Q^{\alpha}(s) W^{\alpha}\left(\mathbf{C}^{\alpha}_{n(0)}(s)\right) + \int_0^s \frac{m^{\alpha}(\tau)}{\rho(s)} q^{\alpha}(s,\tau) W^{\alpha}\left(\mathbf{C}^{\alpha}_{n(\tau)}(s)\right) d\tau. \quad (2.6)$$

The first part of the strain energy accounts for the contribution of constituents that were present at time zero and still are present at the current time s, where $\rho^{\alpha}(0)$ is the mass density of constituent α that was present at time zero, $\rho(s)$ is the mass density of the mixture at time s, $Q^{\alpha}(s)$ is the fraction of constituent α that was present at time zero and yet remains at time s, and $\mathbf{C}^{\alpha}_{n(0)}(s)$ is the right Cauchy-Green tensor that describes the deformation of constituent α present at time zero, relative to its individual natural configuration, to the current configuration at time s. The second part (integral term) of the strain energy accounts for contributions of constituents produced at any time $\tau \in [0, s]$ that remain at s, where $m^{\alpha}(\tau)$ is the mass density of constituent α produced at time

τ, $q^{\alpha}(s,\tau)$ is the fraction of constituent α produced at time τ that remains at time s, and $\mathbf{C}^{\alpha}_{n(\tau)}(s)$ is the right Cauchy-Green tensor that describes the deformation of constituent α produced at time τ, relative to its individual natural configuration, to the current configuration at time s [105]. This approach has been used previously to model theoretical changes in alignment of newly deposited matrix in a biaxial tissue equivalent under different loading conditions [106]. In these preliminary simulations, it was found that if new matrix is deposited in the direction of greatest principal stretch, the principal Cauchy stresses in the system can be restored to near homeostatic values. For the simulations, the production of new matrix was a function of stress deviation from a preferred level of stress.

States of tissue reorganization with no deposition of new material can also be accounted for in the G&R framework. This is particularly important in short term (~5 days) culture of tissue equivalents where experimental evidence shows there is little to no new matrix deposition [37,107]. Removal and deposition relations would still be needed, but for these early times, any removed constituent would need to be replaced by another one. Conceptually, this would amount to removing a collagen fiber at one orientation and replacing it with another fiber in a new orientation.

Current models for the evolution of tissue equivalents take into account some mechanical cues, but they do not directly account for chemical factors that modulate cell behavior. Recall that mechanical perturbations to tissue equivalents can lead to the cellular production of soluble factors that can have a paracrine or autocrine effect on cell-driven remodeling. Within the context of G&R, it would be possible to account naturally for the contribution of such factors in the mass production ($m^{\alpha}(\tau)$) and mass removal

$(Q^{\alpha}(s), q^{\alpha}(s,\tau))$ terms of the stored energy functions. A simple implementation of this approach would be to allow the concentrations of growth factors to modulate the rates at which a constituent is produced or removed. Similarly, the effectiveness of a soluble factor to modulate the tissue equivalent can also depend on the mechanical environment. For example, there is experimental evidence and subsequent network modeling simulations that have shown a reduced rate of enzymatic matrix degradation when a tissue equivalent is strained [108,109].

As with the free-floating lattice, constitutive models for actively applied forces or stresses are needed for constrained tissue equivalents. Similar to the mass production and removal terms, many factors can affect the ability of a cell to apply stress to its surrounding matrix. These can include, but are not limited to, matrix density, composition, and orientation, as well as soluble factors, cell phenotype, and expression levels of integrins and other cell surface proteins and binding domains. Of course, expressions for active cellular stresses would need to account for how the local mechanical environment in which the cells reside may modulate the level of stress a cell can apply.

The coupling of sequential mechanical testing data and G&R simulations may possibly be used to determine parameters related to matrix remodeling. This could be accomplished using an approach proposed to describe G&R of the lens capsule following cataract surgery [110]. Briefly, the mechanical behavior of the tissue equivalent could be described phenomenologically via a standard strain energy function (e.g. Fung-type) at any time during the culture period. This descriptor could then be used in a standard stress analysis to determine stresses and stretches within the construct to determine differences

from homeostatic values that would be expected to modulate the compaction as well as deposition and removal of constituents, which could be captured with a G&R model. The results of the G&R could then be assessed, or compared to experimental data, and used to recalculate the stress and strain state. Iteration of this process could allow one to describe or predict the mechanical evolution of the construct. Minimization of errors between experimentally and computationally determined material parameters via fine-tuning of the deposition and removal parameters would provide general measures of tissue reorganization and potential neo-tissue development and how these parameters may change in time due to changes in material composition (Figure 2.4).

2.5 Summary

Mechanobiological research aims to understand how mechanical loads influence biological responses by cells. This search is often pursued as a one step process, that is, mechanically stimulate a cell or cells and measure some biological entity of interest, as, for example, gene expression or protein production. This, however, is not the case in vivo. Cells often respond to changes in mechanical load by altering their surrounding environment, which in turn alters the mechanical behavior of the tissue and thus the local mechanical loading. Through this process, the cells appear to attempt to establish, maintain, or restore a preferred mechanical environment, a process that is referred to as mechanical homeostasis.

Tissue equivalents represent controllable experimental systems to explore the evolution of biomechanical and mechanobiological properties of tissue engineered constructs and resident cells under well-controlled mechanical and chemical cues. They

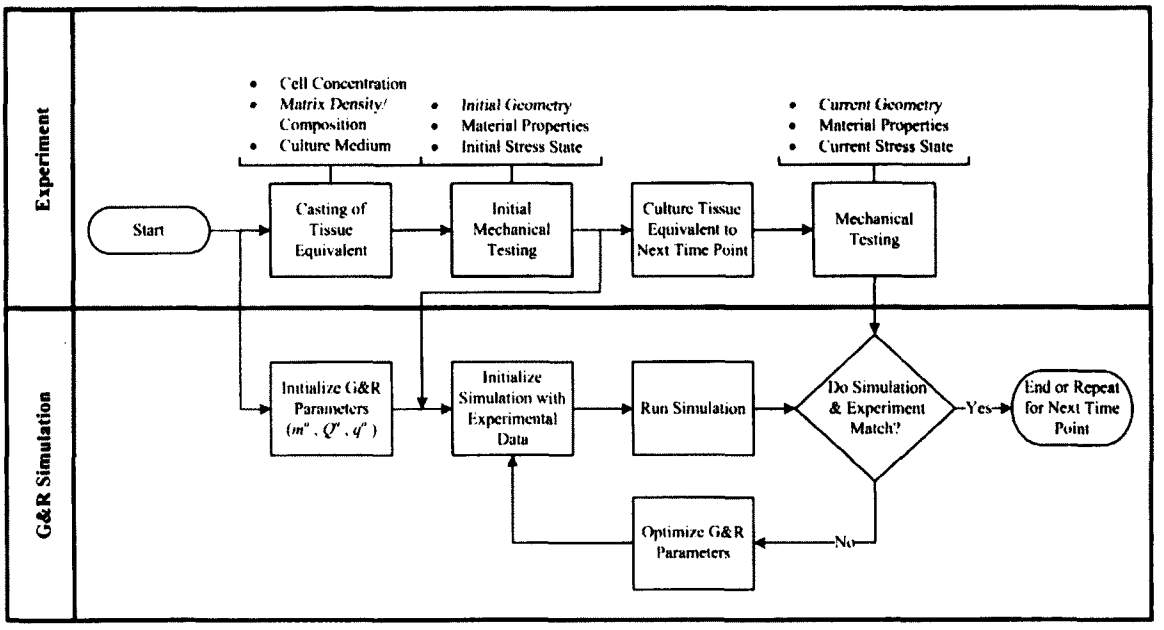

Figure 2.4: Combined Experimental and G&R approach. Example flow chart to implement a combined experimental-computational approach to study the mechanobiology of tissue equivalents.

also provide a platform to examine the biological activity of cells within a 3D matrix environment, which is particularly important for most connective tissue cell types (see Table 2.1 for summary). Finally, modeling of the evolution of tissue equivalents can provide new insight into the interplay between the mechanics and the biology. Models based on tissue equivalent development could also provide a means to simulate the progression of tissue engineering materials and enable more rational design rather than the often trial-and-error experimental approach. Conceptualization of such an approach has been proposed for tissue engineered vascular grafts [111]. Clearly, much has been learned, but much remains to be accomplished. Tissue equivalents promise to remain fundamental to our understanding of cell-matrix interactions and the development and remodeling of soft tissues.

Exp. Type	Parameter	Observation	References
Free-Floating	Cell Concentration	If increased, increases rate/extent of compaction	[2,27]
	Cell Type/Origin	Varies rate/extent of compaction	[29–31,33]
	Matrix Density	If increased, reduces rate/extent of compaction	[2]
	Matrix Type	Can alter rate/extent of compaction	[34,35,37]
	Collagen I w/ Hyaluronan	Increases rate/extent of compaction	[32]
	Collagen I w/ Decorin	Decreases rate/extent of compaction (inhibits TGF-β)	[38]
	Matrix Organization	Alignment parallel to edge, random orientation in center	[27]
	Covalent Cross-linking	If blocked, decreases extent of compaction	[40,41]
	Integrins	Blocking $\alpha_2\beta_1$ and $\alpha_v\beta_3$ reduce/eliminate compaction	[45–48]
	Serum	Required for compaction	[30,50]
	Growth Factors	PDGF and TGF-β1 increase rate/extent of compaction, induce compaction in lieu of serum	[51–54]
	Gene Expression	MMPs vary throughout culture time	[61]
	Collagen I Expression	Decreased (compared to adhered lattice)	[46]
	α-SMA expression	Decreased (compared to adhered lattice), up-regulated by TGF-β1, can regionally vary	[52,62]
	Mechanical Assessment	Residual-type stress field, compressive in center, tensile at outer edge	[90,91]
Uniaxial	Cell Concentration	If increased, increases rate/extent of force generation	[64]
	Cell Type/Origin	Varies rate/extent of force generation	[64,65,68,69]
	Matrix Density	If increased, increases rate/extent of force generation	[64]
	Contractility	Thrombin increases tensile force in system	[65]
	Actin	Disruption eliminates or reduces tensile force in system	[42,65]
	Microtubules	Disruption increases tensile force in system	[65,71]
	Tensional Homeostasis	Cells seek to maintain a preferred level of tension	[43]
	Residual Matrix Tension	Increases even after total force in system plateaus	[42]
	Growth Factors	TGF-β1 increases rate/extent of force generation, overexposure can be inhibitory	[42,72,73]
	Gene Expression	MMP, TIMP levels affected by system prestrain and cyclic loading	[74–76]
Biaxial	Matrix Realignment	Cell-driven, affected by initial geometry and loading during culture	[78–80]
	Load-Induced Matrix Alignment	Mechanical loading results in alignment towards increased force	[82–84]
	Matrix Production	In fibrin-based, collagen deposition can vary regionally based on initial conditions	[85]

Table 2.1: Summary of prior observations from tissue equivalent experiments.

Chapter 3: On a class of admissible constitutive behaviors in free-floating engineered tissues

Portions of this chapter were published in *Int. J. Non-Linear Mech.*, 2012 (47:173-178)

3.1 Introduction

Tissue engineering is a multi-disciplinary field committed to develop living tissue constructs that can be used to repair or replace native tissue following injury or disease (cf. [112]). Despite remarkable advances in tissue engineering over just a few decades, many fundamental questions remain regarding how cells interact with both native extracellular matrix and synthetic polymer scaffolds as they evolve the engineered construct. One of the first, and simplest, tissue-engineered constructs that remains useful for studying basic cell–matrix interactions is the so-called free-floating fibroblast populated collagen lattice (FPCL) [2]. Typically, reconstituted fibrillar collagen is allowed to form a thin "gel" within a circular mold and fibroblasts suspended in an appropriate cell culture media are seeded within the gel at prescribed densities (e.g., on the order of 10^5 cells per ml). When the circular gel is released from the mold, and not otherwise tethered, the cells tend to contract the gel over a period of days, often to less than 50% of the original diameter. Many studies document effects on the rates and extents of contraction as a function of collagen type (e.g., I, II, or III) and density, cell type and density, the presence of exogenous growth factors (e.g., transforming growth factor-beta), and various drug treatments designed to alter cell receptor binding or cytoskeletal integrity. For a nice review of many of these studies, see Dallon and Ehrlich [3].

Amongst the many findings, it appears that fibroblasts use multiple but related methods to contract the gel. In particular, it has been suggested that cells can compact and align collagen fibers as they (1) spread out on and attach to the gel, (2) draw in the collagen fibers via cell extensions and integrin-mediated tractions, or (3) exhibit overall contraction [3,28]. Regardless of the means of contracting the gel, linear momentum balance must be satisfied in this traction free initial-boundary value problem. We consider here a simple homogeneous finite deformation to model the initiation of contraction of an initially thin, amorphous, untethered, circular collagen gel and show that non-trivial solutions can be obtained for a particular class of constitutive behaviors only when the material properties vary radially. We submit that these, and similar future, solutions can increase our ability to interpret the important free-floating FPCL.

3.2 Methods

The collagen gel initially consists of an amorphous mixture of collagen fibers, cells, and water. Consistent with formulations in growth and remodeling biomechanics (e.g., [104]), we use a rule-of-mixtures relation for the Cauchy stress response. For example, conceptually we let the Cauchy stress $\mathbf{t} = -\tilde{p}\mathbf{I} + \phi^s\tilde{\mathbf{t}}^s + \phi^f\tilde{\mathbf{t}}^f$, where $\tilde{p}$ is a Lagrange multiplier enforcing intrinsic incompressibility of the solid constituents or transient motions at a fixed level of contraction, ϕ^s is the mass fraction of the solid, $\tilde{\mathbf{t}}^s$ is the Cauchy stress response of the solid, $\phi^f(= 1 - \phi^s)$ is the mass fraction of the fluid, and $\tilde{\mathbf{t}}^f$ is the Cauchy stress response of the fluid. Although many report that water is exuded during contraction of the gel, we assume that the associated momentum exchanges (from the perspective of mixture theory) are small because of the slowness of

the process. Moreover, consistent with a quasi-static assumption, we let the contribution of the fluid to the overall stress be a hydrostatic pressure and thus lump its contribution together with the arbitrary Lagrange multiplier. Hence, we write $\mathbf{t} = -p\mathbf{I} + \mathbf{t}^S$ where the mass fraction of the solid is embedded in its stress response.

Focusing on early contraction of the gel, we consider homogeneous axisymmetric finite deformations whereby material particles initially at (R, Θ, Z) are mapped to (r, ϑ, z) according to

$$r = \lambda R, \vartheta = \Theta, z = \Lambda Z, \forall r \in [0, r_o], \vartheta \in [0, 2\pi], z \in [-h/2, h/2] \quad (3.1)$$

where r_o is the deformed outer radius, h is the deformed thickness, and λ and Λ are stretch ratios (where $\lambda < 1$ for contraction; see Figure 3.1). Hence, physical components of the deformation gradient are [113]

$$\mathbf{F} = \begin{bmatrix} \frac{\partial r}{\partial R} & \frac{1}{R}\frac{\partial r}{\partial \Theta} & \frac{\partial r}{\partial Z} \\ r\frac{\partial \vartheta}{\partial R} & \frac{r}{R}\frac{\partial \vartheta}{\partial \Theta} & r\frac{\partial \vartheta}{\partial R} \\ \frac{\partial z}{\partial R} & \frac{1}{R}\frac{\partial z}{\partial \Theta} & \frac{\partial z}{\partial Z} \end{bmatrix} = \begin{bmatrix} \lambda & 0 & 0 \\ 0 & \lambda & 0 \\ 0 & 0 & \Lambda \end{bmatrix}. \quad (3.2)$$

Despite reports that fluid is exuded from the gel as it contracts, there are no data on the rate or degree of water loss. Because of this lack of data, and our focus on initial gel contraction, we first assume overall incompressibility. Consequently, $\det \mathbf{F} = 1$ and $\Lambda = 1/\lambda^2$.

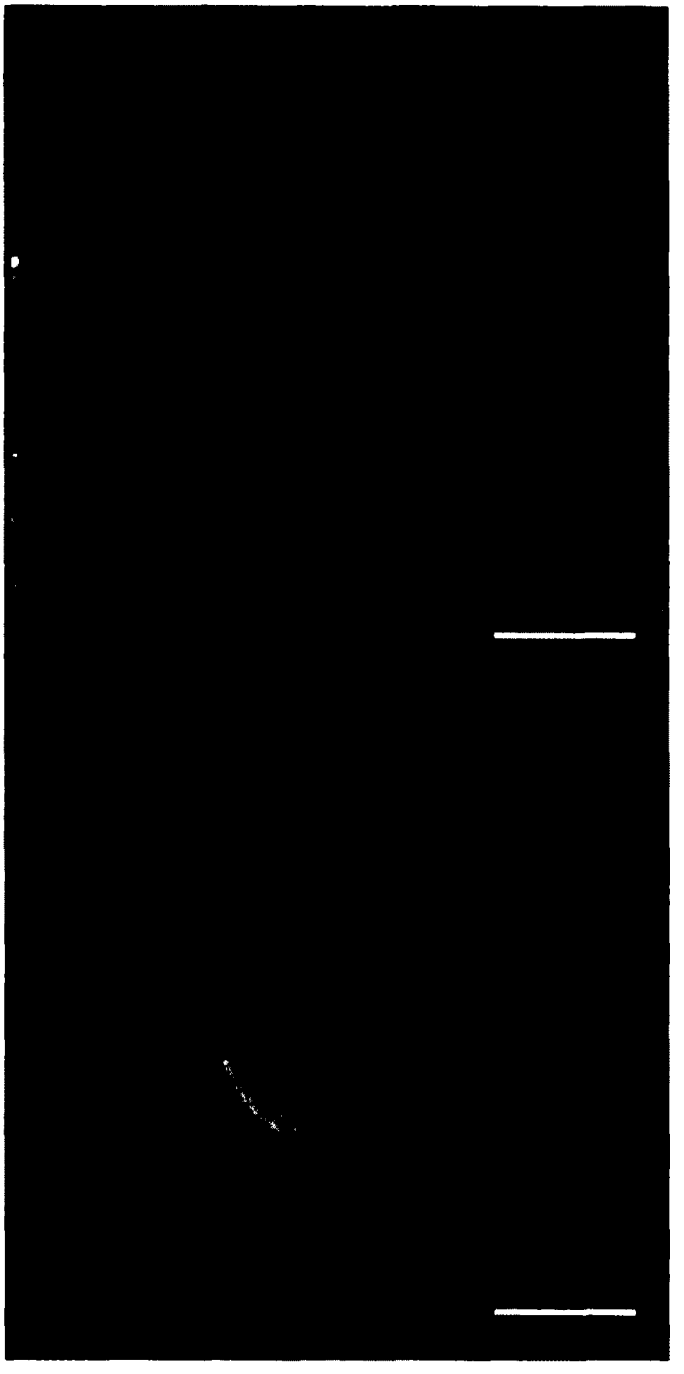

Figure 3.1: Free-floating FPCL compaction example. Representative contraction of an initially circular collagen gel by fibroblasts: initial gel (top) and gel 5 days after seeding with fibroblasts (bottom). Note the retained circularity. Scale bars are 5 mm.

Below, we allow the material properties to vary with radial location, but assume complete axisymmetry and no variations in the z-direction because of the thinness of the gel. Assuming the inertial effects are negligible, we thus enforce equilibrium in this plane stress problem as [113]

$$\frac{\partial t_{rr}}{\partial r} + \frac{1}{r}(t_{rr} - t_{\vartheta\vartheta}) = 0, \frac{\partial t_{\vartheta\vartheta}}{\partial \vartheta} = 0, \frac{\partial t_{zz}}{\partial z} = 0. \tag{3.3}$$

The last two equations reveal that the Lagrange multiplier may depend on the radial direction at most; hence, we must only satisfy radial equilibrium. Our traction-free boundary conditions are $t_{zz}(z = \pm h/2) = 0$ and $t_{rr}(r = r_o) = 0$.

3.3 Results

3.3.1 Homogenous properties

Let us now contrast results for multiple potential descriptors of the constitutive behavior of the solid, which consists of hydrated collagen and cells. Given that the gels are initially very compliant, and the collagen fibers initially distributed randomly, let us begin by considering a neo-Hookean (isotropic) behavior for collagen, namely $\mathbf{t} = -p\mathbf{I} + 2\mu\mathbf{B}$, where μ is a mass averaged shear modulus (i.e., the mass fraction is absorbed within this parameter) and $\mathbf{B} = \mathbf{F}\mathbf{F}^T$ is the left Cauchy–Green tensor. That is, let us first consider the case when the cells do not generate any (contractile) stress, for which

$$t_{rr} = -p + 2\mu\lambda^2, t_{\vartheta\vartheta} = -p + 2\mu\lambda^2, t_{zz} = -p + 2\mu\frac{1}{\lambda^4}. \tag{3.4}$$

Enforcing the traction-free condition on the upper and lower faces requires $0 = -p + 2\mu/\lambda^4$, whereby

$$t_{rr} = 2\mu\left(\lambda^2 - \tfrac{1}{\lambda^4}\right), t_{\vartheta\vartheta} = 2\mu\left(\lambda^2 - \tfrac{1}{\lambda^4}\right). \tag{3.5}$$

Notice that this constant equibiaxial state of plane stress satisfies radial equilibrium (Eq. (3.3_1)) identically, but the traction-free condition at the outer radius $t_{rr}(r = r_o) = 0$ requires further that $\lambda \equiv 1$, the trivial solution. That is, a thin, traction-free, circular specimen endowed with a neo-Hookean behavior cannot deform via Eq. (3.1).

Without repeating the mathematical details, one arrives at the same conclusion for a mixture of isotropic collagen (described by a neo-Hookean constitutive relation) and cells that exhibit an isotropic active (i.e., contractile) stress $t_a\mathbf{I}$. That is, if $\mathbf{t} = -p\mathbf{I} + 2\mu\mathbf{B} + t_a\mathbf{I}$, then the traction-free upper and lower surfaces require $0 = -p + 2\mu/\lambda^4 + t_a$ and the stress state is identical to that in Eq. (3.5); in other words, the only solution possible for this traction-free problem is again the trivial solution, $\lambda \equiv 1$ with no uniform isotropic cell contraction.

Among others, Costa et al. [63] noted that cells tend to align parallel to traction-free surfaces. Hence, let us consider the stress response for an isotropic collagen matrix plus circumferentially oriented active cells, namely $\mathbf{t} = -p\mathbf{I} + 2\mu\mathbf{B} + t_c\mathbf{e}_\vartheta \otimes \mathbf{e}_\vartheta$, where t_c denotes an anisotropic cell contraction. The traction-free condition on the upper and lower surfaces again requires $0 = -p + 2\mu/\lambda^4$, hence the stress field is

$$t_{rr} = 2\mu\left(\lambda^2 - \frac{1}{\lambda^4}\right), t_{\vartheta\vartheta} = 2\mu\left(\lambda^2 - \frac{1}{\lambda^4}\right) + t_c. \tag{3.6}$$

Again, however, the traction-free boundary condition at the outer radius requires $\lambda \equiv 1$. Moreover, these two conditions leave $\mathbf{t} = t_c \mathbf{e}_\vartheta \otimes \mathbf{e}_\vartheta$, which satisfies radial equilibrium if and only if $t_c = 0$, thus yielding the trivial solution. In other words, a thin, traction-free, circular specimen endowed with a uniform neo-Hookean response by the collagen and a uniform uniaxial cell contraction cannot deform via Eq. (3.1).

It is also known, of course, that collagen fibers often align parallel to the cells that maintain them [3,63], which motivates inclusion of a transversely isotropic term for the collagen fibers as well (with the circumferential direction preferred). For example, consider a stored energy function for collagen of the form $W(I_C, IV_C)$ where $I_C = tr\mathbf{C}$ and $IV_C = \mathbf{M} \cdot \mathbf{CM}$, with $\mathbf{C} = \mathbf{F}^T\mathbf{F}$ the right Cauchy–Green tensor and $\mathbf{M}$ a unit vector denoting the original orientation of a locally parallel family of fibers (which give rise to a transverse-isotropy). In this case, the associated Cauchy stress for the collagen is given by $\mathbf{t} = -p\mathbf{I} + 2W_1\mathbf{B} + 2W_4\alpha^2\mathbf{m} \otimes \mathbf{m}$, where $W_1 = \partial W/\partial I_C$, $W_4 = \partial W/\partial IV_C$, and α is the stretch of a collagen fiber that was originally oriented in direction $\mathbf{M}$ but after deformation is oriented at direction $\mathbf{m}$. Because of the initial low stiffness of these collagen gels, we let $W(I_C, IV_C) = \mu(I_C - 3) + c(IV_C - 1)^2$ where μ and c are material parameters; the first term captures the same neo-Hookean (isotropic) contribution used above. If we let the direction $\mathbf{M}$ be circumferential, then $\alpha \equiv \lambda$ and the material exhibits transverse-isotropy with the preferred direction being circumferential. Assuming this combined isotropic—transversely isotropic form of the stored energy for the collagen

plus both an isotropic ($t_a\mathbf{I}$) and a transversely isotropic ($t_c\mathbf{e}_\vartheta \otimes \mathbf{e}_\vartheta$) contribution to the Cauchy stresses by cell contraction, the associated stresses are

$$t_{rr} = -p + 2\mu\lambda^2 + t_a \tag{3.7}$$

$$t_{\vartheta\vartheta} = -p + 2\mu\lambda^2 + t_a + 4c(\lambda^4 - \lambda^2) + t_c \tag{3.8}$$

$$t_{rr} = -p + 2\mu\frac{1}{\lambda^4} + t_a. \tag{3.9}$$

The traction-free top and bottom surfaces again require 0=−p+2μ/λ4+ta, whereby the state of plane stress reduces to

$$t_{rr} = 2\mu\left(\lambda^2 - \frac{1}{\lambda^4}\right), t_{\vartheta\vartheta} = 2\mu\left(\lambda^2 - \frac{1}{\lambda^4}\right) + 4c(\lambda^4 - \lambda^2) + t_c. \tag{3.10}$$

Note again that a uniform isotropic contractile stress is not admitted in the final stress field. Moreover, it is easy to see that the traction-free condition at the outer radius again does not admit a contraction of the gel (i.e., $\lambda \equiv 1$), both with and without isotropic or transversely isotropic cell activation. Finally, because the two boundary conditions leave $\mathbf{t} = t_c\mathbf{e}_\vartheta \otimes \mathbf{e}_\vartheta$, radial equilibrium requires that $t_c = 0$, thus yielding the overall trivial solution yet again.

It appears, therefore, that a homogeneous, axisymmetric contraction of a fully traction-free, thin, circular specimen under plane stress does not admit a uniform isotropic or transversely isotropic (circumferential) response of the class of constitutive relations considered for either the collagen or the cells.

3.3.2 Heterogeneous properties

Next, consider radially varying material properties, which can be modeled via a rule-of-mixtures relation for the stress with appropriate mass fractions ϕ_j varying with radial location. Consistent with the above, we can assume forms of the stored energy function for collagen to be $W_{iso} = \mu(I_C - 3)$ and $W_{aniso} = c(IV_C - 1)^2$ and similarly let the contractile cells exhibit either isotropic ($t_a\mathbf{I}$) or transversely isotropic ($t_c\mathbf{m} \otimes \mathbf{m}$) contractile responses (such an additive split into isotropic and anisotropic contributions is consistent with that advocated by Holzapfel and Ogden in other biomechanical applications; [114]). Hence, we consider the following general form for the stress response

$$\mathbf{t} = -p\mathbf{I} + \phi_{iso}(r)(2\mu\mathbf{B} + t_a\mathbf{I}) + \phi_{aniso}(r)(4c(\lambda^4 - \lambda^2) + t_c)\mathbf{m} \otimes \mathbf{m} \qquad (3.11)$$

where we let $\mathbf{m} \equiv \mathbf{e}_\vartheta$ herein. For the deformation in Eq. (3.1), therefore, the Cauchy stress response is

$$t_{rr} = -p + \phi_{iso}(r)(2\mu\lambda^2 + t_a) \qquad (3.12)$$

$$t_{\vartheta\vartheta} = -p + \phi_{iso}(r)(2\mu\lambda^2 + t_a) + \phi_{aniso}(r)(4c(\lambda^4 - \lambda^2) + t_c) \qquad (3.13)$$

$$t_{zz} = -p + \phi_{iso}(r)(2\mu/\lambda^4 + t_a) \qquad (3.14)$$

where the mass fractions must sum to unity, namely $\phi_{iso} + \phi_{aniso} = 1$ at each point.

Traction-free upper and lower surfaces require $0 = -p + \phi_{iso}(r)(2\mu/\lambda^4 + t_a)$, which reveals that the Lagrange multiplier can now vary with radial location. The state of plane stress thus reduces to

$$t_{rr} = 2\mu\phi_{iso}(r)\left(\lambda^2 - \frac{1}{\lambda^4}\right) \tag{3.15}$$

$$t_{\vartheta\vartheta} = 2\mu\phi_{iso}(r)\left(\lambda^2 - \frac{1}{\lambda^4}\right) + \phi_{aniso}(r)(4c(\lambda^4 - \lambda^2) + t_c). \tag{3.16}$$

Note, again, that a possible isotropic cell contraction cannot contribute to the stress field even if allowed to vary with position. Next, consider two specific cases of regional variations.

First, consider a linear variation in material properties, that is, $\phi_{aniso} = r/r_o$ and thus $\phi_{iso} = 1 - r/r_o$. In other words, we let the material exhibit an isotropic response at the center ($r = 0$) but a strongly transversely isotropic response at the outer edge ($r = r_o$); at increasing radial positions between the center and edge we have an increasingly stronger transverse isotropy (Figure 3.2). Notice from Eq. (3.15) that the traction-free condition is satisfied identically at $r = r_o$ because $\phi_{iso}(r = r_o) = 0$. Radial equilibrium (Eq. (3.3)) thus requires

$$2\mu\left(\lambda^2 - \frac{1}{\lambda^4}\right)\left(-\frac{1}{r_o}\right) - \left(\frac{1}{r_o}\right)(4c(\lambda^4 - \lambda^2) + t_c) = 0\ \forall r. \tag{3.17}$$

Consequently, if there is no anisotropic contractile contribution by the cells (i.e., $t_c \equiv 0$), then $2\mu(1/\lambda^4 - \lambda^2) = 4c(\lambda^4 - \lambda^2)$. For arbitrary values of the material

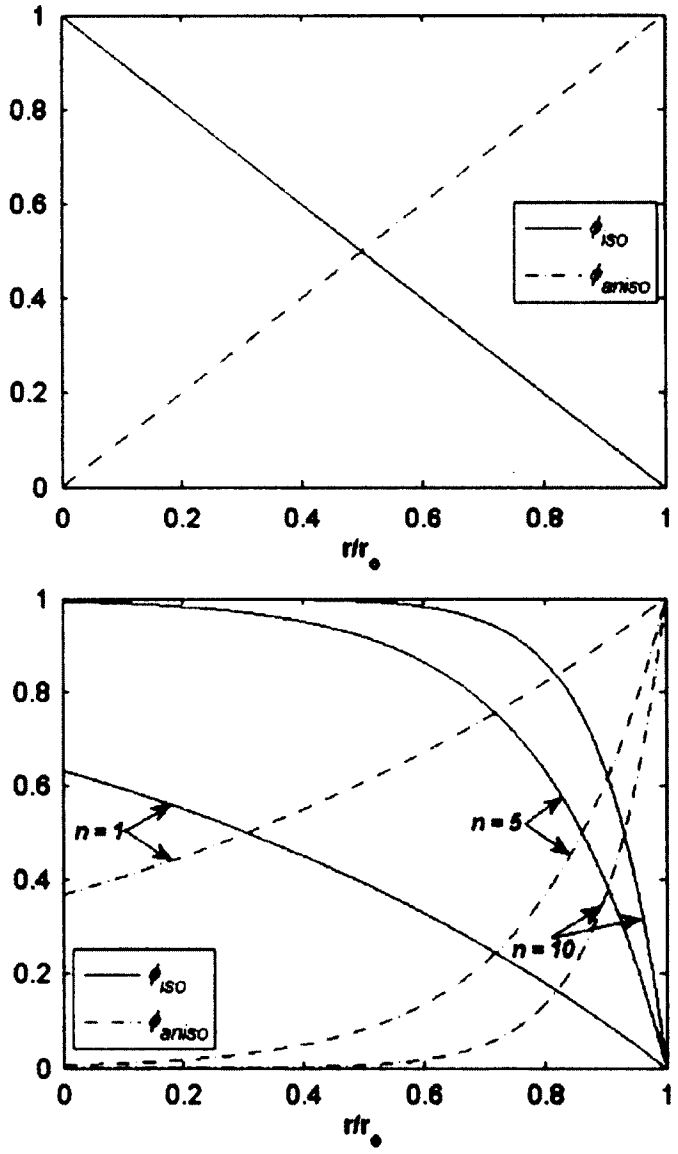

Figure 3.2: Radial distributions of mass fractions. ϕ_{iso} and ϕ_{aniso} for an assumed linear (top) or exponential (bottom) variation. The exponential case is shown for the parameter $n = 1, 5, \& 10$, which reveals that for n large enough one can model a material that transitions from purely isotropic at the center to strongly transversely isotropic at the edge similar to that for the linear variation.

parameters μ and c, it can be shown numerically that the only solution is the trivial one, $\lambda \equiv 1$. In contrast, solving Eq. (3.17) for a non-zero transversely isotropic active stress, $t_c = -2\mu(\lambda^2 - 1/\lambda^4) - 4c(\lambda^4 - \lambda^2)$, with $\lambda < 1$ for contraction of the gel, the final state of plane stress becomes

$$t_{rr} = 2\mu\left(\lambda^2 - \frac{1}{\lambda^4}\right)\left(1 - \frac{r}{r_o}\right), t_{\vartheta\vartheta} = 2\mu\left(\lambda^2 - \frac{1}{\lambda^4}\right)\left(1 - \frac{2r}{r_o}\right). \tag{3.18}$$

Note again that the radial traction-free boundary condition is satisfied automatically at the outer edge ($r = r_o$). Figure 3.3 shows associated distributions of stress, normalized with respect to the material parameter μ, for multiple degrees of contraction ($\lambda < 1$). As would be expected in this traction-free problem, one obtains a "residual-type" distribution of stresses wherein regions of compression balance those of tension for the circumferential stress.

Second, and finally, consider an exponential regional variation in properties, namely $\phi_{iso} = 1 - \exp[n(r/r_o - 1)]$ and therefore $\phi_{aniso} = \exp[n(r/r_o - 1)]$. For large enough values of n, this distribution again yields essentially an isotropic response at the center ($r = 0$) but a strongly transversely isotropic response at the outer edge ($r = r_o$); at radial positions between the center and edge we have an increasingly stronger transverse isotropy (Figure 3.2). Albeit involving slightly more algebra, one finds a result similar to that for the linear radial variation in properties. Absence of an anisotropic cell-mediated contraction again yields the trivial solution. In contrast, enforcing radial equilibrium for a non-zero t_c yields a non-trivial solution. In particular, $t_c = -2\mu(\lambda^2 - 1/\lambda^4)(nr/r_o) - 4c(\lambda^4 - \lambda^2)$. Hence, the final state of plane stress becomes

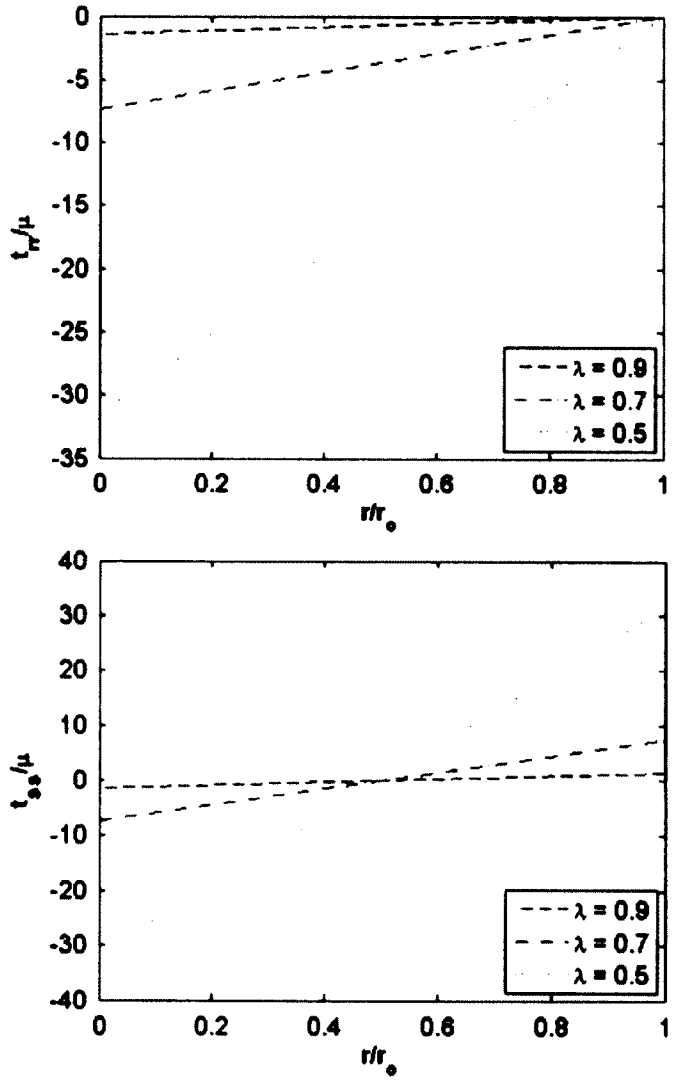

Figure 3.3: Stresses for linear material distribution. Predicted distributions of radial (top) and circumferential (bottom) stress in a model fibroblast seeded collagen gel for a linearly changing radial heterogeneity in material properties ($\phi_{aniso} = r/r_o$ and $\phi_{iso} = 1 - r/r_o$) and different degrees of contraction ($\lambda = 0.9, 0.7, \& 0.5$). Note that stress is non-dimensionalized using the material parameter μ.

$$t_{rr} = 2\mu\left(1 - \exp\left[n\left(\frac{r}{r_o} - 1\right)\right]\right)\left(\lambda^2 - \frac{1}{\lambda^4}\right) \tag{3.19}$$

$$t_{\vartheta\vartheta} = 2\mu\left(1 - \left(1 + \frac{nr}{r_o}\right)\exp\left[n\left(\frac{r}{r_o} - 1\right)\right]\right)\left(\lambda^2 - \frac{1}{\lambda^4}\right). \tag{3.20}$$

Figure 3.4 shows illustrative results for $n = 10$ and multiple levels of contraction ($\lambda < 1$), again normalized with respect to the material parameter μ. The results are qualitatively similar to those for the case of linear variations in material properties, but as expected, focusing the anisotropy near the outer edge creates stronger gradients in the radial distribution of stress.

3.4 Discussion

Prior studies of fibroblast populated collagen lattices have focused on what cells do when various experimental conditions are altered, but they have not addressed the more fundamental question, why do cells contract the gels and thus compact the collagen? We do not claim to resolve this issue, but consider the following. Although the cells are traction free when in suspension, and thus when introduced into the traction-free gel, once they contact the gel they appear to spread out and begin to pull on the extracellular matrix; indeed, they continue to pull on the matrix for long periods. By pulling on the matrix, which in turn pulls back, the cells can establish a stressed environment in which to reside under stress themselves. Note, therefore, that diverse observations consistently suggest that cells seek to establish and maintain a "tensional

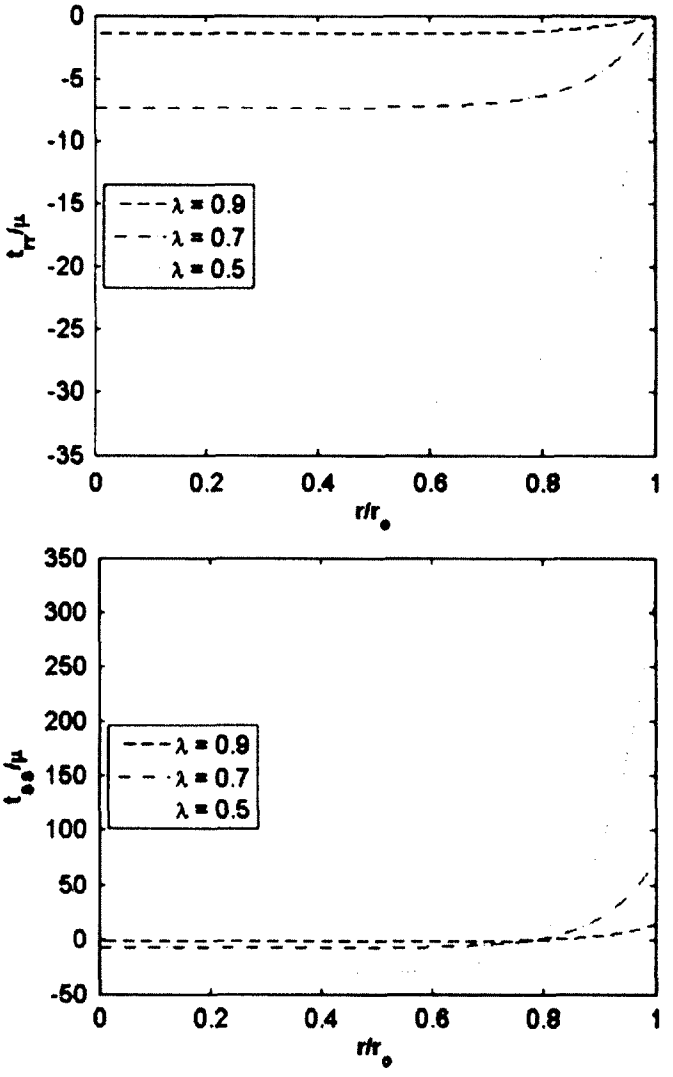

Figure 3.4: Stresses for exponential material distribution. Predicted distributions of radial (top) and circumferential (bottom) stress in a model fibroblast seeded collagen gel for an exponentially changing radial heterogeneity in material properties ($\phi_{iso} = 1 - \exp[n(r/r_o - 1)]$ and $\phi_{aniso} = \exp[n(r/r_o - 1)]$ with $n = 10$) and different degrees of contraction ($\lambda = 0.9, 0.7, \& 0.5$). Albeit not shown, results for other values of n larger were similar.

homeostasis" in connective tissues [43], that is, a target state of mechanical loading [44]. We suggest that the contraction of the gel may be an attempt by the cells to establish such a preferred, or at least a more favorable, mechanical environment that is fundamental to optimal cell function. Similar processes appear to be operative in diverse clinical settings, including lens epithelial cell responses following cataract surgery [115].

The present analysis revealed that cells within a thin, circular, traction-free gel cannot satisfy both equilibrium and boundary conditions by uniformly contracting isotropically. Indeed, they similarly cannot satisfy these fundamental mechanical requirements by uniformly contracting transversely isotropically or by uniformly organizing the collagen circumferentially. Rather, it appears that one way to satisfy both equilibrium and boundary conditions for the class of constitutive relations considered, while avoiding a non-trivial situation (i.e., no deformation, no contraction), is to generate a radially varying contractile response that becomes increasingly transversely isotropic with respect to the circumferential direction with increasing radius (i.e., moving towards the edge of the gel). This simple consequence of the mechanics is consistent with observations that myofibroblasts (which generate greater contractile stresses) tend to be found only near the outer edge of free-floating collagen gels [116] and that the collagen similarly tends to align only near the outer edge in moderate cell density free-floating collagen gels [27]. Indeed, this consequence of the mechanics is also consistent with clever in vitro observations in tethered collagen gels reported by Costa et al. [63] wherein they found that fibroblasts tend to align parallel to a traction-free surface. Based on their observations, Costa and colleagues further suggested that "Similar to Saint-Venant's principle in linear elasticity theory, it appears that the influence of boundary conditions

decreases with increasing distance from the boundary. Therefore, heterogeneity of cell alignment naturally arises." Our theoretical results support their fundamental claim. The values of the transversely isotropic active stresses, at a given level of contraction, were also required by equilibrium and boundary conditions to increase in proportion to the matrix stiffness (gel parameters μ and c). This finding also appears to be consistent with some reports that contractility is higher on or in stiffer matrices [22].

In addition to in vitro experimental findings, it is becoming increasingly evident in vivo that cells often deposit and/or organize matrix in a regionally heterogeneous manner to offset complexities in geometry and applied loads that would otherwise result in a non-homogeneous state of stress and, by definition, a mechanical environment that is not equally optimal for all cells in different regions. Examples of such regional heterogeneities can be found both in health (e.g., the native lens capsule; [115]) and in disease (e.g., cerebral aneurysms; [117]), and also appear to be consistent with the existence of residual stresses in arteries that help homogenize the transmural distribution of stress [118].

The free-floating FPCL preparation has proven convenient for studying many aspects of cell–matrix interaction (cf. [3]), yet the present analysis reveals that it imposes highly restrictive mechanical constraints on the cells. Because the outer edge and the upper/lower surfaces remain traction free, the gross state of stress must either be zero (trivial case) or residual (with self-equilibrating compressive and tensile circumferential stresses), neither of which can satisfy the potential cellular goal of establishing a uniform, non-zero state of mechanical loading that is homeostatic. Indeed, it may be for this reason that the fibroblasts tend to enter the cell death cycle prematurely (i.e., undergo apoptosis),

first in the central region, in free-floating but not in constrained collagen gels [4]. We emphasize, however, that the present analysis reveals that such an unfavorable fate for the cells need not arise because the cells and matrix remain stress free, as suggested by many (e.g., [89,119,120]). Rather, the unfavorable fate may result from the residual-type stress field that is admitted by the mechanics, but is nevertheless not optimal biologically. We note, however, that a residual-type stress field does allows tensile circumferential stresses at and near the outer traction-free edge (cf. Figure 3.3 and Figure 3.4), hence the collagen fibers could align in the direction of the maximum tensile stress consistent with many observations (cf. [121]) and not be forced to behave differently at a traction-free surface (cf. [63]). Indeed, allowing strong gradients in the material properties and hence stresses (cf. Figure 3.2 and Figure 3.4) may allow the majority of the collagen fibers to remain nearly isotropically distributed (in the central region) as reported by some (cf. [4]). In other words, the simple solution offered herein yields results consistent with many seemingly confusing experimental findings (cf. [3]). It is interesting in this regard that Winer et al. [122] note the importance of accounting for the non-linear elasticity under finite deformations as we did. They write "local strain stiffening [due to non-linear elasticity] allows an initially isotropic matrix to reinforce cell-applied mechanical anisotropy and transmit forces between cells up to half a millimeter apart. In this way isolated cells can create far-reaching mechanical gradients and produce a global pattern." In other words, consistent with the findings herein, cells may, under particular conditions, create gradients in matrix stress (and thus stiffness) that enable cooperative behaviors, perhaps as they seek together to establish or maintain a mechanical homeostasis.

To the best of our knowledge, there has not been a comparable mechanical analysis of this experimental preparation. Among others, Barocas and colleagues (e.g., [123]) have considered cell-driven compaction of collagen and fibrin gels that are tethered to fixtures, but this is a very different situation. Independent of differences in the basic initial-boundary value problems considered, the mechanical model used by Barocas and colleagues is also very different from that used herein. For example, they model the collagen matrix as a homogeneous Maxwell fluid to endow the highly hydrated gel with viscoelastic behavior. It is not clear that viscoelasticity plays a strong role in the cell-mediated contraction of the free-floating gel considered herein. John et al. [89] modeled the collagen as linearly elastic, homogeneous, and isotropic. The associated contractile response was simulated using an equivalent "thermal contraction," which necessarily resulted in a uniform zero stress field.

Theory should always guide experiments. The present analysis suggests that regional material properties and cell behaviors may be needed to satisfy equilibrium and boundary conditions in the free-floating FPCL, which gives rise to a non-uniform (residual-type) stress field. We suggest, therefore, that there is a need to carefully measure potential radial gradients in collagen orientation, cell phenotype, and cell status (e.g., contractile or apoptotic). In other words, because of expected gradients in the stress field – with radial gradients in the always compressive radial stresses and similarly radial gradients in the self-equilibrating tensile and compressive circumferential stresses – and the mechanosensitivity of fibroblasts (e.g., [124]), there is a need to determine if similar gradients exist in cell response. Indeed, if different cell responses exist at different radial locations, then more complete correlations of cell response with mechanical stress may

be possible within a single experiment. We emphasize, therefore, that although the present study can provide both insight into prior reports of evolving tissue equivalents and additional guidance for new experiments, there is clearly a need for more data to refine the theoretical framework. Even in the first report by Bell et al. [2], it was suggested that "When cells are incorporated into hydrated collagen lattices, the lattice is contracted and water is squeezed out." Whereas the time-course of changing gel diameter, or area, has been measured and used as a primary indicator of cell activity, complete information on the amount and rate of fluid loss is not available. There is clearly a need for such data and an associated refinement of the analysis to exploit poroelastic or mixture descriptions of the behavior of the gel. Regardless, continued use of a rule-of-mixtures approach, wherein radial gradients in properties can be introduced via mass fractions rather than by allowing material parameters to vary regionally (cf. Eqs. (3.18-20)), appears to confer some utility. It has also been reported that when contracting the gel, the fibroblasts repress their synthetic capability [125]. For this reason, we did not consider potential growth and remodeling of the gel (cf. [104]). Ultimately, however, the desire to understand the initial mechanics of a tissue engineered construct is to understand the stimuli that eventually begin to drive growth and remodeling. There will be a need, therefore, to extend the present studies to include subsequent evolution of the construct as additional matrix is produced and removed (cf. [111]).

Chapter 4: Mechanical restrictions on biological responses by adherent cells within collagen gels

Portions of this chapter were published in *J. Mech. Behav. Biomed. Mater.*, 2012 (14: 216-226)

4.1 Introduction

Interactions between adherent cells and extracellular matrix are fundamental to diverse tissue-level processes, including morphogenesis, development, adaptation, disease progression, and wound healing [5,25,44,126–128]. Not only does the extracellular matrix (often consisting primarily of elastic fibers, collagens, and proteoglycans) endow tissues with important mechanical properties, it sequesters diverse biomolecules (e.g., growth factors, cytokines, and proteinases) and its mechanical state (e.g., stiffness, stress, or strain) can contribute both directly and indirectly to the regulation of cell proliferation, migration, differentiation, and even contraction. For example, mechanical stress can participate in the release or activation of transforming growth factor-beta within the extracellular matrix and cells can participate mechanically in this process [129]. There are many reasons, therefore, to understand better the mechanics of cell-matrix interactions and attendant effects on the mechanobiology and pathobiology.

Considerable information has been gleaned by observing the behavior of cells plated on substrates consisting of, or structures functionalized with, different extracellular matrix proteins [22,23], yet adherent interstitial cells typically behave very differently on 2D surfaces than within 3D matrix [24,25]. For this reason, cell-seeded collagen and fibrin gels (or, tissue equivalents) have become particularly useful model systems [4,5]. Notwithstanding tremendous information gained by studying cellular responses in such

constructs, there has been little attention devoted to the associated mechanics. This state of affairs is surprising given that mechanobiology seeks to quantify changes in cellular activity in response to changes in mechanical stimuli, and it is only via mechanics that we can quantify how these stimuli change as a function of changes in the geometry and mechanical properties of the tissue or tissue equivalent as well as the changes in the applied loads that act on them. We present here mathematical arguments relevant to one of the most commonly used assays for studying cell-matrix interactions, cell-induced contraction of thin, untethered, circular collagen gels. It is shown that, for the class of deformations and constitutive behaviors considered, mechanics (namely, equilibrium and boundary conditions) imposes strong mathematical restrictions on otherwise physically unrestricted (free-floating) constructs that implicate cell behaviors consistent with many observations reported in the literature.

4.2. Methods

4.2.1 Theoretical Framework

Newton's second and third laws can be stated simply: the rate of change of linear momentum must balance the sum of all forces acting on a body relative to an appropriate reference frame (2nd law) and for every action, there must be an equal and opposite reaction (3rd law). Due largely to extensions by L. Euler, A. Cauchy, and other savants, the modern statements of these two laws for continua are $\operatorname{div}\mathbf{t} + \rho\mathbf{b} = \rho\mathbf{a}$ and $\mathbf{T}^{(\mathbf{n})} = -\mathbf{T}^{(\mathbf{n})}$, where $\mathbf{t}$ is the Cauchy (true) stress tensor, ρ the mass density, $\mathbf{b}$ the body force

vector, **a** the acceleration vector, and $\mathbf{T}^{(\mathbf{n})}$ the traction vector (having units of stress)[1] that associates with an outward unit normal vector **n** on a differential area of interest via the relation $\mathbf{T}^{(\mathbf{n})} = \mathbf{t} \cdot \mathbf{n}$ [113]. Effects of gravity have been reported to be negligible in thin collagen gels [63] and it is intuitive that inertial effects are negligible in cell-mediated remodeling processes that occur over periods of hours to days [104]. Hence, we assume that cell-mediated contraction of an untethered collagen gel can be studied as a series of quasi-static equilibria in the absence of body forces.

Although we will allow the material properties to vary with radial location, respecting axisymmetry, and assuming no variations in the z-direction because of the thinness of the gel (e.g., on the order of 0.05 to 0.1 cm relative to diameters ranging from 0.5 to 2.2 cm), equilibrium and boundary conditions reduce to [90]

$$\frac{\partial t_{rr}}{\partial r} + \frac{1}{r}(t_{rr} - t_{\vartheta\vartheta}) = 0, t_{zz}(z = \pm h/2) = 0, t_{rr} = (r = r_o) = 0 \qquad (4.1)$$

for all $r \in [0, r_o]$, $\vartheta \in [0, 2\pi]$, and $z \in [-h/2, h/2]$, where r_o is the current outer radius and h is the associated thickness. That is, we must satisfy equilibrium and traction continuity at all (r, ϑ, z), including traction continuity on the traction-free upper and lower surfaces as well as around the periphery of the untethered circular gel.

Cell-mediated contraction of these gels results in large deformations (cf. [3]), but there is no evidence of dominant viscoelastic effects over the long time scales of interest. Hence, we employ methods of nonlinear elasticity to study the boundary value problem

[1] Terms such as stress (tensor) and traction (vector) have precise meanings in mechanics, but they are used loosely and inconsistently in mechanobiology. For example, the word traction is often used in biology to delineate actomyosin based force generation by cells that differs from classical muscle contraction.

of interest, including a traditional semi-inverse approach wherein one prescribes the deformation (motivated by laboratory observations) and then computes the associated stresses that satisfy Eqs. (4.1). Restricting our attention to a sub-class of gels that are initially circular and that remain circular and uniformly thin, which is supported by empirical observations under certain conditions, consider homogeneous axisymmetric finite deformations whereby material particles originally at (R, Θ, Z) are mapped to (r, ϑ, z) according to

$$r = \lambda R, \vartheta = \Theta, z = \Lambda Z \tag{4.2}$$

where λ and Λ are radial and axial stretch ratios, respectively (with $\lambda < 1$ for contraction of the gel). Associated physical components of the deformation gradient tensor $\mathbf{F}$ are [113]

$$\mathbf{F} = \begin{bmatrix} \frac{\partial r}{\partial R} & \frac{1}{R}\frac{\partial r}{\partial \Theta} & \frac{\partial r}{\partial Z} \\ r\frac{\partial \vartheta}{\partial R} & \frac{r}{R}\frac{\partial \vartheta}{\partial \Theta} & r\frac{\partial \vartheta}{\partial R} \\ \frac{\partial z}{\partial R} & \frac{1}{R}\frac{\partial z}{\partial \Theta} & \frac{\partial z}{\partial Z} \end{bmatrix} = \begin{bmatrix} \lambda & 0 & 0 \\ 0 & \lambda & 0 \\ 0 & 0 & \Lambda \end{bmatrix}. \tag{4.3}$$

Because of reports that fluid is exuded from the gel as it contracts (cf. [2]), we assume an overall compressible behavior for the hydrated gel. Hence, the standard measure of volume changes, $J = \det \mathbf{F} = \lambda^2 \Lambda$, need not equal unity as in incompressible problems. Note, too, that based on preliminary calculations, we neglected the small, near hydrostatic pressure that is exerted on these gels while immersed in culture medium.

Unfortunately, there has been little careful work on the likely evolving mechanical properties of free-floating collagen or fibrin gels. Nevertheless, it appears that these gels initially exhibit a low tensile stiffness (~2 to 24 kPa) and that they are initially isotropic [42,96]; the compressive stiffness is expected to be even lower (~0.015 to 0.075 kPa) due to the high porosity and permeability [87,130]. Hence, we assume that these gels can be characterized initially by a Blatz-Ko constitutive model (cf. [113,131]). In addition, however, observations suggest that both the cells and matrix can align parallel to the outer edge [3,63], hence inducing a potentially radially varying transverse-isotropy (with a preferred circumferential direction). For illustrative purposes, consider an "extended Blatz-Ko" constitutive behavior of the form

$$W(II_C, III_C, IV_C) = \varphi_{iso}(r)\frac{\mu}{2}\left(\frac{II_C}{III_C} + 2III_C^{1/2} - 5\right) + \varphi_{aniso}(r)\frac{c}{4}(IV_C - 1)^2 \quad (4.4)$$

at each time during contraction, where $\varphi_{iso}(r) \in [0,1]$ and $\varphi_{aniso}(r) \in [0,1]$ are "mass fractions" that capture the isotropic and potentially radially varying transversely isotropic contributions, respectively. Moreover, $\varphi_{iso}(r) + \varphi_{aniso}(r) = 1$ for all $\in [0, r_o]$, μ and c are material parameters that model the matrix stiffness (having units of kPa), at any particular time, and the coordinate invariant measures of deformation are

$$2II_C = (\mathrm{tr}\,\mathbf{C})^2 - \mathrm{tr}\,\mathbf{C}^2, III_C = \det\mathbf{C}, IV_C = \mathbf{M}\cdot\mathbf{CM} \quad (4.5)$$

with $\mathbf{C} = \mathbf{F}^T\mathbf{F}$ the right Cauchy-Green tensor and $\mathbf{M}$ a unit vector that denotes the preferred (transversely isotropic) direction in the reference configuration. Note that

$\alpha\mathbf{m} = \mathbf{FM}$, where α is the stretch ratio of a line element originally oriented in direction $\mathbf{M}$, which has direction $\mathbf{m}$ after deforming. We consider only a circumferential transverse isotropy, hence for the prescribed deformations $\mathbf{m} \equiv \mathbf{e}_\vartheta$.

It can be shown that the Cauchy stress response, with $\mathbf{t} = 2\mathbf{F}(\partial W/\partial \mathbf{C})\mathbf{F}^T/\det \mathbf{F}$, for the extended Blatz-Ko material defined by Eq. (4.4) is

$$\mathbf{t} = \varphi_{iso}(r)\frac{\mu}{III_C^{1/2}}\left(III_C^{1/2}\mathbf{I} - \mathbf{B}^{-1}\right) + \varphi_{aniso}(r)\frac{c}{III_C^{1/2}}(IV_C^2 - IV_C)\mathbf{e}_\vartheta \otimes \mathbf{e}_\vartheta \qquad (4.6)$$

where $\mathbf{I}$ is the identity tensor, $\mathbf{B} = \mathbf{F}\mathbf{F}^T$ is the left Cauchy-Green tensor, and $\otimes$ denotes the tensor product. Finally, to generalize Eq. (4.6) to account for possible radial variations in cell-induced contraction, we introduce isotropic ($t_a\mathbf{I}$) and transversely-isotropic ($t_c\mathbf{e}_\vartheta \otimes \mathbf{e}_\vartheta$) active contributions to the Cauchy stress whereby

$$\mathbf{t} = \varphi_{iso}(r)\left(\frac{\mu}{III_C^{1/2}}\left(III_C^{1/2}\mathbf{I} - \mathbf{B}^{-1}\right) + t_a\mathbf{I}\right)$$
$$+\varphi_{aniso}(r)\left(\frac{c}{III_C^{1/2}}(IV_C^2 - IV_C) + t_c\right)\mathbf{e}_\vartheta \otimes \mathbf{e}_\vartheta. \qquad (4.7)$$

That is, given our current lack of understanding of cellular contractile behavior in tissue equivalents, we do not specify the specific functional forms a priori.

4.2.2 Preparation of Cell-seeded Collagen Gels

NIH/3T3 fibroblasts (ATCC) were maintained in Dulbecco's modified Eagle's medium (DMEM), 10% calf serum, and 1% antibiotic-antimycotic (Invitrogen) in an

incubator at 37°C and 5% CO2. They were passaged at 70-80% confluence to obtain cells from passages 4 to 6 for seeding the collagen gels, which were prepared using a protocol modified from [27,78]. Briefly, 50,000 cells were suspended in 554 μL of the seeding culture medium consisting of DMEM with 10% fetal bovine serum (HyClone), 10% porcine serum (Invitrogen), penicillin G (100 U/mL, Sigma), ascorbic acid (50 μg/mL, Sigma), CuSO4 (3 ng/mL, Sigma), proline (50 μg/mL, Sigma), alanine (20 μg/mL, Sigma), glycine (50 μg/mL, Sigma), HEPES (0.01M, Invitrogen), basic fibroblastic growth factor (10 ng/mL, R&D Systems), and platelet-derived growth factor-BB (10 ng/mL, R&D Systems) – see [111]. Alternatively, some cells were suspended in medium that also contained transforming growth factor-β1 (10 ng/mL, Sigma).

This suspension including cells was mixed with a collagen solution containing 146 μL of concentrated type I rat tail collagen (8.58 mg/mL, BD Biosciences), 200 μL of 5X DMEM, and 100 μL of a 10X reconstitution buffer (0.1N NaOH and 20M HEPES) (cf. [78]) and then cast in a 12-well plate (note, each well is 22.2 mm in diameter). The final solution of 1 mL thus contained 50,000 cells and 1.25 mg of collagen. The 12-well plate was placed in the incubator for 30 min for gelation. Gels were then released from the wells by suspending them in their seeding medium and transferred to 60 mm diameter dishes and maintained for up to 7 days in the incubator. Culture medium was replaced at 1, 3, and 5 days. Images of the free-floating gels were acquired, using a Motic DMW143 Digital Stereo Microscope, every 4 hours from 0 to 16, every 12 hours from 24 to 120 (5 days), and at day 7, with all times recorded following release of the gel from the 12-well plate. Changes in radius were measured easily at each time whereas changes in thickness required destructive tests. Hence, one gel at each of the 14 times was used to estimate

thickness. Briefly, each gel was fixed in a 10% formalin solution to prevent changes in dimensions when sectioning of the gel. A 1 to 2 mm wide by ~5 mm long strip was sectioned from each gel and the stereo microscope was used to image the thickness along the axial aspect of the gel strips.

The state of stress in the gels was assessed qualitatively using additional gels cast either with or without fibroblasts. First, to assess the possible presence of a residual stress field (i.e., tensile circumferential stresses at the outer edge of the gels and compressive circumferential stresses in the inner region), a radial cut from the center to outer edge was introduced using a razor blade and any subsequent opening angles were recorded using the stereo microscope. Second, to assess the possible presence of a nearly equibiaxial compressive stress field in the central region of the gel, a 1 mm diameter biopsy punch (Miltex, outer diameter of 1.05 mm) was used to excise a circular portion of the gel from an off-center location and the dimensions of the newly introduced hole were measured and compared to the dimensions of the biopsy punch.

4.2.3 Histology

Intact gels at 0, 5, and 7 days were fixed in a 10% formalin solution for 24 hours at 4°C, then rinsed 3 times in phosphate-buffered saline and subsequently preserved in a 70% ethanol solution. Preserved gels were embedded in paraffin and sectioned at 5 to 8 μm. Half of the sections were stained with picrosirius red (PSR) to examine collagen fiber orientation while the others were immunohistochemically stained for α-smooth muscle actin (αSMA) and counter-stained with hematoxylin to examine cell phenotype and orientation, respectively. Images were acquired at 200X or 300X magnification using

an Olympus BX51 microscope with the PSR section examined under circularly polarized light to show birefringent collagen. Collagen alignment was assessed using the 2D discrete Fourier transform (2D-DFT) power spectrum as described previously [132]. Briefly, PSR images are converted to grayscale and 256 x 256 pixel regions of interest were cropped. These images were processed using a custom MATLAB code that calculates the 2D-DFT of an image, shifts the low frequency components to the image center, calculates the power spectrum as the squared amplitude of the 2D-DFT and rotates it 90 degrees to align the data to the initial image, and maps the result into polar coordinates (ρ, θ). A line average is taken along ρ for each single degree value of θ to determine the spatial frequency averaged intensity as a function of θ, $I(\theta)$, and the angle with the maximum intensity identified as the dominant angle. $I(\theta)$ for each image was normalized by the total intensity and shifted so the dominant angle was at 0 degrees with ±90 degrees plotted on either side. Randomly oriented fibers result in random power spectrum distributions while highly organized or aligned fibers will exhibit a well-defined peak in distributions at the corresponding dominant angle.

4.3 Results

4.3.1 Theoretical Findings

For the deformation given by Eq. (4.2), the non-trivial components of Cauchy stress are as follows:

$$t_{rr} = \varphi_{iso}(r)\left(\mu\left(1-\frac{1}{\lambda^4\Lambda}\right)+t_a\right) \tag{4.8}$$

$$t_{\vartheta\vartheta} = \varphi_{iso}(r)\left(\mu\left(1-\frac{1}{\lambda^4\Lambda}\right)+t_a\right)+\varphi_{aniso}(r)\left(\frac{c}{\lambda}(\lambda^2-1)+t_c\right) \tag{4.9}$$

$$t_{zz} = \varphi_{iso}(r)\left(\mu\left(1 - \frac{1}{\lambda^2\Lambda^3}\right) + t_a\right) \tag{4.10}$$

Note that the traction-free boundary condition at the periphery (Eq. (4.1_3)) is satisfied identically for all functions $\varphi_{iso}(r = r_o) = 0$, which we treat as a restriction on the allowable forms for the radially varying "mass" fractions that dictate material symmetry. Conversely, the traction-free boundary condition on the upper and lower surfaces (Eq. (4.1_2)) requires

$$t_a = -\mu\left(1 - \frac{1}{\lambda^2\Lambda^3}\right) \quad \forall r \in [0, r_o] \tag{4.11}$$

which reveals that the cell-mediated isotropic contraction stress must remain proportional to the (possibly evolving) isotropic matrix stiffness. Let us now consider two special cases defined by particular forms for the mass fractions.

First, consider a linear variation in material properties whereby $\varphi_{aniso}(r) = r/r_o$ and thus $\varphi_{iso}(r) = 1 - r/r_o$. In other words, we let the material exhibit an isotropic response at the center ($r = 0$) but a strongly transversely isotropic (circumferential) response at the periphery ($r = r_o$); at increasing radial positions between the center and edge we have an increasing transverse isotropy. Clearly, this choice of mass fractions satisfies the traction-free condition at the periphery. Radial equilibrium (Eq. (4.1_1)) thus requires, at all radial locations

$$-\mu\left(\frac{1}{\lambda^2\Lambda^3} - \frac{1}{\lambda^4\Lambda}\right) = \frac{c}{\Lambda}(\lambda^2 - 1) + t_c \; or \; t_c = -\mu\left(\frac{1}{\lambda^2\Lambda^3} - \frac{1}{\lambda^4\Lambda}\right) - \frac{c}{\Lambda}(\lambda^2 - 1) \tag{4.12}$$

with $\lambda < 1$ for contraction of the gel. Note, again, that the cell-mediated contraction stress must be proportional to matrix stiffness. Our final state of plane stress thus becomes

$$t_{rr}(r) = \mu\left(1 - \frac{r}{r_o}\right)\left(\frac{1}{\lambda^2\Lambda^3} - \frac{1}{\lambda^4\Lambda}\right), \quad t_{\vartheta\vartheta}(r) = \mu\left(1 - \frac{2r}{r_o}\right)\left(\frac{1}{\lambda^2\Lambda^3} - \frac{1}{\lambda^4\Lambda}\right) \tag{4.13}$$

which can be written equivalently as,

$$t_{rr}(r) = \mu\left(1 - \frac{r}{r_o}\right)\left(\frac{\lambda^4}{J^3} - \frac{1}{\lambda^2 J}\right), \quad t_{\vartheta\vartheta}(r) = \mu\left(1 - \frac{2r}{r_o}\right)\left(\frac{\lambda^4}{J^3} - \frac{1}{\lambda^2 J}\right) \tag{4.14}$$

where $J = \det \mathbf{F} = \lambda^2\Lambda$ is the aforementioned measure of volume changes. It can be shown numerically, as would be expected in this traction-free problem, that one obtains a "residual stress type" distribution of stresses wherein regions of compression balance those of tension (cf. [90]). This type of stress field is also seen in the second case, which is considered in more detail below.

Second, consider an exponential radial variation in material symmetry, namely let $\varphi_{aniso}(r) = \exp[n(r/r_o - 1)]$ and therefore $\varphi_{iso}(r) = 1 - \exp[n(r/r_o - 1)]$. Albeit involving slightly more algebra, one finds a result similar to that for the linear radial variation in symmetry. Specifically, radial equilibrium requires

$$t_c = -\left(\frac{r}{r_o}\right) n\mu\left(\frac{1}{\lambda^2\Lambda^3} - \frac{1}{\lambda^4\Lambda}\right) - \frac{c}{\Lambda}(\lambda^2 - 1) \tag{4.15}$$

which reveals that the anisotropic contribution of active cell stress must now vary radially as well. The overall plane state of stress can thus be written

$$t_{rr}(r) = \mu\left(1 - e^{n(r/r_o - 1)}\right)\left(\frac{\lambda^4}{J^3} - \frac{1}{\lambda^2 J}\right),$$

$$t_{\vartheta\vartheta}(r) = \mu\left(1 - (1 + nr/r_o)e^{n(r/r_o - 1)}\right)\left(\frac{\lambda^4}{J^3} - \frac{1}{\lambda^2 J}\right). \tag{4.16}$$

Figures 4.1 through 4.4 show illustrative parametric studies for $n = 10$, which pushes the transversely isotropic contributions to matrix stiffness and cell contractility towards the periphery. Specifically, Figure 4.1 shows radial distributions of stress, normalized with respect to the material parameter μ, for multiple degrees of contraction ($\lambda = 0.6, 0.5, 0.4$) and a representative fixed value of $J = 0.25$, (i.e., a 75% loss of volume upon contraction). Figure 4.2 similarly shows associated radial distributions for a 50% contraction ($\lambda = 0.5$) for multiple possible values of volume change ($J = 0.75, 0.50, 0.25$). Although these results – particularly, the existence of a self-equilibrating residual stress field – are qualitatively similar to those for the case of linear radial variations in material properties (not shown), focusing the anisotropy near the periphery creates stronger gradients in the distribution of stress.

If we introduce the non-dimensional parameter $\Gamma = c/\mu$, then distributions of cell-induced active stress can also be normalized by the Blatz-Ko modulus μ and plotted as a general function of radius. Figure 4.3 shows results similar to Figure 4.1 (i.e., $J = 0.25$ and multiple degrees of overall contraction of the gel), except for levels of isotropic and oriented cell contractility that yield $\Gamma = c/\mu = 1$. Figure 4.4 shows results

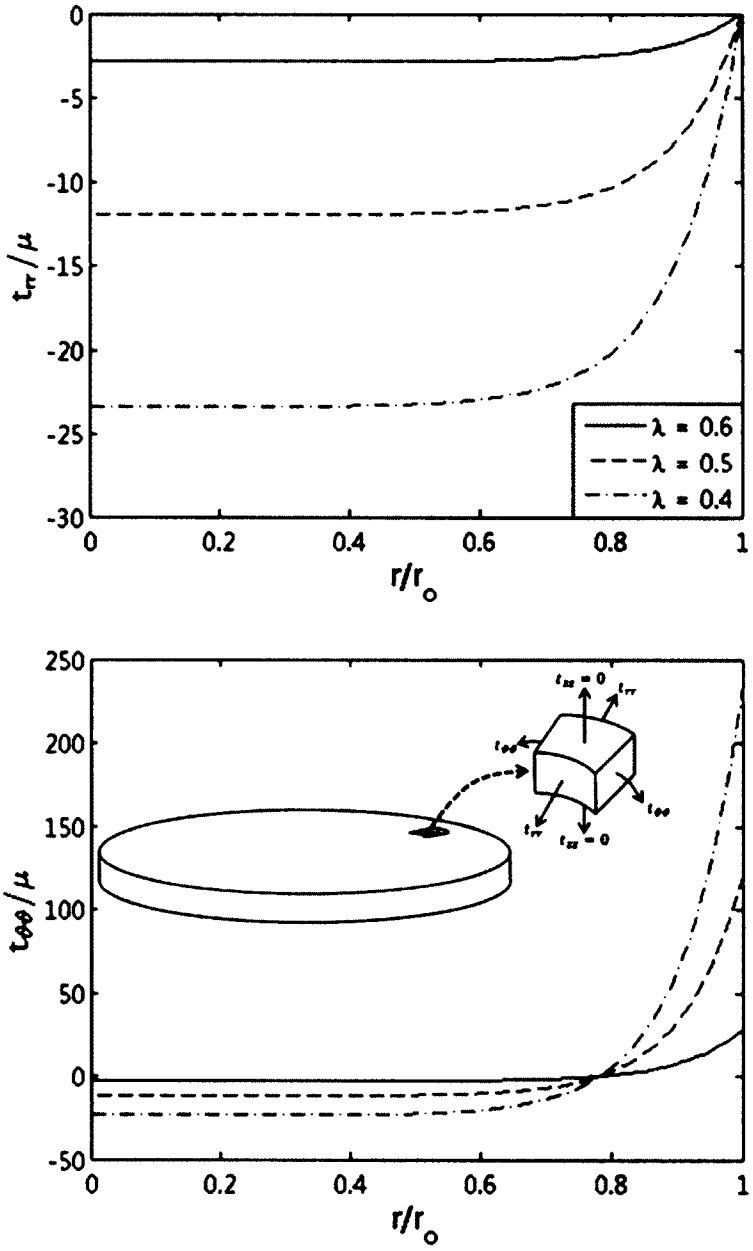

Figure 4.1: Stress distributions for different stretches. Predicted spatial distributions of radial (top) and circumferential (bottom) Cauchy stress, normalized by the isotropic matrix stiffness μ, in a model fibroblast-seeded thin collagen gel for an exponentially varying radial anisotropy (Eq. (4.16) with $n = 10$) and different degrees of contraction ($\lambda = 0.6, 0.5, \& 0.4$) for a fixed degree of volume change ($J = 0.25$). Note that the value of μ would be expected to evolve with increased contraction and that changes in volume should parallel changes in contraction; the present model allows both. Results are intended for illustrative purposes only, not to describe a particular experiment. The schema in the bottom panel shows the components of stress at a generic radial location.

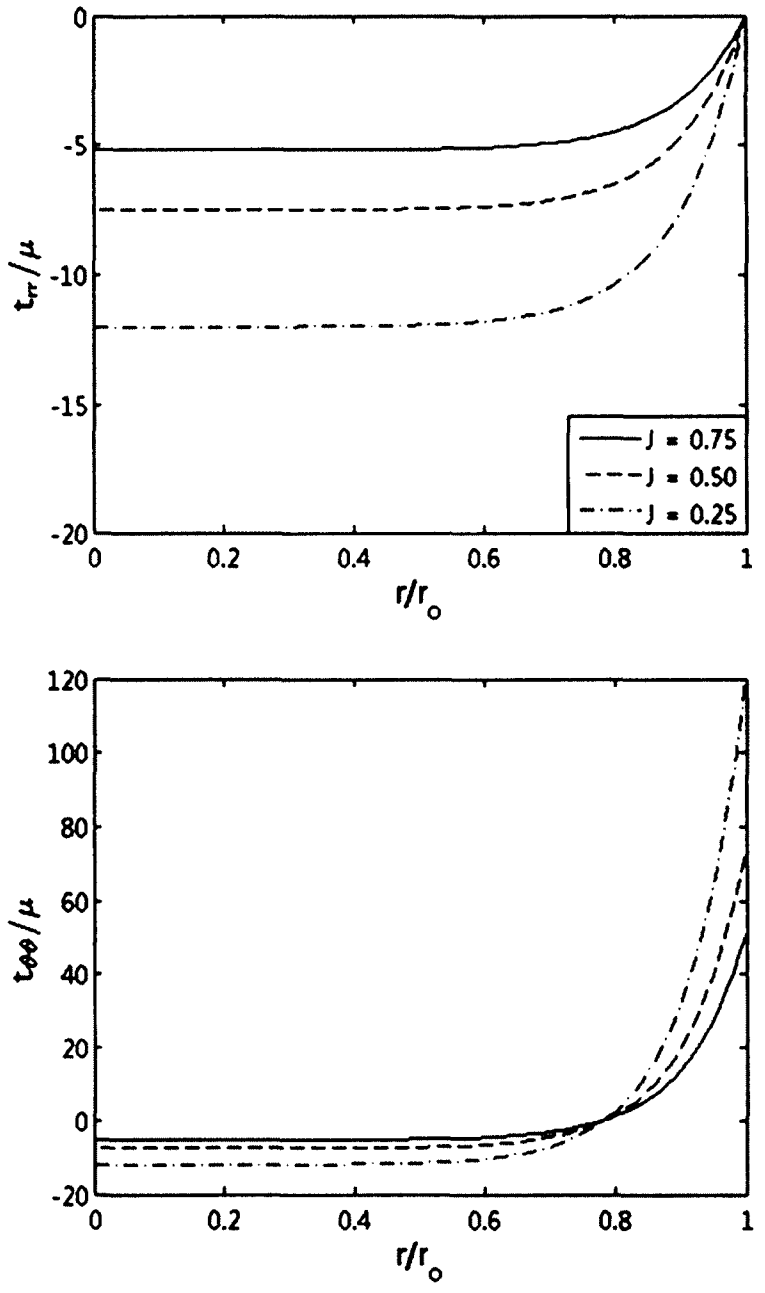

Figure 4.2: Stress distributions for different volume changes. Similar to Figure 4.1 except for different degrees of volume change ($J = 0.75, 0.50, \& 0.25$) at a fixed degree of contraction ($\lambda = 0.5$). See Eq. (4.16).

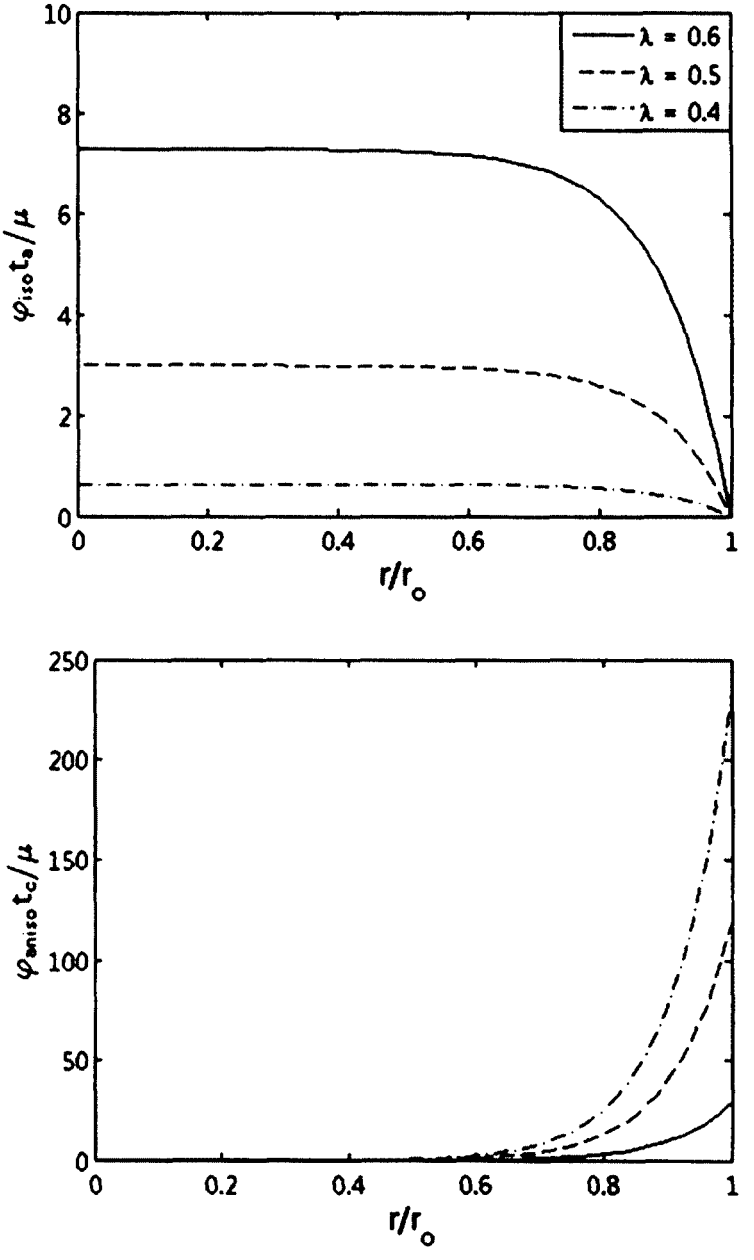

Figure 4.3: Distribution of cell stress for different stretches. Predicted spatial distributions of the isotropic cell stress given by Eq. (4.11) (top) and the transversely-isotropic (circumferential) cell stress given by Eq. (4.15) (bottom). Both stresses are normalized by the isotropic matrix stiffness μ, with $\Gamma = c/\mu = 1$, and are shown for different degrees of contraction ($\lambda = 0.6, 0.5, \& 0.4$) for a fixed degree of volume change ($J = 0.25$).

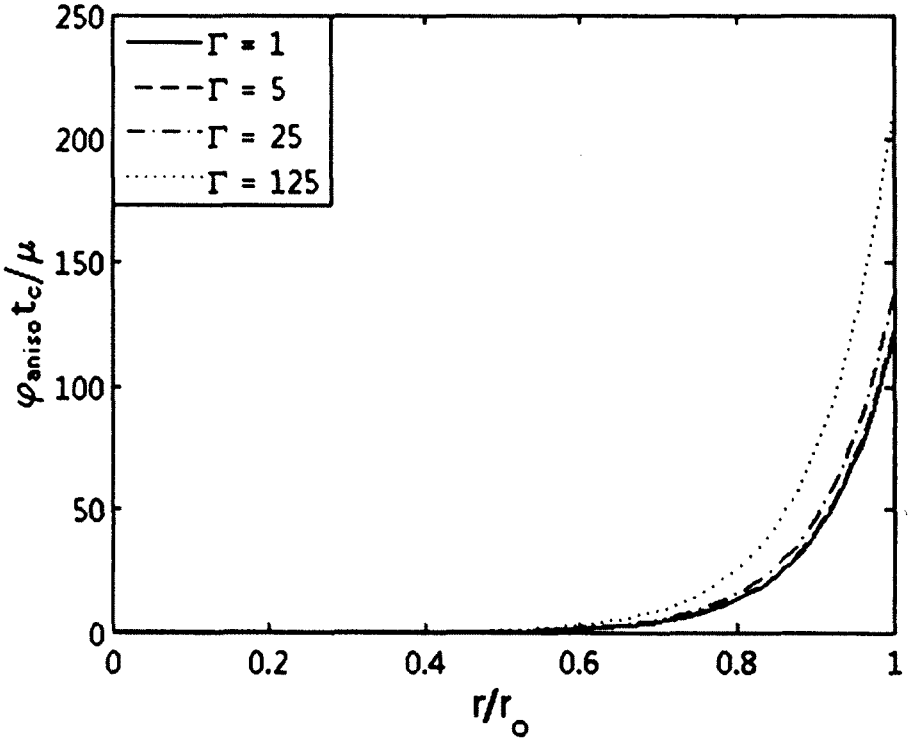

Figure 4.4: Transversely isotropic cell stress. Predicted distributions of the transversely-isotropic cellular stress (Eq. (4.15)) for different values of $\Gamma = c/\mu$ and a fixed contraction ($\lambda = 0.5$) and volume change ($J = 0.25$). Note that the results are not sensitive to the ratio $\Gamma = c/\mu$.

for $\Gamma = c/\mu = 1,5,25,125$, with $\lambda = 0.5$ and $J = 0.25$, which reveals that such results are not very sensitive to this parameter.

4.3.2 Experimental Findings

When cultured for 5 days, fibroblast-seeded collagen gels had a final normalized outer radius of 0.34±0.04 (mean ± SD), that is, a mean radial stretch ratio $\lambda = 0.34$ (Figure 4.5 Panel A, middle column). PSR-stained images of the gels revealed a dramatic change in organization of the collagen fibers from day 0 to day 5. Collagen fibers in the central region were randomly oriented at both day 0 and day 5 (Figure 4.5 Panel A, left column), but matrix compaction was much greater at day 5. In contrast, there was a stark difference in the organization of fibers at the outer edge at day 5 (Figure 4.5 Panel A, right column). Whereas the fibers were randomly oriented at the periphery at day 0, similar to the fibers within the central region, they showed a high degree of preferential alignment parallel to the outer edge (i.e., circumferential direction) at day 5 (Figure 4.5 Panel B). That is, there appeared to be an abrupt transition from a random to a preferred orientation near the periphery. Moreover, the collagen fibers near the periphery appeared red under polarized light, which suggested, more compacted, thicker, or more mature fibers.

The radial cut tests were consistent with a cell-mediated development of a residual stress field, with self-equilibrating tensile stresses at the periphery and compressive circumferential stresses within the central region of the gels (Figure 4.6). The associated "opening angles" were 20.60±6.42 degrees for days 1 through 5. In

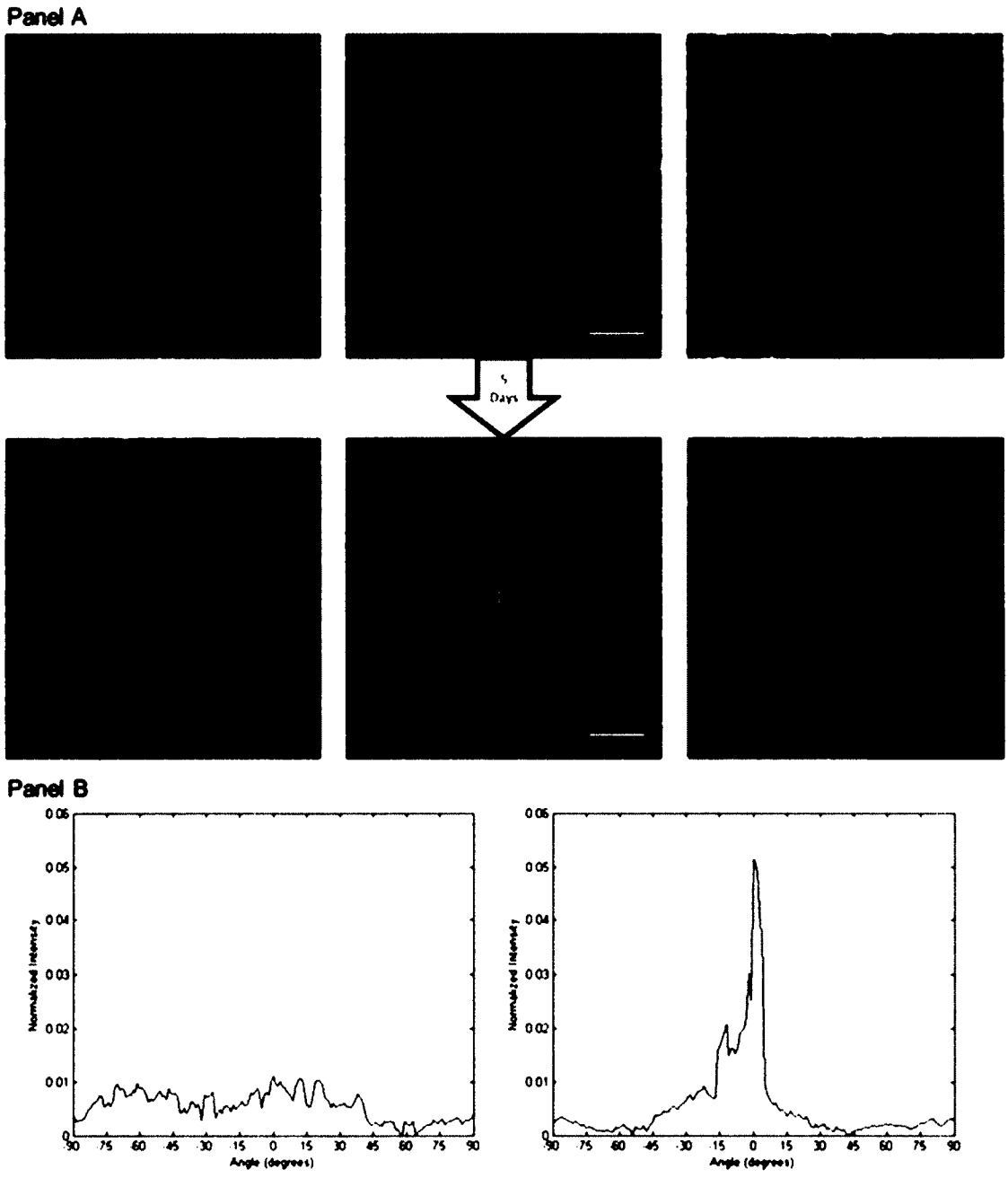

Figure 4.5: Collagen orientation. (Panel A) Circularly polarized light images of picrosirius red-stained sections (left and right columns) from gels at day 0 (top row) and day 5 (bottom row); the middle column shows the entire gel as viewed via the stereo microscope. Note further that the left column shows collagen in the central region of the gels, which compacts but retains its isotropic character at day 5. In contrast, the right column shows collagen at the periphery of the gels, which appears both compacted and aligned parallel to the edge at day 5. White scale bar is 5 mm and yellow scale bar is 50 μm. (Panel B) Assessment of collagen fiber orientation, using a 2D-DFT Power Spectrum, in the central region (left) and at the outer edge (right) of a cell-seeded gel at day 5. The results indicate a lack of preferred direction in the central region, but a high degree of circumferential alignment (shifted to angle 0) of fibers at the outer edge. For visual simplicity, the power spectrums were plotted for ±90 degrees about the measured dominant angle, which was shifted to 0 degrees.

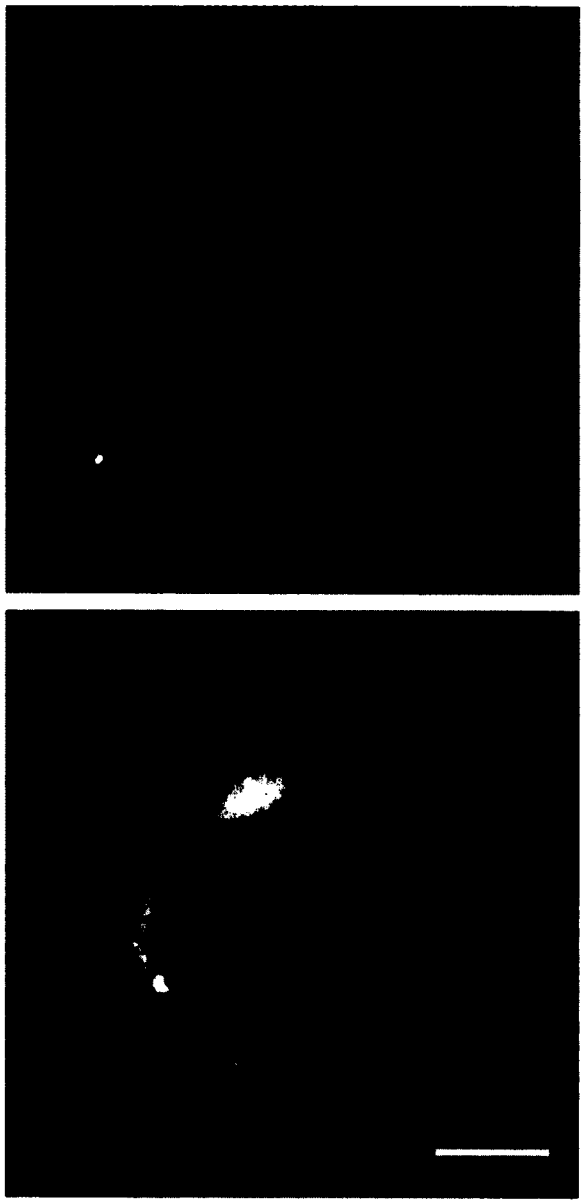

Figure 4.6: Free-floating FPCL opening angle. Collagen gels at day 2 either without (top) or with (bottom) fibroblasts shown 15 min after introducing a radial cut. Whereas the cell-free gels showed little to no appreciable opening angle, the cell-seeded gels exhibited considerable opening angles at all times examined (days 1 through 5) except day 0. Such opening angles are consistent with the radial cut relieving residual stresses, particularly tensile circumferential stresses at the periphery and compressive circumferential stresses in the central region. The scale bar is 5 mm.

contrast, the 0 day gels with cells showed no considerable opening angle, with measured values of 2.39±1.18 degrees (likely reflecting the width of the razor blade). Finally, gels without cells also exhibited no substantial opening angle, with values of 2.36±1.31 degrees (likely due to the thickness of the razor blade) measured at days 0 through 5.

The off-center biopsy punch tests were consistent with the development of equibiaxial compressive stresses in the central region of the cell-seeded gels (Figure 4.7). The punched holes at days 1 to 5 had measured diameters of 0.82±0.06 mm, whereas those at day 0 retained diameters of 1.00±0.03 mm. In gels without cells, the punched holes also maintained diameters similar to the outer diameter of the biopsy punch (1.03±0.06 mm vs. 1.05 mm) at days 0 to 5.

Sections stained with antibodies against αSMA and hematoxylin revealed an increase in cell density at the periphery of the 5 day cell-seeded gel, with a high degree of orientation parallel to the edge similar to that for the collagen (cf. Figures 4.8-A & B). Strong αSMA expression (brown) was present in most oriented cells, which suggested a phenotypic change from fibroblast to myofibroblast. Day 7 gels showed trends similar to the day 5 gels except that changes near the periphery were more dramatic (Figure 4.8-C). As noted in 4.2 Methods, some gels were cultured in the presence of exogenous TGF-β1. These gels compacted to a higher degree ($\lambda \sim 0.15$), but did not maintain an overall flat, disk-shaped geometry. As seen in Figure 4.8-D, the cells were even more highly aligned and densely packed at the periphery. The majority of cells at this edge were also positive for αSMA as were many of the cells in the central region.

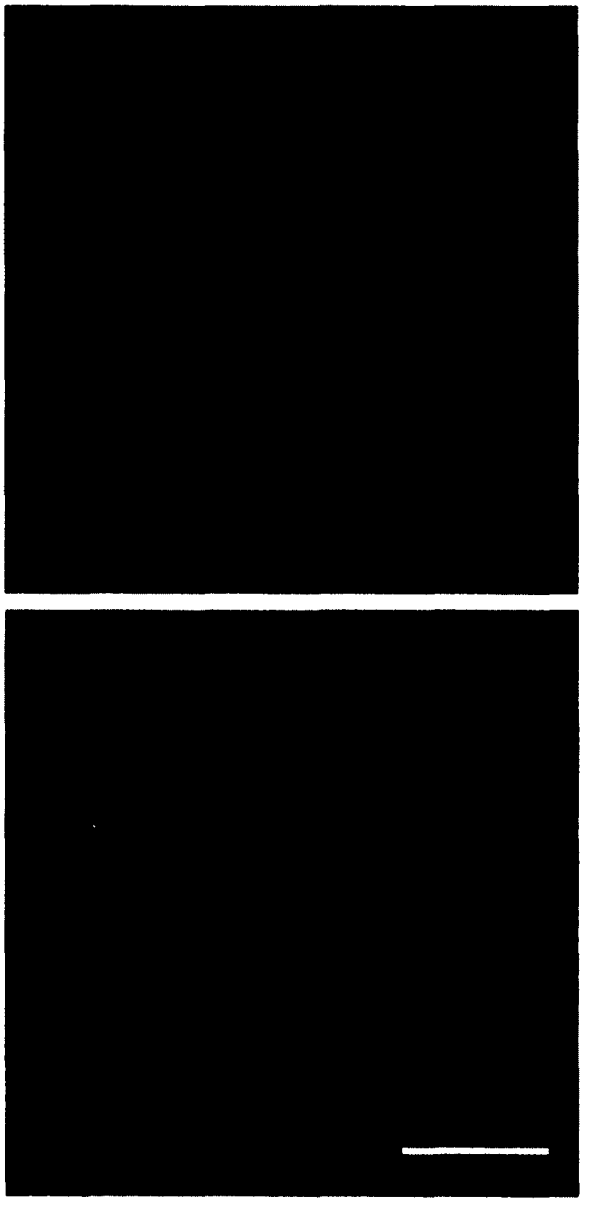

Figure 4.7: Free-floating FPCL equibiaxial compression assessment. Collagen gels at day 2 either without (top) or with (bottom) fibroblasts shown 15 min after introducing a circular hole in the central region. Whereas holes in the cell-free gels maintained dimensions similar to the biopsy punch, those in the cell-seeded gels closed in at all times examined (days 1 through 5) except day 0. Reduction in hole size while retaining a roughly circular shape is consistent with a nearly equibiaxial compressive stress field in the central region. The scale bar is 0.5 mm.

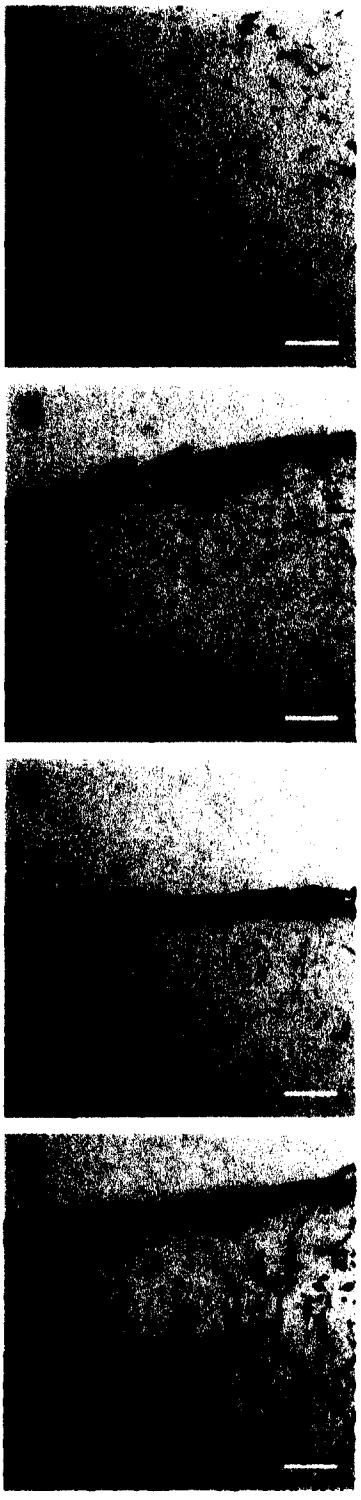

Figure 4.8: αSMA expression. Sections of collagen gels immunostained for αSMA and stained with hematoxylin. Brown indicates positive staining for αSMA and purple the cell nuclei. (A) Cells in the central region of a day 5 gel. (B) Cells near the periphery of a day 5 gel. (C) Cells near the periphery of a day 7 gel. (D) Cells near the periphery of a day 5 gel cultured with exogenous TGF-β1. Scale bars are 50 μm.

4.4 Discussion

The circular, free-floating fibroblast-populated collagen lattice (FPCL) studied theoretically herein was introduced experimentally over thirty years ago by Bell et al.[2]. Many investigators point to this work as possibly the beginning of tissue engineering. Regardless, free-floating gels have since been the focus of over one hundred studies of cell-matrix interactions (cf. [3]). It has been shown, for example, that the rate and extent of cell-mediated gel contraction depends on the initial density of the collagen, the initial density of the cells, and the availability of particular growth factors. It has also been shown that fibroblasts can contract gels consisting of type III collagen more rapidly and to a greater extent than those consisting of type I collagen [116] and, although exposed to the same biochemical milieu, fibroblasts from different tissues contract gels to different extents [133]. These and similar findings remind us that specific results depend on the particular experimental conditions. Nevertheless, many general findings have surfaced. Of particular interest herein, the initial remodeling and compaction of collagen is accomplished by fibroblasts repeatedly extending podial protrusions into the gel, attaching to the collagen via appropriate integrins, and retracting the collagen via actomyosin based mechanisms [27]; similar observations have also been reported by others in complementary experiments [133–135]. After a gel contracts significantly under typical conditions, fibroblasts within the outermost region begin to differentiate into myofibroblasts [116], a process that is typically characterized by the addition of αSMA to the stress fibers, the maturation of focal adhesions to larger "super" focal adhesions, and the ability to sustain a larger contractility [126]. Note, therefore, that increased matrix stiffness, mechanical stress, and the presence of cytokines that are typically present in

culture medium containing serum (e.g., TGF-β1), collectively represent a strong stimulus for fibroblasts to differentiate into myofibroblasts. One would expect, therefore, that significant tensile stresses develop in the outer region of the contracted gel as cells reorient and compact the collagen, which in turn could increase the stiffness locally and anisotropically. Indeed, it has also been reported that cell density tends to be higher in this outer region, with the cells preferentially aligned parallel to the free boundary and the collagen aligned with the cells [3,116]. These localized effects at the boundary can be particularly dramatic in gels having an initially high density ($> 6 \times 10^5$ cells/ml) of cells [27]. Conversely, it appears that cells within the central region of the gel retain their fibroblast phenotype, but experience increased apoptosis. Because normal levels of mechanical stress are thought to diminish apoptosis [120], the relative lower rate of apoptosis in the outermost region further supports the possibility of increased tensile stress in that region.

Interestingly, however, many investigators have assumed that free-floating fibroblast populated collagen gels remain stress free. For example, Grinnell wrote, "if the matrix is floating ... the matrix does not develop tension; that is, it remains mechanically unloaded"[4]. Albeit said in different ways, others have suggested similarly. Bride et al. wrote, "In contracting free floating collagen lattices, the tension is distributed isotropically and the extracellular matrix remains mechanically relaxed during contraction of the gel,"[120] whereas Tomasek et al. suggested that, "Mechanical tension cannot develop in untethered lattices."[5] More recently, John et al. used a thermoelastic analog (finite element) model to simulate a uniform contraction of homogeneous,

isotropic gels and similarly concluded that stresses remain minimal in free-floating gels [89].

Assuming that both the collagenous matrix and active cell stress are both uniform and isotropic, (i.e., $\varphi_{iso}(r) = 1$ with $t_a \neq 0$ and $t_c = 0$), our theoretical results (not shown) confirmed a possible non-trivial solution that allows compaction of a gel via a uniform zero-stress field whereby the active (tensile) cell stress balances everywhere the (compressive) stress in the matrix. This solution requires equal radial and axial deformations (i.e., $\lambda = \Lambda$). Because our measurements of radial contraction and axial thinning revealed that at every time considered (Figure 4.9), this special solution appears to be admissible mathematically, but not realized experimentally. In other words, we submit that free-floating collagen gels are not stress-free as suggested previously.

Using arguments of incompressible finite strain elasticity to model the initiation of contraction in free-floating gels, we previously showed that it is essential to respect in an associated mechanical analysis the reported observations of radial heterogeneities and thus to allow radial variations in both cell contractility and cell-mediated remodeling of the matrix [90]. Herein, we extended our prior results by allowing the gel to be compressible (cf. Figure 4.9). We again found that a residual-type plane stress field can develop whereby the outermost region experiences a tensile circumferential stress and the innermost region experiences a compressive circumferential stress; the radial stress was found to be everywhere compressive except at the periphery where it must vanish to satisfy a traction-free boundary condition (cf. Figures 4.1-4). This non-uniform stress field appears to be consistent with both our general understanding of cell mechanobiology [25,126–128] and observations from free-floating gel experiments

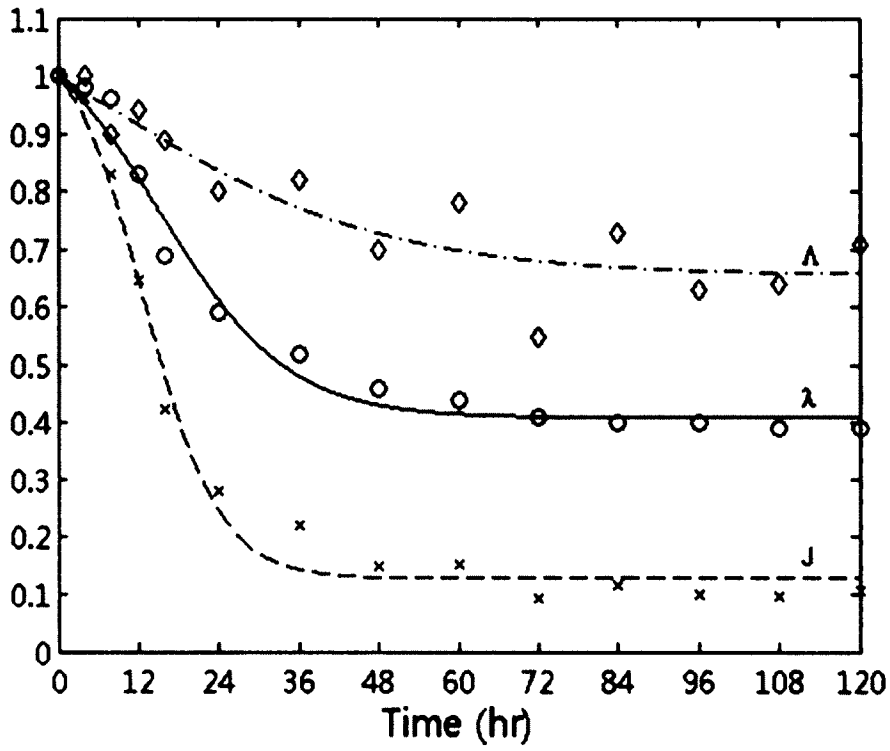

Figure 4.9: Free-floating FPCL geometric changes over time. Experimentally measured mean changes in gel thickness (open diamonds), radial contraction (open circles), and overall volume (x) over 5 days. Note the strongly compressible behavior and that changes in radial contraction and thickness were not the same (i.e., $\lambda \neq \Lambda$), which excludes the mathematically admissible solution of a uniform stress-free gel (see text).

[3,4,116]. Note, therefore, that cells in solution are initially stress-free when introduced within the initially stress-free gels. Substantial evidence now suggests that normally adherent cells seek to achieve and maintain a target level of stress [44], which in collagen gels appears to translate into a target level of tissue-level stress – a process that has been referred to as "tensional homeostasis" [43]. For example, fibroblasts in tethered collagen gels tend to develop and maintain stresses on the order of 4.5 kPa [65]. Interestingly, stresses at focal adhesions in fibroblasts similarly tend to be maintained at ~3 to 5.5 kPa [136], which is consistent from the perspective of traction continuity. We suggest, therefore, that the contraction of a free-floating gel by seeded cells is an attempt at tensional homeostasis. Because of the lack of tethering, however, the cells can only generate a residual-type stress field, which appears to be mechanobiologically more favorable for fibroblasts in the outermost portion of the circular gel where the stresses can be tensile. Indeed, it may be that, in combination with sufficient growth factors, it is the more favorable cell-generated mechanical environment within this outermost region that permits the fibroblasts to differentiate into myofibroblasts as observed by many. Because the fibroblasts in the central region experience only a small biaxial compressive stress, however, it appears that this encourages increased apoptosis, which again has been observed by many. That is, in contrast with the many prior suggestions that free-floating gels cannot develop any stress, our identification of a residual-type stress field is consistent with prior observations of aligned collagen and myofibroblasts near the periphery and nonaligned collagen and apoptotic fibroblasts in the central region.

The present histological results suggest that the transition from an isotropic central region to an anisotropic outer region may be abrupt, with circumferential

alignment of cells and fibers being highly localized to the outer edge of the gel. This steep gradient can be accounted for by our model by adjusting the parameter n in the exponential function for the "symmetry mass fractions," namely φ_{iso} and φ_{aniso}. Small values for n ($\sim$5) result in a gradual transition from an isotropic to anisotropic matrix whereas larger values of n can create a steep gradient that results in a highly localized anisotropic state at the outer edge (Figure 4.10).

Referring to early mechanical models of interactions between cells and the substrates on which they are cultured, Discher et al. suggested that "A major challenge in all such modeling is to clarify the principal enigma: how contractive traction forces exerted by a cell tend to increase with stiffness of the cell's substrate."[22] Although we did not address this particular experimental set-up herein, we found that for the class of deformation and constitutive behaviors considered, forcing cells to respect basic laws of continuum mechanics revealed that the level of contraction must be proportional to matrix stiffness to satisfy equilibrium and boundary conditions (cf. Eqs. (4.11) and (4.15) and Figures 4.3 and 4.4). Indeed, mathematical restrictions resulting from the axisymmetry, thinness, and traction-free surfaces enabled a complete closed-form solution without prescribing the specific functional form for the active stresses a priori. It appears, therefore, that the present solution, which suggests the development of a cell-mediated residual stress field, is consistent with both general observations and experiment-specific observations, including new findings herein that radially-cut gels open up as would be expected with the relief of residual stresses and that interior punched-holes close nearly uniformly as would be expected for a local equibiaxial compressive stress field (Figure 4.6 & 4.7).

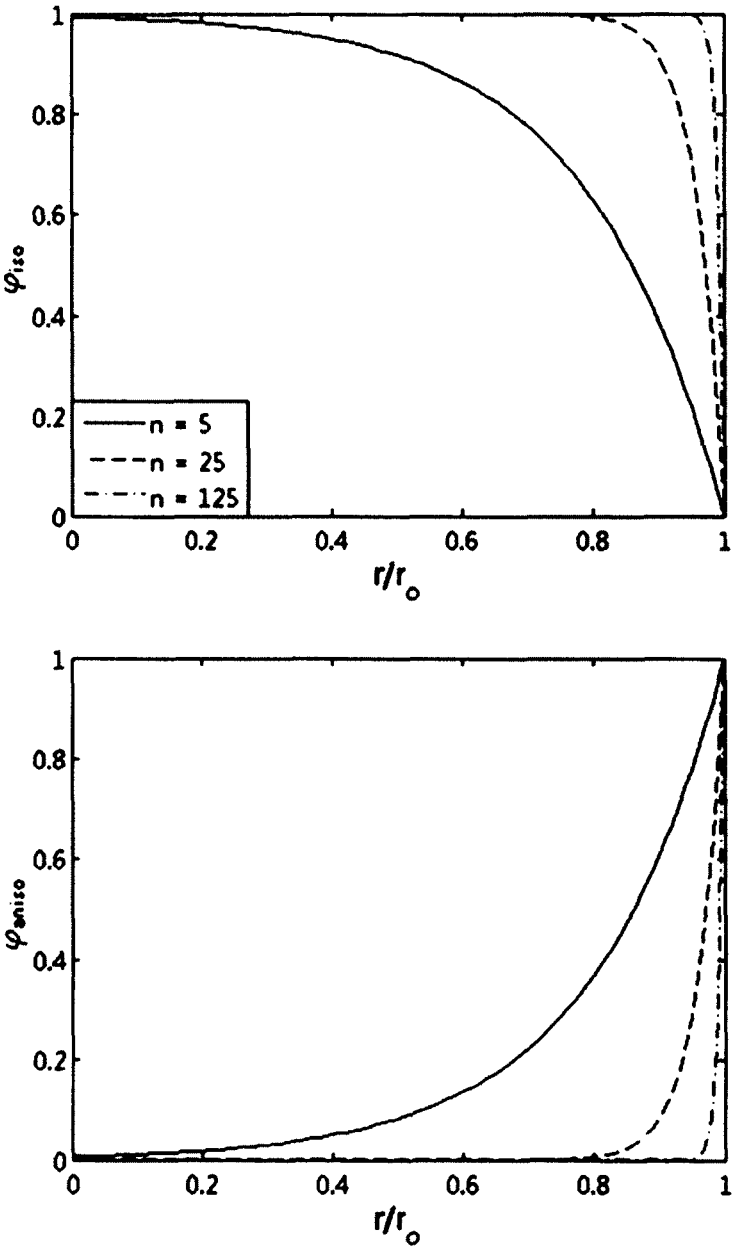

Figure 4.10: Radial distribution parameterization. Parameterization of n for the radially varying functions for material symmetry, φ_{iso} (top) and φ_{aniso} (bottom). Increasing values of n localize the anisotropy closer to the traction-free edge while satisfying equilibrium and boundary conditions, thus showing that changes from isotropy to transverse-isotropy can be both abrupt and highly localized to the outer edge.

In summary, most investigators agree that mechanics plays a central role in dictating cell behaviors in tissues and tissue equivalents, yet most prior papers on cell seeded gels have speculated on roles of the mechanics rather than considering the mechanics explicitly (cf. [122]). Not only can such speculations be ill founded, the mechanics can often expand our insight and enrich our understanding. Hence, we agree with Tomasek et al. that the "inescapable mechanical laws that are integral to the regulation of myofibroblasts"[5] and other mechanoresponsive cells must be considered.

Chapter 5: Tissue transglutaminase, not lysyl oxidase, mediates early calcium-dependent remodeling of fibroblast-populated collagen lattices

5.1 Introduction

Since its introduction in 1979 [2], the free-floating fibroblast-populated collagen lattice (FPCL) and its variants have been used in hundreds of studies to examine diverse aspects of cell-matrix interactions [3,91], including the relative effects of different matrix densities, cell concentrations, and cell types (e.g., neonatal versus mature, dermal versus cardiac). Complementary work using uniaxially constrained FPCLs has shown further that embedded fibroblasts actively seek to establish, maintain, or restore a preferred mechanical environment through a mechanism referred to as "tensional homeostasis" [43]. This endogenous tension appears to arise as the cells actively deform the matrix and then entrench the remodeled collagen, a process that can be repeated until the tension reaches the preferred level. The term "residual matrix tension" has been introduced to describe that part of the overall tension that remains after removing the active cell contribution at any degree of gel compaction [42]. The question remains, however, as to how the cells entrench the matrix deformations and develop this residual tension.

Various reports have directly assessed the contractile mechanisms and pathways that can affect the compaction of FPCLs (for a review, see [3]). Blocking calcium (Ca^{2+}) ion channels or inhibiting calmodulin can reduce or slow the extent of compaction [50]; inhibiting the Rho-kinase pathway can similarly impede the compaction [137,138]. Independent of the specific contractile pathway, entrenching the remodeled matrix would seem to be energetically favorable for the cells. Toward this end, covalently cross-linking

the collagen could entrench the induced deformations and thus tension. Two of the primary enzymatic crosslinkers of collagen are lysyl oxidase (LOX) and tissue transglutaminase (tTG). LOX oxidizes select lysines within collagen to form aldehydes that react to form covalent bonds and stabilize the molecules within fibers [39]. Absence of LOX-mediated crosslinking results in weak collagen fibers and fragile collagenous tissues [139]. tTG crosslinks a number of extracellular matrix proteins, including type I collagen, primarily through the formation of a Nε(γ-glutamyl)lysine bond between two molecules [140]. tTG has been shown to be a key player in wound healing and inflammation as well as in pathological states such as fibrosis and arthritis [141].

Although it has long been thought that the free-floating FPCL remains stress-free since it is traction-free [4,5], we recently showed that a residual-type stress field can both exist and explain many prior observations regarding differences in the matrix and cells between the central region and periphery of the gel [3,91]. We hypothesize, therefore, that although mechanical restrictions on the free-floating FPCL prevent most of the cells from establishing a homeostatic environment, they will nevertheless attempt to achieve tensional homeostasis. Hence, this common assay can be used to explore whether LOX or tTG, or both, play a role in the process of matrix remodeling and subsequent entrenchment.

5.2 Methods

5.2.1 Cell Culture and Preparation of Collagen Gels

NIH/3T3 fibroblasts (ATCC) were maintained in Dulbecco's modified Eagle's medium (DMEM) with 10% calf serum and 1% antibiotic/antimycotic (Life

Technologies) in a 37 °C, 5% CO_2 incubator. Cells were passaged at 70-80% confluence and cells from passages 4 to 8 were used for experiments. Collagen gels were prepared as previously described [91]. Briefly, for each gel, 146 μL of concentrated type I rat tail collagen (8.56 mg/mL, BD Biosciences), 200 μL of 5X DMEM, and 100 μL of a 10X reconstitution buffer (0.1 N NaOH and 20 mM HEPES, Sigma) were combined with 554 μL of the experimental culture medium (described in following subsection) containing 50,000 cells. The final 1 mL solution contained 50,000 cells and 1.25 mg of collagen; it was then cast into a single well of a 12-well plate and placed in the incubator for 30 minutes to gel. The casting solution for cell-free gels was the same minus the 50,000 cells. Gels were then suspended in 3 mL of their respective experimental medium and transferred to 35 mm dishes and allowed to float freely in the medium; they were cultured for up to 4 days with media replaced on day 2.

5.2.2 Experimental Conditions

The culture media used for experiments consisted of DMEM with 10% fetal bovine serum (HyClone), 10% porcine serum (Life Technologies), ascorbic acid (50 μg/mL, Sigma), $CuSO_4$ (3 ng/mL, Sigma), proline (50 μg/mL, Sigma), alanine (20 μg/mL, Sigma), glycine (50 μg/mL, Sigma), HEPES (0.01 M), basic fibroblastic growth factor (10 ng/mL, R&D Systems), platelet-derived growth factor (10 ng/mL, R&D Systems), and 1% antibiotic/antimycotic [142]. The additional amino acids constitute significant portions of the collagen structure while ascorbic acid is required to facilitate the hydroxylation of proline and lysine [143]. The additional growth factors are known to stimulate collagen production [144] and the $CuSO_4$ provides copper, which is necessary

for LOX activity [39]. Control gels were maintained in this media formulation (n = 30 for day 0, n = 22 for all other times).

To inhibit LOX, the media was supplemented with β-aminopropionitrile (BAPN; 100 or 1000 μM, Sigma; $n \geq 12$ for each treatment at each time) [41]. To inhibit tTG, the media was supplemented with either the non-specific, competitive inhibitor cystamine (100, 316, or 1000 μM, Sigma; $n \geq 9$ for each treatment at each time) [145] or the irreversible active site inhibitor Boc-DON (6 μM, Zedira; n = 10 at each time) [146]. Cell-free gels were also maintained in control media or media containing either 150 ng/mL LOX (Origene; $n \geq 10$ at each time) [147] or 67 mU/mL tTG (Sigma; $n \geq 10$ at each time) [145] to determine effects of crosslinkers alone. Gels were imaged at 24 hour intervals from 0 to 4 days (Figure 5.1A).

5.2.3 Cell Contractility and Matrix Entrenchment

Possible effects of matrix entrenchment and cell contractility on gel compaction were assessed by removing actively applied stress to the matrix by the cells. Cell-seeded gels were prepared and maintained as described above. At 24 hour intervals from 1 to 4 days, images were taken of the gels to determine radii before removing the deformations maintained actively by the cells. Specifically, TritonX-100 was added to the culture media to a final concentration of 1% (v/v) to lyse the cells [148]. After 30 minutes, another image of each gel was taken and the measured radii were compared to those before exposure to determine the percent radial dilation (Figure 5.1B). Other control gels were exposed for 30 minutes to either the calcium chelator ethylene glycol tetraacetic acid (EGTA; 4mM, Calbiochem) or the myosin II inhibitor blebbistatin (30 μg/mL,

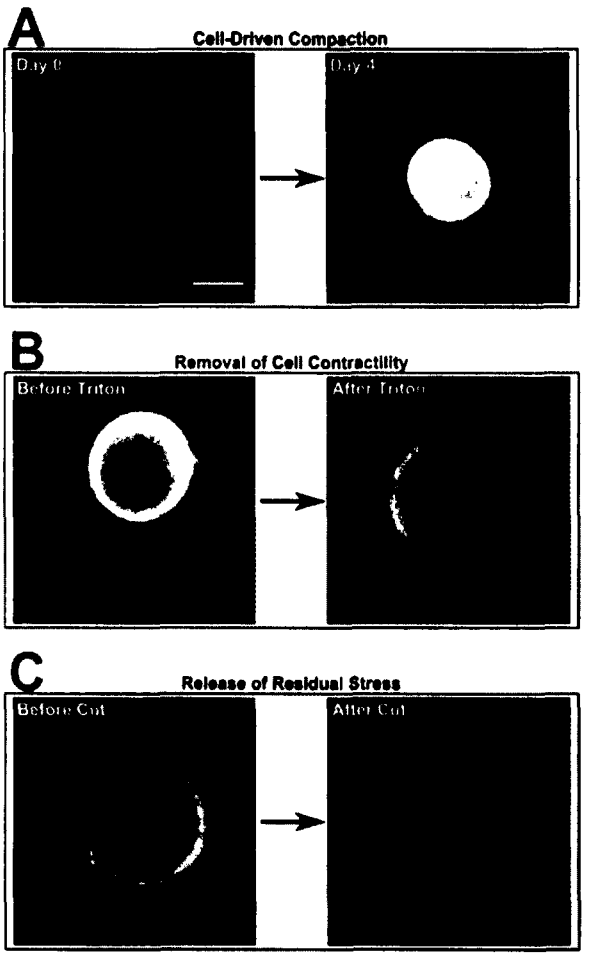

Figure 5.1: Experimental examples. Representative images of collagen gels illustrate three of the empirical manipulations. A) Seeding the gels with 3T3 fibroblasts resulted in significant compaction over the 4 days of observation (right), relative to day 0 (left). B) Exposure of a BAPN-treated (1000 μM), 4-day gel to TritonX-100 lysed the cells and resulted in a dilatation of the gel (right), relative to the state prior to treatment (left). C) Introduction of a radial cut within a 2-day control gel released residual stresses within the gel as evidenced by an "opening up" of the cut (right), relative the state prior to the cut (left). The bar in panel A denotes 5 mm and all images are at the same magnification.

Sigma) to assess roles of, respectively, Ca^{2+}-dependent contractility and myosin II in the active compaction of the collagen gels by the cells (n = 10 for all cases at each time). Although tTG is a calcium-dependent enzyme, the EGTA was only used acutely to sequester calcium during the assessment of contractility, not during the full duration of culture. Note, too, that Ca^{2+} is not required for cell adhesion to type I collagen, thus EGTA should not have caused cell detachment from the matrix [149,150]. Following administration of either EGTA or blebbistatin, images were similarly taken to assess radial dilation, then TritonX-100 was added to eliminate any remaining active cell contraction with further radial dilation measured, if any (n = 5 for each group). Matrix entrenchment and cell contractility were also assessed in gels treated with BAPN, Boc-DON, or cystamine via subsequent exposure to 1% TritonX-100 (n = 8 for all treatments at each time). After eliminating cell contractility, the gels were either used for the residual stress test (Figure 5.1C; described below) or discarded.

Matrix entrenchment was assessed as the percent overall radial Green strain, relative to day 0, that remained following elimination of cell contractility via treatment with TritonX-100; it was calculated using the following equation:

$$\%Entrench = \frac{{}^{1}/_{2}(\lambda_{Triton}^{2}-1)}{{}^{1}/_{2}(\lambda_{Before}^{2}-1)} \times 100 \qquad (5.1)$$

where λ_{Before} is the radial stretch ratio of the gel before TritonX-100 relative to day 0 and λ_{Triton} is the radial stretch ratio of the same gel 30 minutes after exposure to TritonX-100, also relative to day 0. This measure can thus be thought of as the percent overall radial strain relative to day 0 that remained after removal of cell contractility.

Note, for this metric of entrenchment, the circumferential Green strain could be employed as well as it is equal to the radial Green strain in the case of uniform radial compaction.

5.2.4 Residual Stress Test

As shown in [91], the introduction of a radial cut in a collagen gel can be used to assess the presence of a residual-type state of stress. A radial cut from the center to outer edge was introduced using a #10 scalpel blade in control and treated gels following the elimination of cell contractility using TritonX-100 (n = 8 for all cases at each time). Gels were imaged 15 minutes after the cut, and opening angles were quantified using ImageJ (Figure 5.1C).

5.2.5 Cell Viability

Cells were seeded at subconfluent (10,000 cells/well) or confluent (50,000 cells/well) levels in collagen I coated 96-well plates (BD Biosciences) and incubated for 4 hours to allow the cells to attach. After 4 hours, culture media was aspirated off and replaced with control media or media containing BAPN, cystamine, or Boc-DON and cultured for an additional 24 hours. Cell viability was determined using the XTT Cell Viability Assay (Biotium), which is reduced by metabolically active mitochondria. Cells maintained in control media alone served as positive controls; those maintained in control media but exposed to 1% TritonX-100 for 30 minutes served as negative controls as all the cells were lysed and rendered metabolically inactive. To ensure that differences in absorbance readings were not due to the chemical content of a given media formulation, the culture media from all wells was aspirated and replaced with fresh control media

before adding the XTT solution and activation reagent. The plate was then incubated for 4 hours before measuring absorbance at 490 nm and background absorbance at 655 nm (n = 12 for all cases at each seeding density). Background absorbance was subtracted from the measurement absorbance to correct for any nonspecific absorbance. These corrected absorbance measures were then normalized as follows:

$$Abs_{Norm} = \frac{Abs - \overline{NC}_{10k}}{\overline{PC}_{50k} - \overline{NC}_{10k}} \tag{5.2}$$

where Abs_{Norm} is the normalized absorbance, Abs is the background corrected absorbance for a sample, $\overline{NC}_{10k}$ is the mean background corrected absorbance of the negative control subconfluent wells (initially containing 10,000 cells), and $\overline{PC}_{50k}$ is the mean background corrected absorbance of the positive control confluent wells (initially containing 50,000 cells). Hence, $Abs_{Norm} \in [0,1]$, with a value of 1 indicating an absorbance equal to that for the positive control of 50,000 cells maintained in control media and a value of 0 indicating no living cells.

Note that comparing subconfluent versus confluent cultures helped delineate possible confounding effects of cell proliferation in contrast to metabolic activity alone. Moreover, the positive control for the normalization was selected as the positive control at the confluent density as it gave the largest measured absorbance of the two positive controls due to its higher cell density at 24 hours in culture. The negative control for the normalization was selected as the low density negative control as it had the lowest measured absorbance.

5.2.6 Statistical Analysis

All statistical analysis was performed using Minitab 16 (Minitab). ANOVA accounting for interaction was performed on the radial compaction, cell contractility, entrenchment, and opening angle data to determine effects of treatment and time, and on cell viability data to determine the effects of seeding density and treatment. For the radial compaction, the data were divided into 2 groups: control with LOX-inhibitors and control with tTG-inhibitors. If the interaction of treatment and time was determined to be significant, an ANOVA comparing treatments with the covariant of time was performed to ensure the significance of treatments while correcting for the effects of time. After ensuring significant differences, a one-way ANOVA was performed for a single treatment across all times or for a single time across all treatments. For the viability data, an ANOVA was performed for each seeding density across treatments. Significance ($p < 0.05$) was determined using a Bonferroni correction on the confidence interval, $\alpha = 0.05$. Significance is indicated within times for treatment versus control. All other comparisons are noted in the text and on the figures. Results are reported as mean ± SEM.

5.3 Results

5.3.1 Effects of Exogenous LOX and tTG on Compaction

Cell-free collagen gels maintained in control media showed little to no change in radial dimension (i.e., compaction) over 4 days of culture. The measured radii for LOX-treated (150 ng/mL) and tTG-treated (67 mU/mL) cell-free gels were normalized by their same-day control values, which revealed modest levels of compaction (<3%) that did not

change significantly from 1 to 4 days of culture. Specifically, normalized values at day 4 were 0.989±0.005 for LOX-treatment and 0.972±0.003 for tTG-treatment (cf. day 1 values shown in Figure 5.2). The tTG-treated group was nevertheless significantly different from both the control and LOX-treated groups, suggesting that, though minimal, tTG alone can compact collagen in the absence of cells, though not to the degree seen in cell-populated gels (cf. Figure 5.1A).

5.3.2 Cell Viability under Treatment

Cell viability was examined to determine whether treatment with inhibitors had a potential cytotoxic effect that could prevent gel compaction by impairing the cells rather than inhibiting the crosslinks. Figure 5.3 reveals for the subconfluent cells that all of the cystamine-treated groups exhibited significantly lower absorbance levels compared with the positive controls, thus suggesting either reduced metabolic activity or proliferation, or both. The 100 μM cystamine alone was significantly different from the negative controls, however, thus suggesting possible cytotoxicity only at 316 and 1000 μM cystamine. All other treatments at the subconfluent density were either comparable to the subconfluent positive control, thus indicating normal cellular activity, or had significantly higher absorbance levels, thus suggesting an increase in proliferation or possibly metabolic activity. Figure 5.3 reveals further for the confluent seeding density that only the 1000 μM cystamine group showed a significantly lower absorbance compared with the positive control. This group was yet significantly different from the negative control, thus suggesting that cells maintained some metabolic activity but likely experienced some cytotoxic effects from this level of cystamine treatment.

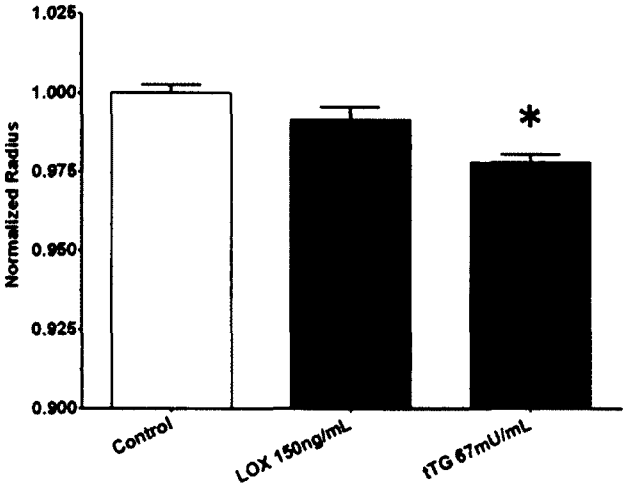

Figure 5.2: Effects of crosslinkers. Introduction of exogenous lysyl oxidase (LOX) and tissue transglutaminase (tTG) into cell-free collagen gels caused only modest compaction after 1 day (cf. Figure 5.4). Data are shown for 1-day gels, but results remained essentially unchanged over the 4-day study period. Bars indicate the standard error of the mean and the * denotes a significant difference ($p < 0.05$) compared with the day 0 untreated control.

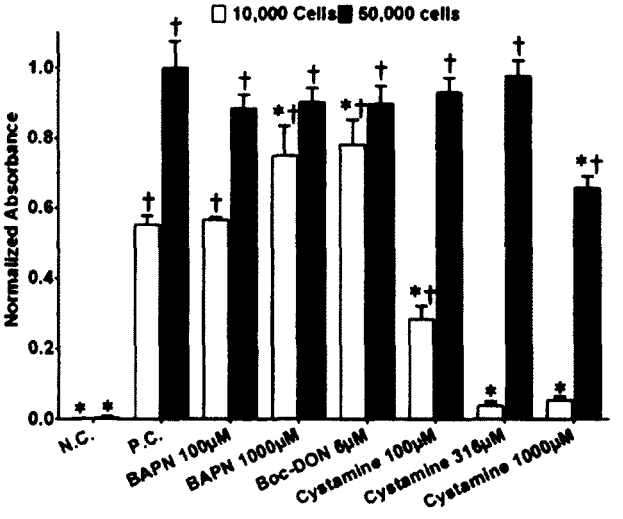

Figure 5.3: Cell viability under treatment. Normalized absorbance values from an XTT cell viability assay for sub-confluent (10,000 cells) and confluent (50,000 cells) seeding densities in 96 well plates, not within collagen gels. The † denotes a significant difference compared with the same seeding density negative control (N.C.), namely, cells lysed with TritonX-100; the * denotes a significant difference compared with the same seeding density positive control (P.C.), namely, untreated cells. Decreased values for the confluent groups (from 1) suggested varying degrees of treatment-induced cell death. Decreased values in the sub-confluent group (from ~0.55) suggested either cell death or reduced proliferation, the latter of which can be entertained based on the increased values in normalized absorbance in two cases relative to their positive control.

5.3.3 Effects of Crosslinker Inhibition on Compaction

Gels maintained in the control media showed the largest degree of compaction during the first day of culture (normalized radius of 0.656±0.023 on day 1 vs. 1.00±0.005 on day 0), with the rate of compaction slowing over the next few days but yielding a final normalized radius of 0.440±0.026 on day 4 (Figure 5.4). Recall that some gels were treated with BAPN to inhibit LOX throughout the 4-day study period. BAPN at 100 μM did not significantly change the extent of overall compaction compared with the control group at any time (Figure 5.4A). In contrast, the 1000 μM BAPN group appeared to reach a near steady level of compaction by day 2 (normalized radius equal to 0.545±0.19 on day 2 and 0.527±0.022 on day 4; Figure 5.4A), yet the day 4 gels alone were statistically different from control. These findings are consistent with the work of Redden and Doolin [41], which showed that LOX inhibition by BAPN only affects gel compaction after 2 to 3 days.

Gels were also treated with cystamine and Boc-DON to inhibit the activity of tTG throughout the 4-day study period. The 316 μM (Figure 5.5C) and 1000 μM (similar, not shown) concentrations of cystamine prohibited essentially any compaction of the collagen gels, consistent with possible cytotoxicity. In contrast, the compaction levels on days 1 and 2 were significantly different from the control for both the 6 μM Boc-DON (Figure 5.5A) and 100 μM cystamine (Figure 5.5B) treatments. By days 3 and 4, however, the normalized radial values for these two groups were not statistically different from the corresponding control values. These day 3 and 4 results suggested, therefore, that neither the 6 μM Boc-DON nor the 100 μM cystamine treatments inhibited the cells'

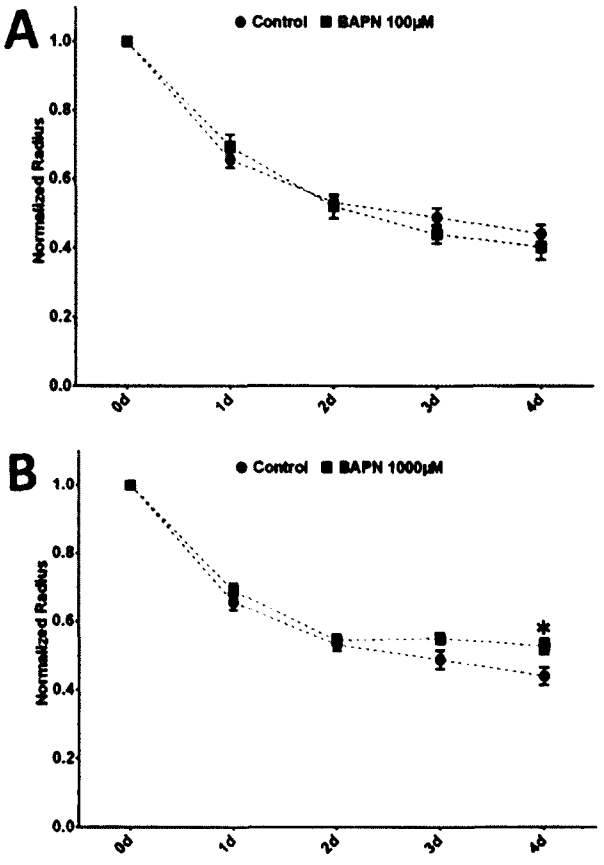

Figure 5.4: Effects of lysyl oxidase inhibition. Time course of fibroblast mediated compaction of collagen gels (i.e., outer radii normalized relative to day 0 starting values) over the 4-day study period for two concentrations of the lysyl oxidase inhibitor BAPN: A) 100 µM and B) 1000 µM. Error bars denote the standard error of the mean and the * denotes a significant difference compared with the same day control mean. BAPN had no effect on cell-mediated compaction over the first 3 days and only a modest effect on day 4 at the higher concentration.

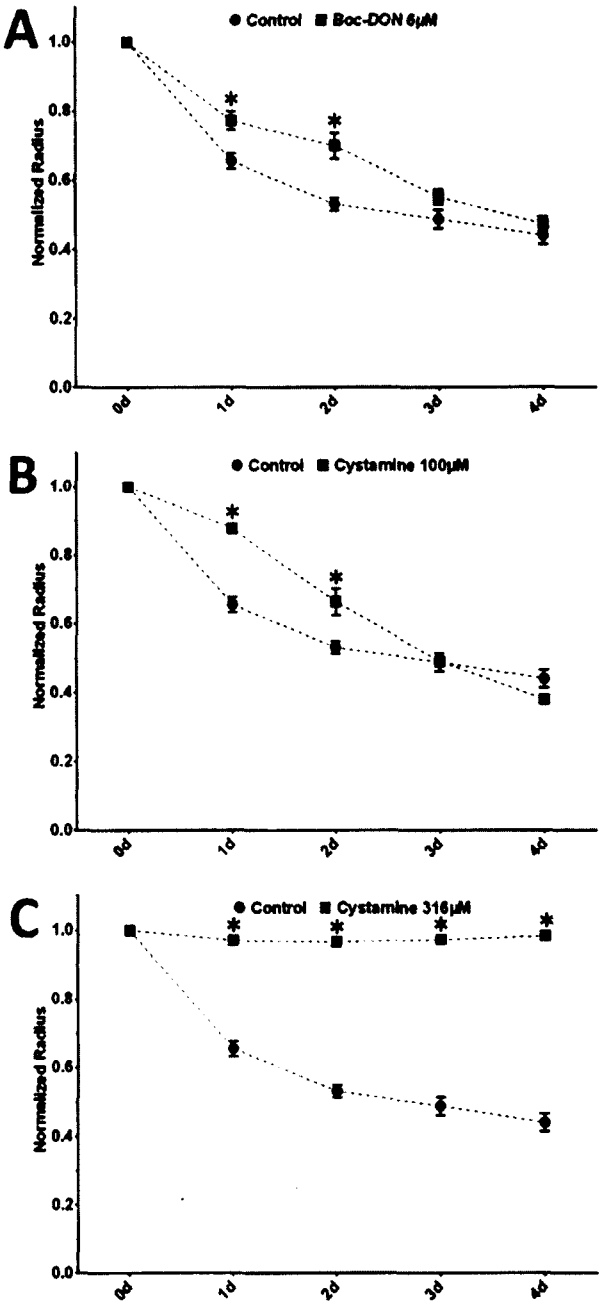

Figure 5.5: Effects of tissue transglutaminase inhibition. Similar to Figure 5.4 except for the time course of cell mediated gel compaction over the 4-day study period for two inhibitors of tissue transglutaminase, one of which was administered at two concentrations: A) 6 μM Boc-DON, B) 100 μM cystamine, and C) 316 μM cystamine. The * denotes a significant difference compared to the same day control. The Boc-DON and low concentration of cystamine consistently reduced compaction on days 1 and 2, relative to day 0 controls, though the gels achieved control values on days 3 and 4. In contrast, the high concentration of cystamine inhibited cell-mediated compaction on all days.

ability to compact the gels, hence suggesting further that collagen crosslinking by tTG plays a significant role during the early remodeling and compaction of the collagen gels.

5.3.4 Cell Contractility and Matrix Entrenchment

A 30 minute exposure to 1% TritonX-100 resulted in mostly uniform radial dilations of control gels at all times (from a minimum of 7.84±0.13% on day 2 to a maximum of 9.63±0.35% on day 4; Figure 5.6A). Dilation caused by a 30 minute exposure to the calcium chelator EGTA was maximal on day 1 (5.35±0.29%) and decreased to a minimum on day 4 (0.06±0.20%). In contrast, a 30 minute exposure to the myosin II inhibitor blebbistatin resulted in a minimal dilation on day 1 (2.33±0.13%) and a maximal dilatation on day 4 (7.67±0.36%). Subsequent exposure of the blebbistatin- and EGTA-gels to TritonX-100 resulted in final radial dilations that were not significantly different from those treated with TritonX-100 alone (not shown). These findings suggest that early (up to day 2) compaction may be driven primarily by rapid, Ca^{2+}-dependent contractions, while later cell contractility may be primarily Ca^{2+}-independent and more sustained.

Gels treated with crosslink inhibitors were also exposed to TritonX-100 at each time to assess that part of the compaction that was maintained by active cell contraction. The 316 μM cystamine group showed effectively no dilation when the cells were lysed, which was expected since no compaction was seen for this group (Figure 5.6B). The other experimental groups (1000 μM BAPN and 6 μM Boc-DON) showed no significant difference in dilation when compared with the same day controls, though the day 2 Boc-DON dilations trended to be smaller. The day 2 Boc-DON value was significantly

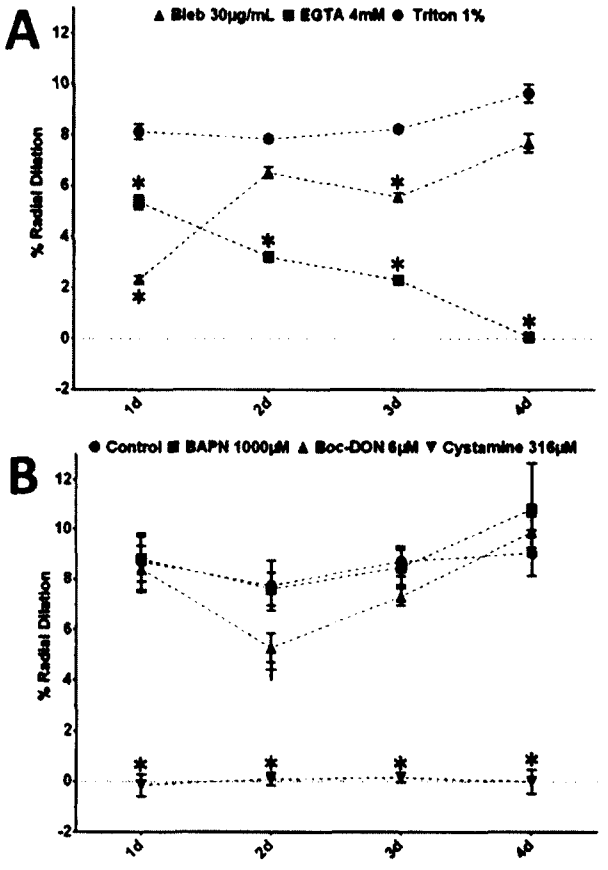

Figure 5.6: Dilation due to contractility release. The percent radial dilation (i.e., partial release of compaction relative to same day controls) is shown on each of the 4 days for two protocols. A) Control gels were exposed to blebbistatin to inhibit myosin activity, EGTA to chelate the calcium, or TritonX-100 to lyse the cells. B) Control gels and gels treated with either BAPN (to inhibit LOX) or Boc-DON or cystamine (to inhibit tTG) were exposed to TritonX-100. The * denotes a significant difference compared with the same day control mean. The † denotes a significant difference compared to the day 1, 3, and 4 day Boc-DON means.

different than Boc-DON-treated values at all other times, and similarly, the values of dilation for all groups trended smaller on day 2.

Matrix entrenchment amongst the control, 1000 μM BAPN, and 6 μM Boc-DON groups was not statistically different on any day, though the Boc-DON value trended lower than control and BAPN values on days 1 and 2 (Figure 5.7). The percent entrenchment for each group tended to increase from day 1 to day 2 or 3 with day 1 control (85.4±2.6%) and day 1 1000 μM BAPN (80.7±2.8%) being significantly different from days 2 through 4 (93.3±1.1% for control and 89.9±2.3% for BAPN on day 4), and day 1 Boc-DON (72.3±5.6%) being significantly different from days 3 and 4 (94.4±0.6% on day 4). These results suggested that tTG inhibition may reduce the rate of matrix entrenchment compared with controls.

5.3.5 Opening Angles

The presence of a residual stress field was assessed qualitatively by introducing a radial cut, from the center to the outer edge of a gel, following the elimination of cell contractility using TritonX-100 and measuring any appreciable opening angle. Day 0 gels showed small opening angles (4.5±1.0°; Figure 5.8), with the majority of any angle presence likely due to the width of the cutting blade. This observation suggests there is little to no residual stress present within the gels immediately after casting. Gels treated with 316 μM cystamine had opening angles on all four days that were not significantly different from the day 0 controls, again consistent with possible cytotoxicity. In contrast, the day 1 control gels exhibited significant opening angles (22.6±1.2°), which suggests the development of a tensile circumferential stress at the outer edge and compressive

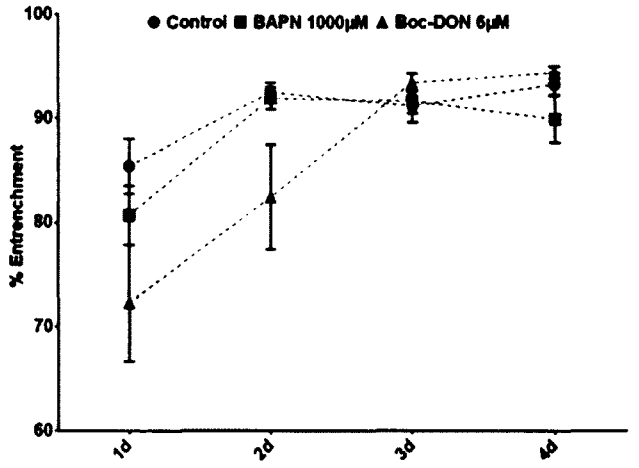

Figure 5.7: Matrix Entrenchment. Time-course of the percent gel compaction that was entrenched (i.e., not recovered upon removal of active cell tension by lysing the cells with TritonX-100) on each of the 4 days of study for three groups: control, BAPN-treated, and Boc-DON-treated. Entrenchment was quantified as the percent change in the total radial Green strain due to TritonX-100 treatment relative to day 0. Note that 316 μM cystamine group not included as little to no compaction was measured for this group compared to day 0 gels.

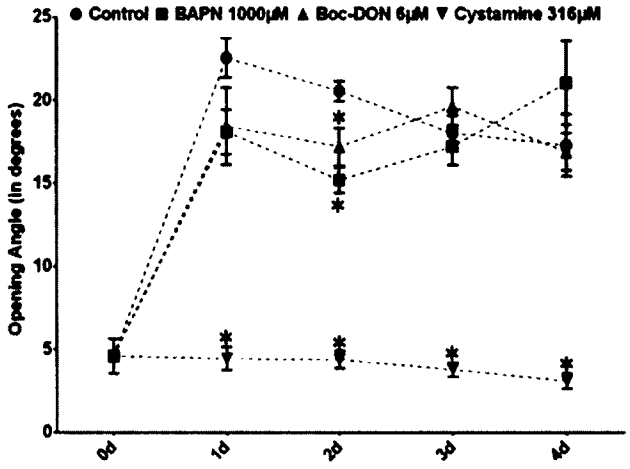

Figure 5.8: Opening Angles. Time course of radial-cut related opening angles (cf. Figure 5.1C) over the 4-day study period for four groups: control, LOX-inhibited (BAPN) and tTG-inhibited (both Doc-DON and high concentration cystamine) gels. The * denotes a significant difference compared with the same day control. Surprisingly, the treatments with BAPN and Boc-DON had similar effects at all times; in contrast, treatment with 316 μM of cystamine disallowed any matrix remodeling and associated development of residual stress. The value of 5 degrees for the opening angle likely represents the width of the cut alone, and can be considered to be an experimental offset.

stress within the central region of the gels. The opening angles tended to decrease slightly from day 1 to day 4 (17.3±1.9°) with day 3 and 4 values being significantly different from day 1. Finally, gels treated with 1000 μM BAPN and 6 μM Boc-DON had opening angles that tended to be lower on days 1 and 2, with the day 2 values being significantly different compared with the control value (20.6±0.6° for control compared with 15.2±0.8° for BAPN and 17.2±1.1° for Boc-DON). Results from the BAPN and Boc-DON groups were not different from the controls on days 3 and 4.

5.4 Discussion

The development, maintenance, remodeling, or repair of collagenous tissues results from de novo deposition of new matrix, remodeling of extant matrix, or both. Both of these mechanisms require cells to actively work on the matrix via actomyosin activity and integrin engagement. As shown many years ago by Paye et al. [125], however, fibroblasts tend not to synthesize matrix when compacting initially stress free collagen gels. Rather, these cells appear first to actively deform the matrix and "lock-in" or entrench such deformations in an incremental fashion. Such entrenchment can change the overall geometry and material properties of the matrix, which dictates the local mechanical environment in which the cells reside. With regards to in vitro studies using the FPCL, extensive work has revealed intracellular mechanisms [2,3,27,151,152] and cell-matrix interactions via integrins [32,45–49] that are necessary for cells to deform their surrounding matrix. An important question, however, has been how the cells, after deforming the matrix, entrench the applied deformations and thereby develop or attempt

to develop a preferred mechanical environment that does not require continued actomyosin activity and thus energetic expenditures to maintain.

Direct application of tissue transglutaminase or lysyl oxidase to cell-free gels showed that tTG, but not LOX, was capable of modestly, yet significantly, compacting the collagen in the absence of cells. This finding suggested that the initial collagen matrix had available binding sites for tTG but not LOX, or else that LOX-induced changes require cell mediation. This latter finding is consistent with the primary role of LOX to support the consolidation of collagen molecules and fibrils into fibers following new deposition by cells [39], noting that the initial collagen used in the gel seeding was already at a fiber diameter. It would be expected that LOX could affect cell-free gel compaction if pepsin-degraded collagen was used, which would allow LOX-aided fibril consolidation.

Roles of tTG in the remodeling of collagenous tissue have been examined in vivo using diverse animal models. Of note is small artery remodeling following a ligation-induced reduction in flow, which was studied using either tTG inhibition in normal rats [145] or lack of expression in a $tTG^{-/-}$ mouse [153]. As expected, low flow controls exhibited extensive remodeling and had reduced vessel diameters after only two days. Inhibition of tTG and lack of tTG expression both resulted in vessel diameters comparable to normal flow controls despite the low flow conditions, thus suggesting the importance of tTG in early arterial remodeling to restore preferred wall shear stresses. Our results are consistent with these findings as tTG inhibition in the absence of cytotoxicity slowed early matrix remodeling, that is, the remodeling of the gels on days 1 and 2 (Figure 5.5). Note, too, that it was also shown in [153] that $tTG^{-/-}$ vessels had

nevertheless remodeled after 7 days to levels similar to those of the low flow controls, thus revealing a longer-term (compensatory) mechanism to reestablish the preferred flow conditions independent of tTG. Our 3 and 4 day results showed a similar compensation as the measured radii for the tTG-inhibited gels were comparable to controls on those days. We note, of course, that endogenous LOX was not inhibited in the tTG-inhibited gels.

tTG activity has also been shown to play a role in some cell-matrix interactions [141,154]. In its closed confirmation, extracellular tTG can attach to fibronectin and aid in cell adhesion to these substrates through α_v integrins. With regard to type I collagen, however, there has not been any report of tTG aiding or being necessary for fibroblast adhesion via β_1 integrins. Conversely, it has been shown that proteolysis of extracellular tTG may increase the binding affinity of $\alpha_1\beta_1$ integrins to type I collagen [154]. It appears, therefore, that inhibition of tTG in collagen lattices should not induce cell detachment, which could slow or inhibit gel compaction.

With regard to lysyl oxidase, Redden and Doolin showed that inhibition via 1000 μM BAPN treatment had little effect on matrix compaction by adult human lung fibroblasts during the first two days of treatment [41]. After day 2, however, gel compaction either stalled or the gels dilated before compaction resumed by day 4. They concluded that the matrix compaction was bimodal with later (after day 2) compaction requiring de novo collagen synthesis facilitated by LOX activity. Our results followed a similar trend for the same concentration of BAPN, with treated gels being significantly larger than controls on day 4. While our results with regards to LOX inhibition coincide with this prior study, our results related to tTG inhibition are consistent with tTG-

mediated crosslinking contributing to early remodeling, which is not due to cell contraction alone.

We wanted to ensure cell viability for all of our experimental conditions. Of greatest concern was the treatment of cells with cystamine [146]. At low seeding densities, all concentrations of cystamine showed significantly lower signal compared with the positive control (cf. Figure 5.3). Because differences in cell number can influence the overall signal measured, the low values of absorbance may have only indicated an attenuation of cell proliferation by cystamine. Results from the higher seeding density would seem to support this possibility as the absorbance signal for the low and middle concentrations of cystamine were statistically the same as the positive control. This finding is concerning with respect to some reports in the literature, however, as use of cystamine to inhibit tTG either in vivo or in vitro may confound the desired results. Cells treated with high levels of cystamine may stop proliferating, have reduced metabolic activity, or be induced to undergo apoptosis. Such effects would result in less active cells compared with control groups and thus make it difficult to determine if differences between controls and cystamine-treated groups were due to tTG inhibition or just a reduced cell number or cell activity. The Boc-DON results herein were thus preferred as indicators of tTG inhibition.

Cell contractility plays a key role in the compaction of FPCLs. Before the matrix can be crosslinked in a new geometry, it must first be actively deformed by the resident cells. We used 30 minute exposures to 1% TritonX-100 to lyse the cells (cf. Appendix B, Figures B.1 and B.2) and thereby assess the contribution to compaction by the actively applied cell tension. Regardless of treatment, the resulting dilations following

administration of TritonX-100 were not significantly different across experimental groups at any time. Note, therefore, that it has been shown experimentally that the stress actively applied by a cell on its substrate increases with increased substrate stiffness [22]. Indeed, it has been shown mathematically for the free-floating FPCL that the actively applied cell stress must be proportional to the matrix stiffness [3,91]. It is possible, therefore, that matrix stiffness was comparable, at least over most of the gel, regardless of the degree of entrenchment achieved in this study. Alternatively, if the bulk stiffnesses were different at different levels of compaction, the applied cell stresses would also be different as well. For example (cf. Figure 5.8), the 6 μM Boc-DON treated gels showed less overall compaction on day 1 compared with the control and 1000 μM BAPN gels, indicating less remodeling and, likely, lower bulk stiffness. The deformations associated with the applied cell stress were statistically equal, however. Hence, if the matrix stiffness is lower in the day 1 Boc-DON treated gels but the cell-associated deformations were the same across all treatments, the applied cell stresses would be lower in the less compact Boc-DON treated matrices.

We also examined the mode of cell contractility via acute exposure to EGTA, to sequester Ca^{2+}, or blebbistatin, to inhibit myosin II. Results from these experiments suggested a temporal variation in the primary mode of cell contractility. While day 1 appeared to be dominated by a Ca^{2+}-dependent activity, days 2 to 4 appeared to be dominated by a Ca^{2+}-independent pathway, perhaps mediated by Rho-kinase since the day 4 data showed essentially no acute effects of Ca^{2+} removal. The results from days 1 and 2 are consistent, however, with an interplay between Ca^{2+}-dependent and Ca^{2+}-independent modes of contraction, as reported by Castella et al. [155]. They showed that

a single myofibroblast in 2D culture can utilize both modes of contraction: Ca^{2+}-independent contraction to maintain tension on the culture surface and Ca^{2+}-dependent contraction to apply small deformations to the surrounding matrix. The model they proposed suggests that a sustained contraction via the Rho-kinase pathway allows the cell to locally unload the matrix tension whereas Ca^{2+}-dependent contractions allow the cell to reorganize the unloaded matrix or orient newly deposited material. Our results similarly suggest that both modes of contractility may be present, perhaps with one dominating at different times during compaction, though we did not directly examine the associated signaling pathways.

By day 4, removal of Ca^{2+} had no appreciable effect with regards to the removal of cell contractility while the result for inhibition of myosin II was statistically the same as that for the TritonX-100. Multiple factors may affect this result, including possible apoptosis [156,157], likely in the central compressive region of the gel, as has been suggested previously [91,156]. Conversely, the cells at the outer edge of the gel may begin to differentiate into myofibroblasts [3,62,91,116] (see Appendix B, Figure B.3), which have been shown to maintain contractility via the Rho-kinase pathway [158].

The opening angle results indicate if there is radial compaction of the gel, there is development of a residual stress field. At all times, the BAPN and Boc-DON treated groups had similar opening angles even though the overall amounts of compaction may be different. For example, at day 2, the opening angles for each group are similar while the overall compaction is different. This does not necessarily mean that both groups had similar stress fields. To determine what may give rise to this phenomenon, 2 day gels that were cultured in control media and gels treated with either BAPN or Boc-DON were

examined histologically and stained with picrosirius red. The gels were imaged under circularly polarized light to show only birefringent collagen. Day 2 gels for both treatment groups and controls showed similar levels of collagen alignment at the outer region (Appendix B, Figure B.4). The picrosirius red images also show that the fibers in the control and BAPN gels at the outer edge are thicker and denser compared to the Boc-DON group which likely leads to stiffer material behavior. The similar matrix alignment may allow for the different groups to have similar opening angle values even when the degree of compaction is different and bulk material properties are likely different as well.

Based on our general observations (Figure 5.9), we propose a possible timeline for free-floating FPCL remodeling. Cells are initially cast in a dilute collagen gel with little to no mechanical stress. As previously noted, work by Brown et al. [43] and Mizutani et al. [159] suggests that the cells seek to establish or maintain a preferred mechanical state via a process referred to as "tensional homeostasis." Initially being at a zero stress state, the cells likely seek quickly to develop stress within the matrix, which in turn could stress the cells themselves. Following a time lag in which cells are initially adhering to and spreading within the matrix, they will begin contracting to stress the surrounding matrix, which begins the process of compaction because of the traction-free boundary conditions. Ca^{2+}-dependent contractility may be initially utilized during this early, rapid deformation and reorganization of the collagen; the Rho-kinase pathway could also be engaged to allow the cells to sustain the local deformation while utilizing Ca^{2+}-dependent contractions to reorganize the surrounding collagen [155]. To entrench the incrementally achieved deformations, the fibroblasts appear to use tTG early on to

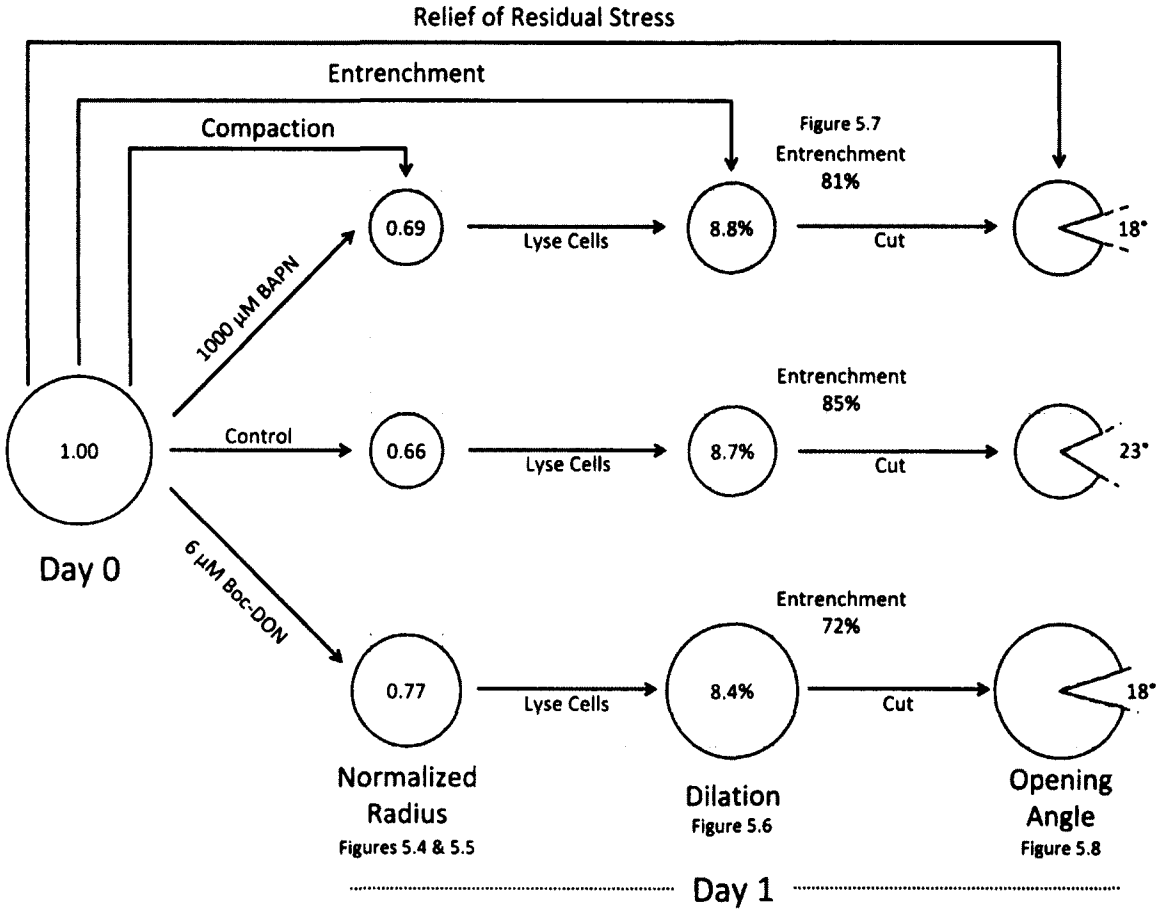

Figure 5.9: Illustrative example of results. Schematic drawing illustrating some of the primary metrics of interest based on day-1 results; specific results were different on other days, but qualitatively represented here. Note, in particular, that inhibition of tissue transglutaminase (i.e., Boc-DON treatment), but not lysyl oxidase (BAPN treatment), reduced both early matrix compaction and entrenchment. Nevertheless, the active cell-mediated compaction was similar across all groups (indicated by the ~8.5% dilatation following exposure to TritonX-100) independent of the degree of entrenchment.

covalently crosslink the remodeled collagen fibers. Upon entrenchment, the cells can relax and possibly spread out or reorient. Such a process could allow the cells to repeatedly contract, entrench, and spread to apply small, repetitive deformations that lead over time to the global shrinkage of the FPCL.

As the cells continue to contract and entrench the gel, a residual-type stress field appears to develop within the matrix [90,91]. The central region is mechanically characterized as in equibiaxial compression while a tensile circumferential stress develops at the outer edge. Cells at or near the outer edge may find this mechanical environment to be tolerable or preferred. Nearby cells may begin to migrate toward the outer edge, possibly driven by durotaxis (in response to the radially changing matrix stress or stiffness) or chemotaxis (in response to cytokines produced by cells in the more favorable environment). Such a migration could contribute to the increased cell density seen near the outer edge of compacted gels [91,116]. Because the cells in the central region would nevertheless remain in a nearly equibiaxial compressive stress environment, they may begin to undergo apoptosis which could possibly account for the reduced amount of Ca^{2+}-dependent contractility at later times.

The tensile environment of the outer edge could also lead to the differentiation of the fibroblasts in this region into myofibroblasts, which has been previously reported [3,62,91,116]. As the cells establish a preferred level of stress, their primary mode of contraction may switch from Ca^{2+}-dependent to a sustained contractile phenotype supported by the Rho-kinase pathway. If the cells could achieve their homeostatic target (unlikely in the free floating gel), they could then switch from a state of remodeling extant matrix to a state of tissue maintenance.

At later times (3 to 4 days), the effects of tTG inhibition appeared to have been diminished while LOX inhibition appeared to stall further FPCL compaction. Though not measured in this study, this may be due to new collagen deposition. When fibroblasts achieve a preferred or tolerable level of stress, they may begin to deposit new collagen either to maintain or develop further their preferred mechanical environment. Inhibition of LOX would prevent the transition of newly produced soluble collagen molecules into insoluble fibrils and fibers [39,160]. Also, by days 3 and 4, tTG activity may become minimal as available crosslinking sites on the initial collagen fibers become bound. New collagen deposition may be necessary to further alter the organization of the FPCL [41].

To understand more fully the nature of FPCL remodeling, more work is needed to characterize well the evolving mechanical environment. Until recently, the mechanical state of the compacting gel has been largely ignored or assumed to be negligible [4,5]. Yet, new insight into the mechanics of the free-floating FPCL has suggested that the cells develop a residual-type stress field (compression in the center and tension at the outer edge) through matrix remodeling and the development of radially varying matrix organization [90,91]. As the cells contract and remodel the matrix, differences in local mechanical environments could lead to heterogeneous rates and methods of remodeling as well as variations in gene expression and cell viability. Here, we have characterized the global mode of remodeling. Further work is needed to not only characterize potential regional variations within the FPCL, but also to correlate cell activity with any variations in the local mechanical environment. To this end, we need a better understanding of the evolving mechanical environment of the FPCL.

In summary, tissue transglutaminase, not lysyl oxidase, appears to play a primary role in the early remodeling and entrenchment of extant fibers in the free-floating FPCL, with Ca^{2+}-dependent contractility dominating early on as cells attempt to quickly remodel their surrounding matrix. LOX is not necessary for the early remodeling of the matrix as new matrix production is likely minimal. At later times, however, LOX may be required as new collagen is produced either to continue remodeling the matrix or to begin the process of tissue maintenance if the cells have established a homeostatic mechanical state. Similarly, our results suggest Ca^{2+}-independent contractility dominates at later times, suggesting cells are switching to a state of sustained contractility that is a hallmark of the myofibroblast phenotype.

Chapter 6: Computational model of matrix remodeling and entrenchment in the free-floating fibroblast-populated collagen lattice

6.1 Introduction

Mechanobiology is the study of the biological responses of cells to mechanical stimuli [20]. The biological responses can then lead to changes in the material composition of tissues and cause changes in their mechanical behavior. The altered mechanical environment would then change the mechanical stimuli on the cells potentially causing further cell responses. This makes the correlation of mechanical stimuli to biological response challenging to discern. For example, mechanobiological studies are difficult in nature to carry out in vivo as results are readily confounded by the complex biological environment and multiple mechanical loads. Tissue equivalents provide simplified, controllable in vitro systems. One of the simplest tissue equivalents is the free-floating fibroblast-populated collagen lattice (FPCL) and its many variants [2,161]. Until recently, however, the mechanical environment of the free-floating FPCL had not been explicitly examined [90,91]. Previously, the mechanical environment was assumed to be negligible, or that the stress was approximately zero everywhere within the construct as there are no external constraints for the cells to tense the matrix against [5,120].

For the free-floating FPCL to be a useful tool in mechanobiology, the mechanical environment needs to be characterized carefully to allow proper correlation of mechanical stimuli to biological responses. Mechanical analysis has been carried out for other tissue equivalents as constrained uniaxial and biaxial geometries allow for the direct measurement of forces within the system, which allows for easier approximation of the

material properties and estimation of internal stresses. Some of the current models even seek to model to mechanical responses of individual collagen or matrix fibers within a construct and how this relates to the overall state of the tissue equivalent [82,83]. These models allow for the determination of the mechanical environment at distinct time points, but they currently due not provide a means to predict the evolution of the mechanical behavior as the cells remodel the tissue.

There is a need for a more comprehensive analysis of the mechanics of the free-floating FPCL and a predictive model of its remodeling to enlighten our understanding of mechanobiological responses of cells within three-dimensional environments. These would provide a means to correlate mechanical stimuli to cellular activity in a simple system. Further, a predictive model of free-floating FPCL remodeling would also allow an in silico framework to test hypotheses to guide benchtop experiments.

We present here a computational model of the remodeling of the free-floating FPCL. This model is based on our previously proposed mechanical model of the free-floating FPCL [91] and utilizes the growth and remodeling (G&R) theory to describe the tissue remodeling in a mechanically-mediated manner [104]. This methodology has been used in multiple in vivo- and in vitro-based simulations to describe mechanical and material changes in different vascular pathologies and the evolution of tissue engineered vascular grafts (see [105,111,162,163]). This model may provide a preliminary framework to explore the evolving mechanical stimuli experienced by resident cells and guide future models in discerning the mechanobiological and biomechanical behaviors of tissue equivalents.

6.2 Methods

6.2.1 Constrained Mixture Formulation

Our computational model is based on the prior motivation and theoretical framework set forth in [44,110,162] and follows a rule-of-mixtures approach. Briefly, it is assumed that $k = 1, \ldots, n$ mechanically significant constituents can exhibit different material properties, production and removal rates, and different stress-free or natural configurations; however, these constituents are constrained to deform with the composite material. The deformations of each individual constituent k can be quantified in a straightforward manner (via the deformation gradient $\mathbf{F}^{k}_{n(\tau)}$, where $n(\tau)$ denotes the constituent-specific natural configurations and $\tau \in [0, s]$ is the G&R time of deposition; see Figure 6.1) if the deformation of the composite material and deposition-related deformations of each constituent are known.

For the model presented herein, we employ the "extended Blatz-Ko" constitutive behavior presented in [91] to determine the stresses within the composite material. The general Cauchy stress equation, **t**, takes the form

$$\mathbf{t} = \varphi_{iso}(\hat{r})\mu\left(\mathbf{I} - \frac{1}{J}\mathbf{B}^{-1}\right) + \varphi_{ani}(\hat{r})\frac{c}{J}(IV_C^2 - IV_C)\mathbf{m} \otimes \mathbf{m} \tag{6.1}$$

where $\varphi_{iso}(\hat{r}) \in [0,1]$ and $\varphi_{ani}(\hat{r}) \in [0,1]$ are "mass fractions" that capture the radially varying isotropic and transversely isotropic contributions, respectively (where $\varphi_{iso}(\hat{r}) + \varphi_{ani}(\hat{r}) = 1$ at any generalized radial location, $\hat{r}$, with $\hat{r} = R$, ρ, or r depending on the configuration of interest and $\varphi_{ani}(\hat{r} = \hat{r}_o) = 1$ where $\hat{r}_o$ denotes the outer edge), μ and c are material parameters that model the material stiffness (units of Pa or kPa), **I** is the

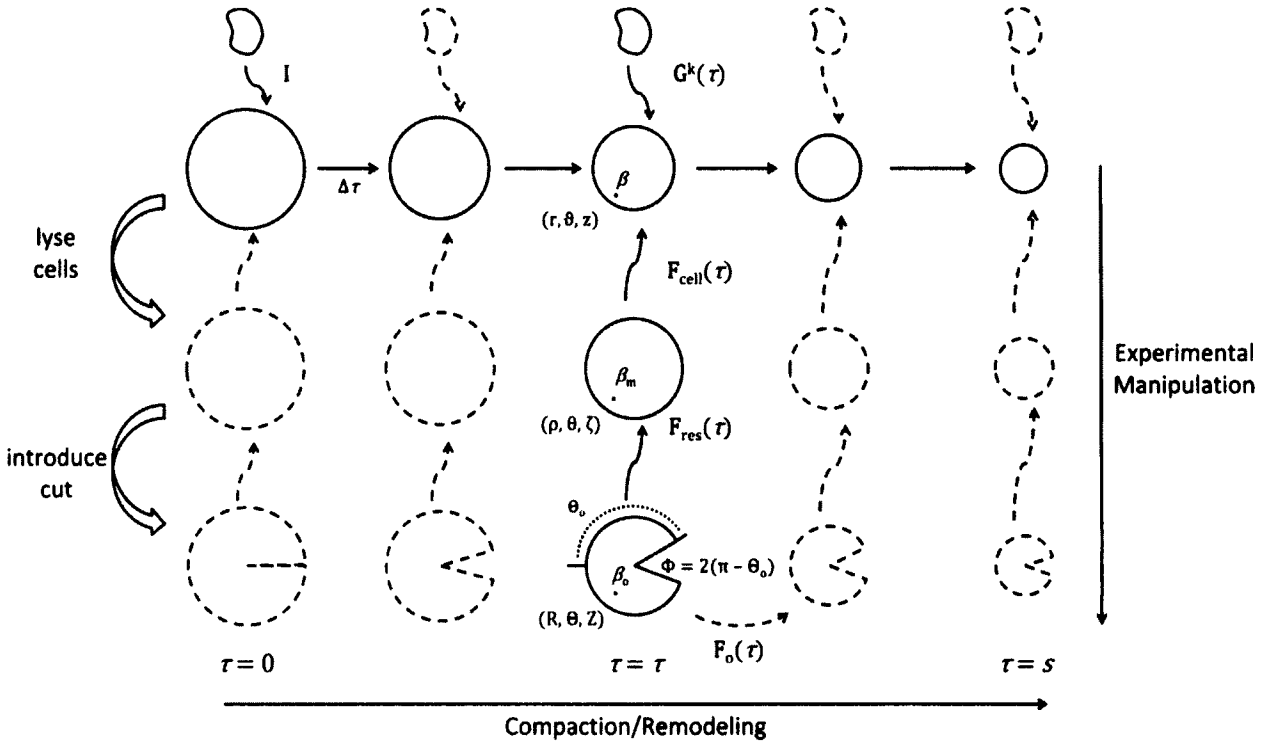

Figure 6.1: G&R schema. This schema shows the evolution of the free-floating FPCL from time 0 to time *s* and the deformation gradients associated with the transformations between different material configurations. From bottom to top, the represented configurations are the reference configurations, residually stressed configurations, cell stressed configurations, and natural or stress free configurations of the remodeled matrix. The different configurations of the free-floating FPCL are assessed experimentally through the methods indicated on the left. The current stress is calculated by deforming the reference configuration to the residually stressed configuration (via $\mathbf{F}_{res}$) and then to the cell stressed configuration (via $\mathbf{F}_{cell}$). Once the stress field is known, the remodeling is applied with the remodeled material being deformed into the cell stressed configuration (via $\mathbf{G}^k$). The new reference configuration is found by deforming the new composite material back to the initial reference and determining the deformation needed for the average stress of the material to be zero (via $\mathbf{F}_o$).

identity tensor, $J = \det \mathbf{F}$, $\mathbf{B} = \mathbf{F}\mathbf{F}^T$ is the left Cauchy-Green tensor, and $IV_C = \mathbf{M} \cdot \mathbf{C}\mathbf{M}$ is the fourth invariant of $\mathbf{C} = \mathbf{F}^T\mathbf{F}$, the right Cauchy-Green tensor, with $\mathbf{M}$ a unit vector that denotes the preferred (transversely isotropic) direction in the reference configuration. After deformation this preferred direction is denoted by the unit vector $\mathbf{m}$. For our case, we consider a circumferential transverse isotropy where $\mathbf{M} = (0,1,0)$, whereby $\mathbf{m} = \mathbf{e}_i$ ($i = \Theta, \theta$, or ϑ depending on the configuration of interest). Finally, $\otimes$ denotes a tensor product.

The Cauchy stress within the composite mixture, $\mathbf{t}_m$, is the sum of stresses for the original or "old" material and the remodeled or "new" material, and takes the form

$$\mathbf{t}_m = \mathbf{t}_o + \mathbf{t}_n^{iso} + \mathbf{t}_n^{ani} \tag{6.2}$$

where $\mathbf{t}_o$ is the stress in the original material (both isotropic and transversely isotropic) and $\mathbf{t}_n^{iso}$ and $\mathbf{t}_n^{ani}$ are the stresses in the remodeled isotropic matrix and transversely isotropic matrix, respectively.

With the composite material, we want to determine the new reference geometry following remodeling. To accomplish this, we assume the new reference geometry is a deviation from the previous reference geometry with associated deformation gradient for the original material of the form

$$\mathbf{F}_o = \begin{bmatrix} \delta_R & 0 & 0 \\ 0 & \delta_\Theta & 0 \\ 0 & 0 & \delta_Z \end{bmatrix} \tag{6.3}$$

where δ_R, δ_Θ, and δ_Z are radial, circumferential, and axial stretch ratios (see Figure 6.1).

The new material would be deposited into the fully stressed material at a prescribed deposition stretch described by the deformation gradient

$$\mathbf{G}^k = \begin{bmatrix} G_r^k & 0 & 0 \\ 0 & G_\vartheta^k & 0 \\ 0 & 0 & G_z^k \end{bmatrix} \tag{6.4}$$

where $k \in \{iso, ani\}$. To describe the full deformation of the remodeled material, we must first deform it back to the reference configuration for the original material from the fully stressed state. This results in the following form for the deformation gradient of the remodeled material:

$$\mathbf{F}_n^k = \mathbf{F}_o \mathbf{F}_{res}^{-1} \mathbf{F}_{cell}^{-1} \mathbf{G}^k \tag{6.5}$$

where $\mathbf{F}_{res}$ is the deformation gradient associated with the residually stressed configuration and $\mathbf{F}_{cell}$ is the deformation gradient associated with the cell stressed configuration.

With these deformations, the original material stress is

$$\mathbf{t}_o = \alpha(r)\varphi_{iso}(R)\mu\left(\mathbf{I} - \frac{1}{J_o}\mathbf{B}_o^{-1}\right) + \alpha(r)\varphi_{ani}(R)\frac{c}{J_o}(IV_o^2 - IV_o)\mathbf{e}_\Theta \otimes \mathbf{e}_\Theta \tag{6.6}$$

and the remodeled material stresses are

$$\mathbf{t}_n^{iso} = \omega_{iso}(r)\mu_{dep}\left(\mathbf{I} - \frac{1}{{}^{iso}J_n}\,{}^{iso}\mathbf{B}_n^{-1}\right) \tag{6.7}$$

$$\mathbf{t}_n^{ani} = \omega_{ani}(r)\frac{c_{dep}}{{}^{ani}J_n}\left({}^{ani}IV_n^2 - {}^{ani}IV_n\right)\mathbf{e}_\Theta \otimes \mathbf{e}_\Theta \tag{6.8}$$

where μ_{dep} and c_{dep} are the material properties of the remodeled material. Here, $\alpha(r)$ is a survival function that describes the fraction of original material remaining after remodeling. $\omega_{iso}(r)$ and $\omega_{ani}(r)$ are functions that describe the fractions of original material remodeled into new isotropic and transversely isotropic configurations, respectively. The functional forms of $\alpha(r)$, $\omega_{iso}(r)$, and $\omega_{ani}(r)$ are described in the *G&R Constitutive Theory* section (6.2.3) in more detail. One special case to consider is that of no remodeling (i.e., $\alpha(r) = 1, \omega_{iso}(r) = \omega_{ani}(r) = 0\ \forall r$) where we recover Eq. (6.1) and use this to solve the boundary value problem in the next section to determine the stresses that lead to remodeling.

Although we expect $\mathbf{t} = \mathbf{0}$ in the reference configuration, to determine the values of $\mathbf{F}_o = \mathrm{diag}[\delta_R, \delta_\Theta, \delta_Z]$, we assume the average stress along the radius for any principal direction should be equal to zero (e.g., $\int_o^{R_o} t_{RR}dR = 0$ for the radial component and similarly for $t_{\Theta\Theta}$ and t_{ZZ}). The values of $\mathbf{F}_o$ are then used to determine the new reference geometry via

$$R_o(s) = \delta_R R_o(\tau) \tag{6.9}$$

$$\Theta_o(s) = \frac{\delta_\Theta}{\delta_R}\Theta_o(\tau) \tag{6.10}$$

$$H(s) = \delta_Z H(\tau) \tag{6.11}$$

where τ indicates the stress-free geometry before remodeling, and s indicates the stress-free geometry after remodeling. R_o, Θ_o, and H are the outer radius, opening angle, and thickness, respectively, in the reference configuration.

6.2.2 Boundary Value Problem

The constitutive relation proposed in [91] to determine the state of stress in free-floating FPCLs, which has supporting experimental findings, revealed the presence of a residual-type stress field within a cell-compacted free-floating FPCL. In particular, application of a radial cut to a compacted gel results in an opening angle that is indicative of a tensile circumferential stress in the outer region of the gel and a compressive stress within the central region; that the latter is equibiaxial was revealed by punching a hole in the central region, which decreased axisymmetrically. Here, we extend our prior theoretical framework to include explicitly the deformations associated with the residual stress problem. Full derivation of this boundary value problem is shown in Appendix C.

Briefly, at any given time, τ, the free-floating FPCL has some known reference configuration, β_o, and its material properties are known. The free-floating FPCL is first deformed from this stress-free reference geometry to its residually stressed configuration, β_m, via the deformation gradient, $\mathbf{F}_{res}$. The principal values of $\mathbf{F}_{res}$ can be found by enforcing the axial traction-free boundary conditions (e.g., $t_{\zeta\zeta}(\pm\eta/2) = 0$, where η is the free-floating FPCL thickness in the residually stressed configuration) and satisfying radial equilibrium. The opening angle is known from the geometry.

Once the contribution of the residual deformations is accounted for in the passive gel, the full stress in the cell-stressed configuration can be found by including the active cell stresses, namely

$$\mathbf{t} = \varphi_{iso}\left(\mu\left(\mathbf{I} - \tfrac{1}{J}\mathbf{B}^{-1}\right) + t_a\mathbf{I}\right) + \varphi_{ani}\left(\tfrac{c}{J}(IV^2 - IV) + t_c\right)\mathbf{e}_\vartheta \otimes \mathbf{e}_\vartheta \tag{6.12}$$

where t_a and t_c are the isotropic and transversely isotropic cell-induced stresses, respectively [91].

Although we previously showed that equilibrium stresses can be found at any state without prescribing functional forms of $t_a\mathbf{I}$ and $t_c\mathbf{m} \otimes \mathbf{m}$ explicitly [91], it proves useful here to propose forms to facilitate study of the evolution of the cell stresses. Consider, for example,

$$t_a = T_a f_e\left(1 - \left(\frac{(V - V_{max})V_o}{(V_o - V_{max})V}\right)^2\right)d(s) \tag{6.13}$$

$$t_c = T_c f_e\left(1 - \left(\frac{(V - V_{max})V_o}{(V_o - V_{max})V}\right)^2\right)d(s) \tag{6.14}$$

where T_a and T_c are maximum isotropic and transversely isotropic cell stresses, respectively, f_e is an effective volume fraction (i.e., the ratio of overall volume the cells can influence mechanically; this is updated and will increase as the overall volume is decreased), V is the current volume, V_{max} is the volume at which maximum stress can be applied, V_o is the volume at which cells cannot actively stress the matrix, and $d(s)$ is a time delay function to account for initial cell adhesion and spreading. This functional

form for the cell stresses is motivated by the cell stress relation proposed in [86] where it is modeled as an induced "negative pressure" or tensile stress, and further influenced by a model proposed in [164] and modified by [165] for the active stress applied by smooth muscle cells in arteries. In the smooth muscle cell model, there is a level of stretch at which a maximal stress is generated, and deviations from this value decrease the induced stress. For our model, there is likely a mass density at which cells can maximally adhere to and contract the matrix and deviations from this density will reduce the overall cell contraction. Since we are modeling pure remodeling (i.e., no net mass production or removal) it is convenient to use volumes instead of mass densities.

For illustrative purposes, let $d(s)$ be prescribed as a sigmoid function of the form

$$d(s) = 1 - \frac{1+\exp(-bt_{1/2})}{1+\exp\left(b(s-t_{1/2})\right)} \tag{6.15}$$

where s is the current remodeling time, $t_{1/2}$ is the approximate time at which half the cells are adhered and capable of actively applying stress, and b is a parameter that alters the slope of the sigmoid.

With the prescribed cell stresses, the principal values of the cell-induced deformation gradient, $\mathbf{F}_{cell}$, can be found by satisfying the traction-free axial boundary condition and radial equilibrium. With all deformations known, as well as all material properties, the stresses can be calculated.

6.2.3 G&R Constitutive Theory

Mass deposition for prior vascular-based G&R simulations has been prescribed as a basal mass density production with a linear dependence on the deviation from the preferred or homeostatic value of stress [166]. This concept is in line with the concept of "tensional homeostasis" [43]; that is, cells seek to develop and maintain a preferred mechanical environment or level of stress. For mass density remodeling, we take a similar approach. The mass density remodeling rate takes the form

$$m_n = \dot{m}_n \Delta\sigma d(s) \tag{6.16}$$

where $\dot{m}_n = N f_e \tilde{\rho}(s)$ is the maximum remodeling rate, N is the fraction of f_e that can be remodeled per unit time, $\tilde{\rho}(s)$ is the current mass density, and $\Delta\sigma = \frac{\sigma_h - \sigma}{\sigma_h}$ is the deviation of the current stress, $\sigma = \sqrt{t_{rr}^2 + t_{\vartheta\vartheta}^2}$, from the homeostatic (preferred) level of stress, σ_h. Note, if $\sigma = 0$, then $\Delta\sigma$ is maximal with a value of 1. For the purposes of our model, we constrain $\Delta\sigma \geq 0$ to ensure the remodeling deposition does not become negative; that is, if $\sigma \geq \sigma_h$, no remodeling will ensue. The delay function, $d(s)$, is used here as well to account for the lag time before cells begin to actively remodel the matrix.

Finally, we need to prescribe rules for how matrix is reorganized to new orientations. From our prior work, we know the center of the free-floating FPCL is in equibiaxial compression while the outer edge is in a uniaxial tension [91]. Therefore, we use the difference in the principal stresses to prescribe the deposition distribution. The deposition equations take the following forms:

$$\omega_{iso}(r) = \frac{m_n}{\bar{\rho}(s)}\Delta\tau(1-\xi) = Nf_e\Delta\sigma d(s)\Delta\tau(1-\xi) \tag{6.17}$$

$$\omega_{ani}(r) = \frac{m_n}{\bar{\rho}(s)}\Delta\tau\xi = Nf_e\Delta\sigma d(s)\Delta\tau\xi \tag{6.18}$$

$$\xi = \frac{|t_{\vartheta\vartheta} - t_{rr}|}{\max(|t_{\vartheta\vartheta} - t_{rr}|)} \tag{6.19}$$

where, again, ω_{iso} and ω_{ani} are the remodeled matrix deposition distributions for the isotropic and transversely isotropic materials, respectively, and $\Delta\tau$ is the time step over which the deposition takes place. Here, ξ is a function that prescribes the deposition of anisotropic material based on the current principal stresses, t_{rr} and $t_{\vartheta\vartheta}$, where a value of 1 indicates only anisotropic material is deposited. Note, since both t_{rr} (radial stress) and $t_{\vartheta\vartheta}$ (circumferential stress) vary radially, the distribution functions will vary radially as well. Since we are assuming pure remodeling with no mass removed or new mass added, the survival function takes the following form

$$\alpha(r) = 1 - \omega_{iso}(r) - \omega_{ani}(r). \tag{6.20}$$

6.2.4 Computational Framework

The process flow of our simulation is shown in Figure 6.2 and the approach we take is modified from [110,162]. The computational model was implemented in a custom Matlab (The MathWorks) script. The simulation is first initialized by prescribing material properties, maximal cell stresses, geometry, and mass deposition parameters. With these current parameter values, both the residual and active cell stress boundary value problems are solved to determine the current deformations. Deformations are found using

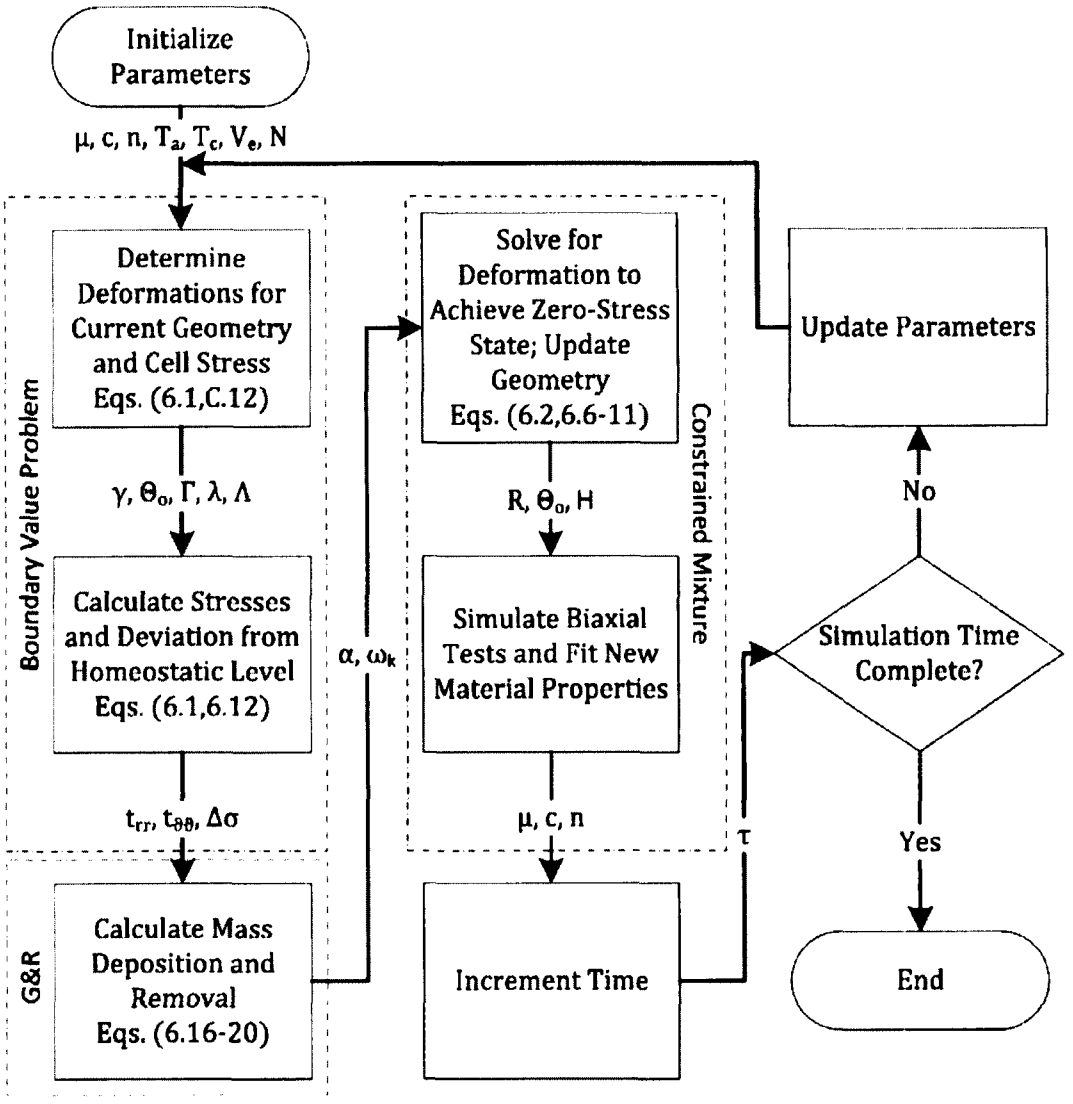

Figure 6.2: Computational flow chart. This flow chart shows the overall process flow of the computational model. The dashed line boxes indicate the processes associated with the boundary value problem, G&R constitutive assumptions, and the constrained mixture problem. The important equations for each process are indicated and as well as the primary outputs of each process.

Newton's Method. Next, current stresses and the deviation from the homeostatic stress level are determined and subsequently used to calculate mass density remodeling which takes place in the cell-stressed configuration (β; cf. Figure 6.1). After applying the removal and deposition functions, we solve for the deformations of the new composite material (remaining original matrix plus remodeled matrix) that satisfy an average zero-stress state to determine the evolution of the reference configuration (β_o).

Then, equibiaxial mechanical tests ($\lambda_R = \lambda_\Theta = \lambda, \lambda \in [0.5,1.5]$ in relation to the new reference configuartion) are simulated at the center, outer edge, and an intermediate point along the radius of the composite material. A least-squares nonlinear regression is performed by minimization of Eq. (6.1) against the three equibiaxial test results to determine the material parameters, μ, c, and n (this parameter is related to the cell stress and matrix distributions and is described in the *Parameter Initialization* section, 6.2.5), for a new material. By refitting the material parameters, we can simplify the G&R process by allowing each time step to start with a new "stress-free" material with a known reference geometry. We can now proceed to the next time step or terminate the simulation if the final time step has been reached. A time step of 0.1 hours or 6 minutes is used for the simulations discussed herein.

6.2.5 Parameter Initialization

Table 6.1 shows parameter values that were used in the baseline simulation. We sought to model the geometric changes from our prior experiments [91] and Chapter 5. The parameter f_e was estimated by

	Parameter	Notation	Value	Reference	Notes
1.)	Initial isotropic stiffness	μ_o	1	[87,130]	Non-dimensional value, 15 Pa in real units
2.)	Initial transversely isotropic stiffness	c_o	0		Initially Isotropic Matrix
3.)	Initial material and cell distribution	n_o	250		Accounts for inability of cells at outer edge to apply radial tractions, can only apply circumferential tractions
4.)	Homeostatic stress value	σ_h	$\frac{1000}{3}$	[65,136]	Non-dimensional Value, 5000 Pa in real units
5.)	Max isotropic cell stress	T_a	$\frac{\sigma_h}{\sqrt{3}}$	[65,136]	$\|\|T_a\mathbf{I}\|\| = \sigma_h$
6.)	Max transversely isotropic cell stress	T_c	σ_h	[65,136]	
7.)	Isotropic deposition stretch	$G_{r,\vartheta}^{iso}$	1.07		
8.)	Isotropic deposition volume	V_{iso}	1.1		$V_{iso} = \det \mathbf{G}^{iso}$ $G_z^{iso} = \frac{V_{iso}}{G_r^{iso} G_\vartheta^{iso}}$
9.)	Transversely isotropic deposition stretch	G_ϑ^{ani}	1.12		
10.)	Transversely isotropic deposition volume	V_{ani}	1.1		$V_{ani} = \det \mathbf{G}^{ani}$ $G_r^{ani} = G_z^{ani} = \left(\frac{V_{ani}}{G_\vartheta^{ani}}\right)^{1/2}$
11.)	Deposition isotropic stiffness	μ_{dep}	σ_h		Non-dimensional
12.)	Deposition transversely isotropic stiffness	c_{dep}	$200\sigma_h$		Non-dimensional
13.)	Initial effective volume fraction	f_e	0.01	[167]	Non-dimensional
14.)	Remodeling fraction rate	N	0.1		Units of hr^{-1}
15.)	Volume of max cell stress	V_{max}	0.1	[91]	Non-dimensionalized by original volume
16.)	Volume of no cell stress	V_o	100		Non-dimensionalized by original volume, arbitrarily high to account for significantly dilute matrix
17.)	Half-time for cell activity	$t_{1/2}$	8		By 8 hours, cell activity at ~50%
18.)	Slope modulator of cell activity function	b	0.44		

Table 6.1: Initial parameter values for the baseline simulation

$$f_e = \frac{N_{cells} L^3}{V_i} \tag{6.21}$$

where $N_{cells} = 50{,}000$ is the number of cells, $L \approx 50\ \mu m$ is a characteristic cell length [167], and $V_i = 0.5\ cm^3$ is the initial volume of the gel. Gels from our prior experiments [91] were seeded at 1 cm^3 volumes, but physical measurements indicated that settling of the collagen resulted in an initial volume closer to 0.5 cm^3. This results in $f_e \approx 0.01$ and this value increases as the current volume decreases by multiplying by V_i/V, where V is the current total volume.

Due to the lack of data on the mechanical environment, we used non-dimensionalized stress values normalized to the original isotropic material parameter. The compressive stiffness of dilute type I collagen has been previously shown to be in the range of ~15-75 Pa [87,130]. We chose 15 Pa as our normalizing factor for variables that have units of stress. Prior experiments in tethered tissue equivalents and on micropatterned substrates have shown the steady-state values of stress for the whole tissue and at focal adhesions to be ~5 kPa [65,136]. This was used to estimate both the homeostatic stress value, σ_h, and magnitude of the maximum cell stresses, T_a and T_c.

For this study, we used exponential-based "mass fraction" equations of the form [91]

$$\varphi_{iso} = 1 - \exp[n(r/r_o - 1)],\ \varphi_{ani} = \exp[n(r/r_o - 1)] \tag{6.22}$$

where n changes the steepness of the exponential as r approaches r_o. Because homogenous deformations are assumed, r/r_o can be replaced by ρ/ρ_o or R/R_o,

depending on the configuration of interest. The remaining parameters were determined by trial and error to provide best fits compared to available geometric data from prior experiments [91] and Chapter 5.

6.2.6 Competing Hypotheses for Constitutive Assumptions

To examine the effects of proposed constitutive assumptions on the model results, we examined competing hypotheses. First, to ensure that the sigmoid shape of the time delay function, $d(s)$, was not the responsible for the observed sigmoidal trend in the geometric results, the following form was examined as well:

$$d(s) = \begin{cases} \frac{s}{2t_{1/2}}, s < 2t_{1/2} \\ 1, \ s \geq 2t_{1/2} \end{cases} \tag{6.23}$$

where $d(s)$ increases linearly from 0 to 1 until reaching $s = 2t_{1/2}$.

For the stress-mediated mass density remodeling rate (Eq. (6.16)), the stress magnitude is used as the metric for the current stress level. Another potential metric would be the average stress level, that is,

$$\sigma = \frac{1}{2}(t_{rr} + t_{\vartheta\vartheta}). \tag{6.24}$$

This form of the stress metric is capable of accounting for compressive stresses as the values are not squared as they are in determining the magnitude.

Another alternative hypothesis is for the stress-mediated deposition functions, namely different functional forms of ξ (Eq. (6.19)). The proposed form uses the difference in the principal stresses to prescribe the deposition profile. Gradients in the mechanical environment (e.g., spatial stress gradients) have been suggested as the mechanical inputs into cells [167,168]. A competing hypothesis for matrix deposition would be to utilize the stress gradients in the radial direction to determine matrix redeposition. The form of ξ for this case would be

$$\xi = \frac{\left|\frac{\partial t_{\theta\theta}}{\partial r} - \frac{\partial t_{rr}}{\partial r}\right|}{\max\left(\left|\frac{\partial t_{\theta\theta}}{\partial r} - \frac{\partial t_{rr}}{\partial r}\right|\right)}. \tag{6.25}$$

For the geometric results to remain realistic, the value of n_o is increased to 500 for this case.

The final hypothesis test is related to the deposition stiffnesses or material properties, μ_{dep} and c_{dep}. For the baseline model, these values are kept constant. It is likely that these values would change over time due to myriad factors, including the current matrix density and the effects of crosslink formation. As proposed for the active cell stresses, there may be a matrix density at which crosslinker activity is maximal; that is, there is likely a matrix density at which the enzyme kinetics of the crosslinkers are optimized. Similar to the cell stress constitutive relations, it is more convenient to use volumes instead of mass densities and the possible relations for the deposition stiffnesses take the following forms:

$$\mu_{dep} = M_{dep}\left(1 - \left(\frac{(V-V_{max})V_o}{(V_o-V_{max})V}\right)^2\right) \tag{6.26}$$

$$c_{dep} = C_{dep}\left(1 - \left(\frac{(V-V_{max})V_o}{(V_o-V_{max})V}\right)^2\right) \tag{6.27}$$

where M_{dep} and C_{dep} are the maximal deposition stiffnesses for the isotropic and transversely isotropic materials, respectively, and they are modulated by the current volume, V. For this simulation, $M_{dep} = 4.5\sigma_h$ and $C_{dep} = 800\sigma_h$.

6.2.7 Additional Experiments and Mechanical Characterization of Free-Floating FPCLs

Free-floating FPCL experiments were carried out to determine opening angles at earlier time points (before 24 hours in culture) to provide additional experimental values to compare the simulations against. Additionally, experiments were carried out to examine the evolution of free-floating FPCL mechanical behavior. Free-floating FPCLs were cast a previously described in [91]. Briefly, a 1 mL solution containing 1.25 mg rat tail type I collagen (BD Biosciences) and 50,000 NIH/3T3 fibroblasts (ATCC) was cast into a single well of a 12-well plate and placed in a 37°C incubator to gel. After 30 minutes, gels were released from the mold and transferred to 35mm dishes and free-floated in 3 mL of Dulbecco's modified Eagle's medium (DMEM; Life Technologies) with 10% fetal bovine serum (HyClone), 10% porcine serum (Life Technologies), ascorbic acid (50 μg/mL, Sigma), $CuSO_4$ (3 ng/mL, Sigma), proline (50 μg/mL, Sigma), alanine (20 μg/mL, Sigma), glycine (50 μg/mL, Sigma), HEPES (0.01 M), basic fibroblastic growth factor (10 ng/mL, R&D Systems), platelet-derived growth factor (10

ng/mL, R&D Systems), and 1% antibiotic/antimycotic [142]. Gels were cultured at 37°C and 5% CO_2 for a maximum of 2 days. Opening angle experiments were carried out at 4 hour intervals from 4 to 16 hours. Terminal mechanical testing protocols were performed at 24 hour intervals from day 0 to day 2.

Opening angle experiments were performed as described in Chapter 5. Briefly, the free-floating FPCLs are treated with a 1% TritonX-100 solution for 30 minutes to lyse the cells and remove actively applied stresses. A #10 scalpel blade was used to introduce a radial cut from the center of the gel to the outer edge. The gels were imaged after 15 minutes and opening angles were measured using ImageJ.

The central region of free-floating FPCLs was assessed mechanically using an indentation method previously used by [169]. Briefly, a single FPCL was kept in its 35mm culture dish and submersed in culture media. It was placed on the weighing pan of a 100 μg precision analytic balance (Mettler-Toledo) and 1 mm diameter stainless steel ball bearing attached to a micrometer-driven stage was used to indent the apical surface of the FPCL in the center. The micrometer distance and analytic balance measurements were recorded via a custom LabView (National Instruments) program. The mechanical data was plotted as

$$F = \frac{8R^{1/2}}{3}\frac{G}{1-\nu}e^{3/2} \tag{6.28}$$

where F is the measured load in Newtons, e is the indentation depth in meters, R is the radius of the indenter in meters, G is the linear shear modulus, and ν is Poisson's ratio. Eq. (6.28) is the classic Hertzian model for the indentation of an elastic material by a

spherical indenter. Linear regression was performed to determine the value of the lumped parameter, $G/(1-\nu)$, for a given sample against the experimental data. Only the loading data was used for the regression. Samples were tested at 0, 1, and 2 days with the mean and standard error of the mean for $G/(1-\nu)$ values being reported for each day.

To examine the tensile properties of the outer region, free-floating FPCLs were cultured as described above and tested on days 0, 1, and 2. Gel thicknesses were estimated from the indentation testing results. Before testing, a biopsy punch (Accuderm) was used to remove the central region of the gel to leave an approximately 2 mm thick ring (i.e., if the gel was 10 mm in diameter, a 6 mm diameter punch was used to leave 2 mm on either side of the remaining ring). Because of the size of the day 0 samples, a 7 mm diameter punch was first used to create a smaller disk and a 3 mm punch was used to create the ring for these samples. The ring samples were then loaded on to the tissue holders of a Myobath system (World Precision Instruments) and force was measured using a 50 gram force transducer. For the loading protocol, gels were lengthened at a rate of 0.3 mm every five seconds until failure. Because the gels exhibit little to no resistance to bending, they were treated as uniaxial samples.

The first Piola-Kirchhoff stress was calculated as the force on one side of the ring (i.e., half the measured force) divided by the original cross sectional area of the ring, which is the 2 mm multiplied by the estimated thickness from the indentation tests. This measure of stress is likely underestimated as the cross sectional area of the ring changes greatly as the gel is stretched to find the initiation of force generation where the stretch is assumed to be equal to 1. The stress was plotted against the stretch with a stretch range

from 1 to 1.4. To estimate material properties, the following equation for the uniaxial stress was used:

$$P = \mu\left(\frac{1}{\lambda^{1/2}} - \frac{1}{\lambda^3}\right) + c(\lambda^3 - \lambda) \tag{6.29}$$

where P is the first Piola-Kirchhoff stress in the direction of loading, λ is the stretch ratio in the direction of loading, μ is the isotropic material property (modeled here as a Blatz-Ko material), and c is the material property for the anisotropic or aligned material. This is related to Eq. (6.1) with the mass fractions combined into the material properties. The Blatz-Ko, however, is not suitable for most material behaviors when stretches in the loading direction are greater than 1. Because of this, combined with the low bending stiffness of the material, the samples were assumed to be wholly anisotropic in uniaxial tension, that is

$$P = c(\lambda^3 - \lambda) = (\phi_{iso}c_{iso} + \phi_{ani}c_{ani})(\lambda^3 - \lambda) \tag{6.30}$$

where c_{iso} is the material property of the isotropic material in tension, c_{ani} is the material property of the anisotropic material in tension, and ϕ_{iso} and ϕ_{ani} are the associated mass fractions for the isotropic and anisotropic materials, respectively, with $\phi_{iso} + \phi_{ani} = 1$. For day 0, c_{ani} and ϕ_{ani} are assumed to be zero. On days 1 and 2, c_{iso} is assumed to be equal to the value found for day 0. The values for ϕ_{iso} and ϕ_{ani} are not known for days 1 and 2, so the values of c_{ani} are parameterized for different values of ϕ_{ani}. Values for c_{ani} were found through nonlinear regression via a least squares minimization of Eq. (6.30)

against the combined average experimental data for each time point to determine c and the subsequent parameterization of the mass fractions and the assumed value of c_{iso}.

6.3 Results

6.3.1 Baseline Simulation Results

Our model is able to capture the geometric changes associated with the compaction of the free-floating FPCL. Namely, experiments have shown both the radial and axial dimensions are reduced during compaction with the radial dimension being reduced more than the axial [91]. Our baseline simulation leads to a marked reduction in radius (Figure 6.3A) and a smaller reduction in the thickness (Figure 6.3B) that are comparable to experimental data. Also, the removal of cell stress leads to a dilatation of the radial dimension (Figure 6.3A). Our model also predicts the formation of an opening angle that rapidly develops in the first 24 hours (Figure 6.3C). The experimental results are offset by the 0 hour mean from Chapter 5 to account for the potential systematic error in the application of the radial cut.

The results of our baseline simulation also show an evolution of the stress state of the free-floating FPCL (Figure 6.4). At early times (16 hours) the stresses are minimal with the radial stress being wholly compressive along the radius and 0 at the outer edge (Figure 6.4A), but there is still the development of a residual-type stress field in the circumferential direction (Figure 6.4B). The center ($r = 0$) is also in a state of equibiaxial compression. At later times, the stress values increase with the radial stress becoming more compressive and by 48 hours, the tensile stress at the outer edge is ~225 (non-dimensional; Figure 6.4B) while the target homeostatic value is ~333.

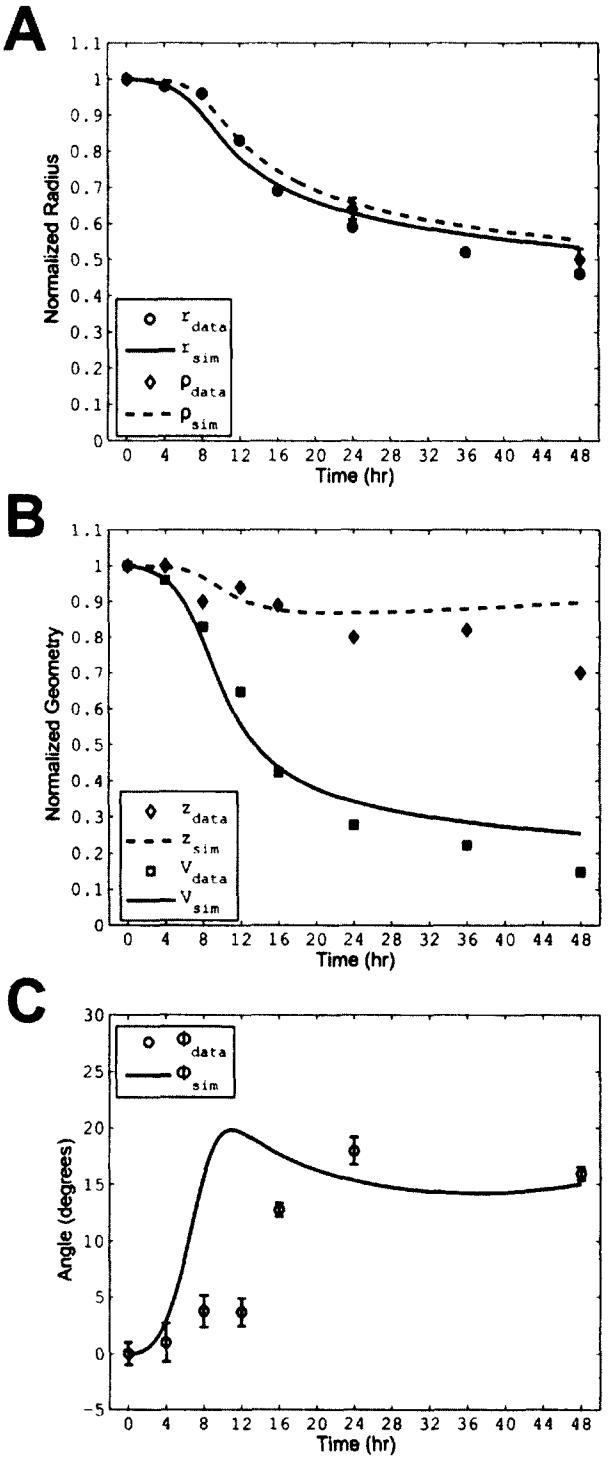

Figure 6.3: Baseline simulation geometric results with experimental data. (A) The evolution of the radius in the cell stressed configuration (r) and the residually stressed configuration (ρ). (B) The evolution of the thickness (z) and volume (v) in the cell stressed configuration. (C) The evolution of the opening angle (Φ, cf. Figure 6.1) in the reference configuration. The subscript "data" indicates the prior experimental results and the subscript "sim" indicates the baseline simulation results. For the experimental data, values are the mean ± SEM.

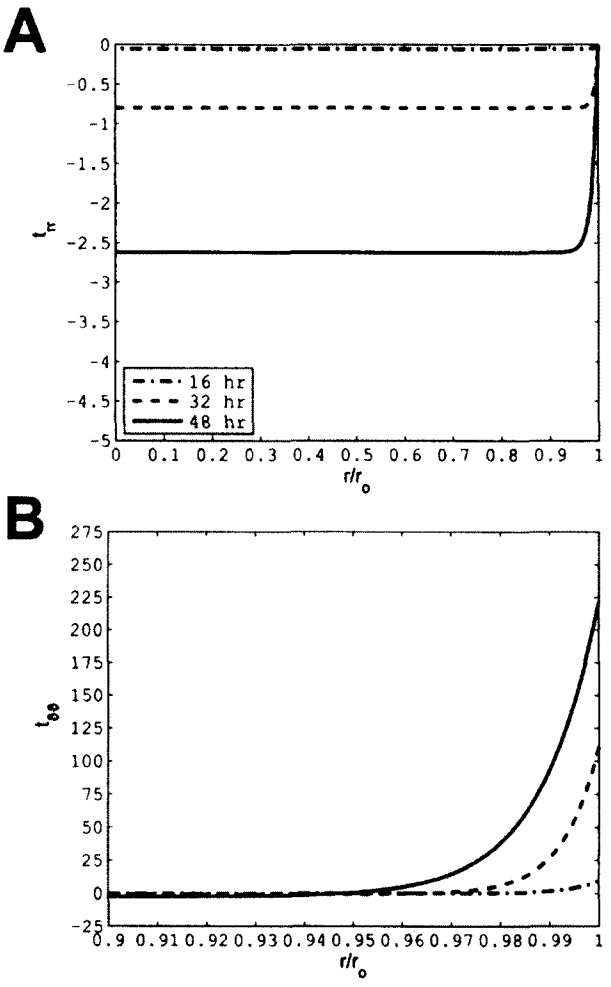

Figure 6.4: Baseline simulation stress evolution. (A) The non-dimensional radial stress (t_{rr}) values along the radius at 16, 32, and 48 hours. (B) The non-dimensional circumferential stress ($t_{\theta\theta}$) values along the radius at 16, 32, and 48 hours. For the circumferential stress, only the non-dimensional radial values from 0.9 to 1 are shown.

The active cell stresses also evolve with time. As time increases, both the isotropic (Figure 6.5A) and the transversely isotropic (Figure 6.5B) cell stresses increase, with the transversely isotropic cell stress having the largest maximum value at the outer edge. The cell stress distribution remains highly dominated by the isotropic population with the transversely isotropic cell stress being localized to the outer edge.

We also examined the changing material properties of the free-floating FPCL over time. From an initial value (non-dimensional) of 1, μ increases gradually during remodeling to a final value of ~24 at 48 hours (Figure 6.6A). The material and cell distribution parameter, n, decreases over time (Figure 6.6A), meaning as the material is remodeled, there is an inward propagation of the transversely isotropic constituent and cell stress. The final value for n at 48 hours, however, is ~85, which indicates that the transversely isotropic material is still highly localized to the outer region of the free-floating FPCL and is in line with the experimental finding of [91].

The transversely isotropic material parameter, c, starts from an initial value of 0 to approximately simulate an initial wholly isotropic material. As time increases, the value of c undergoes large changes (Figure 6.6B). This results in the transversely isotropic constituent being significantly stiffer compared to the isotropic constituent and allows for the stresses in the outer region to develop to levels near the homeostatic value. The final non-dimensional value of c at 48 hours is ~4500.

We also examined the material behavior at multiple time points in more detail (Figure 6.7). As noted in the methods, at the end of each time point, new material parameters are determine by simulating equibiaxial tests at multiple points along the radius and minimizing the difference between these tests and the original stress equation,

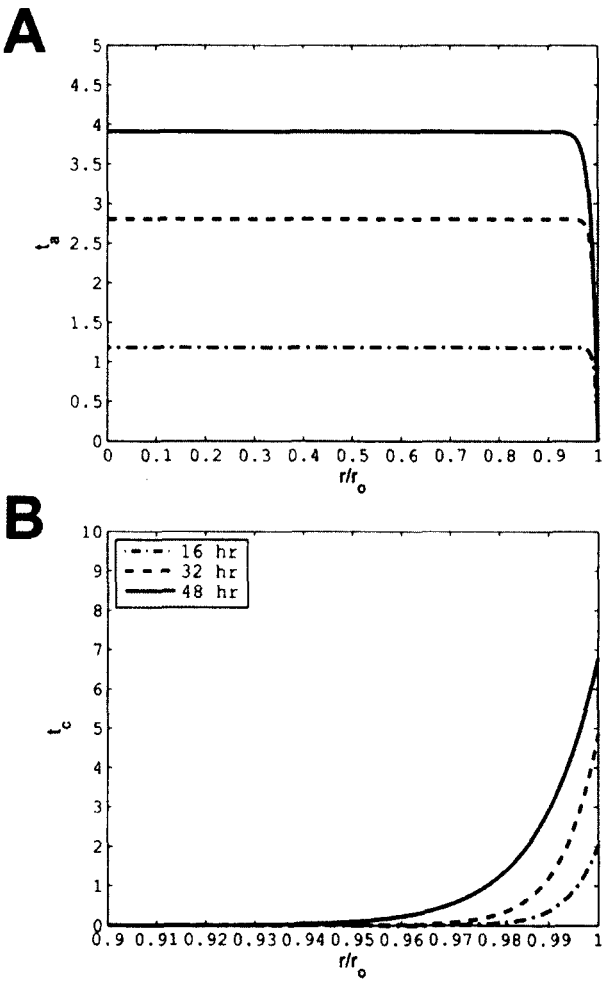

Figure 6.5: Baseline simulation cell stress evolution. (A) The non-dimensional isotropic cell stress (t_a) values along the radius at 16, 32, and 48 hours. (B) The non-dimensional transversely isotropic cell stress (t_c) values along the radius at 16, 32, and 48 hours. For the transversely isotropic cell stress, only the non-dimensional radial values from 0.9 to 1 are shown.

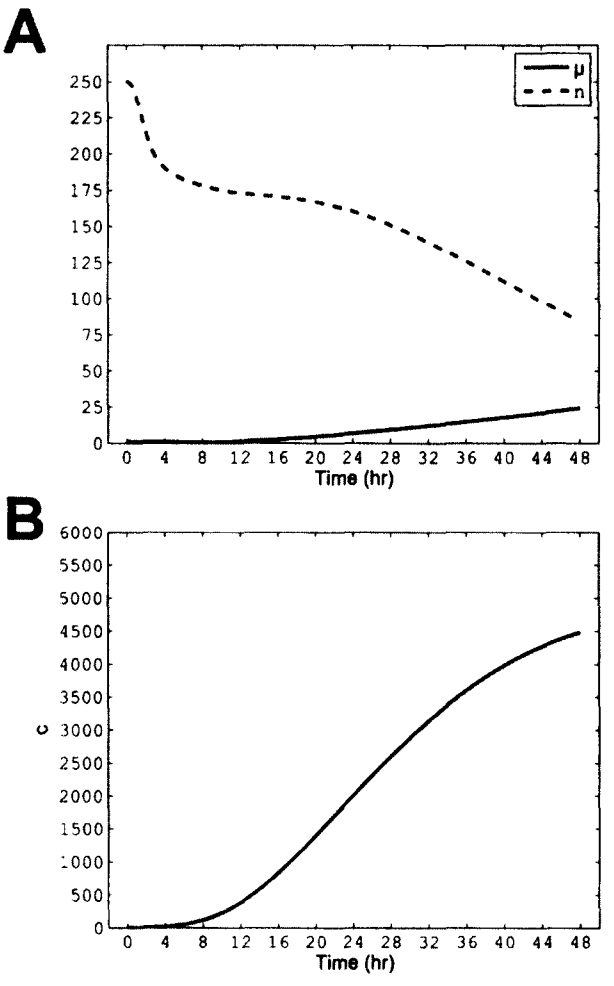

Figure 6.6: Baseline simulation material properties. (A) The evolution of the isotropic material property, μ, and the distribution parameter, n. (B) The evolution of the transversely isotropic material property, c.

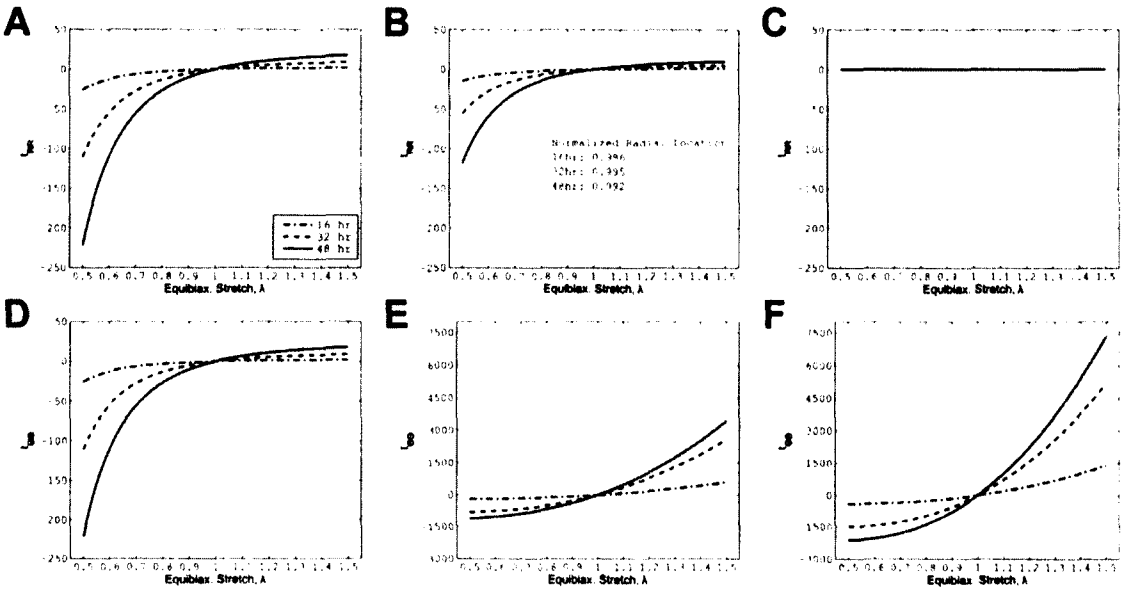

Figure 6.7: Baseline simulation equibiaxial tests. (A-C) The stress response for the radial direction (t_{RR}). (D-F) The stress response for the circumferential direction ($t_{\theta\theta}$). A and D are the tests simulated at the center of the gel. B and E are the tests simulated at the point where the material is approximately half isotropic and half transversely isotropic. The normalized radial location of this point for each time is indicated in B. C and F are the tests simulated at the outer edge where the material is wholly anisotropic or transversely isotropic.

Eq. (6.1). At the center of the free-floating FPCL, the material exhibits an equibiaxial stress behavior ($t_{RR} = t_{\Theta\Theta}$) for the range of stretches simulated (Figure 6.7A and Figure 6.7D). As time increases, the isotropic material property, μ, increases resulting in a stiffer response at later times.

During the simulation, the approximate radial location at which the material is determined to be half isotropic and half transversely isotropic can be determined. For the equibiaxial tests at these locations, there is a shift in material response compared to the central location. In the radial direction, the material response is similar in trend compared to the results for the central region (cf. Figure 6.7A and Figure 6.7B). The magnitude of the response, however, is reduced by a factor of ~2 for the intermediate location as the amount of isotropic material is approximately half. For the circumferential direction (Figure 6.7E), the behavior is dominated by the transversely isotropic material which results in an increased stress magnitude both in tension and compression compared to the radial behavior for the same location. The normalized radial locations for these transition locations are indicated in Figure 6.7B. Note, tested locations for all time points shown are in the outer 1% of the domain as the aligned matrix is highly localized to the outer edge.

Finally, the equibiaxial tests at the outer edge show the behavior of a wholly transversely isotropic material. For the radial direction, there is no stress developed at any value of stretch at any time (Figure 6.7C). In the circumferential direction, the material behavior is stiffer compared to the material at the intermediate location at all times (cf. Figure 6.7E and Figure 6.7F). This type of material behavior would be beneficial for cells in this region as relatively low values of stretch would allow for the development of significantly higher stress magnitudes compared to the other regions tested. For all tested

locations, the simulated tests indicate that the overall mechanical behavior is becoming stiffer over time.

6.3.2 Hypothesis Testing

Hypothesis tests were performed to examine how the constitutive relations proposed for this model affect the emergent behaviors and to determine if there are other potential functional forms for the needed constitutive relations that may require further investigation. First, we examined the nature of the time delay function, $d(s)$. The proposed function is a sigmoid (Eq. (6.15)) and it is noted that the experimental results related to the radius (Figure 6.3A), thickness, and volume (Figure 6.3B) are sigmoidal in trend over time. To ensure the sigmoid form of the time delay is not the cause of the sigmoid trend of the simulated geometries, a linear shaped time delay function (Eq. (6.23)) was examined. The linear function did not result in any significant differences compared to the baseline simulation. Namely, the geometric results showed only minor differences (Figure 6.8) with the linear time delay resulting in a sigmoidal-type evolution for the radius and volume. The trends in the evolution of the material properties was very similar to the baseline model (Figure 6.9) which resulted in stress distributions over time that were comparable (not shown). This indicates that the sigmoid-shaped time delay function for the baseline model is not driving the emergent shape of the geometric trends.

For the baseline model, the stress magnitude was used for comparison to the homeostatic stress level, σ_h, to determine the mass density remodeling rate. For an alternative hypothesis, the average stress (Eq. (6.24)) was examined. The geometric results showed little difference between the baseline and average stress simulations

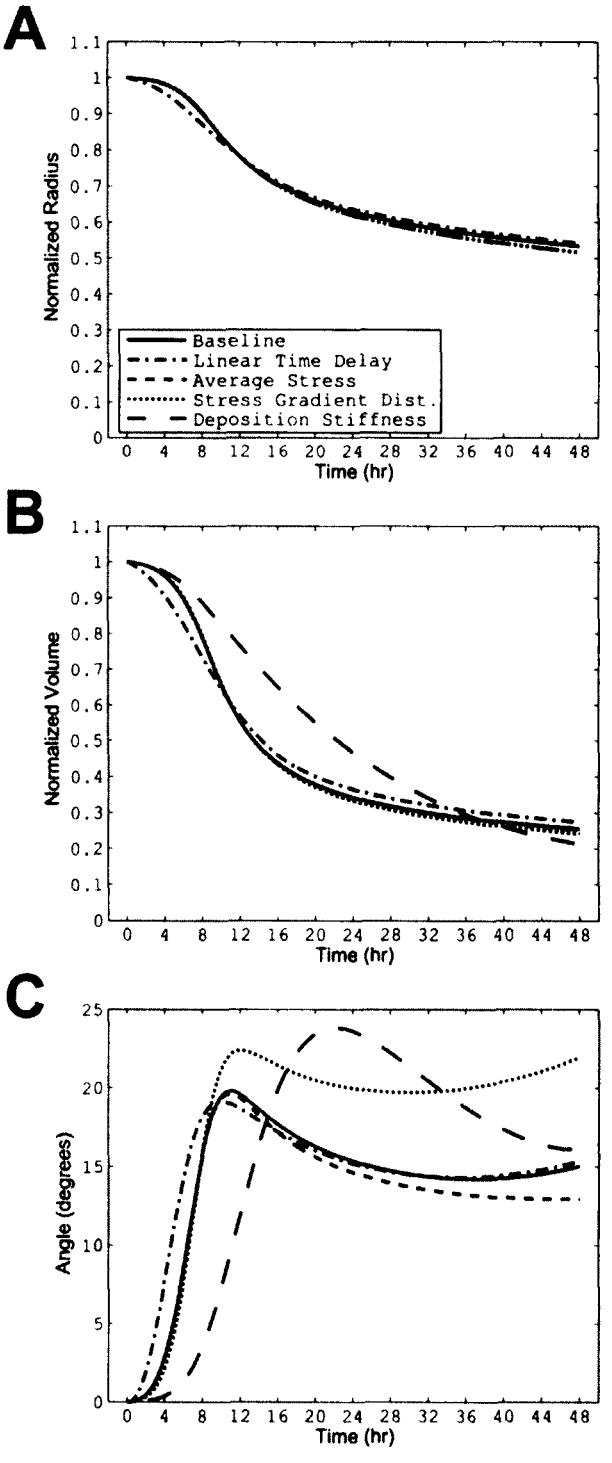

Figure 6.8: Hypothesis testing geometries. (A) The normalized cell stressed radius evolution for each hypothesis test. (B) Normalized cell stressed volume evolution. (C) Opening angle evolution in the reference configuration.

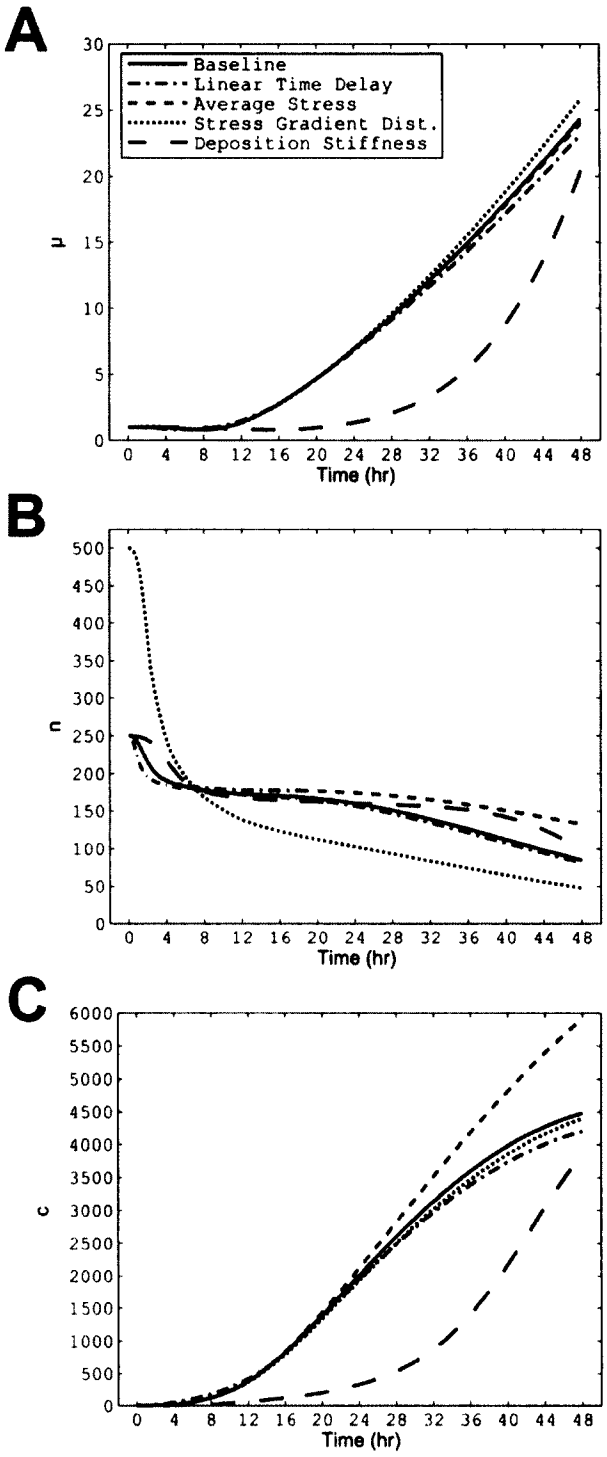

Figure 6.9: Hypothesis testing material properties. (A) Evolution of the isotropic material property, μ. (B) Evoultion of the material property, n. (C) Evolution of the material property, c.

(Figure 6.8). The primary difference was in the material properties. This isotropic parameter, μ, had a comparable evolution related to the baseline model (Figure 6.9A), but the distribution parameter, n, did not reach a similar value (Figure 6.9B). The final n value was significantly higher, indicating that there was less inward development of transversely isotropic matrix in the average stress model. The final value for the transversely isotropic material parameter, c, was also significantly larger in the average stress case (Figure 6.9C). The stress distributions differed, primarily due to the n parameter for the average stress resulting in a more localized transversely isotropic region but the final stress magnitudes were not significantly different (not shown).

As stated previously, it has been suggested that cells may respond to spatial gradients in the stress field in which they reside [167,168]. This provided the basis for an alternative hypothesis for how the remodeled matrix is reoriented. For the baseline model, material redistribution is driven by the difference in principal stresses (Eq. (6.19)). The proposed alternative would be to reorient the matrix based on the difference of the spatial gradients of the principal stresses (Eq. (6.25)). It was found for this hypothesis that the initial value for n needed to be increased for the geometric results to be realistic (i.e., comparable to experimental results). Overall, the geometric results were similar to the baseline model (Figure 6.8). The simulated opening angle values followed similar trend with the stress gradient model values being larger in magnitude. The material properties μ and c had similar evolutions compared to the baseline model (Figure 6.9A and Figure 6.9C). The largest difference was in the progression of the n parameter (Figure 6.9B). Even though the initial value for n was doubled for the stress derivative model, the final value for this case was significantly lower (~50) compared to the

baseline. This suggests that if cells were responding to the stress gradient, the inward propagation of anisotropy would develop quickly, even though this hypothesis also suggests the initial cell stress distribution would be more isotropic compared to the baseline model (due to the needed increase in the initial n value to ensure realistic results).

Finally, the baseline model showed a rapid development of an opening angle, but our expanded experimental results showed that the opening angle develops more gradually over the first 24 hours. The baseline model used static values for the deposition stiffnesses, but it is more likely that these values would evolve as the matrix is altered. For this test, we postulated that the deposition stiffnesses would evolve as the matrix density increases (volume decreases; Eqs. (6.26, 27)). The resulting radial values are similar compared to the baseline model (Figure 6.8A) while the volume decreases more slowly (Figure 6.8B). The largest difference is in the development of the opening angle (Figure 6.8C). For the case of evolving deposition stiffnesses, the opening angle development is more gradual with the maximum angle occurring at about 24 hours, which correlates better to the experimental data compared to the baseline model. The material properties for the case of evolving deposition stiffnesses have different profiles compared to the baseline model (Figure 6.9). For example, the c parameter evolution is more gradual during the first 24 hours before it starts to increase significantly during the last 24 hours. For the baseline case, this parameter increases steadily from about 8 hours before starting to level off near the end of the simulation. This alternative hypothesis of evolving deposition stiffnesses seems to provide a better approximation of the opening

angle development and improved functional forms for this constitutive need to be examined further.

6.3.3 Mechanical Testing Results

Microindentation testing provided estimates of the isotropic material behavior in of the central region of the gels in compression. On day 0, the lumped parameter, $G/(1-\nu)$, was 56.2 ± 17.8 Pa (Figure 6.10). This value increased on day 1 to 121.2 ± 38.5 Pa and again on day 2 to a value of 181.1 ± 52.8 Pa. These results show an increase in the stiffness of the central region of the gels over the period of interest. The final values for G would be decreased as the expected value of ν would be between 0 and 0.5. The final value on day 2 is not the estimated 24 times greater than the day 0 properties from the baseline simulation. This, however, may be related to the hypothesis test examining the evolving deposition stiffnesses that allow for the material properties to evolve more gradually.

The tensile properties also indicate a stiffening of the material from day 0 to day 2 (Table 6.2). Before parameterization with possible mass fractions, the value of c increased from a value of 19.0 Pa on day 0 to a value of 49.2 Pa on day 2. The possible parameter values for c_{ani} were calculated for assumed ϕ_{ani} values of 0.1, 0.01, and 0.001. For the higher mass fraction, the value of c_{ani} on day 2 is 203.1 Pa. If the mass fraction is two orders of magnitude lower, the value increases to 17.1 kPa. This value corresponds well with the baseline simulation where the final non-dimensional value of c is about 4500 times greater than the initial value of μ. The assumed dimensional value of μ was 15 Pa which is three orders of magnitude smaller than the parameter value for the

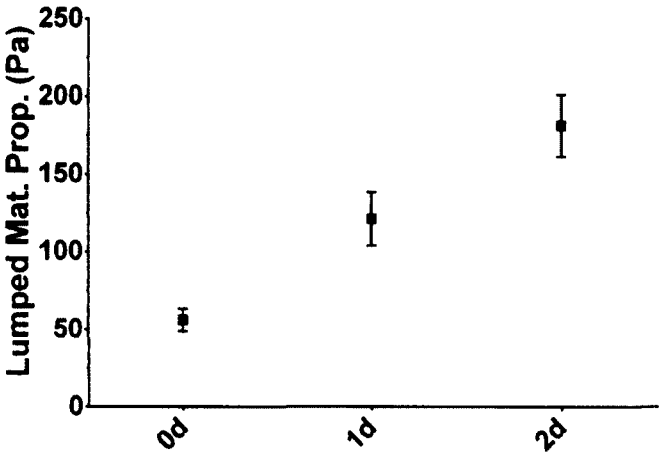

Figure 6.10: Isotropic material behavior. Values of lumped parameter ($G/(1-\nu)$) from microindentation tests with units of Pa. Values are in reported as the mean ± SEM.

	c (Pa)	c_{ani} (Pa)		
		ϕ_{ani} = 0.1	ϕ_{ani} = 0.01	ϕ_{ani} = 0.001
Day 0	19.0	-	-	-
Day 1	34.7	57.8	289.1	2602.1
Day 2	49.2	203.1	1742.1	17132.1

Table 6.2: Material properties from uniaxial tensile tests. Values reported have units of Pa. The first column indicates the value of c from the nonlinear regression. The other columns indicate the values for c_{ani} for different values of ϕ_{ani}.

lowest ϕ_{ani} value. Also, the stress values are expected to be higher than calculated here as the initial cross sectional area at the initial uniaxial stretch of 1 is likely smaller than the values used in these initial approximations.

6.4 Discussion

Experiments with uniaxially constrained collagen tissue equivalents have shown that cells seek to develop and maintain a preferred level of force or stress. This mechanism has been termed "tensional homeostasis" [43]. Cells contract to deform their resident matrix to change the mechanical environment and will entrench the applied deformations to develop and maintain stress within the matrix. In uniaxial tissue equivalents this maintained stress is measureable by removing the active cell stress from the tissue equivalent and observing the remaining force which is called the "residual matrix tension" [42]. While force measurements are not directly possible, this phenomena has been qualitatively observed in free-floating FPCLs as lysing the resident cells leads to only a partial dilatation of the gel, but it does not return to its original geometry as seen in Chapter 5.

Previous mechanics-based models of the free-floating FPCL and its variants were developed to examine the magnitude of cell contractility or traction force necessary to compact collagen lattices. John et al. modeled cell contractility as a thermal change resulting in collagen contraction [89]. For an unconstrained gel, this model results in a uniform compaction with no stress developed within the matrix as the temperature drop is isotropic over the entire domain. Another model sought to determine the value of cell traction, or the force or stress exerted by a cell on the extracellular matrix [86,87]. This

model was implemented on a gel with a spherical geometry having isotropic, linear viscoelastic properties. This model is capable of simulating the geometric changes of the assay and predicts that increases in cell traction will increase the rate and extent of matrix compaction.

Both of these models assumed unchanging material properties, no changes to matrix orientation, and do not account for the development of residual stress within the matrix. To this end, we sought to develop an initial continuum mechanics-based model to describe the remodeling and entrenchment of the free-floating FPCL and the evolution of its mechanical environment. We utilized a G&R approach that captures remodeling via the removal of material constituents and their redeposition at new orientations, deformations, and with altered material properties or stiffnesses. It is this redeposition that allows for the material composition to change and allows for evolution of the mechanical environment. It also allows for regional variations, which manifest experimentally, to develop.

Previous G&R-based models of vascular adaptations use a similar approach to determine new mass depositions (see [166]). For these models, the intramural stress of the artery is perturbed from its homeostatic value. If the stress is increased, matrix production is increased to bring stress levels down while decreased stress leads to a reduction of basal matrix production to allow more material to be removed to restore the preferred stress level. The resulting basic form of mass density deposition is

$$m = m_o(1 + K\Delta\sigma) \tag{6.31}$$

where m_o is a basal mass density production rate, $\Delta\sigma = \frac{\sigma-\sigma_h}{\sigma_h}$ is the deviation of the current stress, σ, from the homeostatic (preferred) level of stress, σ_h, and K is a modulating gain factor. Note, if $\sigma < \sigma_h$, then $\Delta\sigma < 0$ which leads to a reduction in mass production. While suitable for these models of perturbation from a preferred level, this functional form is not useful for the system modeled herein. For example, if $\sigma = 0$ and $K = 1$, $m = 0$. For the free-floating FPCL, the initial stress is zero over the whole domain, so this form of the matrix deposition would result in zero remodeling. The constitutive we proposed for matrix deposition in remodeling (Eq. (6.16)) accounts for cells in an unstressed or under-stressed environment seeking to remodel and develop stress to achieve their preferred environment.

Experimental results for free-floating FPCLs revealed a sigmoidal trend in the evolution of the geometry [91]. For the baseline model, we prescribed a sigmoid time delay to account for the initial "lag" phase of the FPCL culture in which the cells are initially adhering to and spreading within the collagen matrix. For an alternative hypothesis, a linear time delay function was also examined and resulted in simulated geometries very similar to the baseline model. This indicates that the emergent sigmoidal evolution of the geometric results for the baseline simulation is not a direct result of the prescribed time delay function.

Another constitutive that was examined was the stress metric used as a comparison against the postulated homeostatic value. The baseline model used the stress magnitude while the alternative hypothesis used the average stress. The stress magnitude does not account for differences between compressive and tensile stresses, while the average stress does. With the mechanical environment at the outer edge being uniaxial

(i.e., tensile circumferential stress, zero stress radially) the circumferential stress would have to reach a level double that of the homeostatic value. For the baseline case of stress magnitude, the circumferential stress would only need to reach a value equal to the homeostatic.

For the redistribution function, ξ, the alternative hypothesis of the differences in the spatial stress gradients revealed an interesting result. First, for the geometric results to remain realistic or comparable to experimental values, the initial value of n had to be doubled compared to the baseline model. This means that the initial anisotropic response of cells at or near the gel periphery is more localized than in the baseline simulation. Regardless, the gradient-based distribution function resulted in a final n value smaller than the baseline, indicating a greater amount of matrix redistribution in the circumferential direction. As mentioned previously, some reports have suggested some cellular responses may be related to the gradient of stress and not directly to the local stress magnitude [167,168]. For our alternative hypothesis, this can be likened to the cells sensing that the stress is changing more in one direction as compared to another. That is, the stress in both radial and circumferential directions may be compressive which is not preferred by fibroblasts. For the baseline model, if the local values of stress are not vastly different, the redeposited matrix would be predominately isotropic. For the alternative hypothesis, the stress gradients may be different, likely with the circumferential gradient indicating a shift in the stress for that direction towards the preferred tensile environment. Cells would then be able to more quickly align collagen in the circumferential direction and be able to develop, at least in the outer region of the gel, a preferred mechanical

environment. Further investigation of the local cellular responses needs to be carried out to understand the nature of the mechanical cues to which the cells are responding.

The final hypothesis test focused on a potential relation to prescribe the material properties of the remodeled and redeposited matrix. Collagen entrenchment after remodeling is likely mediated via covalent crosslinking which may be dominated by tissue transglutaminase for the length of time we simulated in this model (see Chapter 5). The crosslinking of collagen is known to alter the its material properties and increase its apparent stiffness [170,171]. The precise effect of how the collagen stiffness is modulated, however, is not known. As an initial guess of how the deposition stiffnesses can be altered, we assumed a similar relation with the matrix density that was also used for the active cell stresses (Eqs (6.13, 14)). At low matrix densities (large FPCL volumes) crosslinking is not optimized as there can be large distances between substrate sites for the crosslinkers. For high matrix densities (small FPCL volumes), crosslinker efficiency may be reduced as the matrix is too tightly compact or binding sites are obstructed. There may be a matrix density at which crosslinker activity is optimized and the effect on deposition stiffness is greatest. The results of this test showed a gradual early development of material parameters compared to the baseline model (cf. Figure 6.9). After 24 hours, both the μ and c parameters begin to undergo significant changes with the final values reaching levels comparable to the baseline simulation. With regard to the geometry, the variable deposition stiffnesses delay the opening angle development. The simulated values for this hypothesis follow more closely angle development seen experimentally.

The mechanical testing data showed that the material properties of the free-floating FPCLs increase over time. While the material property of the central region did not increase 24 fold as indicated in the baseline simulation, the value changed from the order of tens of Pa to hundreds of Pa in the two day time period. Refinement of the deposition stiffness evolution, as indicated in the hypothesis testing, may provide a more comparable evolution of the material behavior.

Without precise knowledge of the material distribution, it is difficult to determine the material properties of the anisotropic material. Prior experiments have shown that the anisotropic collagen is highly restricted to the periphery of the gel [91]. The parameterization of the mass fractions indicates it is possible for the c parameter to approach values on the order of tens of kPa. Secondly, for the method of testing performed, it was not possible to determine the cross sectional area of the sample at the initiation of force development. The area value used for the stress calculations was likely too large which results in an underestimation of the actual stresses. If the stress values are actually larger, the resulting material properties would also increase.

Like all computational models, this one is not without simplifying assumptions. One of the major assumptions of this model is that of homogeneous deformations. It is likely that there are regional differences in the deformation both radially and axially. Regionally varying deformations would result in changes to the stress distribution within the free-floating FPCL. These variations in the stress field would lead to different distributions in the redistribution of material and further variation of local material behavior. This may also affect cell contractility and further effect the nature of local cell

behavior. Future models should allow for local variation in deformation and explore how this changes the free-floating FPCL evolution.

Similarly, our model assumes a homogeneous distribution of cells and that cells remain uniformly distributed throughout the simulation. The cell orientation is allowed to change, but there is no net migration of cells. This simplifies the model but does not account for prior experimental results. Previous studies have shown an increase cell density in the outer region of the gel compared to the central region [62,91]. Other work has shown that there can be significant apoptosis of cells within the free-floating FPCL even in the first day of compaction [156,172]. Differences in local cell populations would affect not only the local active cell stress magnitude, but also the rate of local remodeling as increases or decreases in local cell density would change the local rate of remodeling.

The final step of each iteration of our model fits simulated biaxial data of the composite material (remaining original material and remodeled material) to determine new material parameters and establish the mechanical behavior for the start of the next iteration. This simplifies the modeling of the mechanical behavior by homogenizing the material behavior of the composite, but this does not allow for the tracking of the condition of constituents deposited at different times as they deform with the composite and the determination of failure of an individual constituent is not possible.

Alterations would need to be made to the constitutive formulations for the active cell stress as well as the removal and distribution functions. They need to account for cell migration, cell viability, as well as the alterations to orientation. The constitutive relations would also need to account for any modulation due to stress to account for cell mechanobiological responses. In line with this is the need to account for cell

differentiation. Multiple reports have shown that cells in the outer region of the free-floating FPCL align parallel to the outer edge, which is accounted for in our model, but also differentiate into myofibroblasts [62,91,116]. The myofibroblast phenotype is capable of more forceful contractions and would lead to changes in the maximum cell stress value [5].

The scope of this model could also be expanded to allow for longer duration simulations. Currently, we simulate 48 hours of free-floating FPCL compaction as there is negligible matrix production and deposition in this time frame. Longer simulation times would need to account for new matrix production as well as the remodeling of existing collagen. It has been postulated that new matrix deposition is necessary to account for at least a portion of the compaction observed after 2 days of culture [41]. This idea is supported by the inhibition of lysyl oxidase, the enzymatic crosslinker necessary to consolidate collagen molecules and fibrils into fibers, in free-floating FPCL experiments [39,41] and Chapter 5. Longer simulation times may also need to account for cell proliferation as well.

In summary, we have developed a continuum-based computational model to simulate the cell-induced compaction and remodeling of the free-floating fibroblast-populated collagen lattice. This is the first model of this assay to account for the experimentally observed matrix remodeling, gross geometric changes, and development of a residual-type stress field within the construct. Further improvements will better our understanding of cell-matrix interactions, mechanobiological responses, and the mechanisms by which cells attempt to develop a preferred mechanical environment.

Chapter 7: Conclusions and Future Direction

7.1 Conclusions

Mechanobiological studies can be confounded by the nature and complexity of biological tissues. As cells are stimulated mechanically, they can alter their local environment leading to changes in the mechanical behavior of this tissue and changing the applied mechanical stimuli. Tissue equivalents can provide simplified systems that allow for careful control of externally applied mechanical loads as well as precise control over the initial biological composition and the chemical environment. Control over the experimental conditions allows for more precise correlation of the mechanical environment to the resulting biological responses of the cells.

The free-floating fibroblast-populated collagen lattice (FPCL) and its variants provide a simple 3D in vitro system to study mechanobiological responses of cells. The traction-free boundary conditions limit the admissible constitutive models that permit compaction of the construct by the resident cells. Chapter 3 provides an initial incompressible model of the free-floating FPCL that examines the nature of the initiation of gel compaction by the resident cells. If the free-floating FPCL behaves nearly incompressible as cells initially spread and begin contracting the matrix, nontrivial deformations are only admissible if both the material behavior and actively-applied cell stress behavior vary radially in the construct. Prior assumptions of the tissue equivalent being wholly isotropic do not allow nontrivial deformations. This initial model also showed that stresses could develop within the construct and that the stress field has a residual-type distribution, meaning compressive stress in the central region transitioning

to tension in the circumferential direction as one moves along the radius to the outer edge.

Chapter 4 expands upon the findings of Chapter 3 to allow for deformations and material behaviors previously exhibited in the free-floating FPCL. The constitutive model for the free-floating FPCL is changed to allow for the compressible behavior exhibited by the tissue equivalent as the cells compact and remodel the matrix resulting in an overall change in the volume of the construct. While mathematically admissible, the prior assumption of isotropy requires radial and axial deformations to be equal, which is not observed experimentally. The theoretical model presented in this chapter indicates, as the model in Chapter 3 also indicated, the presence of a residual-type stress distribution as the result of cell-induced compaction and this requires the radial variation of the material properties and the active cell stresses. The presence of this stress-distribution was confirmed qualitatively through radial cut experiments, which resulted in opening angles that indicate the presence of residual stress in the circumferential direction. The presence of an equibiaxial compressive stress in the center of the free-floating FPCL was also confirmed through the application of a circular hole in the center of the gel that partially closed indicating a lengthening of the surrounding tissue. Finally, this chapter presented the idea that the stresses developed in the free-floating FPCL were the result of the fibroblasts seeking to develop a preferred mechanical environment. Because of the lack of external constraints, however, the cells are only able to develop a residual-type distribution. In this type of stress field, the cells in the outer region may be able to achieve a preferred tensile environment and can even differentiate into myofibroblasts,

but it is at the expense of the cells in the central region of the gel which may begin to undergo apoptosis as they are in a non-optimal mechanical environment.

In Chapter 5, the mechanisms by which cells seek to achieve their preferred mechanical environment were examined experimentally. To develop stress within the matrix, the cells need to be able to entrench applied deformations. The inhibition of the covalent crosslinker tissue transglutaminase (tTG) resulted in reduced or completely inhibited compaction of free-floating FPCLs at early times while the inhibition of lysyl oxidase only resulted in changes of compaction after 2 days in culture. These results suggest tTG as the primary crosslinker responsible for the entrenchment of cell-applied deformations in early remodeling of extant matrix and necessary for the development of residual stress within the tissue equivalent. Also examined was the mode of cell contractility through the removal of cell contractility after set periods of compaction. These results indicated that initial compaction may be mediated primarily by calcium-dependent contractility while at later times calcium-independent pathways such as the Rho-kinase pathway are the preferred means of contractility.

Finally, Chapter 6 expands upon the prior mechanical models to account for the development of the residual stress distribution and the associated deformations. This expanded theoretical model is then used as the foundation for a computational model of free-floating FPCL compaction and remodeling. The computational model is driven by the concept of tensional homeostasis [43], that the cells seek to develop and maintain a preferred mechanical environment. To account for this, remodeling is accounted for via growth and remodeling (G&R) theory-based constitutive relations. That is, the rate of remodeling is dependent upon the deviation of the current mechanical state compared to

the preferred one. Remodeling is increased the larger the difference between the actual stress and the preferred stress. The initial model simulation was performed to closely match previous experimental data and the simulation results were examined to assess the evolution and radial distribution of cell and material behavior.

Using a continuum mechanics-based approach, the theoretical, experimental and computational findings of this work provide greater insight into the cell-driven compaction and remodeling of the free-floating FPCL. This work provides a means to begin correlating the biological responses of cells to mechanical stimuli and the computational model offers an initial model to assess the evolving material properties and subsequent changes in the mechanical environment. Better understanding of cellular mechanobiological responses will increase our understanding of not only normal cell responses and adaptations to perturbations in mechanical stimuli, but also increase our understanding of adaptations or maladaptations associated with various pathologies. Furthermore, the computational model of the evolving free-floating FPCL provides an in silico framework to test hypotheses and guide experimental work.

7.2 Future Direction

7.2.1 Free-floating FPCL Computation Model Improvements

The computational model presented here provides the first model to assess both matrix remodeling and, at least qualitatively, estimate the evolution of the mechanical environment of the free-floating FPCL. As proposed in Chapter 6, the model is not without simplifying assumptions. The greatest need of this model is experimental data related to the mechanical properties. Initial mechanical testing was performed but the

nature of the constructs may make it difficult to properly assess the material properties. Free-floating FPCLs are cast as dilute collagen solutions which lead them to be delicate and easily torn if improperly handled. There has been some previous work done to characterize the initial material properties of dilute collagen gels [87,130]. These studies estimate the compressive stiffness of the collagen gels to be in the range of 15-75 Pa. This is very soft when compared to the tensile properties of constrained collagen gels which can be in range of 2-24 kPa [42,96]. Secondly, as the free-floating FPCL is compacted, collagen in the outer region is reoriented circumferentially which will change the material behavior in this region. The amount of matrix that is reoriented, however, is minimal when compared to the isotropic central region. Directly assessing the mechanical properties of this region has proven to be difficult.

Improved mechanical testing methods should seek to allow testing at multiple radial locations. Indentation testing with smaller indenters would allow for this. Improved methodology is also need to directly determine the mechanical behavior of the outer aligned region of the gel

As mentioned in Chapter 6, it is likely that the cell-applied deformations can vary regionally in a similar manner compared to the material properties. The current form of the computational model assumes homogeneous deformations, meaning the deformations are uniform throughout the simulated domain. This allows the initial boundary value problem and subsequent constrained mixture problem to be solved analytically. If nonhomogeneous deformations are allowed, a finite element model would need to be implemented in order to solve for the potentially radially varying deformations. This also needs to be verified experimentally by determining the local material deformations

during cell-induced remodeling. Such a model would provide refinement of local material properties and in turn provide a better estimation of local mechanical environments. These improved estimations would allow for a more precise correlation of mechanical stimuli to biological responses.

7.2.2 Biaxial Bioreactor

The free-floating FPCL provides a simple, unconstrained, high throughput system to study mechanobiological responses. Being unconstrained, however, provides no external means to directly control the mechanical environment of the tissue equivalent. Planar biaxial tissue equivalents allow for the precise control of external loads on the construct along two axes. As stated in Chapter 2, these types of tissue equivalents have been assessed mechanically and preliminary computational simulations have been carried out examining their growth and remodeling [78,81,82,99,106]. Mechanical assessment of biaxial tissue equivalents has been focused on the material behavior at a given time point or on the time-dependent changes through the terminal testing of different samples at different time points.

Secondly, current biaxial tissue equivalent systems are capable of only loading the tissue constructs statically via either a constant force application or a held displacement [78,81–83,99]. These types of mechanical loads allow the assessment of mechanobiological responses to a single, initial stimulus. In vivo, however, many mechanical stimuli are applied cyclically such as the repetitive motion of a ligament or tendon during physical activity or the cyclic distension of a large artery due to cardiac output.

To this end, we designed a planar biaxial bioreactor that allows for the cyclic loading of tissue equivalents in culture and should allow for an individual sample to be tested at multiple time points to examine the changes in material behavior within a single construct.

7.2.2.1 Bioreactor Design

Our bioreactor design is a modification of previously proposed and implemented biaxial systems [78,106]. A schematic representation is shown in Figure 7.1 and the technical drawings can be found in Appendix D. Briefly, the main chamber (Figure 7.1-A) is constructed from a single piece of glass-filled polycarbonate. The chamber is bored out in a cruciform shape to limit the amount of culture medium necessary to submerge the tissue equivalent. Through holes on the sides of the chamber allow stainless steel loading arm to be connected to linear acme screws (Figure 7.1-B; Thomson BSA). A submersible force transducer (Honeywell) is included for each axis to allow for the measurement of force. The linear screws are driven by hermetically-sealed NEMA-17 stepper motors (Advanced Micro Systems) to allow for continuous use within the humid environment of the cell culture incubator. The lid of the chamber has ports to attach filters to allow for sterile gas exchange and a central glass window for the imaging of the sample during mechanical testing. These components can then be attached to a polycarbonate baseplate. A camera is required to track deformations during mechanical testing, so a kinematic baseplate (Figure 7.1-C; ThorLabs) is also attached to the main baseplate. This allows for the camera (Figure 7.1-D; Allied Vision Technologies) and its

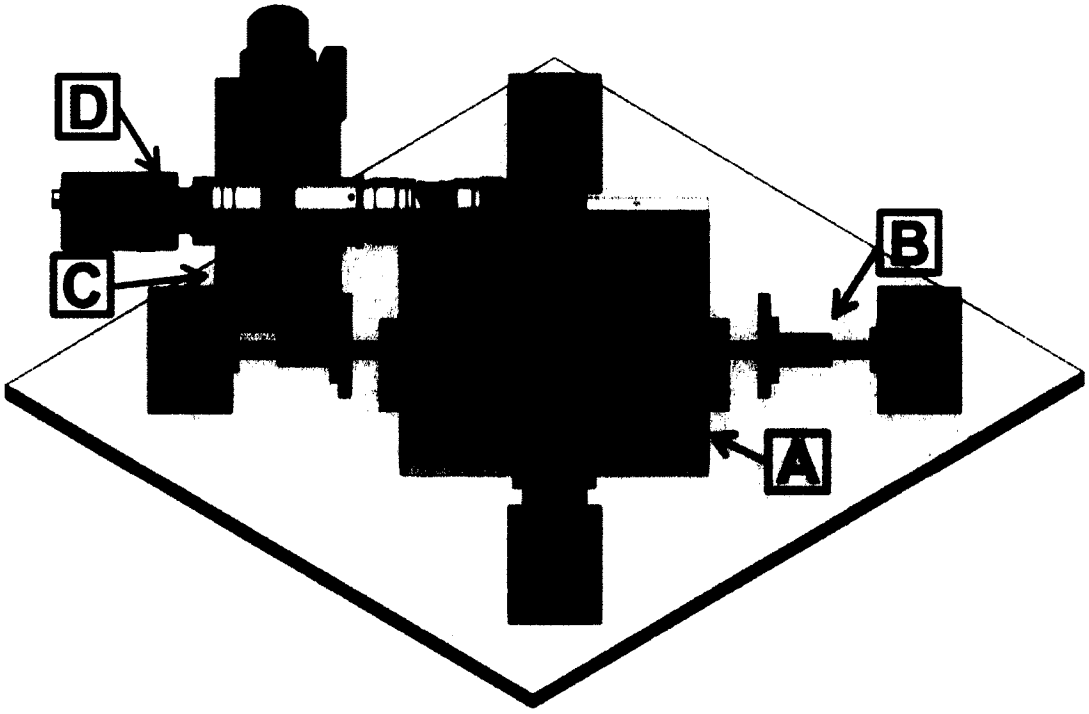

Figure 7.1 Schematic representation of biaxial bioreactor. Key components are labeled as follows: (A) culture chamber, (B) linear screw, (C) kinematic base for camera stand, (D) CCD camera.

stand to be connected to the baseplate to perform mechanical testing within the incubator chamber.

The key advantage of this design is that it allows for culture protocols and mechanical testing to be performed using the same system. The hardware control and data collection are performed using custom LabView (National Instruments) programs. The culture program allows for equibiaxial, nonequibiaxial (different level of stretch on each axis), and strip biaxial (one axis held statically while other is stretched cyclically) cyclic loading protocols. The mechanical testing program is designed to perform automated equibiaxial stretch, and constant stretch (one axis held at a fixed stretch while the other axis is stretched at a constant rate from the minimum stretch level to the maximum and back to the minimum) protocols.

7.2.2.2 Tissue Culture Conditions

The initial collagen casting solution should be similar to that of the free-floating FPCL. Modifications may be necessary in the initial collagen concentration and cell density. Because these tissue equivalents are to be cyclically loaded, the initial collagen concentration will likely need to be increased to allow the construct to bear the applied loads. Increasing the collagen concentration also would require an increase in cell density if remodeling rates similar to those of the free-floating FPCL are wanted.

Another modification to the initial collagen solution is the inclusion of 100 μm diameter black microspheres (IMT/Stason Pharmaceuticals) which are used as markers to track motions during mechanical testing. These markers are not neutrally buoyant and settle to the bottom of the mold during gelation. This is advantageous as after gelation the

tissue equivalent can be inverted and the markers will be attached to the now apical surface and not embedded within the tissue. Finally, the collagen is cast into a cruciform-shaped mold with rectangular sections of a porous, hydrophilically-treated polyethylene sheet at the ends of the arms. The collagen solution penetrates into the polyethylene before gelation, allowing the tissue equivalent to be attached to the loading arms by gripping the polyethylene.

7.2.2.3 Preliminary Results

Initial tests with the bioreactor system examined the initial culture conditions to allow for successful culturing of the tissue equivalents. The initial testing was performed using an equibiaxial culture protocol with a loading frequency of 1 Hz and a grip-to-grip stretch of 2.5%. It was found that an initial collagen concentration 2.5 mg/mL was capable of being cyclically loaded. Lower concentrations would regularly tear. Even at a concentration 2.5 mg/mL, cruciforms were still susceptible to tearing. Tearing usually occurs at the edge of a polyethylene grip and seemed to happen due to cellular contraction and remodeling against the cyclic loading as tearing would only occur after 3 to 4 days of cyclic loading. A possible improvement to possibly prevent tearing would be to include tTG in the initial seeding solution to augment the initial material properties of the tissue equivalent. Increased initial collagen density may also help, but this will slow the rate of remodeling.

With the biaxial tissue equivalents needing higher collagen concentrations compared to the free-floating FPCLs, high cell densities are needed as well to obtain similar remodeling or compaction rates. For initial tests, cell concentrations of 500,000

cells/mL were used. This density was necessary to see appreciable remodeling, or gross geometric changes, within 24 hours of culture (see Figure 7.2 for example of geometric changes over 5 days of cyclic loading).

Finally, initial mechanical testing has been attempted will minimal success. One difficulty is the determination of the unloaded configuration as force levels at early time points may be minimal (<1 gram of force (gf) compared to 50 gf range of the force transducer). Secondly, the range of stretch values that can be used in the mechanical testing has been less than previously estimated (max stretch expected ~1.1 [81,82,99], specimens are tearing at ~1.04). It is not known, however, if this is possibly due to the cyclic loading as prior testing on statically loaded specimens has shown the constructs to be more compliant.

Figure 7.3 shows the loading curves for both the x and y axis of a specimen that was cyclically stretched 2.5% equibiaxially for 5 days. Only loading curves are shown as one of the x-axis arms tore at a stretch of ~1.03. The specimen showed a characteristic isotropic response that is expected for an equibiaxially loaded specimen. Also, the specimen exhibited a nonlinear response related to stretch.

In connection with the experimental system, a computational model of biaxial tissue equivalents needs to be examined. Prior work has been done on this front [106] and implementation of a model comparable to the one proposed in Chapter 6 would provide a computational framework that can be readily optimized against experimental data via the schema proposed in Chapter 2 (Figure 2.4). The implementation and verification of this combined experimental and computational approach would provide a controllable and

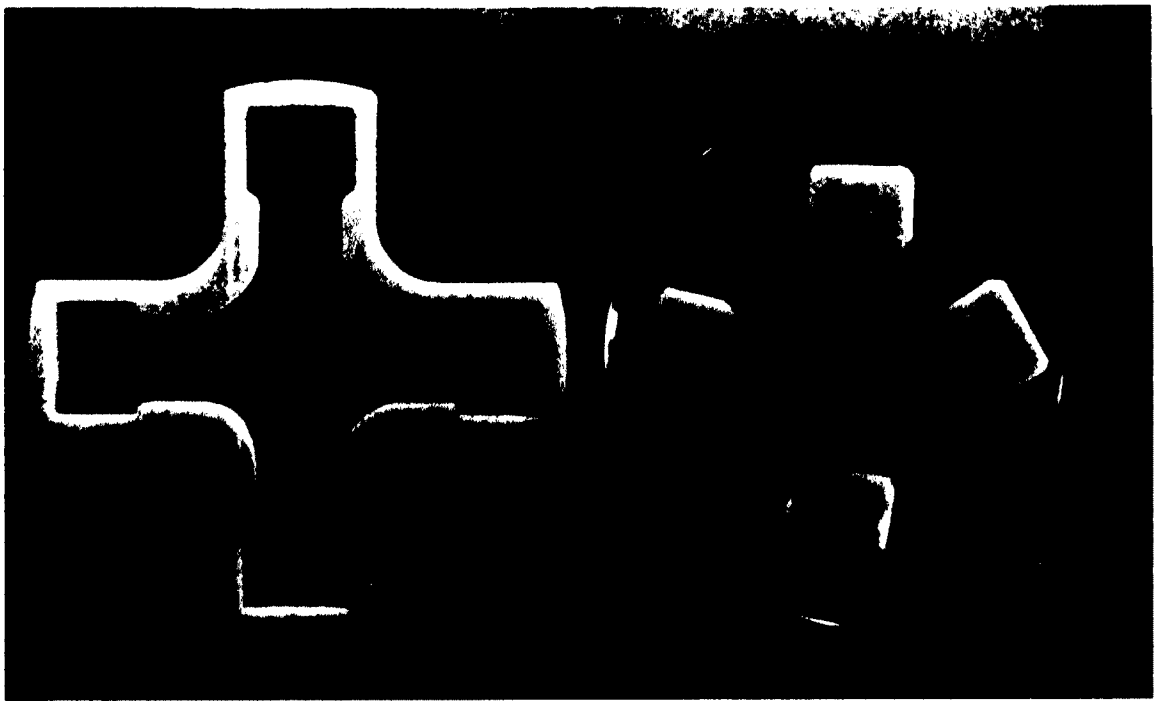

Figure 7.2 Biaxial tissue equivalent example. Representative image of cruciform-shaped biaxial tissue equivalent. The cruciform mold, *left*, and a 5 day cyclically loaded gel, *right*, are shown. Note the thinning of the cruciform arms in the compacted gel compared to the dimensions of the mold.

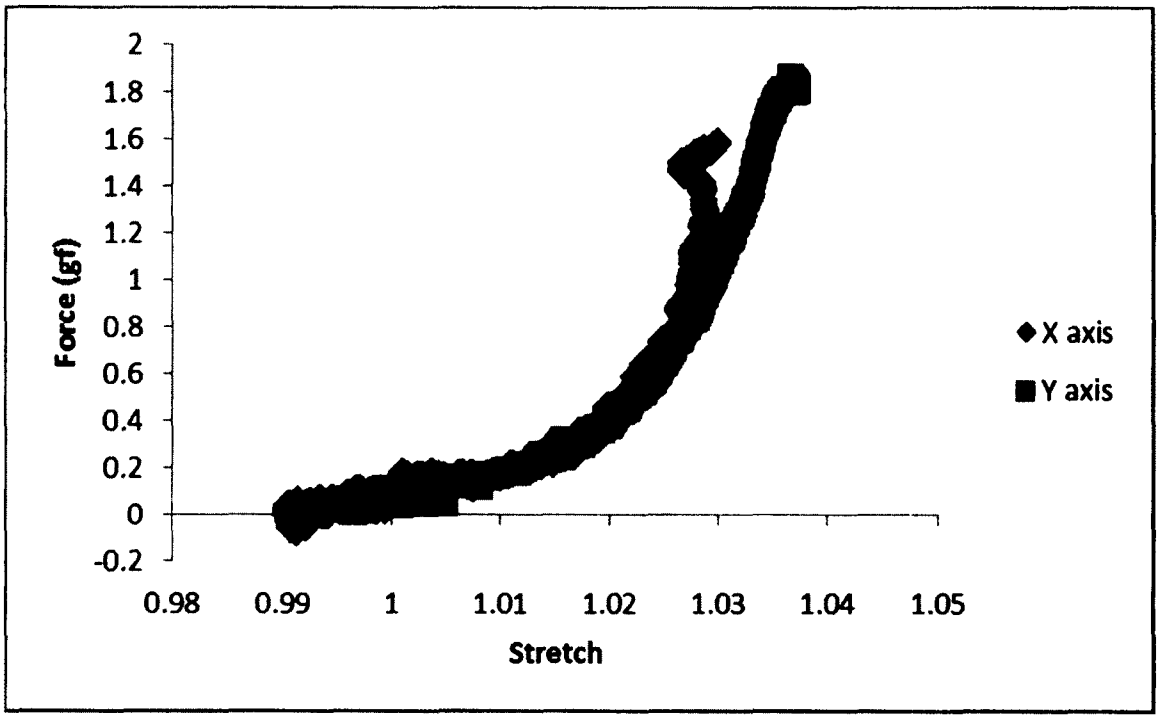

Figure 7.3 Example equibiaxial testing data. Loading curve of a biaxial tissue equivalent during equibiaxial mechanical testing.

tunable system to examine mechanobiological responses of multiple cell and tissue types to a wide array of mechanical stimuli.

References

[1] Jaklenec, A., Stamp, A., Deweerd, E., Sherwin, A., and Langer, R., 2012, "Progress in the Tissue Engineering and Stem Cell Industry 'Are we there yet?,'" Tissue Eng. Part B Rev., **18**(3), pp. 155–166.

[2] Bell, E., Ivarsson, B., and Merrill, C., 1979, "Production of a tissue-like structure by contraction of collagen lattices by human fibroblasts of different proliferative potential in vitro.," Proc. Natl. Acad. Sci. U. S. A., **76**(3), pp. 1274–8.

[3] Dallon, J. C., and Ehrlich, H. P., 2008, "A review of fibroblast-populated collagen lattices.," Wound Repair Regen., **16**(4), pp. 472–9.

[4] Grinnell, F., 2003, "Fibroblast biology in three-dimensional collagen matrices," Trends Cell Biol., **13**(5), pp. 264–269.

[5] Tomasek, J. J., Gabbiani, G., Hinz, B., Chaponnier, C., and Brown, R. A., 2002, "Myofibroblasts and mechano-regulation of connective tissue remodelling," Nat. Rev. Mol. Cell Biol., **3**(5), pp. 349–363.

[6] Prockop, J. D., 1995, "Collagens: Molecular Biology, Diseases, and Potentials for Therapy," Annu. Rev. Biochem., **64**(1), pp. 403–434.

[7] Birk, D. E., and Brückner, P., 2011, "Collagens, Suprastructures, and Collagen Fibril Assembly," The Extracellular Matrix: an Overview, R.P. Mecham, ed., Springer Berlin Heidelberg, pp. 77–115.

[8] Laurent, G. J., 1987, "Dynamic state of collagen: pathways of collagen degradation in vivo and their possible role in regulation of collagen mass," Am. J. Physiol. - Cell Physiol., **252**(1), pp. C1–C9.

[9] Klingberg, F., Hinz, B., and White, E. S., 2013, "The myofibroblast matrix: implications for tissue repair and fibrosis," J. Pathol., **229**(2), pp. 298–309.

[10] Wight, T. N., Toole, B. P., and Hascall, V. C., 2011, "Hyaluronan and the Aggregating Proteoglycans," The Extracellular Matrix: an Overview, R.P. Mecham, ed., Springer Berlin Heidelberg, pp. 147–195.

[11] Barczyk, M., Carracedo, S., and Gullberg, D., 2010, "Integrins," Cell Tissue Res., **339**(1), pp. 269–280.

[12] Sorrell, J. M., and Caplan, A. I., 2009, "Chapter 4 Fibroblasts—A Diverse Population at the Center of It All," International Review of Cell and Molecular Biology, Kwang W. Jeon, ed., Academic Press, pp. 161–214.

[13] Vedrenne, N., Coulomb, B., Danigo, A., Bonté, F., and Desmoulière, A., 2012, "The complex dialogue between (myo)fibroblasts and the extracellular matrix during skin repair processes and ageing," Pathol. Biol., **60**(1), pp. 20–27.

[14] Darby, I., Skalli, O., and Gabbiani, G., 1990, "Alpha-smooth muscle actin is transiently expressed by myofibroblasts during experimental wound healing," Lab. Investig. J. Tech. Methods Pathol., **63**(1), pp. 21–29.

[15] Nathan, C., and Sporn, M., 1991, "Cytokines in context.," J. Cell Biol., **113**(5), pp. 981–986.

[16] Pierce, G. F., Mustoe, T. A., Altrock, B. W., Deuel, T. F., and Thomason, A., 1991, "Role of platelet-derived growth factor in wound healing," J. Cell. Biochem., **45**(4), pp. 319–326.

[17] Sigal, L. H., 2012, "Basic Science for the Clinician 57 - Transforming Growth Factor Beta," J. Clin. Rheumatol., **18**(5), pp. 268–272.

[18] Jayme, D. W., 2001, "Cell Culture Media," eLS, John Wiley & Sons, Ltd.
[19] Hayenga, H. N., Thorne, B. C., Yen, P., Papin, J. A., Peirce, S. M., and Humphrey, J. D., 2013, "Multiscale Computational Modeling in Vascular Biology: From Molecular Mechanisms to Tissue-Level Structure and Function," Multiscale Computer Modeling in Biomechanics and Biomedical Engineering, A. Gefen, ed., Springer Berlin Heidelberg, pp. 209–240.
[20] Wang, J. H. C., and Thampatty, B. P., 2006, "An introductory review of cell mechanobiology," Biomech. Model. Mechanobiol., **5**(1), pp. 1–16.
[21] Nagatomi, J., 2011, Mechanobiology Handbook, Taylor & Francis US.
[22] Discher, D. E., Janmey, P., and Wang, Y., 2005, "Tissue cells feel and respond to the stiffness of their substrate," Science, **310**(5751), pp. 1139–1143.
[23] Chen, C. S., 2008, "Mechanotransduction–a field pulling together?," J. Cell Sci., **121**(20), pp. 3285–3292.
[24] Cukierman, E., Pankov, R., Stevens, D. R., and Yamada, K. M., 2001, "Taking Cell-Matrix Adhesions to the Third Dimension," Science, **294**(5547), pp. 1708–1712.
[25] Chiquet, M., Gelman, L., Lutz, R., and Maier, S., 2009, "From mechanotransduction to extracellular matrix gene expression in fibroblasts," Biochim. Biophys. Acta BBA - Mol. Cell Res., **1793**(5), pp. 911–920.
[26] Ehrlich, H. P., 2003, "The fibroblast-populated collagen lattice," Methods Mol. Med., **78**, pp. 277–291.
[27] Ehrlich, H. P., and Rittenberg, T., 2000, "Differences in the mechanism for high- versus moderate-density fibroblast-populated collagen lattice contraction.," J. Cell. Physiol., **185**(3), pp. 432–9.
[28] Harris, A. K., Wild, P., and Stopak, D., 1980, "Silicone rubber substrata: a new wrinkle in the study of cell locomotion," Science, **208**(4440), pp. 177–179.
[29] Steinberg, B. M., Smith, K., Colozzo, M., and Pollack, R., 1980, "Establishment and transformation diminish the ability of fibroblasts to contract a native collagen gel.," J. Cell Biol., **87**(1), pp. 304–308.
[30] Buttle, D. J., and Ehrlich, H. P., 1983, "Comparative studies of collagen lattice contraction utilizing a normal and a transformed cell line," J. Cell. Physiol., **116**(2), pp. 159–166.
[31] Ehrlich, H. P., Griswold, T. R., and Rajaratnam, J. B. M., 1986, "Studies on vascular smooth muscle cells and dermal fibroblasts in collagen matrices. Effects of heparin.," Exp. Cell Res., **164**(1), pp. 154–62.
[32] Travis, J. A., Hughes, M. G., Wong, J. M., Wagner, W. D., and Geary, R. L., 2001, "Hyaluronan Enhances Contraction of Collagen by Smooth Muscle Cells and Adventitial Fibroblasts Role of CD44 and Implications for Constrictive Remodeling," Circ. Res., **88**(1), pp. 77–83.
[33] Orlandi, A., Ferlosio, A., Gabbiani, G., Spagnoli, L. G., and Ehrlich, H. P., 2005, "Phenotypic heterogeneity influences the behavior of rat aortic smooth muscle cells in collagen lattice.," Exp. Cell Res., **311**(2), pp. 317–27.
[34] Ehrlich, H. P., 1988, "The modulation of contraction of fibroblast populated collagen lattices by types I, II, and III collagen," Tissue Cell, **20**(1), pp. 47–50.

[35] Tiollier, J., Dumas, H., Tardy, M., and Tayot, J.-L., 1990, "Fibroblast behavior on gels of type I, III, and IV human placental collagens," Exp. Cell Res., **191**(1), pp. 95–104.

[36] Frey, J., Chamson, A., Raby, N., and Rattner, A., 1995, "Collagen bioassay by the contraction of fibroblast-populated collagen lattices," Biomaterials, **16**(2), pp. 139–143.

[37] Lorimier, S., Gillery, P., Hornebeck, W., Chastang, F., Laurent-Maquin, D., Bouthors, S., Droulle, C., Potron, G., and Maquart, F.-X., 1996, "Tissue origin and extracellular matrix control neutral proteinase activity in human fibroblast three-dimensional cultures," J. Cell. Physiol., **168**(1), pp. 188–198.

[38] Zhang, Z., Garron, T. M., Li, X. J., Liu, Y., Zhang, X., Li, Y. Y., and Xu, W. S., 2009, "Recombinant human decorin inhibits TGF-β_1-induced contraction of collagen lattice by hypertrophic scar fibroblasts," Burns, **35**(4), pp. 527–537.

[39] Kagan, H. M., 2000, "Intra- and extracellular enzymes of collagen biosynthesis as biological and chemical targets in the control of fibrosis," Acta Trop., **77**(1), pp. 147–152.

[40] Woodley, D. T., Yamauchi, M., Wynn, K. C., Mechanic, G., and Briggaman, R. A., 1991, "Collagen Telopeptides (Cross-Linking Sites) Play a Role in Collagen Gel Lattice Contraction," J. Invest. Dermatol., **97**(3), pp. 580–585.

[41] Redden, R. A., and Doolin, E. J., 2003, "Collagen crosslinking and cell density have distinct effects on fibroblast-mediated contraction of collagen gels," Skin Res. Technol., **9**(3), pp. 290–293.

[42] Marenzana, M., Wilson-Jones, N., Mudera, V., and Brown, R. A., 2006, "The origins and regulation of tissue tension: Identification of collagen tension-fixation process in vitro," Exp. Cell Res., **312**(4), pp. 423–433.

[43] Brown, R. A., Prajapati, R., McGrouther, D. A., Yannas, I. V., and Eastwood, M., 1998, "Tensional homeostasis in dermal fibroblasts: Mechanical responses to mechanical loading in three-dimensional substrates," J. Cell. Physiol., **175**(3), pp. 323–332.

[44] Humphrey, J. D., 2008, "Vascular Adaptation and Mechanical Homeostasis at Tissue, Cellular, and Sub-cellular Levels," Cell Biochem. Biophys., **50**(2), pp. 53–78.

[45] Schiro, J. A., Chan, B. M. C., Roswit, W. T., Kassner, P. D., Pentland, A. P., Hemler, M. E., Eisen, A. Z., and Kupper, T. S., 1991, "Integrin $\alpha 2\beta 1$ (VLA-2) mediates reorganization and contraction of collagen matrices by human cells," Cell, **67**(2), pp. 403–410.

[46] Langholz, O., Röckel, D., Mauch, C., Kozlowska, E., Bank, I., Krieg, T., and Eckes, B., 1995, "Collagen and collagenase gene expression in three-dimensional collagen lattices are differentially regulated by alpha 1 beta 1 and alpha 2 beta 1 integrins.," J. Cell Biol., **131**(6), pp. 1903–1915.

[47] Kelynack, K. J., Hewitson, T. D., Nicholls, K. M., Darby, I. A., and Becker, G. J., 2000, "Human renal fibroblast contraction of collagen I lattices is an integrin-mediated process," Nephrol. Dial. Transplant., **15**(11), pp. 1766–1772.

[48] Cooke, M. E., Sakai, T., and Mosher, D. F., 2000, "Contraction of collagen matrices mediated by alpha2beta1A and alpha(v)beta3 integrins.," J. Cell Sci., **113** (**Pt 1**, pp. 2375–83.

[49] Grundström, G., Mosher, D. F., Sakai, T., and Rubin, K., 2003, "Integrin αvβ3 mediates platelet-derived growth factor-BB-stimulated collagen gel contraction in cells expressing signaling deficient integrin α2β1," Exp. Cell Res., **291**(2), pp. 463–473.

[50] Ehrlich, H. P., Buttle, D. J., and Bernanke, D. H., 1989, "Physiological variables affecting collagen lattice contraction by human dermal fibroblasts," Exp. Mol. Pathol., **50**(2), pp. 220–229.

[51] Montesano, R., and Orci, L., 1988, "Transforming Growth Factor β Stimulates Collagen-Matrix Contraction by Fibroblasts: Implications for Wound Healing," Proc. Natl. Acad. Sci. U. S. A., **85**(13), pp. 4894–4897.

[52] Arora, P. D., Narani, N., and McCulloch, C. A. G., 1999, "The Compliance of Collagen Gels Regulates Transforming Growth Factor-β Induction of α-Smooth Muscle Actin in Fibroblasts," Am. J. Pathol., **154**(3), pp. 871–882.

[53] Grinnell, F., Ho, C.-H., Lin, Y.-C., and Skuta, G., 1999, "Differences in the Regulation of Fibroblast Contraction of Floating Versus Stressed Collagen Matrices," J. Biol. Chem., **274**(2), pp. 918–923.

[54] Ikuno, Y., and Kazlauskas, A., 2002, "TGFβ1-dependent contraction of fibroblasts is mediated by the PDGFα receptor," Invest. Ophthalmol. Vis. Sci., **43**(1), pp. 41–46.

[55] Jiang, H., Rhee, S., Ho, C. H., and Grinnell, F., 2008, "Distinguishing fibroblast promigratory and procontractile growth factor environments in 3-D collagen matrices," FASEB J., **22**(7), pp. 2151–2160.

[56] Battegay, E. J., Raines, E. W., Seifert, R. A., Bowen-Pope, D. F., and Ross, R., 1990, "TGF-β induces bimodal proliferation of connective tissue cells via complex control of an autocrine PDGF loop," Cell, **63**(3), pp. 515–524.

[57] Ignotz, R. A., and Massagué, J., 1987, "Cell adhesion protein receptors as targets for transforming growth factor-β action," Cell, **51**(2), pp. 189–197.

[58] Heino, J., Ignotz, R. A., Hemler, M. E., Crouse, C., and Massague, J., 1989, "Regulation of cell adhesion receptors by transforming growth factor-beta. Concomitant regulation of integrins that share a common beta 1 subunit.," J. Biol. Chem., **264**(1), pp. 380–388.

[59] Leof, E. B., Proper, J. A., Getz, M. J., and Moses, H. L., 1986, "Transforming growth factor type β regulation of actin mRNA," J. Cell. Physiol., **127**(1), pp. 83–88.

[60] Lin, Y. C., and Grinnell, F., 1993, "Decreased level of PDGF-stimulated receptor autophosphorylation by fibroblasts in mechanically relaxed collagen matrices," J. Cell Biol., **122**(3), pp. 663–672.

[61] Daniels, J. T., Cambrey, A. D., Occleston, N. L., Garrett, Q., Tarnuzzer, R. W., Schultz, G. S., and Khaw, P. T., 2003, "Matrix metalloproteinase inhibition modulates fibroblast-mediated matrix contraction and collagen production in vitro," Invest. Ophthalmol. Vis. Sci., **44**(3), pp. 1104–1110.

[62] Ehrlich, H. P., and Rajaratnam, J. B. M., 1990, "Cell locomotion forces versus cell contraction forces for collagen lattice contraction: An in vitro model of wound contraction," Tissue Cell, **22**(4), pp. 407–417.

[63] Costa, K. D., Lee, E. J., and Holmes, J. W., 2003, "Creating alignment and anisotropy in engineered heart tissue: role of boundary conditions in a model three-dimensional culture system," Tissue Eng., **9**(4), pp. 567–577.

[64] Delvoye, P., Wiliquet, P., Levêque, J.-L., Nusgens, B. V., and Lapière, C. M., 1991, "Measurement of Mechanical Forces Generated by Skin Fibroblasts Embedded in a Three-Dimensional Collagen Gel," J. Invest. Dermatol., **97**(5), pp. 898–902.

[65] Kolodney, M. S., and Wysolmerski, R. B., 1992, "Isometric contraction by fibroblasts and endothelial cells in tissue culture: a quantitative study," J. Cell Biol., **117**(1), pp. 73–82.

[66] Eastwood, M., McGrouther, D. A., and Brown, R. A., 1994, "A culture force monitor for measurement of contraction forces generated in human dermal fibroblast cultures: evidence for cell-matrix mechanical signalling," Biochim. Biophys. Acta BBA-Gen. Subj., **1201**(2), pp. 186–192.

[67] Mauch, C., Mark, K. van der, Helle, O., Mollenhauer, J., Pfäffle, M., and Krieg, T., 1988, "A defective cell surface collagen-binding protein in dermatosparactic sheep fibroblasts.," J. Cell Biol., **106**(1), pp. 205–211.

[68] Porter, R. A., Brown, R. A., Eastwood, M., Occleston, N. L., and Khaw, P. T., 1998, "Ultrastructural changes during contraction of collagen lattices by ocular fibroblasts," Wound Repair Regen., **6**(2), pp. 157–166.

[69] Hall, S. M., Soueid, A., Smith, T., Brown, R. A., Haworth, S. G., and Mudera, V., 2007, "Spatial differences of cellular origins and in vivo hypoxia modify contractile properties of pulmonary artery smooth muscle cells: lessons for arterial tissue engineering.," J. Tissue Eng. Regen. Med., **1**(4), pp. 287–95.

[70] Nirmalanandhan, V. S., Levy, M. S., Huth, A. J., and Butler, D. L., 2006, "Effects of cell seeding density and collagen concentration on contraction kinetics of mesenchymal stem cell-seeded collagen constructs," Tissue Eng., **12**(7), pp. 1865–1872.

[71] Brown, R. A., Talas, G., Porter, R. A., McGrouther, D. A., and Eastwood, M., 1996, "Balanced mechanical forces and microtubule contribution to fibroblast contraction," J. Cell. Physiol., **169**(3), pp. 439–447.

[72] Brown, R. A., Sethi, K. K., Gwanmesia, I., Raemdonck, D., Eastwood, M., and Mudera, V., 2002, "Enhanced Fibroblast Contraction of 3D Collagen Lattices and Integrin Expression by TGF-β1 and-β3: Mechanoregulatory Growth Factors?," Exp. Cell Res., **274**(2), pp. 310–322.

[73] Bisson, M. A., Beckett, K. S., McGrouther, D. A., Grobbelaar, A. O., and Mudera, V., 2009, "Transforming Growth Factor-β1 Stimulation Enhances Dupuytren's Fibroblast Contraction in Response to Uniaxial Mechanical Load Within a 3-Dimensional Collagen Gel," J. Hand Surg., **34**(6), pp. 1102–1110.

[74] Karamichos, D., Brown, R. a, and Mudera, V., 2007, "Collagen stiffness regulates cellular contraction and matrix remodeling gene expression.," J. Biomed. Mater. Res. A, **83**(3), pp. 887–94.

[75] Prajapati, R. T., Chavally-Mis, B., Herbage, D., Eastwood, M., and Brown, R. A., 2000, "Mechanical loading regulates protease production by fibroblasts in three-dimensional collagen substrates," Wound Repair Regen., **8**(3), pp. 226–237.

[76] Prajapati, R. T., Eastwood, M., and Brown, R. A., 2000, "Duration and orientation of mechanical loads determine fibroblast cyto-mechanical activation: Monitored by protease release," Wound Repair Regen., **8**(3), pp. 238–246.

[77] Knezevic, V., Sim, A. J., Borg, T. K., and Holmes, J. W., 2002, "Isotonic biaxial loading of fibroblast-populated collagen gels: a versatile, low-cost system for the study of mechanobiology," Biomech. Model. Mechanobiol., **1**(1), pp. 59–67.

[78] Hu, J.-J., Humphrey, J. D., and Yeh, A. T., 2009, "Characterization of engineered tissue development under biaxial stretch using nonlinear optical microscopy.," Tissue Eng. Part A, **15**(7), pp. 1553–64.

[79] Jhun, C.-S., Evans, M. C., Barocas, V. H., and Tranquillo, R. T., 2009, "Planar biaxial mechanical behavior of bioartificial tissues possessing prescribed fiber alignment.," J. Biomech. Eng., **131**(8), p. 081006.

[80] Thomopoulos, S., Fomovsky, G. M., and Holmes, J. W., 2005, "The Development of Structural and Mechanical Anisotropy in Fibroblast Populated Collagen Gels," J. Biomech. Eng., **127**(5), p. 742.

[81] Lee, E. J., Holmes, J. W., and Costa, K. D., 2008, "Remodeling of engineered tissue anisotropy in response to altered loading conditions," Ann. Biomed. Eng., **36**(8), pp. 1322–1334.

[82] Sander, E. A., Stylianopoulos, T., Tranquillo, R. T., and Barocas, V. H., 2009, "Image-based biomechanics of collagen-based tissue equivalents," IEEE Eng. Med. Biol. Mag., **28**(3), pp. 10–18.

[83] Sander, E. A., Stylianopoulos, T., Tranquillo, R. T., and Barocas, V. H., 2009, "Image-based multiscale modeling predicts tissue-level and network-level fiber reorganization in stretched cell-compacted collagen gels," Proc. Natl. Acad. Sci., **106**(42), pp. 17675–17680.

[84] Raghupathy, R., Witzenburg, C., Lake, S. P., Sander, E. A., and Barocas, V. H., 2011, "Identification of regional mechanical anisotropy in soft tissue analogs," J. Biomech. Eng., **133**(9), p. 091011.

[85] Sander, E. a, Barocas, V. H., and Tranquillo, R. T., 2011, "Initial fiber alignment pattern alters extracellular matrix synthesis in fibroblast-populated fibrin gel cruciforms and correlates with predicted tension.," Ann. Biomed. Eng., **39**(2), pp. 714–29.

[86] Moon, A. G., and Tranquillo, R. T., 1993, "Fibroblast-populated collagen microsphere assay of cell traction force: Part 1. Continuum model," AIChE J., **39**(1), pp. 163–177.

[87] Barocas, V. H., Moon, A. G., and Tranquillo, R. T., 1995, "The fibroblast-populated collagen microsphere assay of cell traction force--Part 2: Measurement of the cell traction parameter," J. Biomech. Eng., **117**(2), pp. 161–170.

[88] Ramtani, S., 2004, "Mechanical modelling of cell/ECM and cell/cell interactions during the contraction of a fibroblast-populated collagen microsphere: theory and model simulation," J. Biomech., **37**(11), pp. 1709–1718.

[89] John, J., Quinlan, A. T., Silvestri, C., and Billiar, K., 2010, "Boundary Stiffness Regulates Fibroblast Behavior in Collagen Gels," Ann. Biomed. Eng., **38**(3), pp. 658–673.

[90] Simon, D. D., and Humphrey, J. D., 2012, "On a class of admissible constitutive behaviors in free-floating engineered tissues," Int. J. Non-Linear Mech., **47**(2), pp. 173–178.
[91] Simon, D. D., Horgan, C. O., and Humphrey, J. D., 2012, "Mechanical restrictions on biological responses by adherent cells within collagen gels," J. Mech. Behav. Biomed. Mater., **14**, pp. 216–226.
[92] Waldman, S. D., and Lee, J. M., 2002, "Boundary conditions during biaxial testing of planar connective tissues. Part 1: Dynamic Behavior," J. Mater. Sci. Mater. Med., **13**(10), pp. 933–938.
[93] Waldman, S. D., and Lee, J. M., 2005, "Effect of sample geometry on the apparent biaxial mechanical behaviour of planar connective tissues," Biomaterials, **26**(35), pp. 7504–7513.
[94] Stylianopoulos, T., and Barocas, V. H., 2007, "Volume-averaging theory for the study of the mechanics of collagen networks," Comput. Methods Appl. Mech. Eng., **196**(31–32), pp. 2981–2990.
[95] Voytik-Harbin, S. L., Roeder, B. A., Sturgis, J. E., Kokini, K., and Robinson, J. P., 2003, "Simultaneous Mechanical Loading and Confocal Reflection Microscopy for Three-Dimensional Microbiomechanical Analysis of Biomaterials and Tissue Constructs," Microsc. Microanal., **9**(01), pp. 74–85.
[96] Roeder, B. A., Kokini, K., Robinson, J. P., and Voytik-Harbin, S. L., 2004, "Local, three-dimensional strain measurements within largely deformed extracellular matrix constructs.," J. Biomech. Eng., **126**(6), pp. 699–708.
[97] Tower, T. T., Neidert, M. R., and Tranquillo, R. T., 2002, "Fiber alignment imaging during mechanical testing of soft tissues.," Ann. Biomed. Eng., **30**(10), pp. 1221–33.
[98] Billiar, K. L., and Sacks, M. S., 2000, "Biaxial Mechanical Properties of the Native and Glutaraldehyde-Treated Aortic Valve Cusp: Part II—A Structural Constitutive Model," J. Biomech. Eng., **122**(4), pp. 327–335.
[99] Thomopoulos, S., Fomovsky, G. M., Chandran, P. L., and Holmes, J. W., 2007, "Collagen Fiber Alignment Does Not Explain Mechanical Anisotropy in Fibroblast Populated Collagen Gels," J. Biomech. Eng., **129**(5), pp. 642–650.
[100] Baek, S., Gleason, R. L., Rajagopal, K. R., and Humphrey, J. D., 2007, "Theory of small on large: Potential utility in computations of fluid–solid interactions in arteries," Comput. Methods Appl. Mech. Eng., **196**(31–32), pp. 3070–3078.
[101] Rodriguez, E. K., Hoger, A., and McCulloch, A. D., 1994, "Stress-dependent finite growth in soft elastic tissues," J. Biomech., **27**(4), pp. 455–467.
[102] Kroon, M., 2010, "Modeling of Fibroblast-Controlled Strengthening and Remodeling of Uniaxially Constrained Collagen Gels," J. Biomech. Eng., **132**(11), pp. 111008–111008.
[103] Kroon, M., 2010, "On the correlation between continuum mechanics entities and cell activity in biological soft tissues: Assessment of three possible criteria for cell-controlled fibre reorientation in collagen gels and collagenous tissues," J. Theor. Biol., **264**(1), pp. 66–76.
[104] Humphrey, J. D., and Rajagopal, K. R., 2002, "A constrained mixture model for growth and remodeling of soft tissues," Math. Models Methods Appl. Sci., **12**(03), pp. 407–430.

[105] Baek, S., Rajagopal, K. R., and Humphrey, J. D., 2006, "A theoretical model of enlarging intracranial fusiform aneurysms.," J. Biomech. Eng., **128**(1), pp. 142–9.
[106] Humphrey, J. D., Wells, P. B., Baek, S., Hu, J.-J., McLeroy, K., and Yeh, A. T., 2008, "A theoretically-motivated biaxial tissue culture system with intravital microscopy.," Biomech. Model. Mechanobiol., **7**(4), pp. 323–34.
[107] Nusgens, B., Merrill, C., Lapiere, C., and Bell, E., 1984, "Collagen Biosynthesis by Cells in a Tissue Equivalent Matrix In Vitro," Coll. Relat. Res., **4**(5), pp. 351–363.
[108] Bhole, A. P., Flynn, B. P., Liles, M., Saeidi, N., Dimarzio, C. A., and Ruberti, J. W., 2009, "Mechanical strain enhances survivability of collagen micronetworks in the presence of collagenase: implications for load-bearing matrix growth and stability," Philos. Trans. R. Soc. Math. Phys. Eng. Sci., **367**(1902), pp. 3339–3362.
[109] Hadi, M. F., Sander, E. A., Ruberti, J. W., and Barocas, V. H., 2012, "Simulated remodeling of loaded collagen networks via strain-dependent enzymatic degradation and constant-rate fiber growth," Mech. Mater., **44**, pp. 72–82.
[110] Pedrigi, R. M., and Humphrey, J. D., 2011, "Computational Model of Evolving Lens Capsule Biomechanics Following Cataract-Like Surgery," Ann. Biomed. Eng., **39**(1), pp. 537–548.
[111] Niklason, L. E., Yeh, A. T., Calle, E. A., Bai, Y., Valentín, A., and Humphrey, J. D., 2010, "Enabling tools for engineering collagenous tissues integrating bioreactors, intravital imaging, and biomechanical modeling," Proc. Natl. Acad. Sci., **107**(8), pp. 3335–3339.
[112] Guilak, F., Butler, D. L., Goldstein, S. A., and Mooney, D., eds., 2003, Functional Tissue Engineering, Springer.
[113] Humphrey, J. D., 2002, Cardiovascular Solid Mechanics: Cells, Tissues, and Organs, Springer.
[114] Holzapfel, G. A., and Ogden, R. W., 2006, Mechanics of Biological Tissue, Springer.
[115] Pedrigi, R. M., Dziezyc, J., Kalodimos, H. A., and Humphrey, J. D., 2009, "Ex vivo quantification of the time course of contractile loading of the porcine lens capsule after cataract-like surgery," Exp. Eye Res., **89**(6), pp. 869–875.
[116] Ehrlich, H. P., 1988, "Wound closure: evidence of cooperation between fibroblasts and collagen matrix," Eye, **2**(2), pp. 149–157.
[117] Ryan, J. M., and Humphrey, J. D., 1999, "Finite Element Based Predictions of Preferred Material Symmetries in Saccular Aneurysms," Ann. Biomed. Eng., **27**(5), pp. 641–647.
[118] Cardamone, L., Valentín, A., Eberth, J. F., and Humphrey, J. D., 2009, "Origin of axial prestretch and residual stress in arteries," Biomech. Model. Mechanobiol., **8**(6), pp. 431–446.
[119] Grinnell, F., 1994, "Fibroblasts, myofibroblasts, and wound contraction," J. Cell Biol., **124**(4), pp. 401–404.
[120] Bride, J., Viennet, C., Lucarz-Bietry, A., and Humbert, P., 2004, "Indication of fibroblast apoptosis during the maturation of disc-shaped mechanically stressed collagen lattices," Arch. Dermatol. Res., **295**(8), pp. 312–317.
[121] Baaijens, F., Bouten, C., and Driessen, N., 2010, "Modeling collagen remodeling," J. Biomech., **43**(1), pp. 166–175.

[122] Winer, J. P., Oake, S., and Janmey, P. A., 2009, "Non-Linear Elasticity of Extracellular Matrices Enables Contractile Cells to Communicate Local Position and Orientation," PLoS ONE, **4**(7), p. e6382.
[123] Ohsumi, T. K., Flaherty, J. E., Evans, M. C., and Barocas, V. H., 2008, "Three-dimensional simulation of anisotropic cell-driven collagen gel compaction," Biomech. Model. Mechanobiol., **7**(1), pp. 53–62.
[124] Laurent, G. J., Chambers, R. C., Hill, M. R., and McAnulty, R. J., 2007, "Regulation of matrix turnover: fibroblasts, forces, factors and fibrosis," Biochem. Soc. Trans., **35**(4), p. 647.
[125] Paye, M., Nusgens, B. V., and Lapière, C. M., 1987, "Modulation of cellular biosynthetic activity in the retracting collagen lattice," Eur. J. Cell Biol., **45**(1), pp. 44–50.
[126] Hinz, B., 2010, "The myofibroblast: paradigm for a mechanically active cell," J. Biomech., **43**(1), pp. 146–55.
[127] Schwartz, M. A., 2010, "Integrins and Extracellular Matrix in Mechanotransduction," Cold Spring Harb. Perspect. Biol., **2**(12).
[128] DuFort, C. C., Paszek, M. J., and Weaver, V. M., 2011, "Balancing forces: architectural control of mechanotransduction," Nat. Rev. Mol. Cell Biol., **12**(5), pp. 308–319.
[129] Wipff, P.-J., Rifkin, D. B., Meister, J.-J., and Hinz, B., 2007, "Myofibroblast contraction activates latent TGF-β1 from the extracellular matrix," J. Cell Biol., **179**(6), pp. 1311–1323.
[130] Harley, B. A., Leung, J. H., Silva, E. C. C. M., and Gibson, L. J., 2007, "Mechanical characterization of collagen-glycosaminoglycan scaffolds.," Acta Biomater., **3**(4), pp. 463–74.
[131] Horgan, C. O., 1996, "Remarks on ellipticity for the generalized Blatz-Ko constitutive model for a compressible nonlinearly elastic solid," J. Elast., **42**(2), pp. 165–176.
[132] Bayan, C., Levitt, J. M., Miller, E., Kaplan, D., and Georgakoudi, I., 2009, "Fully automated, quantitative, noninvasive assessment of collagen fiber content and organization in thick collagen gels," J. Appl. Phys., **105**(10), p. 102042.
[133] Dahlmann-Noor, A. H., Martin-Martin, B., Eastwood, M., Khaw, P. T., and Bailly, M., 2007, "Dynamic protrusive cell behaviour generates force and drives early matrix contraction by fibroblasts," Exp. Cell Res., **313**(20), pp. 4158–4169.
[134] Roy, P., Petroll, W. M., Chuong, C. J., Cavanagh, H. D., and Jester, J. V., 1999, "Effect of Cell Migration on the Maintenance of Tension on a Collagen Matrix," Ann. Biomed. Eng., **27**(6), pp. 721–730.
[135] Meshel, A. S., Wei, Q., Adelstein, R. S., and Sheetz, M. P., 2005, "Basic mechanism of three-dimensional collagen fibre transport by fibroblasts," Nat. Cell Biol., **7**(2), pp. 157–164.
[136] Balaban, N. Q., Schwarz, U. S., Riveline, D., Goichberg, P., Tzur, G., Sabanay, I., Mahalu, D., Safran, S., Bershadsky, A., Addadi, L., and Geiger, B., 2001, "Force and focal adhesion assembly: a close relationship studied using elastic micropatterned substrates," Nat. Cell Biol., **3**(5), pp. 466–472.

[137] Ina, K., Kitamura, H., Tatsukawa, S., Miyazaki, T., Abe, H., and Fujikura, Y., 2007, "Contraction of tubulointerstitial fibrosis tissue in diabetic nephropathy, as demonstrated in an in vitro fibrosis model," Virchows Arch., **451**(5), pp. 911–921.
[138] Bond, J. E., Kokosis, G., Ren, L., Selim, M. A., Bergeron, A., and Levinson, H., 2011, "Wound Contraction Is Attenuated by Fasudil Inhibition of Rho-Associated Kinase," Plast. Reconstr. Surg. Novemb. 2011, **128**(5).
[139] Avery, N. C., and Bailey, A. J., 2008, "Restraining Cross-Links Responsible for the Mechanical Properties of Collagen Fibers: Natural and Artificial," Collagen, P. Fratzl, ed., Springer US, pp. 81–110.
[140] Wang, Z., and Griffin, M., 2012, "TG2, a novel extracellular protein with multiple functions," Amino Acids, **42**(2-3), pp. 939–949.
[141] Griffin, M., Casadio, R., and Bergamini, C. M., 2002, "Transglutaminases: nature's biological glues.," Biochem. J., **368**(Pt 2), pp. 377–96.
[142] Solan, A., Mitchell, S., Moses, M., and Niklason, L., 2003, "Effect of pulse rate on collagen deposition in the tissue-engineered blood vessel," Tissue Eng., **9**(4), pp. 579–586.
[143] Murad, S., Grove, D., Lindberg, K. A., Reynolds, G., Sivarajah, A., and Pinnell, S. R., 1981, "Regulation of collagen synthesis by ascorbic acid.," Proc. Natl. Acad. Sci. U. S. A., **78**(5), pp. 2879–2882.
[144] Ivarsson, M., McWhirter, A., Borg, T. K., and Rubin, K., 1998, "Type I collagen synthesis in cultured human fibroblasts: Regulation by cell spreading, platelet-derived growth factor and interactions with collagen fibers," Matrix Biol., **16**(7), pp. 409–425.
[145] Bakker, E. N. T. P., Buus, C. L., Spaan, J. A. E., Perree, J., Ganga, A., Rolf, T. M., Sorop, O., Bramsen, L. H., Mulvany, M. J., and Vanbavel, E., 2005, "Small artery remodeling depends on tissue-type transglutaminase.," Circ. Res., **96**(1), pp. 119–26.
[146] Schaertl, S., Prime, M., Wityak, J., Dominguez, C., Munoz-Sanjuan, I., Pacifici, R. E., Courtney, S., Scheel, A., and Macdonald, D., 2010, "A Profiling Platform for the Characterization of Transglutaminase 2 (TG2) Inhibitors," J. Biomol. Screen., **15**(5), pp. 478–487.
[147] Baker, A.-M., Bird, D., Welti, J. C., Gourlaouen, M., Lang, G., Murray, G. I., Reynolds, A. R., Cox, T. R., and Erler, J. T., 2013, "Lysyl Oxidase Plays a Critical Role in Endothelial Cell Stimulation to Drive Tumor Angiogenesis," Cancer Res., **73**(2), pp. 583–594.
[148] Zhao, R., Boudou, T., Wang, W.-G., Chen, C. S., and Reich, D. H., 2013, "Decoupling Cell and Matrix Mechanics in Engineered Microtissues Using Magnetically Actuated Microcantilevers," Adv. Mater., **25**(12), pp. 1699–1705.
[149] Martz, E., 1980, "Immune T lymphocyte to tumor cell adhesion. Magnesium sufficient, calcium insufficient.," J. Cell Biol., **84**(3), pp. 584–598.
[150] Grzesiak, J. J., Davis, G. E., Kirchhofer, D., and Pierschbacher, M. D., 1992, "Regulation of alpha 2 beta 1-mediated fibroblast migration on type I collagen by shifts in the concentrations of extracellular Mg2+ and Ca2+," J. Cell Biol., **117**(5), pp. 1109–1117.
[151] Redden, R. A., and Doolin, E. J., 2006, "Complementary roles of microtubules and microfilaments in the lung fibroblast-mediated contraction of collagen gels:

Dynamics and the influence of cell density," Vitro Cell. Dev. Biol. - Anim., **42**(3-4), pp. 70–74.

[152] Ehrlich, H. P., Gabbiani, G., and Meda, P., 2000, "Cell coupling modulates the contraction of fibroblast-populated collagen lattices.," J. Cell. Physiol., **184**(1), pp. 86–92.

[153] Bakker, E. N. T. P., Pistea, A., Spaan, J. a E., Rolf, T. M., de Vries, C. J., van Rooijen, N., Candi, E., and VanBavel, E., 2006, "Flow-dependent remodeling of small arteries in mice deficient for tissue-type transglutaminase: possible compensation by macrophage-derived factor XIII.," Circ. Res., **99**(1), pp. 86–92.

[154] Zemskov, E. A., Janiak, A., Hang, J., Waghray, A., and Belkin, A. M., 2006, "The role of tissue transglutaminase in cell-matrix interactions," Front. Biosci. J. Virtual Libr., **11**, pp. 1057–1076.

[155] Castella, L. F., Buscemi, L., Godbout, C., Meister, J.-J., and Hinz, B., 2010, "A new lock-step mechanism of matrix remodelling based on subcellular contractile events," J. Cell Sci., **123**(10), pp. 1751–1760.

[156] Tian, B., Lessan, K., Kahm, J., Kleidon, J., and Henke, C., 2002, "β1 Integrin Regulates Fibroblast Viability during Collagen Matrix Contraction through a Phosphatidylinositol 3-Kinase/Akt/Protein Kinase B Signaling Pathway," J. Biol. Chem., **277**(27), pp. 24667–24675.

[157] Zhu, Y. K., Umino, T., Liu, X. D., Wang, H. J., Romberger, D. J., Spurzem, J. R., and Rennard, S. I., 2001, "Contraction of fibroblast-containing collagen gels: Initial collagen concentration regulates the degree of contraction and cell survival," Vitro Cell. Dev. Biol. - Anim., **37**(1), pp. 10–16.

[158] Tomasek, J. J., Vaughan, M. B., Kropp, B. P., Gabbiani, G., Martin, M. D., Haaksma, C. J., and Hinz, B., 2006, "Contraction of myofibroblasts in granulation tissue is dependent on Rho/Rho kinase/myosin light chain phosphatase activity," Wound Repair Regen., **14**(3), pp. 313–320.

[159] Mizutani, T., Haga, H., and Kawabata, K., 2004, "Cellular stiffness response to external deformation: Tensional homeostasis in a single fibroblast," Cell Motil. Cytoskeleton, **59**(4), pp. 242–248.

[160] Kagan, H. M., and Ryvkin, F., 2011, "Lysyl Oxidase and Lysyl Oxidase-Like Enzymes," The Extracellular Matrix: an Overview, R.P. Mecham, ed., Springer Berlin Heidelberg, pp. 303–335.

[161] Simon, D. D., and Humphrey, J. D., 2014, "Learning from Tissue Equivalents: Biomechanics and Mechanobiology," Bio-inspired Materials for Biomedical Engineering, A.B. Brennan, and C.M. Kirschner, eds., John Wiley & Sons, Inc, pp. 281–308.

[162] Gleason, R. L., and Humphrey, J. D., 2004, "A mixture model of arterial growth and remodeling in hypertension: altered muscle tone and tissue turnover," J. Vasc. Res., **41**(4), pp. 352–363.

[163] Miller, K. S., Lee, Y. U., Naito, Y., Breuer, C. K., and Humphrey, J. D., 2014, "Computational model of the in vivo development of a tissue engineered vein from an implanted polymeric construct," J. Biomech.

[164] Rachev, A., and Hayashi, K., 1999, "Theoretical Study of the Effects of Vascular Smooth Muscle Contraction on Strain and Stress Distributions in Arteries," Ann. Biomed. Eng., **27**(4), pp. 459–468.

[165] Humphrey, J. D., and Wilson, E., 2003, "A potential role of smooth muscle tone in early hypertension: a theoretical study," J. Biomech., **36**(11), pp. 1595–1601.
[166] Valentin, A., and Humphrey, J. D., 2009, "Parameter Sensitivity Study of a Constrained Mixture Model of Arterial Growth and Remodeling," J. Biomech. Eng., **131**(10), p. 101006.
[167] Lo, C.-M., Wang, H.-B., Dembo, M., and Wang, Y., 2000, "Cell Movement Is Guided by the Rigidity of the Substrate," Biophys. J., **79**(1), pp. 144–152.
[168] Richardson, W. J., Metz, R. P., Moreno, M. R., Wilson, E., and Moore, J., James E., 2011, "A Device to Study the Effects of Stretch Gradients on Cell Behavior," J. Biomech. Eng., **133**(10), pp. 101008–101008.
[169] Yoo, L., Reed, J., Shin, A., Kung, J., Gimzewski, J. K., Poukens, V., Goldberg, R. A., Mancini, R., Taban, M., Moy, R., and Demer, J. L., 2011, "Characterization of Ocular Tissues Using Microindentation and Hertzian Viscoelastic Models," Invest. Ophthalmol. Vis. Sci., **52**(6), pp. 3475–3482.
[170] Spurlin, T. A., Bhadriraju, K., Chung, K.-H., Tona, A., and Plant, A. L., 2009, "The treatment of collagen fibrils by tissue transglutaminase to promote vascular smooth muscle cell contractile signaling," Biomaterials, **30**(29), pp. 5486–5496.
[171] Lee, P.-F., Bai, Y., Smith, R. L., Bayless, K. J., and Yeh, A. T., 2013, "Angiogenic responses are enhanced in mechanically and microscopically characterized, microbial transglutaminase crosslinked collagen matrices with increased stiffness," Acta Biomater., **9**(7), pp. 7178–7190.
[172] Fluck, J., Querfeld, C., Cremer, A., Niland, S., Krieg, T., and Sollberg, S., 1998, "Normal Human Primary Fibroblasts Undergo Apoptosis in Three-Dimensional Contractile Collagen Gels," J. Invest. Dermatol., **110**(2), pp. 153–157.

Appendix A: Strain Energy Contours

A.1 Strain Energy Contours for Incompressible Model

Presented here are example strain energy contours for the incompressible model presented in Chapter 3. The contours are used to assess the convexity of the strain energy functions to check stability and uniqueness. Values are calculated for the non-dimensionalized strain energy shown here:

$$\frac{W_{incomp}}{\mu} = \frac{1}{2}(I_C - 3) + \frac{\Gamma}{4}(IV_C - 1)^2$$

$$= \frac{1}{2}\left(\lambda_r^2 + \lambda_\vartheta^2 + \frac{1}{\lambda_r^2\lambda_\vartheta^2} - 3\right) + \frac{\Gamma}{4}\left(\lambda_\vartheta^2 - 1\right)^2 \qquad \text{(A.1)}$$

where W_{incomp} is the strain energy function for the incompressible model and $\Gamma = c/\mu$ is the ratio of the transverse isotropic material parameter, c, to μ. The strain energy was modified from the form presented in Chapter 3 to allow a more direct comparison to the strain energy contours to be presented in Section A.2.

In Figure A.1, contours are plotted over a range of values for λ_r and λ_ϑ, and each plot is for a different value of Γ. For simplicity, radial variation is not considered in these plots.

A.2 Strain Energy Contours for Compressible Model

Presented here are example strain energy contours for the compressible model presented in Chapter 4. Values are calculated for the non-dimensionalized strain energy shown here:

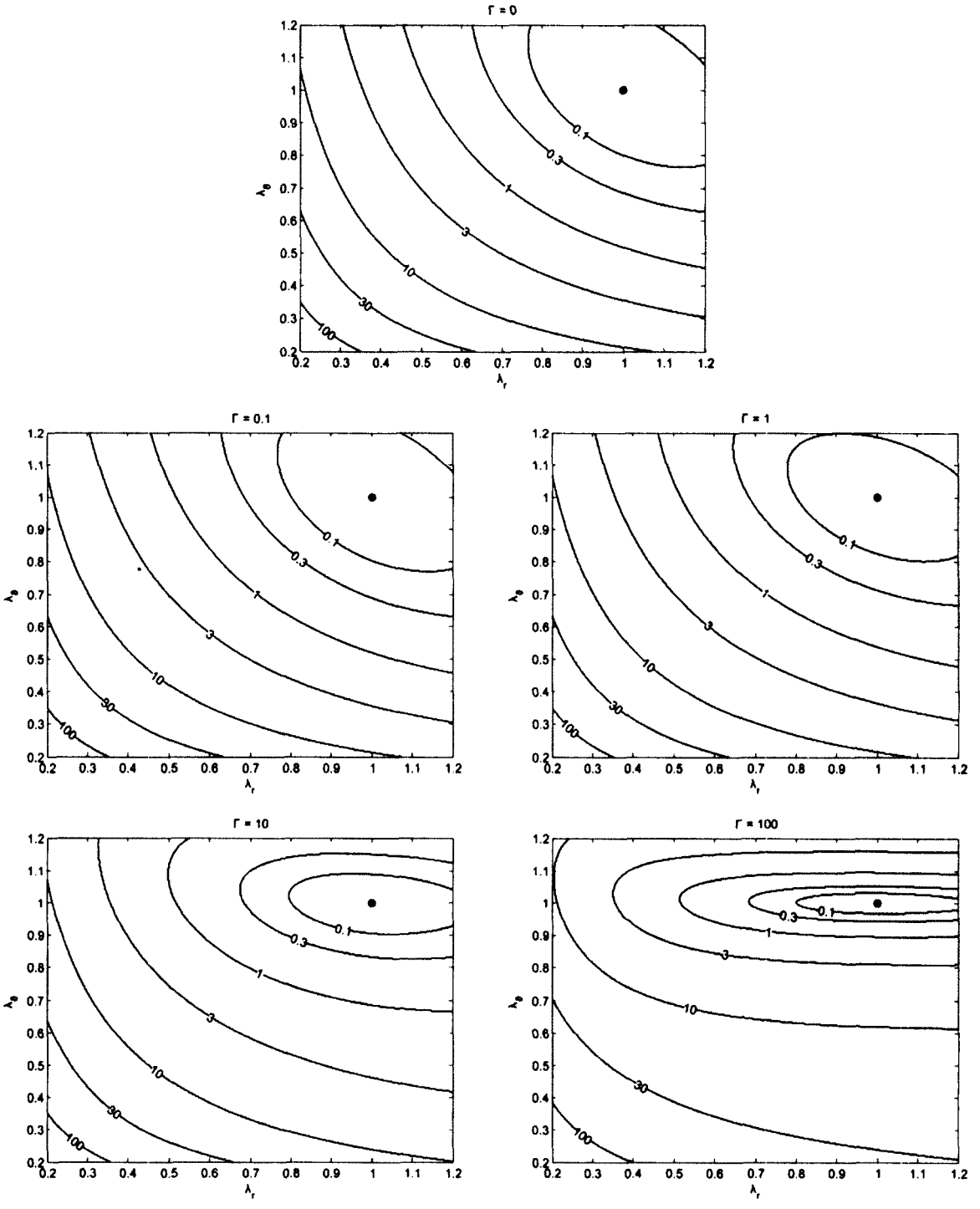

Figure A.1: Strain energy contours for incompressible model. Each plot is for a different level of transverse isotropy compare to isotropy. The minimum energy level is indicated in each plot by a dot.

$$\frac{W_{comp}}{\mu} = \frac{1}{2}\left(\frac{II_C}{III_C} + 2III_C^{1/2} - 5\right) + \frac{\Gamma}{4}(IV_C - 1)^2$$

$$= \frac{1}{2}\left(\lambda_r^{-2} + \lambda_\vartheta^{-2} + \frac{\lambda_r^2\lambda_\vartheta^2}{J^2} + 2J - 5\right) + \frac{\Gamma}{4}\left(\lambda_\vartheta^2 - 1\right)^2 \quad \text{(A.2)}$$

where W_{comp} is the compressible strain energy function.

In Figure A.2, contours are plotted over a range of values for λ_r and λ_ϑ, and each plot is for a different value of Γ. Due to compressibility, each plot also show the contours for cases of no change in volume ($J = 1$) in gray and cases with a 25% decrease in volume ($J = 0.75$) in black.

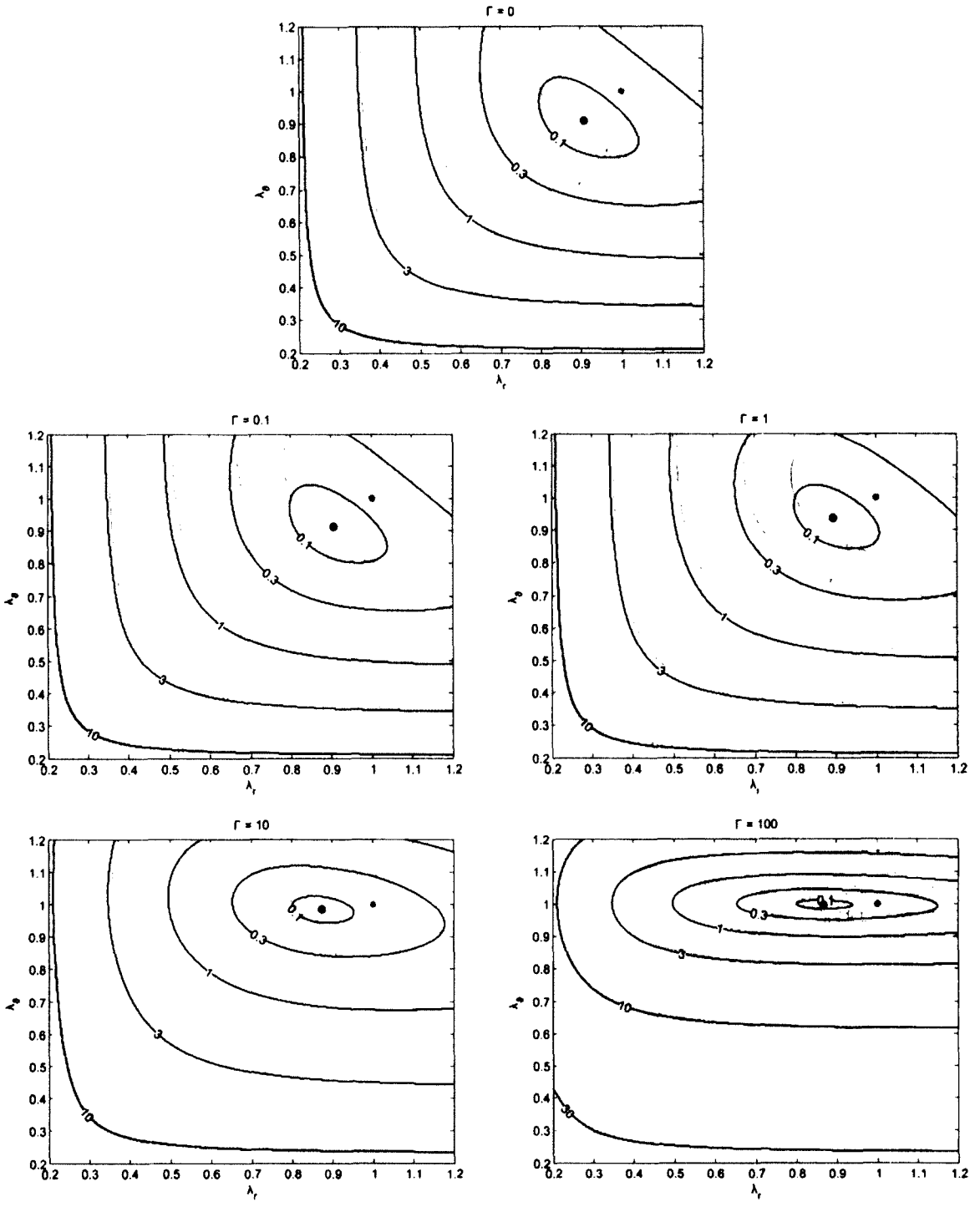

Figure A.2: Strain energy contours for compressible model. Contours are plotted for no volume change ($J = 1$) in gray and a 25% decrease in volume ($J = 0.75$) in black. Minimum energy levels are indicated by the dot. For $J = 0.75$ the minimum energy level is not equal to zero.

Appendix B: Supplemental Figures for Chapter 5

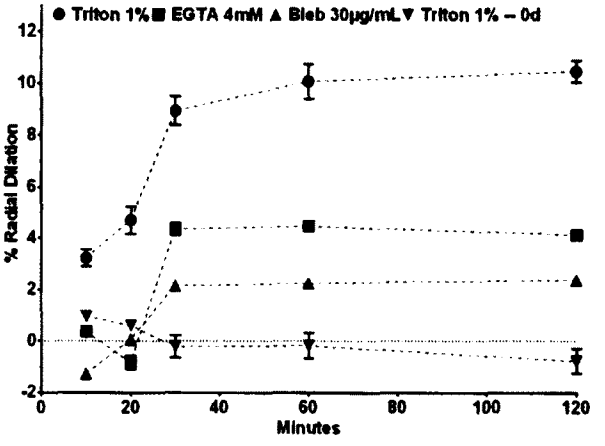

Figure B.1: Time course of contractility release. Illustrative time course (in minutes) of the dilation of 1-day gels upon exposure to 1% TritonX-100 to lyse the cells, EGTA to chelate the calcium, or blebbistatin to inhibit myosin activity, all compared to control (i.e., exposure of 0 day gels prior to cell-mediated compaction).

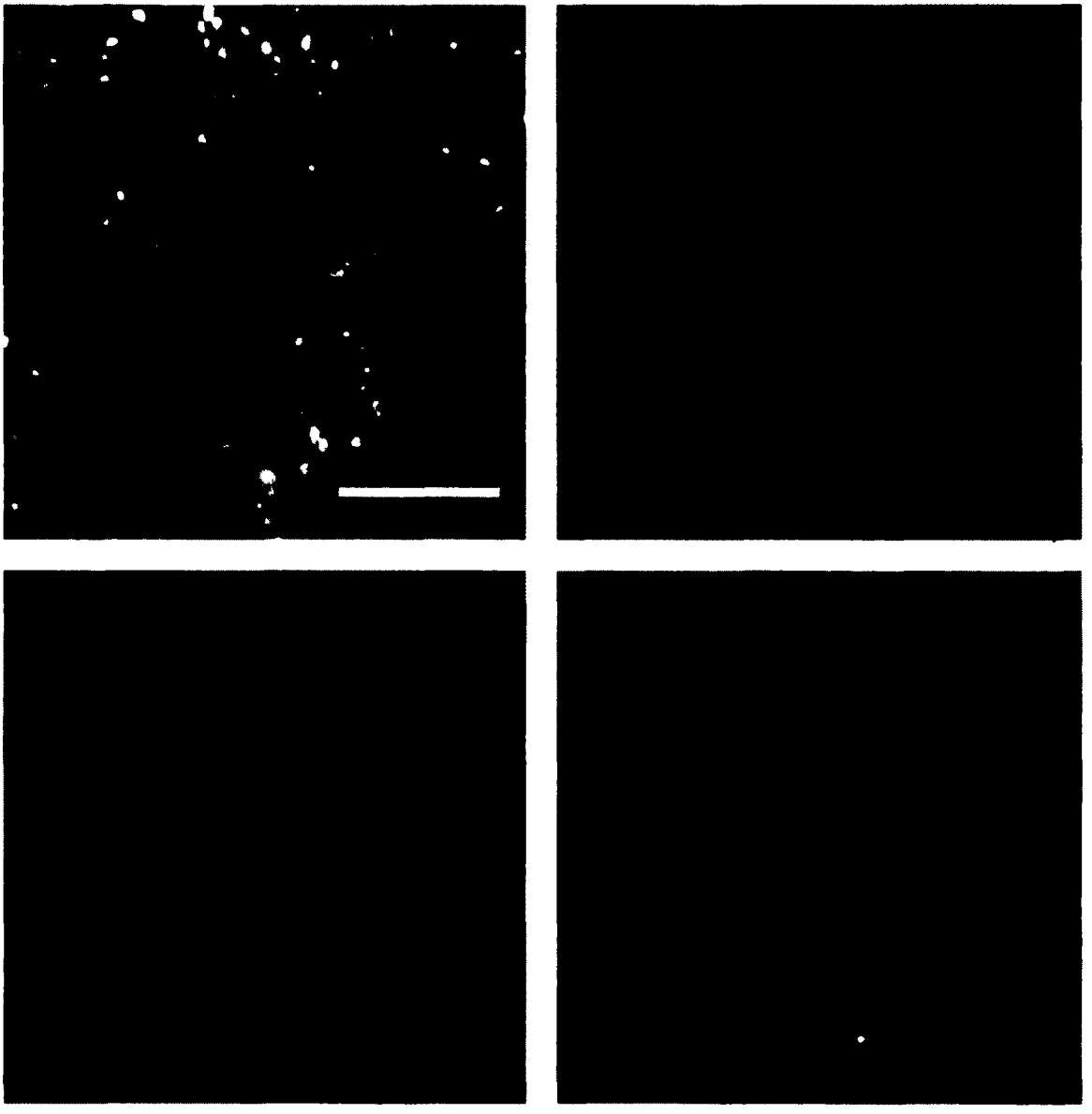

Figure B.2: Live/Dead assay of free-floating FPCL. Live (left) and Dead (right) staining of 5-day collagen gels before (top two panels) and 30 minutes after (bottom two panels) treatment with 1% TritonX-100. Note that the 5-day gels represent a maximum degree of compaction relative to gels studied over 4 days of culture. Scale bar is 200 μm.

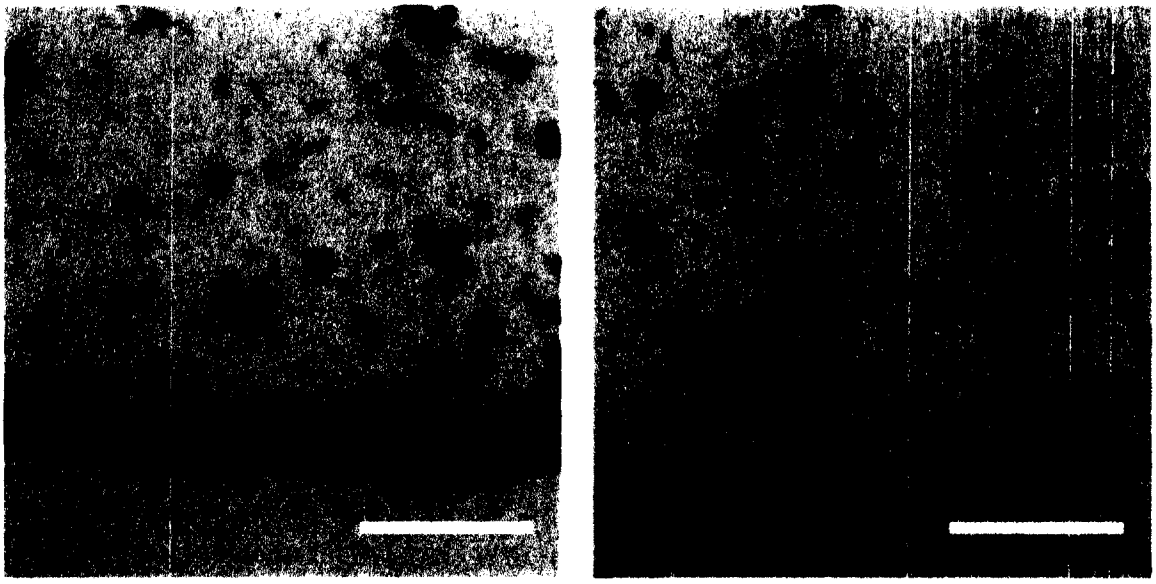

Figure B.3: Confirmation of myofibroblast phenotype. Immunohistological staining for α-smooth muscle actin (brown), with a hematoxylin counter-stain to reveal cell nuclei (blue), suggested a preferential differentiation of fibroblasts into myofibroblasts near the outer periphery of the gels (left) relative to the central region of the gels (right). Gels shown after 4 days of culture. Scale bar is 50 μm.

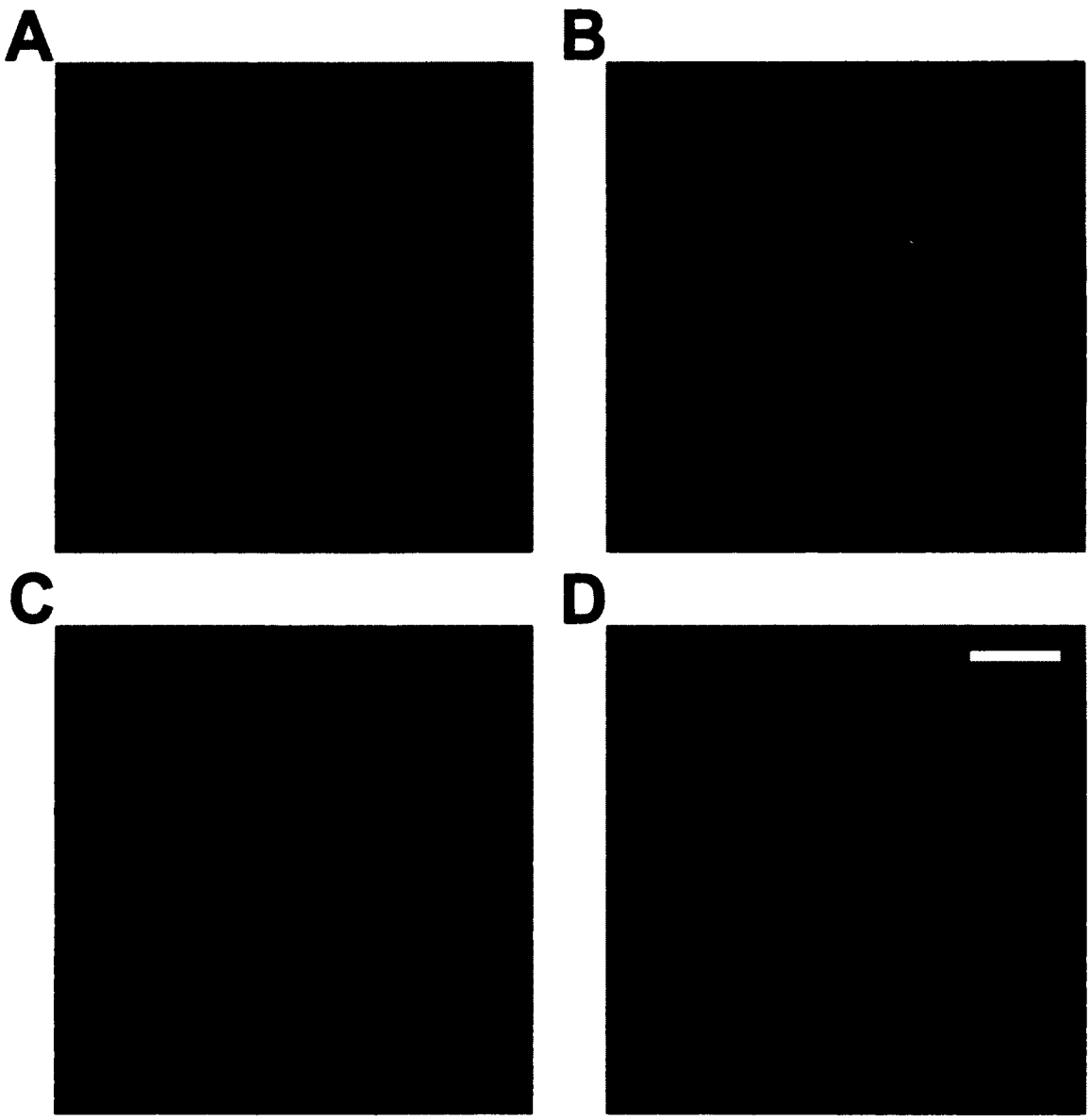

Figure B.4: Picrosirius red images of collagen alignment. Day 2 picrosirius red stained sections of free-floating FPCLs. (A) Central region of a1000 μM BAPN treated gel showing random orientation of the collagen fibers. (B) Control, (C) BAPN-treated, and (D) 6 μM Boc-DON-treated sections at the outer edge of the gels. All show similar levels of collagen alignment with the Boc-DON gel having smaller fibers and possible lower collagen density. Scale bar is 25 μm.

Appendix C: Computational Model Boundary Value Problem Derivation

For the boundary value problem to determine the stresses before remodeling, we first consider homogeneous axisymmetric finite deformations whereby material particles originally at (R, Θ, Z) are mapped to (ρ, θ, ζ) according to

$$\rho = \gamma R, \theta = \frac{\pi}{\Theta_o}\Theta, \zeta = \Gamma Z, \rho \in [0, \rho_o], \theta \in [0, 2\pi], \zeta \in [-\eta/2, \eta/2] \tag{C.1}$$

where γ and Γ are radial and axial stretch ratios, respectively, and Θ_o is a measurable opening angle. The associated physical components of the deformation gradient, $\mathbf{F}_{res}$, are [113]

$$\mathbf{F}_{res} = \begin{bmatrix} \frac{\partial \rho}{\partial R} & \frac{1}{R}\frac{\partial \rho}{\partial \Theta} & \frac{\partial \rho}{\partial Z} \\ \rho\frac{\partial \theta}{\partial R} & \frac{\rho}{R}\frac{\partial \theta}{\partial \Theta} & \rho\frac{\partial \theta}{\partial Z} \\ \frac{\partial \zeta}{\partial R} & \frac{1}{R}\frac{\partial \zeta}{\partial \Theta} & \frac{\partial \zeta}{\partial Z} \end{bmatrix} = \begin{bmatrix} \gamma & 0 & 0 \\ 0 & \gamma\frac{\pi}{\Theta_o} & 0 \\ 0 & 0 & \Gamma \end{bmatrix}, \det \mathbf{F}_{res} = J_{res} = \frac{\pi\gamma^2\Gamma}{\Theta_o}. \tag{C.2}$$

The Cauchy stress (Eq. (6.1)) for the residually-stressed configuration takes the following form:

$$\mathbf{t}_{res} = \varphi_{iso}(\rho)\mu\left(\mathbf{I} - \frac{1}{J_{res}}\mathbf{B}_{res}^{-1}\right) + \varphi_{ani}(\rho)\frac{c}{J_{res}}(IV_{res}^2 - IV_{res})\mathbf{e}_\theta \otimes \mathbf{e}_\theta \tag{C.3}$$

where $\mathbf{B}_{res} = \mathbf{F}_{res}\mathbf{F}_{res}^T$ is the left Cauchy-Green tensor, and $IV_{res} = \mathbf{M} \cdot \mathbf{C}_{res}\mathbf{M}$ is the fourth invariant of $\mathbf{C}_{res} = \mathbf{F}_{res}^T\mathbf{F}_{res}$.

For the constitutive relation, therefore, the residual-type stress field is

$$t_{\rho\rho} = \varphi_{iso}\mu\left(1 - \frac{1}{J_{res}\gamma^2}\right) \tag{C.4}$$

$$t_{\theta\theta} = \varphi_{iso}\mu\left(1 - \frac{\Theta_o^2}{J_{res}\gamma^2\pi^2}\right) + \varphi_{ani}\frac{c}{J_{res}}\left(\frac{\gamma^4\pi^4}{\Theta_o^4} - \frac{\gamma^2\pi^2}{\Theta_o^2}\right) \tag{C.5}$$

$$t_{\zeta\zeta} = \varphi_{iso}\mu\left(1 - \frac{1}{J_{res}\Gamma^2}\right) \tag{C.6}$$

Applying the boundary condition, $t_{\zeta\zeta}(\pm\eta/2) = 0$ where η is the deformed thickness, it can be shown that $\Gamma = \sqrt[3]{\frac{\Theta_o}{\gamma^2\pi}}$. This finding reduces the form of the stresses. Moreover, J_{res} can also be written $J_{res} = \sqrt[3]{\gamma^4\pi^2/\Theta_o^2}$. Hence, the radial and circumferential stresses take the form

$$t_{\rho\rho} = \varphi_{iso}\mu\left(1 - \sqrt[3]{\frac{\Theta_o^2}{\gamma^{10}\pi^2}}\right) \tag{C.7}$$

$$t_{\theta\theta} = \varphi_{iso}\mu\left(1 - \sqrt[3]{\frac{\Theta_o^2}{\gamma^{10}\pi^2}}\right) + \varphi_{ani}c\left(\frac{\gamma^2\pi^3}{\Theta_o^3\Gamma} - \frac{\pi}{\Theta_o\Gamma}\right) \tag{C.8}$$

Now, equilibrium requires $\mathrm{div}\,\mathbf{t} = \mathbf{0}$, the only nontrivial equation of which is

$$\frac{\partial t_{\rho\rho}}{\partial\rho} + \frac{t_{\rho\rho} - t_{\theta\theta}}{\rho} = 0 \tag{C.9}$$

which requires that

$$t_{\theta\theta} = \left(\rho\frac{\partial\varphi_{iso}}{\partial\rho} + \varphi_{iso}\right)\mu\left(1 - \sqrt[3]{\frac{\Theta_o^2}{\gamma^{10}\pi^2}}\right). \tag{C.10}$$

Note, therefore, that $t_{\theta\theta}(\rho = 0) = t_{\rho\rho}(\rho = 0)$ as expected. Finally, noting that Θ_o is known from the geometry, γ can be found by enforcing that Eq. (C.10) equals Eq. (C.8) at each ρ, that is

$$\varphi_{iso}\mu\left(1 - \frac{\Theta_o^2}{J\gamma^2\pi^2}\right) + \varphi_{ani}\frac{c}{J}\left(\frac{\gamma^4\pi^4}{\Theta_o^4} - \frac{\gamma^2\pi^2}{\Theta_o^2}\right)$$
$$= \left(\rho\frac{\partial\varphi_{iso}}{\partial\rho} + \varphi_{iso}\right)\mu\left(1 - \sqrt[3]{\frac{\Theta_o^2}{\gamma^{10}\pi^2}}\right) \forall\rho. \tag{C.11}$$

To ensure homogeneous deformations, we enforce the sufficient condition that Eq. (C.11) must be satisfied at $\rho = \rho_o$ which reduces the equation to

$$\frac{c}{J}\left(\frac{\gamma^4\pi^4}{\Theta_o^4} - \frac{\gamma^2\pi^2}{\Theta_o^2}\right) = \rho_o\frac{\partial\varphi_{iso}}{\partial\rho}\Big]_{\rho_o}\mu\left(1 - \sqrt[3]{\frac{\Theta_o^2}{\gamma^{10}\pi^2}}\right). \tag{C.12}$$

We next consider homogeneous axisymmetric finite deformations whereby material particles, originally mapped from (R, Θ, Z) to (ρ, θ, ζ) in the residual problem, are subsequently mapped to (r, ϑ, z) following cell-induced compaction according to

$$r = \lambda\gamma R,\ \vartheta = \frac{\pi}{\Theta_o}\Theta,\ z = \Lambda\Gamma Z \tag{C.13}$$

where λ and Λ are radial and axial stretch ratios, respectively. The resulting deformation is

$$\mathbf{F} = \mathbf{F}_{cell}\mathbf{F}_{res} = \begin{bmatrix} \lambda\gamma & 0 & 0 \\ 0 & \lambda\gamma\frac{\pi}{\Theta_o} & 0 \\ 0 & 0 & \Lambda\Gamma \end{bmatrix} \tag{C.14}$$

where

$$\mathbf{F}_{cell} = \begin{bmatrix} \lambda & 0 & 0 \\ 0 & \lambda & 0 \\ 0 & 0 & \Lambda \end{bmatrix}. \tag{C.15}$$

Because of assumed compressibility, $\det \mathbf{F} = J \neq 1$, where $\det \mathbf{F}_{cell} \neq 1$ and $\det \mathbf{F}_{res} \neq 1$.

From the residually-stressed configuration, we know the values of γ, Θ_o, and Γ, leaving λ and Λ as the only unknown deformations. Using Eq. (6.12), the axial boundary condition, $t_{zz}(\pm h/2) = 0$ where h is the final deformed thickness, and radial equilibrium (i.e., $\int_0^{r_o}\left(\frac{\partial t_{rr}}{\partial r} + \frac{t_{rr}-t_{\theta\theta}}{r}\right)dr$) provide two equations to solve for the unknown deformations.

Appendix D: Technical Drawings for Biaxial Bioreactor Components

This appendix contains the technical drawings for all of the custom machined components for the planar biaxial bioreactor implemented in Chapter 7. Also contained in this appendix is the parts list for the biaxial culture and mechanical testing system.

D.1 Technical Drawings for Machined Parts

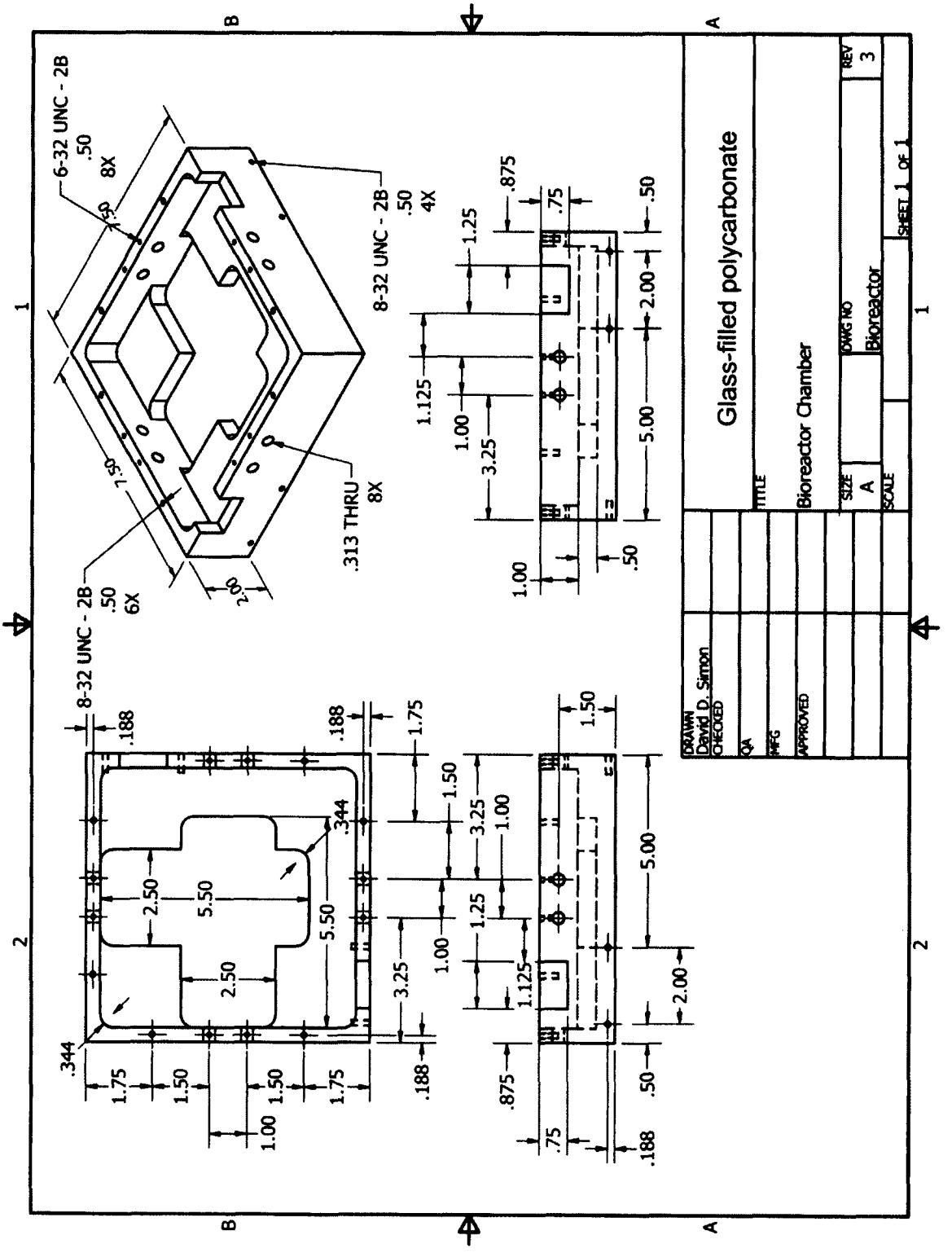

Figure D.1: Bioreactor chamber technical drawing. Units are in inches.

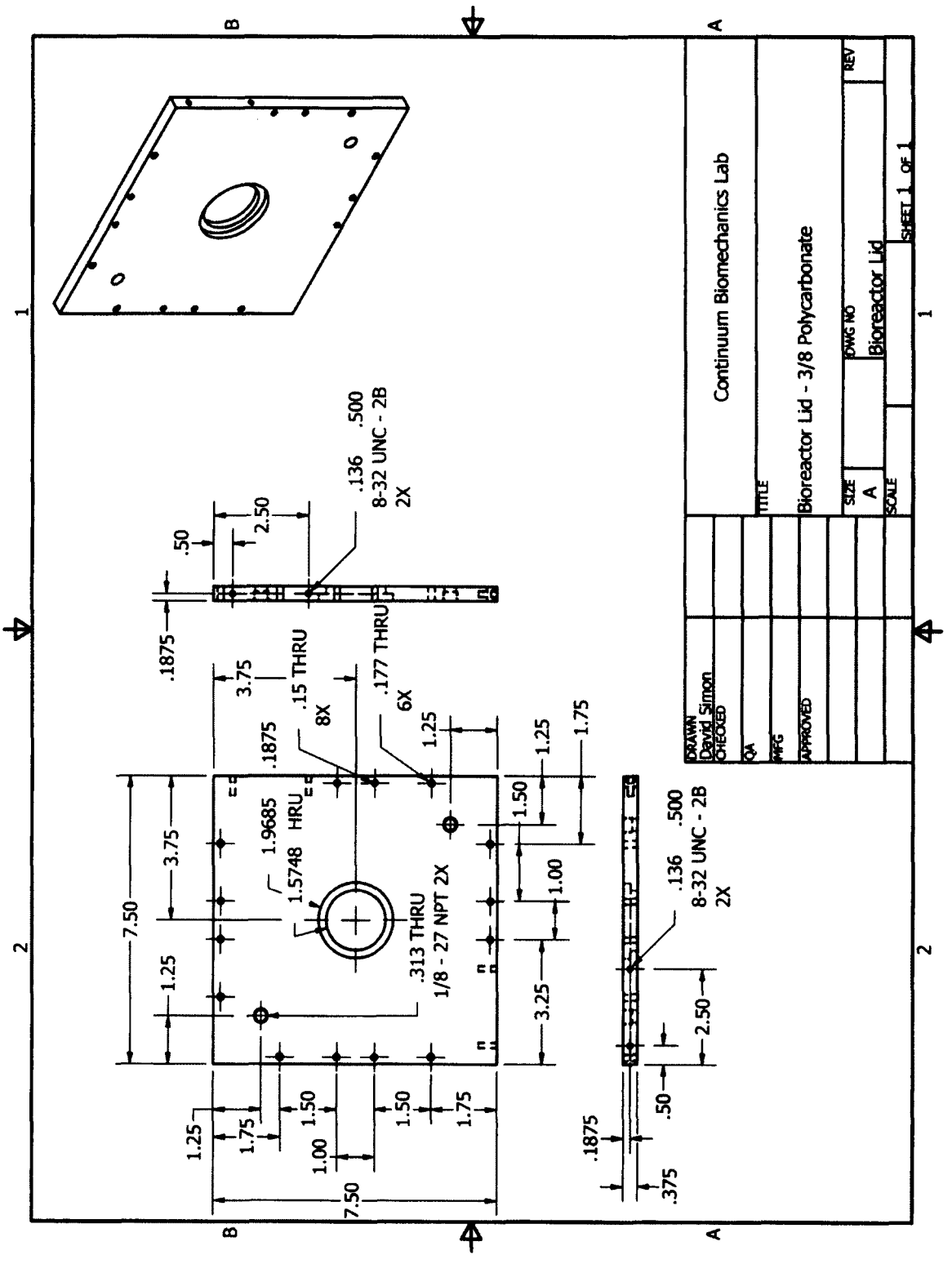

Figure D.2: Bioreactor chamber lid technical drawing. Units are in inches.

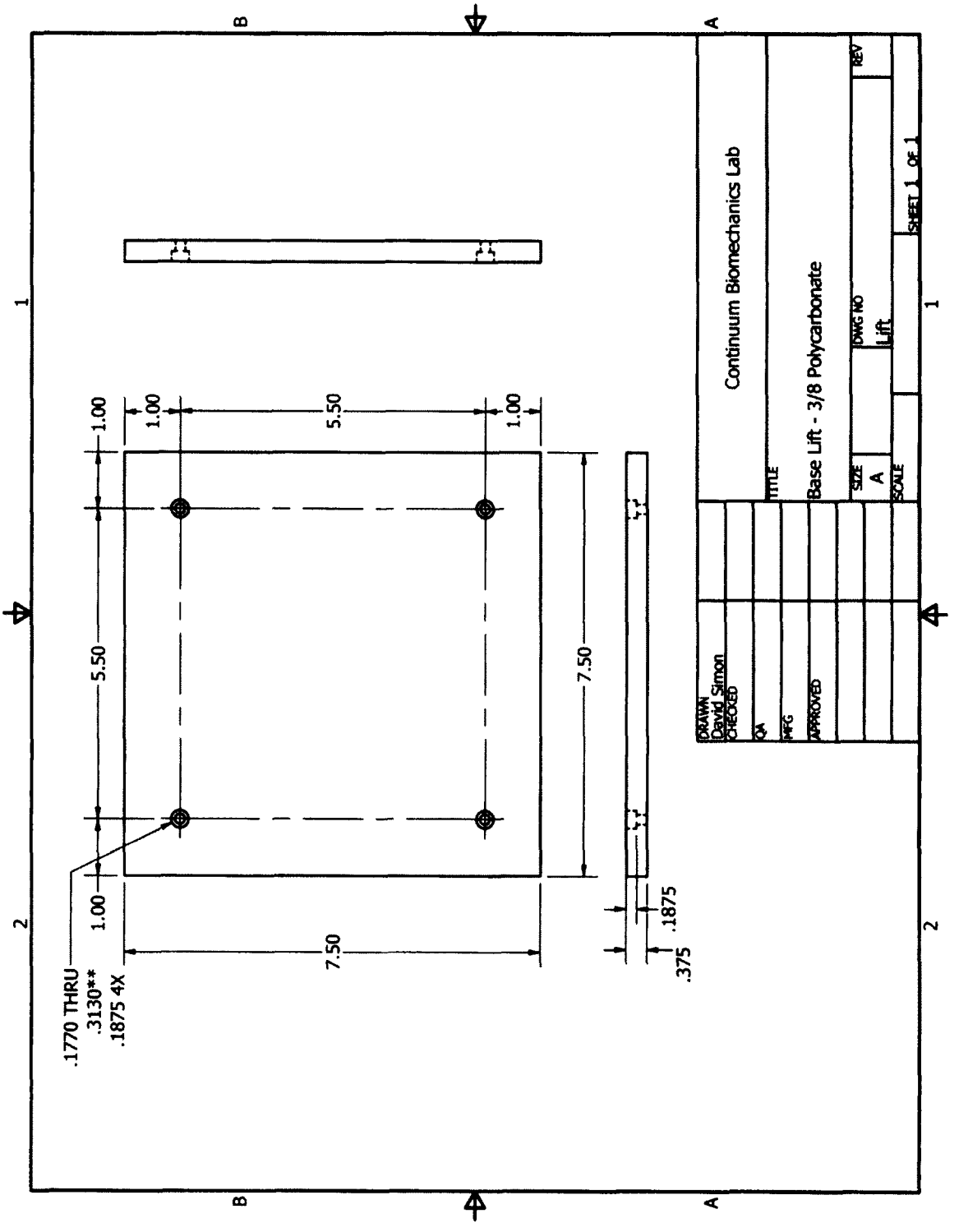

Figure D.3: Bioreactor chamber baseplate technical drawing. This ensures proper alignment of loading arms connected to linear screw. Units are in inches.

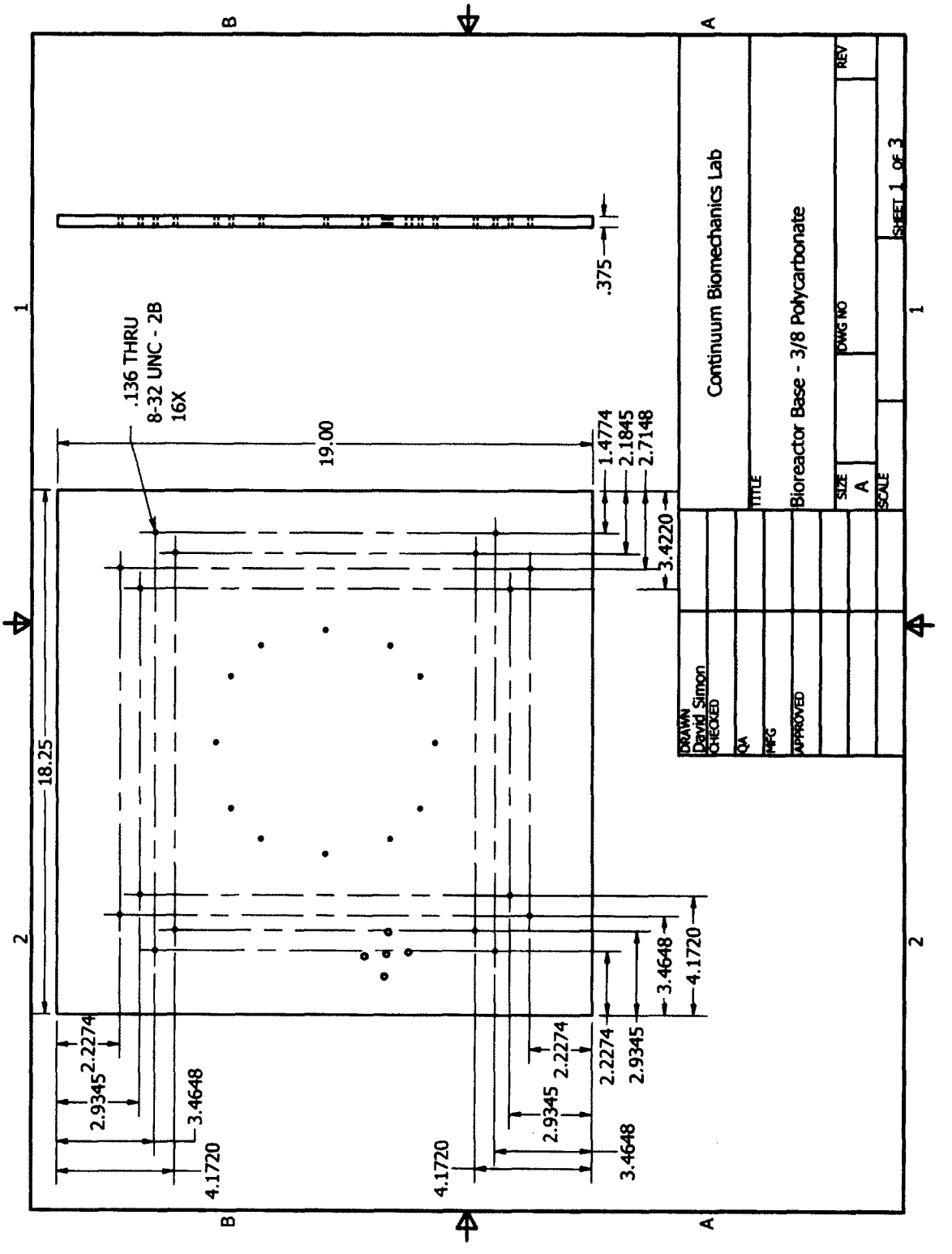

Figure D.4: System baseplate technical drawing #1. Provides overall dimensions of baseplate and tapping locations for linear screw motor mounts. Units are in inches.

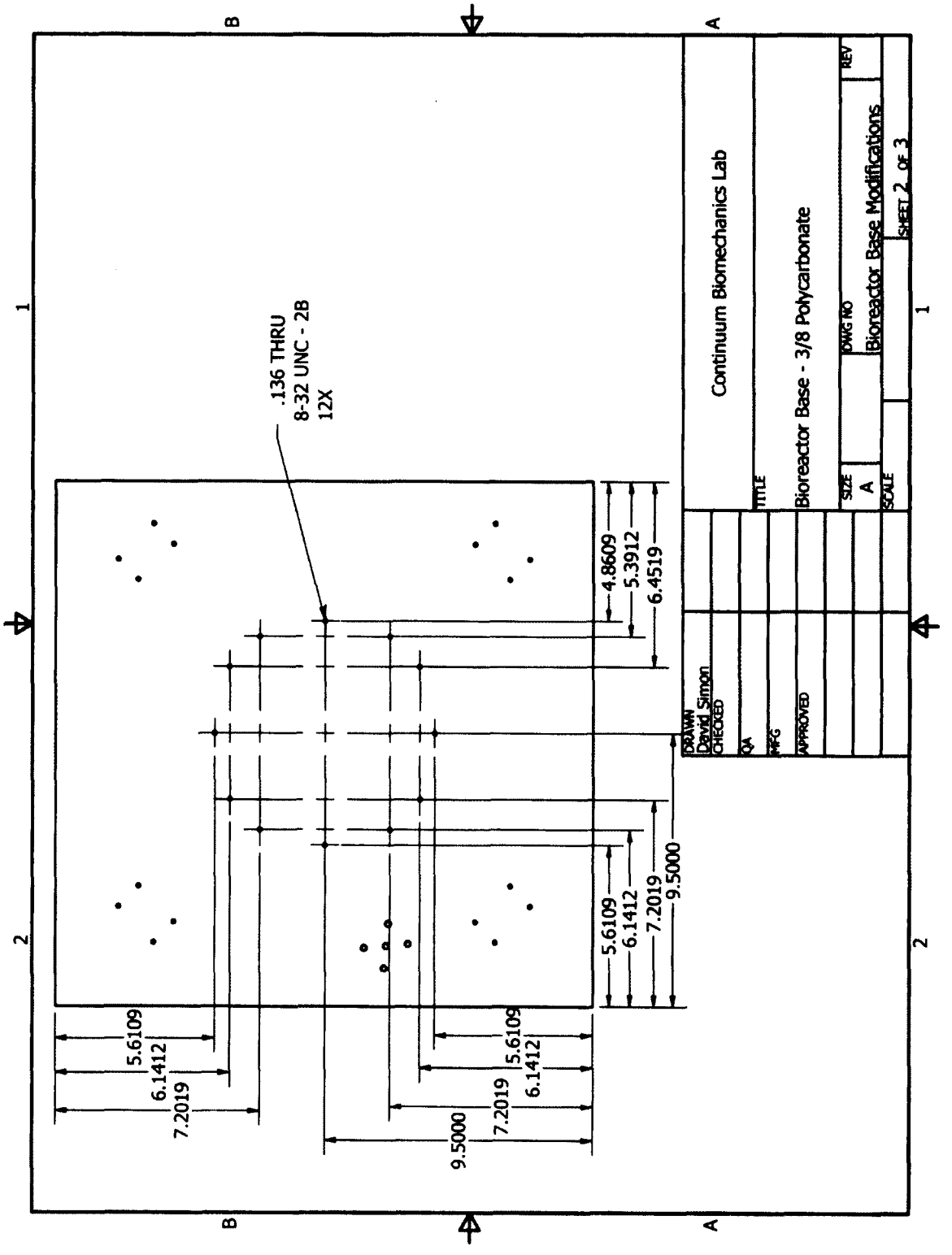

Figure D.5: System baseplate technical drawing #2. Provides locations for bioreactor baseplate tappings and tappings for the linear screw end supports. Units are in inches.

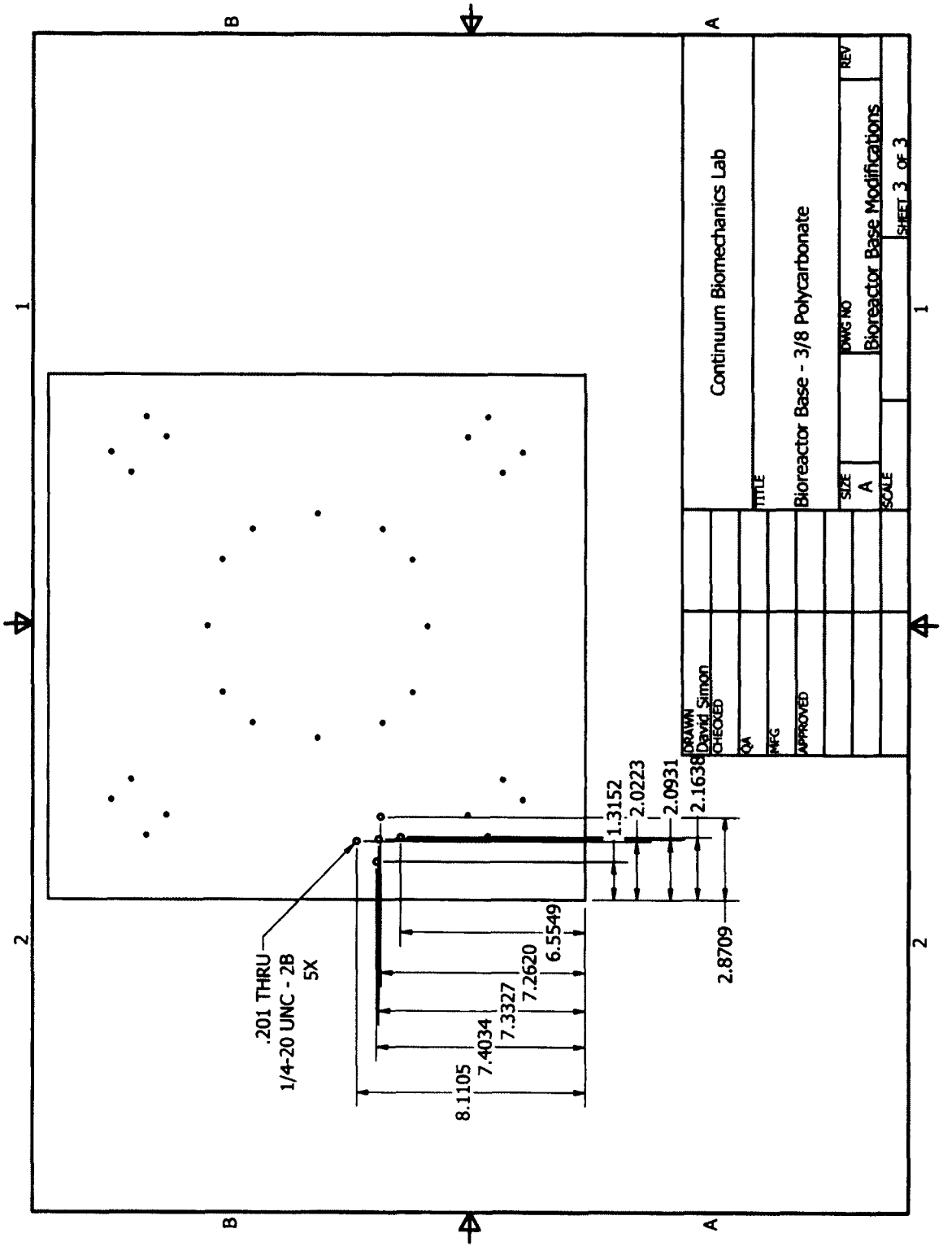

Figure D.6: System baseplate technical drawing #3. Provides locations of tappings for camera support base. Units are in inches.

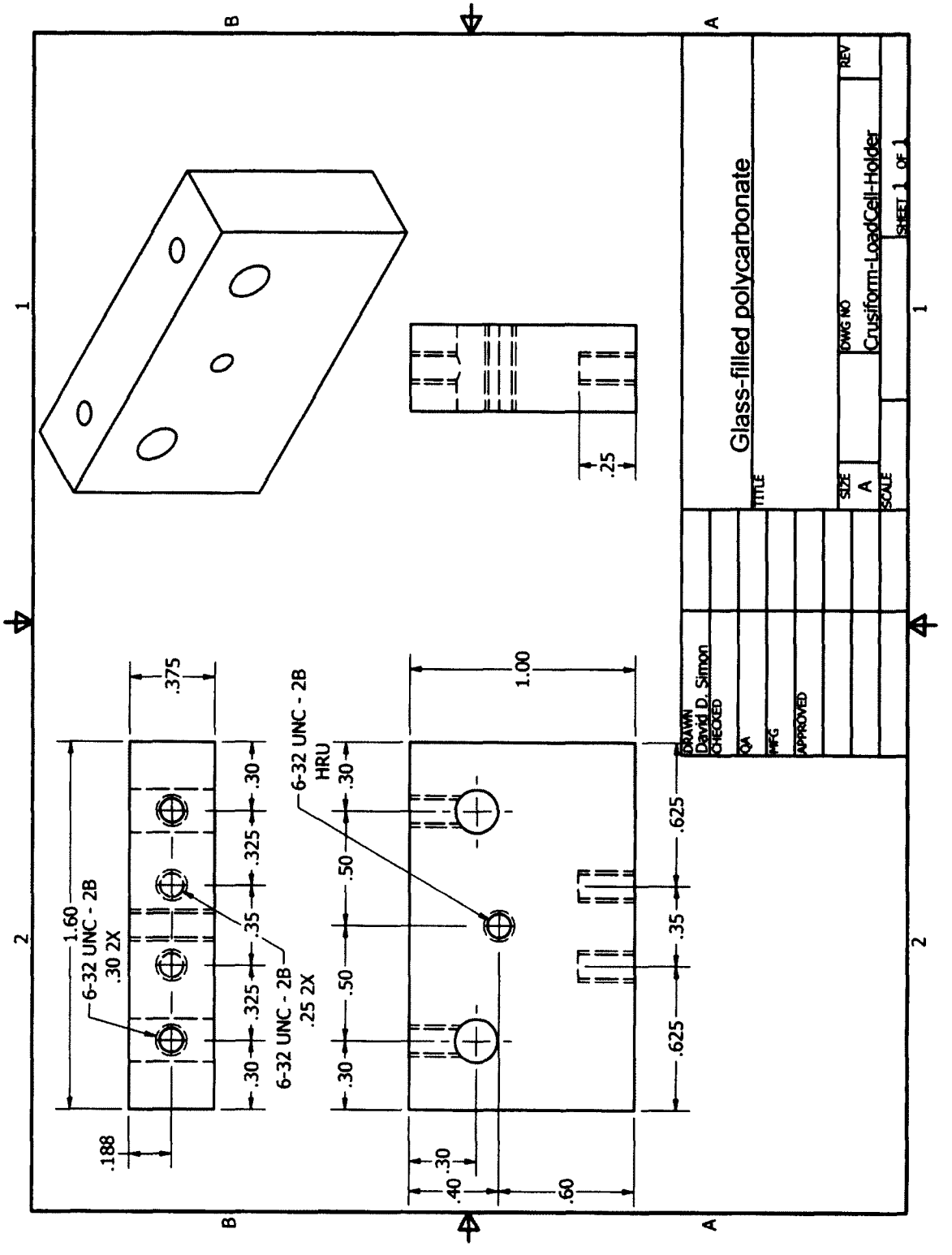

Figure D.7: Cruciform and load cell holder technical drawing. Connect cruciform gels and load cells to loading arms. Units are in inches.

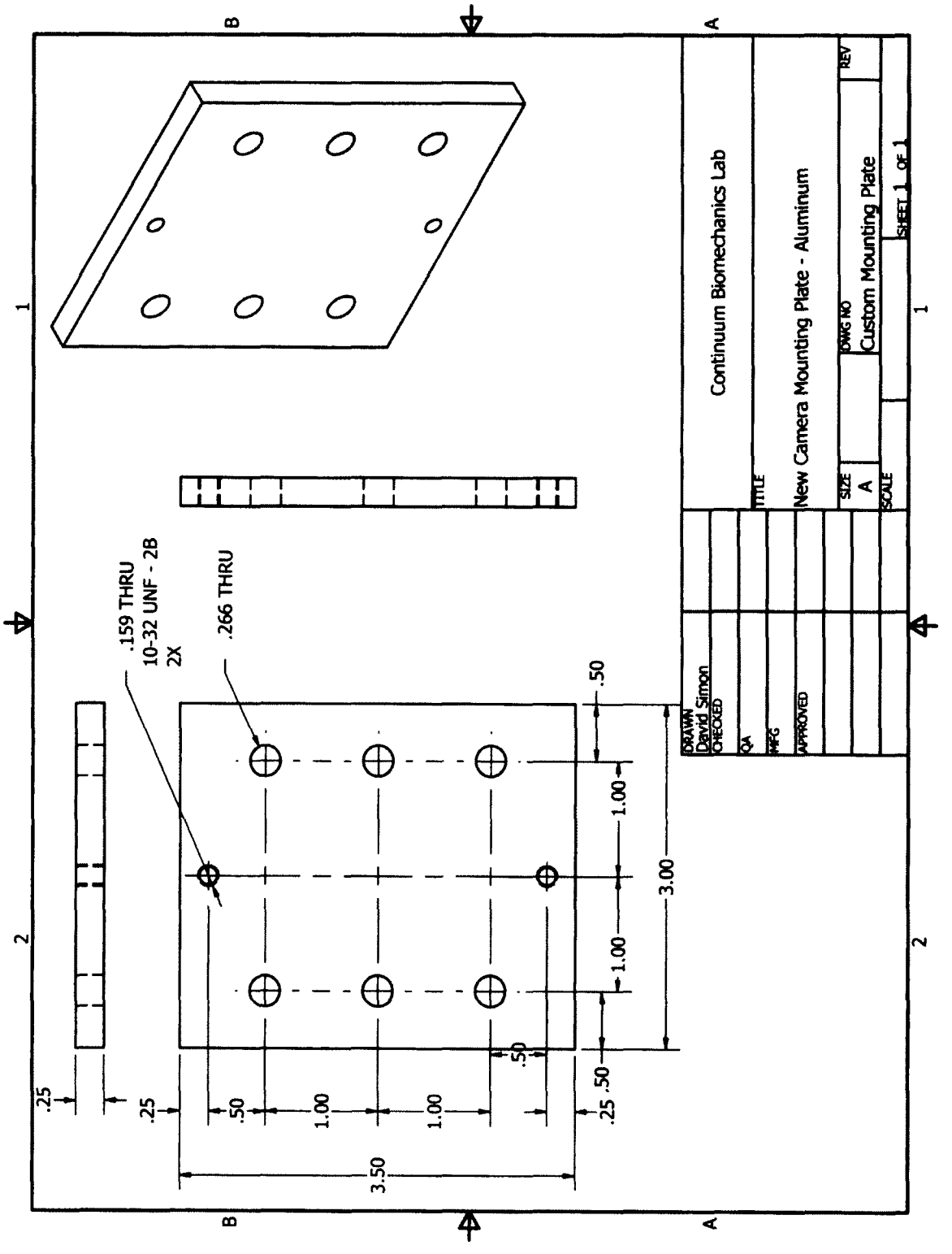

Figure D.8: Camera and optics mounting plate technical drawing. Units are in inches.

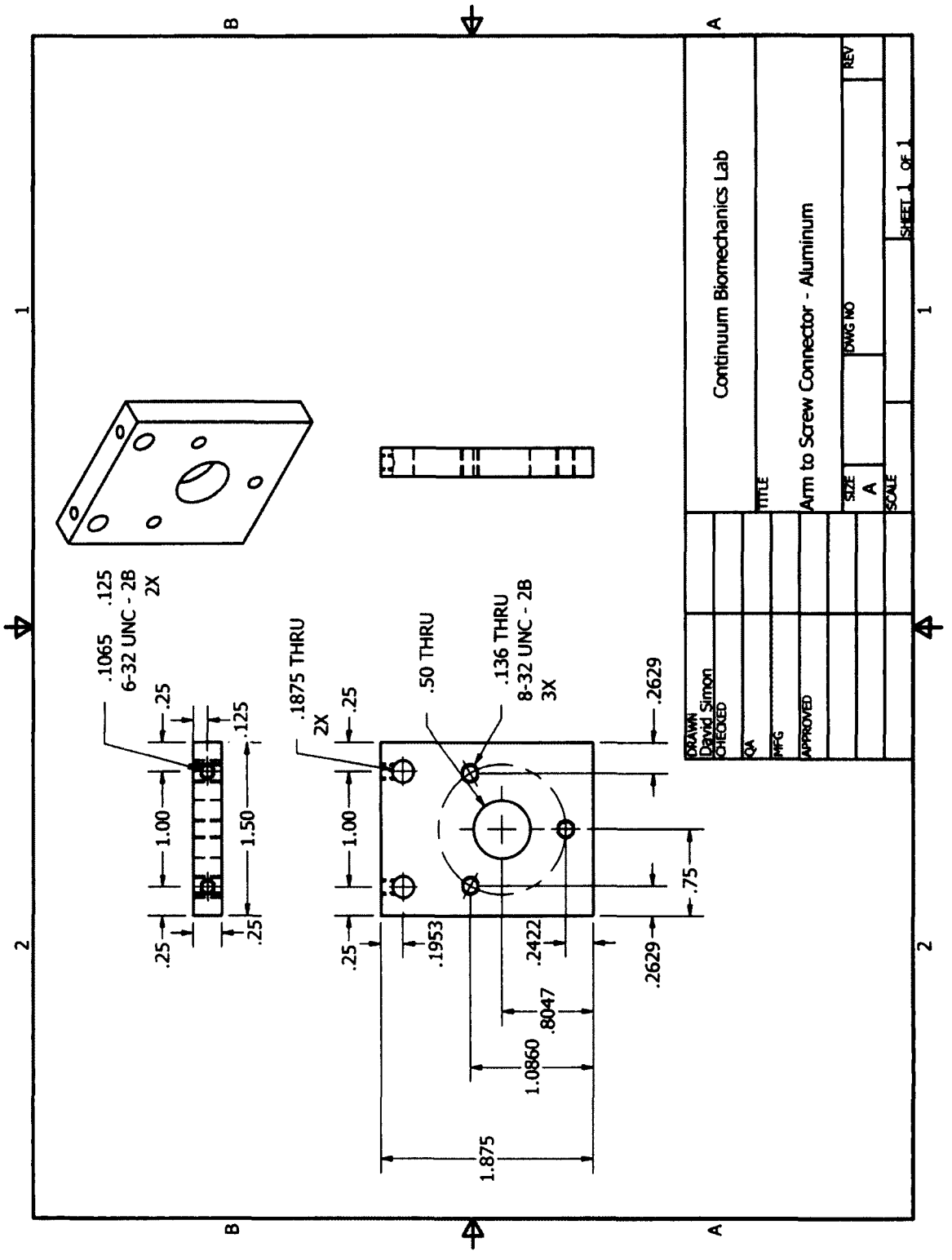

Figure D.9: Loading arm to linear screw connector plate technical drawing. Units are in inches.

D.2 Biaxial System Parts List

Advanced Micro Systems, Inc.

- Motor Controllers X2: MAX-420, Dual Axis 4 Amp. 40V Microstep Control Module with encoder feedback
- COM Port Adapter: SIN-11-USB
- Motors X4: BM17-63-IP65, Motor, High Torque 63 oz-in, Frame Size 17, with IP65 Water & Dust Resistance Rating
    - Lead Extension option: Lead Ext, 4 foot shielded lead extensions

Thomson BSA

- Linear screws X4: M17S4, M17S4-MTS10X2M-2.0" STROKE

ThorLabs

- Kinematic base: KB3X3
- Mounting Post and Base: P4, PB1

Newport Corporation

- 1D Linear Stage X3: TSX-1D
- Rod Clamp: 340-RC

Navitar, Inc.

- 6.5X Zoom Body: 1-6232
- 1X Short Tube Adapter: 1-6245

- C-Mount Coupler: 1-6010
- Right Angle Lens Attachment: 1-62866
- 0.75X Lens Attachment: 1-60111
- Universal Mounting Clamp: 1-6270
- 150W Halogen Light Supply: 8-61172
- Fiberoptic Ring Light: 1-61214

Edmund Optics

- CCD Camera: 68-573, AVT Manta G-032 1/3" Monochrome CCD Camera

National Instruments

- Bridge and Strain Measurement Module: NI USB-9237

Honeywell

- Force Transducer X2: AL311AJ,1A,2U,4A,6I,15C, Model 31 Submersible Load Cell

Electro Industries

- DC Power Supply: 303D

Dell

- Computer: Optiplex 790